Complexity

Iterative Learning and Fractional Order Control for Complex Systems

Lead Guest Editor: Farah Bouakrif
Guest Editors: Ahmad Taher Azar, Christos K. Volos, Jesus M. Muñoz-Pacheco, and Viet-Thanh Pham

Iterative Learning and Fractional Order Control for Complex Systems

Complexity

Iterative Learning and Fractional Order Control for Complex Systems

Lead Guest Editor: Farah Bouakrif
Guest Editors: Ahmad Taher Azar, Christos Volos, Jesus M. Muñoz-Pacheco, and Viet-Thanh Pham

Editorial Board

Contents

Hindawi
Complexity
Volume 2019, Article ID 7958625, 3 pages
https://doi.org/10.1155/2019/7958625

Editorial

Iterative Learning and Fractional Order Control for Complex Systems

Farah Bouakrif,[1] **Ahmad Taher Azar**,[2,3] **Christos K. Volos**,[4] **Jesus M. Muñoz-Pacheco**,[5] **and Viet-Thanh Pham**[6,7]

[1]*Faculty of Science and Technology, University of Jijel, Jijel 18000, Algeria*
[2]*College of Engineering, Prince Sultan University, Riyadh, Saudi Arabia*
[3]*Faculty of Computers and Information, Benha University, Benha 13511, Egypt*
[4]*Laboratory of Nonlinear Systems-Circuits & Complexity (LaNSCom), Department of Physics, Aristotle University of Thessaloniki, 54124 Thessaloniki, Greece*
[5]*Facultad de Ciencias de la Electrónica, Autonomous University of Puebla (BUAP), Av. San Claudio y 18 Sur, Puebla, Pue. 72570, Mexico*
[6]*Faculty of Electrical and Electronic Engineering, Phenikaa Institute for Advanced Study (PIAS), Phenikaa University, Yen Nghia, Ha Dong district, Hanoi 100000, Vietnam*
[7]*Phenikaa Research and Technology Institute (PRATI), A&A Green Phoenix Group, 167 Hoang Ngan, Hanoi 100000, Vietnam*

Correspondence should be addressed to Farah Bouakrif; f.bouakrif@gmail.com

Received 14 April 2019; Accepted 15 April 2019; Published 2 May 2019

Control theory asks how to influence the behavior of a dynamical system with appropriately chosen inputs so that the system's output follows the desired trajectory or final state [1–5]. A key notion in control theory is the feedback process: the difference between the actual and desired output is applied as feedback to the system's input, forcing the system's output to converge to the desired output. Feedback control has deep roots in physics and engineering [6, 7].

Indeed, when a system is performing the same task repeatedly, it is advantageous to use the knowledge from the previous iterations of the same task to reduce the error on successive trials. An example of such a system is robot arm manipulators when the reference trajectory is repeated over given operation time. When the conventional control algorithms with such systems are used, the same error is repeated from cycle to cycle. Iterative Learning Control (ILC) is a relatively new addition to the toolbox of the control algorithm. It is concerned with the performance of systems that operate repetitively. ILC differs from most existing control methods in the sense that it exploits every possibility of incorporating past control information, such as tracking errors and control input signals, into the construction of the present control action to enable the controlled system to perform progressively better from operation to operation. Since the ILC method was proposed by Uchiyama [8] and presented as a formal theory by Arimoto [9], this technique has been the center of interest of many researchers over the last decades [10–19].

Fractional order control systems have also received considerable attention recently, from both an academic and industrial viewpoint, because of their increased flexibility (concerning integer-order systems) which allows more accurate modeling of complex systems and the achievement of more challenging control requirements [20–24].

The overall purpose of this special issue lies in gathering the latest developments, trends, research solutions, and applications of ILC and fractional order control and to explore the more productive avenues for future research. The breadth of scope for the special issue includes both theoretical study and experimental application. We receive a total of 26 submissions where the authors are from geographically distributed countries, denoting the high impact of the proposed topic and the

seniority in the organization of the special issue. After two rounds of rigorous review, only ten papers were accepted.

In the paper "Robust Fractional-Order PID Controller Tuning Based on Bode's Optimal Loop Shaping," L. Liu and S. Zhang present a novel fractional-order PID controller tuning strategy based on Bode's optimal loop shaping which is commonly used for LTI feedback systems. The controller parameters are achieved based on flat phase property and Bode's optimal reference model so that the controlled system is robust to gain variations. Also, the proposed fractional-order PID controller does not have any restriction on the controlled plant so that it can be widely applied to both integer-order and fractional-order systems.

In the paper "A Fractional-Order System with Coexisting Chaotic Attractors and Control Chaos via a Single State Variable Linear Controller," P. Zhou et al. propose a 3D fractional-order nonlinear system with coexisting chaotic attractors. The fractional-order system exhibits chaotic attractors with the order as low as 2.5431. Meanwhile, a control scheme for the stabilization of the unstable equilibrium is suggested via a single state variable linear controller.

In the paper "New Iterative Method for the Solution of Fractional Damped Burger and Fractional Sharma-Tasso-Olver Equations," M. J. Khan et al. apply the new iterative method to obtain the approximate solutions of time-fractional damped Burger and time-fractional Sharma-Tasso-Olver equations. The 2nd-order approximate solutions by the new iterative method are in good agreement with the exact solution as compared to the 5th-order solution by the FRDTM.

In the paper "Consensus of Multi-Integral Fractional-Order Multiagent Systems with Nonuniform Time-Delays," J. Liu et al. study the consensus problems for multi-integral fractional-order multiagent systems (MIFOMASs) with nonuniform time-delays. The consensus conditions for MIFOMASs are obtained by a novel frequency-domain method which properly eliminates consensus problems of the systems associated with nonuniform time-delays. Numerical simulations with different parameters demonstrate the results.

In the paper "The Unique Existence of Weak Solution and the Optimal Control for Time-Fractional Third Grade Fluid System," G. Shao et al. study the third grade fluid system with the time-fractional derivative of the order $\alpha \in (0, 1)$. They first establish a unique existence criterion of weak solutions in the case that the dimension. Then they prove the sufficient condition of optimal pairs.

In the paper "Adaptive Inverse Control Based on Kriging Algorithm and Lyapunov Theory of Crawler Electromechanical System," G. Zhang et al. propose an adaptive inverse control method based on kriging algorithm and Lyapunov theory to improve control accuracy during adaptive driving of the electromechanical system of a crawler. The adaptive travel control law of the crawler was obtained by the Lyapunov theory. Combined with the kriging algorithm, the adaptive driving reverse control method is designed, and the online system is used to update and perfect the inverse system model in real time. The adaptive inverse control method is verified by theoretical analysis and virtual prototype simulation.

In the paper "Complex Dynamics of the Fractional-Order Rössler System and Its Tracking Synchronization Control," H. Wang et al. study the fractional-order Rössler system with a fast discrete iteration using the Adomian decomposition method (ADM) for its implementing on a DSP board. Complex dynamics of the fractional-order chaotic system are analyzed by means of Lyapunov exponent spectra, bifurcation diagrams, and phase diagrams. Moreover, tracking synchronization controllers were theoretically designed and numerically investigated. That lays a foundation for the application of the fractional-order Rössler system.

In the paper "Dynamics Feature and Synchronization of a Robust Fractional-Order Chaotic System," X.-B. Yang et al. introduce a three-dimensional fractional-order chaotic system. The critical finding by analysis is that the position of signal x_3 descends at the speed of $1/c$ as the parameter b increases, and the signal amplitude of x_1, x_2 can be controlled by the parameter m in terms of the power function with the index $-1/2$. Consequently, this system can provide rich encoding keys for chaotic communication. By considering the properties of amplitude and position modulation, the partial projective synchronization and partial phase synchronization are also realized with a linear control scheme. Numerical simulations are executed to confirm the theoretical analysis.

In the paper "Evaluating Fractional PID Control in a Nonlinear MIMO Model of a Hydroelectric Power Station," O. A. Rosas-Jaimes et al. present a fractional PID control for a hydropower plant with six generation units working in an alternation scheme. The parameters and other features of such a set of hydrogeneration units have been used to perform the respective tuning up. To assess the behavior of this controlled system, a model of such nonlinear plant is regulated through a classical PID by classical linearization of its set points, and then a pseudo-derivative part is substituted into a fractional PID. Both sets of resulting signals are compared; the simulations show that the fractional PID has a faster response concerning those plots obtained from the classical PID used.

In the paper "Results on a Novel Piecewise-Linear Memristor-Based Chaotic System," B. Wang studies a kind of piecewise-linear memristor-based chaotic system. Based on a novel and complicated piecewise-linear memristor model, a chaotic system is constructed; then a random sequence extraction approach from the given memristor-based chaotic system is designed. At last the random sequence test is carried out to show the potential application value in encryption field of the new memristor-based chaotic system.

Conflicts of Interest

The editors declare that they have no conflicts of interest regarding the publication of this special issue.

Acknowledgments

The guest editorial team would like to thank and express its deep appreciation to all the authors who have submitted

their works for this special issue. The editors are also grateful to all anonymous reviewers for their rigorous reviews and insightful comments. Additionally, we would like to thank the journal's Editorial Board for being very encouraging and accommodative regarding this special issue. We hope the readers will find this special issue interesting and informative.

Farah Bouakrif
Ahmad Taher Azar
Christos K. Volos
Jesus M. Muñoz-Pacheco
Viet-Thanh Pham

References

[1] A. T. Azar and S. Vaidyanathan, *Advances in Chaos Theory and Intelligent Control*, vol. 337 of *Studies in Fuzziness and Soft Computing*, Springer, Germany, 2016.

[2] F. Bouakrif, "Trajectory tracking control using velocity observer and disturbances observer for uncertain robot manipulators without tachometers," *Meccanica*, vol. 52, no. 4-5, pp. 861–875, 2017.

[3] K. C. Draa, H. Voos, M. Alma, A. Zemouche, and M. Darouach, "LMI-based trajectory tracking for a class of nonlinear systems with application to an anaerobic digestion process," in *Proceedings of the 2018 Annual American Control Conference (ACC)*, pp. 4393–4397, IEEE, Milwaukee, WI, USA, June 2018.

[4] R. A. Garcia and C. E. D'Attellis, "Trajectory tracking in nonlinear systems via nonlinear reduced-order observers," *International Journal of Control*, vol. 62, no. 3, pp. 685–715, 1995.

[5] X. Zhang, X. Huang, and H. Lu, "Forwarding-based trajectory tracking control for nonlinear systems with bounded unknown disturbances," *International Journal of Control, Automation, and Systems*, vol. 14, no. 5, pp. 1231–1243, 2016.

[6] A. T. Azar and S. Vaidyanathan, *Chaos Modeling and Control Systems Design*, vol. 581 of *Studies in Computational Intelligence*, Springer, Germany, 2015.

[7] A. T. Azar and Q. Zhu, *Advances and Applications in Sliding Mode Control systems*, vol. 576 of *Studies in Computational Intelligence*, Springer, Germany, 2015.

[8] M. Uchiyama, "Formulation of high-speed motion pattern of a mechanical arm by trial," *Transactions of the Society of Instrument and Control Engineers*, vol. 14, pp. 706–712, 1978.

[9] S. Arimoto, S. Kawamura, and F. Miyazaki, "Bettering operation of robots by learning," *Journal of Robotic Systems*, vol. 1, no. 2, pp. 123–140, 1984.

[10] F. Bouakrif, "D-type iterative learning control without resetting condition for robot manipulators," *Robotica*, vol. 29, no. 7, pp. 975–980, 2011.

[11] F. Bouakrif, D. Boukhetala, and F. Boudjema, "Velocity observer-based iterative learning control for robot manipulators," *International Journal of Systems Science*, vol. 44, no. 2, pp. 214–222, 2013.

[12] F. Bouakrif and M. Zasadzinski, "High order iterative learning control to solve the trajectory tracking problem for robot manipulators using Lyapunov theory," *Transactions of the Institute of Measurement and Control*, vol. 40, no. 15, pp. 4105–4114, 2018.

[13] F. Bouakrif, "Iterative learning control for strictly unknown nonlinear systems subject to external disturbances," *International Journal of Control, Automation, and Systems*, vol. 9, no. 4, pp. 642–648, 2011.

[14] M. M. Ghazaei Ardakani, S. Z. Khong, and B. Bernhardsson, "On the convergence of iterative learning control," *Automatica*, vol. 78, pp. 266–273, 2017.

[15] J. van Zundert, J. Bolder, and T. Oomen, "Optimality and flexibility in iterative learning control for varying tasks," *Automatica*, vol. 67, pp. 295–302, 2016.

[16] S. Devasia, "Iterative learning control with time-partitioned update for collaborative output tracking," *Automatica*, vol. 69, pp. 258–264, 2016.

[17] X. Li and D. Shen, "Two novel iterative learning control schemes for systems with randomly varying trial lengths," *Systems & Control Letters*, vol. 107, pp. 9–16, 2017.

[18] D. Meng and K. L. Moore, "Convergence of iterative learning control for SISO nonrepetitive systems subject to iteration-dependent uncertainties," *Automatica*, vol. 79, pp. 167–177, 2017.

[19] R. Zhang, Z. Hou, H. Ji, and C. Yin, "Adaptive iterative learning control for a class of non-linearly parameterised systems with input saturations," *International Journal of Systems Science*, vol. 47, no. 5, pp. 1084–1094, 2016.

[20] A. T. Azar, A. G. Radwan, and S. Vaidyanathan, *Mathematical Techniques of Fractional Order Systems*, Elsevier, Amsterdam, Netherlands, 2018.

[21] A. T. Azar, S. Vaidyanathan, and A. Ouannas, *Fractional Order Control and Synchronization of Chaotic Systems*, vol. 688 of *Studies in Computational Intelligence*, Springer, Germany, 2017.

[22] Y. Q. Chen, I. Petráš, and D. Y. Xue, "Fractional order control—a tutorial," in *Proceedings of the American Control Conference (ACC '09)*, pp. 1397–1411, IEEE, June 2009.

[23] S. Victor, R. Malti, H. Garnier, and A. Oustaloup, "Parameter and differentiation order estimation in fractional models," *Automatica*, vol. 49, no. 4, pp. 926–935, 2013.

[24] Z. Yakoub, M. Amairi, M. Chetoui, B. Saidi, and M. Aoun, "Model-free adaptive fractional order control of stable linear time-varying systems," *ISA Transactions®*, vol. 67, pp. 193–207, 2017.

Hindawi
Complexity
Volume 2019, Article ID 8948656, 6 pages
https://doi.org/10.1155/2019/8948656

Research Article

Results on a Novel Piecewise-Linear Memristor-Based Chaotic System

Bo Wang [1,2]

[1] *School of Electrical and Information Engineering, Xihua University, Chengdu 610039, China*
[2] *School of Applied Mathematics, University Electronic Science and Technology of China, Chengdu 610054, China*

Correspondence should be addressed to Bo Wang; coolbie@163.com

Received 20 September 2018; Revised 13 November 2018; Accepted 22 November 2018; Published 2 January 2019

Guest Editor: Christos K. Volos

The paper studies a kind of piecewise-linear memristor-based chaotic system. Based on a novel and complicated piecewise-linear memristor model, a chaotic system is constructed; then a random sequence extraction approach on the basis of the given memristor-based chaotic system is designed; at last the random sequence test is carried out to show the potential application value in encryption field of the new memristor-based chaotic system.

1. Introduction

Chaos phenomenon in circuit was first reported by Leon O. Chua at Waseda University in 1983. Since then, chaos gets a number of attentions from scholars for its potential application in chaotic synchronization [1, 2], secret communication [3, 4], image's encryption [5, 6], and so on.

In 1971, Chua first proposed the concept of memristor [7], which was regarded as the fourth element in electronic circuits. Although the technique to produce the real memristor is not mature so far, memristor model can be used to construct chaotic circuit system. At present, a number of investigations on memristor-based chaotic system have been carried out [8–12]. For example, the chaotic circuit with one memristor is studied in [13, 14], the chaotic circuit with two memristors is concerned in [15, 16], the integer order chaotic memristor circuit is investigated in [17, 18], and the fractional chaotic memristor circuit is researched in [19, 20]. However for the existing piecewise-linear memristive chaotic circuits, the nonlinear device usually adopts Chua's piecewise-linear memristor model, and there are seldom other kinds of piecewise-linear memristor model for selection.

Random number generator is one important application field of chaotic system [21, 22], and how to generate a random sequence with better performance has always been a challenging issue. Although some approaches to extract random sequence based on memristive chaotic system have been proposed up to now, corresponding random sequences are easy to analyze by attackers with the well-known prior knowledge of memristive chaotic system. Hence it is meaningful to build the memristive chaotic system on the basis of the new and complicated memristor model. All these motive our research.

The organization of the paper is as follows: a chaotic system based on a novel piecewise-linear memristor model will be proposed in Section 2, and corresponding analysis will also be provided; then the random sequence test will be carried out in Section 3; the conclusion will be presented in Section 4.

2. Memristor-Based Chaotic System

In this section, a novel memristor-based system is proposed as follows:

$$\begin{aligned} \dot{x} &= \alpha\left(y - x - \overline{W}(w)\, x\right) \\ \dot{y} &= \beta x + (\kappa + \gamma - \beta)\, y - z \\ \dot{z} &= \kappa y - z \\ \dot{w} &= x \end{aligned} \tag{1}$$

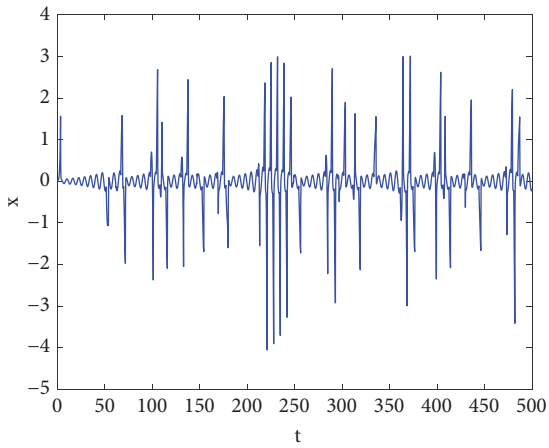

(a) Time response of state variable x(t)

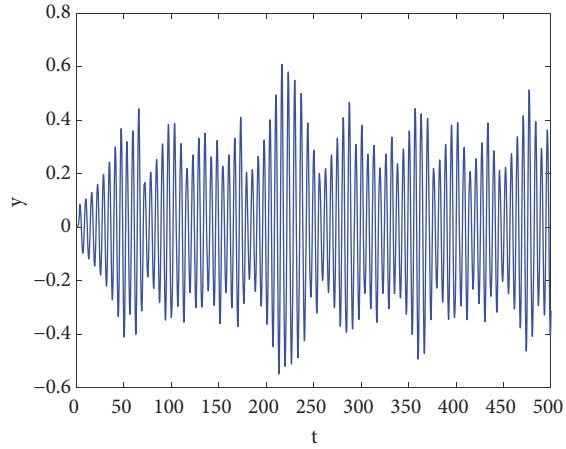

(b) Time response of state variable y(t)

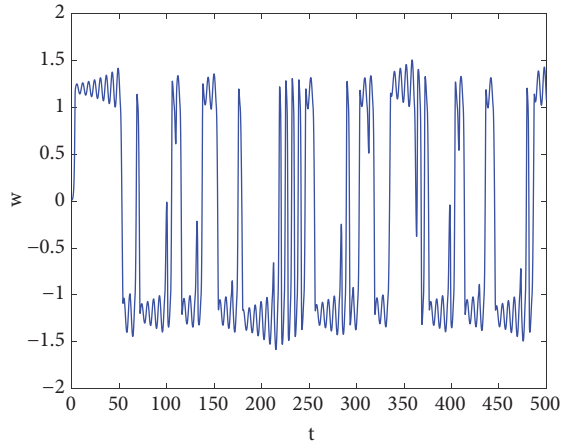

(c) Time response of state variable w(t)

Figure 1: Time response of state variables of the memristor-based system.

where $\overline{W}(w)$ is the constructed memristor model, which satisfies

$$\overline{W}(w) = \begin{cases} A, & |w| \le m, \ |x| \le n \\ B, & |w| > m, \ |x| \le n \\ C, & |w| \le m, \ |x| > n \\ D, & |w| > m, \ |x| > n \end{cases} \tag{2}$$

When $\alpha = 4.7, \beta = 0.061, \gamma = 1, \kappa = 2.1, A = -1.29, B = 0.75, C = -1.17, D = 0.93, m = 1, n = 1.56$, initial value is $[0.01, 0, 0, 0.01]$, and the system dynamics are displayed in Figures 1 and 2.

Remark 1. Figure 1(a) displays the time response of state variable x(t). Figure 1(b) displays the time response of state variable y(t). Figure 1(c) displays the time response of state variable w(t). It can be seen that the state variables of the memristor-based system look chaotic and disorganized visually.

Remark 2. Figure 2(a) displays the phase diagram of y-w. Figure 2(b) displays the phase diagram of x-w. Figure 2(c) displays the phase diagram of x-z. It can be seen that the state variables of the memristor-based system keep moving in a certain attractor and do not converge to a point or diverge to infinity.

Firstly, consider the system dissipativity:

$$\nabla V = \frac{\partial \dot{x}}{\partial x} + \frac{\partial \dot{y}}{\partial y} + \frac{\partial \dot{z}}{\partial z} + \frac{\partial \dot{w}}{\partial w} \tag{3}$$

When $|w| \le m, |x| \le n$, one can get

$$\nabla V = -1.37 \tag{4}$$

When $|w| > m, |x| \le n$, one can get

$$\nabla V = -3.41 \tag{5}$$

When $|w| \le m, |x| > n$, one can get

$$\nabla V = -1.49 \tag{6}$$

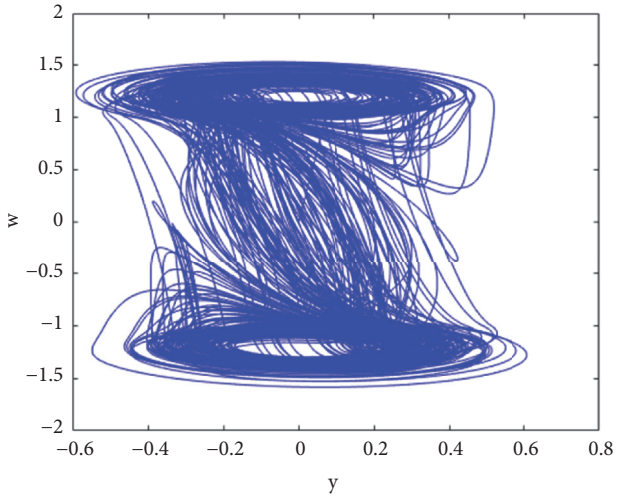

(a) Phase diagram of y-w

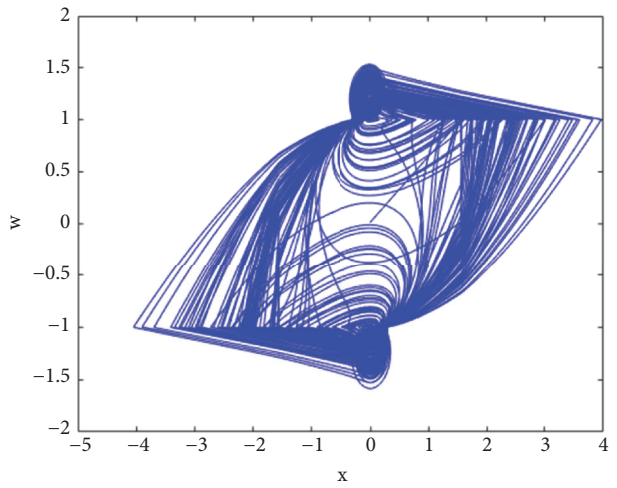

(b) Phase diagram of x-w

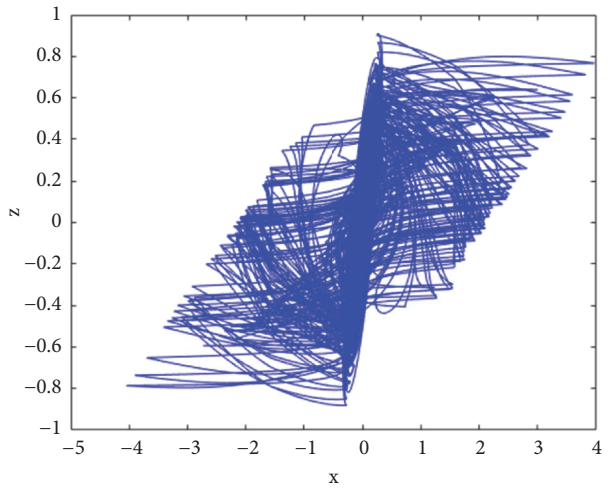

(c) Phase diagram of x-z

FIGURE 2: Phase diagram of state variables of the memristor-based system.

When $|w| > m, |x| > n$, one can get

$$\nabla V = -3.59 \tag{7}$$

From the above it can be concluded that $\nabla V < 0$, which means that the memristor-based system is dissipative.

Next, by adjusting parameter α, consider the dynamics of the given memristor-based system. The simulations are displayed in Figure 3.

Remark 3. Figure 3(a) displays the Lyapunov exponent diagram of the memristor-based system. Figure 3(b) displays the bifurcation diagram of the memristor-based system. It can be seen that the given memristor-based system is in the chaotic state when $\alpha \in [3.5, 7]$.

3. Random Sequence

In this section, we design a new random sequence extraction approach on the basis of the given memristor-based system as follows.

Step 1. Let X=[x,y,z,w]. Set the initial variable of the given memristor-based chaotic system X_0=[0.01, 0, 0, 0.01], the threshold value m=4, and the sequence label j=0.

Step 2. Carry out iterations 1000 times based on the given memristor-based chaotic system, corresponding system state variable is denoted as X(j), and set the sequence label j=1.

Step 3. Carry out an iterative operation based on the given memristor-based chaotic system, and set the sequence label j=j+1.

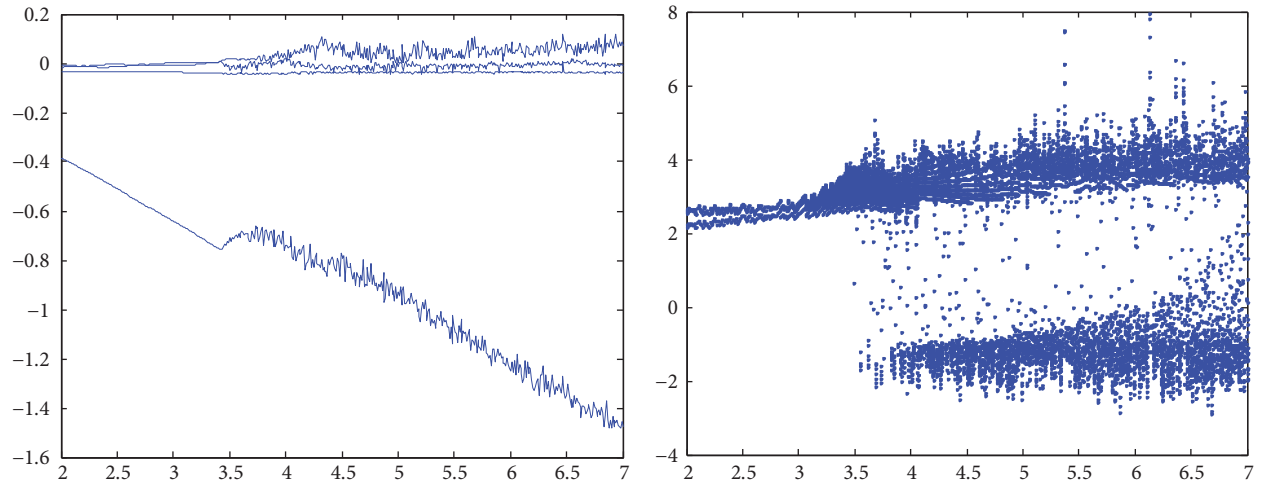

(a) Lyapunov exponent diagram (b) Bifurcation diagram

Figure 3: Dynamics of given memristor-based system with different a.

Table 1: NIST test on random sequences.

Chaos Systems	New system		Chua's system [23]	
Statistical test	P value	Proportion	P value	Proportion
Frequency	0.9735	0.9900	0.7981	0.9800
Block Frequency	0.7362	1.0000	0.6786	1.0000
Cumulative Sums	0.5478	0.9900	0.1222	0.9800
Runs	0.9176	1.0000	0.8343	0.9900
Longest Run	0.5261	0.9900	0.2896	0.9800
Rank	0.6858	1.0000	0.4372	1.0000
Approximate Entropy	0.5247	0.9800	0.1916	0.9800
Serial	0.8653	1.0000	0.5955	1.0000
Linear Complexity	0.4275	0.9900	0.0668	0.9700

Step 4. Determine i:

$i = \mathrm{REM}(z(j),2)$,

where REM (.) is the remainder operation.

Step 5. Determine $P_{t1}(j)$:

when $w_i(j) > 4$, $P_{t1}(j)=1$;

otherwise, $P_{t1}(j)=0$;

where $w_i(j)$ denotes the value of ith decimal place of w(j).

Step 6. Determine the mapping variable M(j) according to i:

if i=0, M(j)=x(j);

if i=1, M(j)=y(j).

Step 7. Determine $P_{s1}(j)$:

when $M_i(j) > 4$,$P_{s1}(j)=1$;

otherwise, $P_{s1}(j)=0$.

where $M_i(j)$ denotes the value of ith decimal place of $M_i(j)$.

Step 8. Determine P_j

$P_j = \mathrm{XOR}(P_{t1}(j), P_{s1}(j))$;

where XOR (.) is the exclusive-or operation.

Step 9. Carry out circulation from Step 3 to Step 8 10 million times; one can obtain the binary random sequence:

$P = \{P_1, P_2, \ldots, P_N\}$

where j=N, and N=10000000 is the required sequence length.

Set the sampling time T as 0.001s, and $h = 5, i = 4$. Extract a binary random sequence with 10 million bits, which is divided into 100 groups and put into a software test kit, NIST, and the NIST test results of random sequences are displayed in Table 1.

Remark 4. Table 1 displays NIST test results of random sequences. The significance level of each test in NIST is set to 0.01, and P value $\geqslant 0.01$ means that the sequence would be random with a confidence of 0.99. It can be noted that P values of all tests on the proposed sequence are all bigger than 0.01, which means our sequence can be regarded as random. In addition, it can be seen that, compared with Chua's system [23], the sequence based on the new memristor-based chaotic system has bigger P value in Frequency test, Block Frequency test, Cumulative Sums test, Runs test, Longest Run test,

Table 2: Statistic test on sequences based on Beker and Piper method.

	Frequency test	Serial test	Poker test			Run test
			m=1	m=2	m=3	
Chua's system [23]	0.23	1.07	0.73	3.24	5.03	1.14
New system	0.08	0.76	0.56	2.87	4.35	0.52
Threshold	3.84	5.99	7.81	14.07	26.00	1.96

Rank test, Approximate Entropy test, Serial test, and Linear Complexity test; hence the proposed sequence has the better overall random statistic characteristics.

Next, the statistic test on 100000 bits of sequence based on Beker and Piper method [24] is carried out. Corresponding test results are shown in Table 2.

Remark 5. Table 2 shows the statistic test results of sequences based on Beker and Piper method. Frequency test, Serial test, Poker test, and Runs test are included in Beker and Piper approach to measure the relative frequencies of '0' and '1' in a section of sequence. The confidence level is set as 0.95, and threshold is introduced to determine the confidence of test results. It can be seen that all results are less than the preset threshold, which means that all tests are passed successfully, and the sequences can be regarded as random signal. In addition, it can be seen that the numerical values of Frequency test, Serial test, Poker test, and Runs test based on the proposed sequence are less than the ones based on Chua's system. More importantly, the proposed sequence is on the basis of chaotic system with the novel piecewise-linear memristor model, which will increase the security of corresponding cryptosystem for its unusual mechanism.

4. Conclusion

In this paper, based on a proposed complicated piecewise-linear memristor model, a new chaotic system has been constructed; then an extraction method on the basis of the given memristor-based system has been designed to obtain the random sequence; finally the random sequence test is carried out to show the potential application value of the new memristor-based chaotic system in encryption field.

Data Availability

The data used to support the findings of this study are included within the article.

Conflicts of Interest

The author declares that there are no conflicts of interests regarding the publication of this paper.

Acknowledgments

This work is partially supported by the Key Laboratory of Fluid and Power Machinery of the Ministry of Education and the National Natural Science Foundation of China (61703150, 11626093).

References

[1] H. Handa and B. B. Sharma, "Novel adaptive feedback synchronization scheme for a class of chaotic systems with and without parametric uncertainty," *Chaos, Solitons & Fractals*, vol. 86, pp. 50–63, 2016.

[2] B. Wang and L. L. Chen, "New Results on Fuzzy Synchronization for a Kind of Disturbed Memristive Chaotic System," *Complexity*, vol. 2018, Article ID 3079108, p. 9, 2018.

[3] H. Huijberts, H. Nijmeijer, and R. Willems, "System identification in communication with chaotic systems," *IEEE Transactions on Circuits and Systems I: Fundamental Theory and Applications*, vol. 47, no. 6, pp. 800–808, 2000.

[4] F. Wang, X. Wang, C.-G. Yuan, and J. Ma, "Generating a prion with bacterially expressed recombinant prion protein," *Science*, vol. 327, no. 5969, pp. 1132–1135, 2010.

[5] D. S. Laiphrakpam and M. S. Khumanthem, "Cryptanalysis of symmetric key image encryption using chaotic Rossler system," *Optik - International Journal for Light and Electron Optics*, vol. 135, pp. 200–209, 2017.

[6] B. Wang, L. L. Chen, and J. Cheng, "New result on maximum entropy threshold image segmentation based on P system," *Optik - International Journal for Light and Electron Optics*, vol. 163, pp. 81–85, 2018.

[7] L. O. Chua, "Memristor—the missing circuit element," *IEEE Transactions on Circuit Theory*, vol. 18, no. 5, pp. 507–519, 1971.

[8] B. Wang, J. Cheng, and F. Zou, "Stochastic finite-time H∞ filtering for nonlinear Markovian jump systems with partly known transition probabilities," *Proceedings of the Institution of Mechanical Engineers, Part I: Journal of Systems and Control Engineering*, 2018.

[9] Y. Babacan and F. Kaçar, "Memristor emulator with spike-timing-dependent-plasticity," *AEÜ - International Journal of Electronics and Communications*, vol. 73, pp. 16–22, 2017.

[10] B. Wang, L. Chen, and Y. Liu, "New results on contrast enhancement for infrared images," *Optik - International Journal for Light and Electron Optics*, vol. 178, pp. 1264–1269, 2019.

[11] J. Wu, L. Wang, G. Chen, and S. Duan, "A memristive chaotic system with heart-shaped attractors and its implementation," *Chaos, Solitons & Fractals*, vol. 92, pp. 20–29, 2016.

[12] B. Wang, D. Zhang, J. Cheng, and J. H. Park, "Fuzzy model-based nonfragile control of switched discrete-time systems," *Nonlinear Dynamics*, vol. 93, no. 4, pp. 2461–2471, 2018.

[13] H. H. Iu, D. S. Yu, A. L. Fitch, V. Sreeram, and H. Chen, "Controlling chaos in a memristor based circuit using a twin-T notch filter," *IEEE Transactions on Circuits and Systems I: Regular Papers*, vol. 58, no. 6, pp. 1337–1344, 2011.

[14] B. Muthuswamy, "Implementing memristor based chaotic circuits," *International Journal of Bifurcation and Chaos*, vol. 20, no. 5, pp. 1335–1350, 2010.

[15] R. K. Budhathoki, M. P. Sah, C. Yang, H. Kim, and L. Chua, "Transient behaviors of multiple memristor circuits based on flux charge relationship," *International Journal of Bifurcation and Chaos*, vol. 24, no. 2, 1430006, 14 pages, 2014.

[16] A. Buscarino, L. Fortuna, M. Frasca, and L. V. Gambuzza, "A chaotic circuit based on Hewlett-Packard memristor," *Chaos: An Interdisciplinary Journal of Nonlinear Science*, vol. 22, no. 2, Article ID 023136, 2012.

[17] R. Riaza, "First order mem-circuits: modeling, nonlinear oscillations and bifurcations," *IEEE Transactions on Circuits and Systems I: Regular Papers*, vol. 60, no. 6, pp. 1570–1583, 2013.

[18] A. Buscarino, L. Fortuna, M. Frasca, and L. V. Gambuzza, "A gallery of chaotic oscillators based on HP memristor," *International Journal of Bifurcation and Chaos*, vol. 23, no. 5, Article ID 1330015, 2013.

[19] I. Petráš, "Fractional-order memristor-based Chua's circuit," *IEEE Transactions on Circuits and Systems II: Express Briefs*, vol. 57, no. 12, pp. 975–979, 2010.

[20] L. Teng, H. H. C. Iu, and X. Wang, "Chaotic behavior in fractional-order memristor-based simplest chaotic circuit using fourth degree polynomial," *Nonlinear Dynamics*, vol. 77, no. 1-2, pp. 231–241, 2014.

[21] H. Hu, L. Liu, and N. Ding, "Pseudorandom sequence generator based on the Chen chaotic system," *Computer Physics Communications*, vol. 184, no. 3, pp. 765–768, 2013.

[22] F. Özkaynak and S. Yavuz, "Security problems for a pseudorandom sequence generator based on the Chen chaotic system," *Computer Physics Communications*, vol. 184, no. 9, pp. 2178–2181, 2013.

[23] T. Matsumoto, "A Chaotic Attractor from Chua's Circuit," *IEEE Transactions on Circuits and Systems II: Express Briefs*, vol. 31, no. 12, pp. 1055–1058, 1984.

[24] H. J. Beker and F. C. Piper, Eds., *Cryptography and coding*, vol. 20 of *The Institute of Mathematics and its Applications Conference Series. New Series*, The Clarendon Press, Oxford University Press, New York, 1989.

Hindawi
Complexity
Volume 2019, Article ID 9367291, 15 pages
https://doi.org/10.1155/2019/9367291

Research Article

Evaluating Fractional PID Control in a Nonlinear MIMO Model of a Hydroelectric Power Station

O. A. Rosas-Jaimes,[1] **G. A. Munoz-Hernandez**,[1] **G. Mino-Aguilar**,[1] **J. Castaneda-Camacho**,[1] **and C. A. Gracios-Marin**[2]

[1]*Benemerita Universidad Autonoma de Puebla, Av. San Claudio and 18 Sur. Puebla, C.P. 72570, Mexico*
[2]*Instituto Tecnologico de Puebla, Av. Tecnologico 420 Puebla, C.P. 72220, Mexico*

Correspondence should be addressed to O. A. Rosas-Jaimes; oscar.rosasj@correo.buap.mx

Received 8 August 2018; Revised 6 November 2018; Accepted 10 December 2018; Published 1 January 2019

Guest Editor: Viet-Thanh Pham

In this paper a Fractional PID Control is presented. This control was designed for a hydropower plant with six generation units working in an alternation scheme. The parameters and other features of such a set of hydrogeneration units have been used to perform the respective tuning up. In order to assess the behavior of this controlled system, a model of such nonlinear plant is regulated through a classical PID by classical linearization of its set points, and then a pseudo-derivative part is substituted into a Fractional PID. Both groups of signals contain variations of voltage suggesting some abrupt changes in the supply of electricity fed to the network. Both sets of resulting signals are compared; the simulations show that the Fractional PID has a faster response with respect to those plots obtained from the classical PID used.

1. Introduction

Hydropower pumped storage stations are important because they have the capacity of releasing, on demand, large amounts of energy to an electrical net (Figure 1). Water is pumped to an upper reservoir from a lower one and released to generate electricity [1]. The model to be used in this work is based on Dinorwig, North Wales, UK [1–3]. It is composed of six reversible pump-turbines of 300 MW each [2, 3]. To modulate the flow, six valves that enclose the turbine inlet are used. Two closed loop control signals are used to determine the guide vane angle: an inner loop controls the generated power, and an outer loop controls the grid frequency. Different works have been published for Dinorwig [1–3]. In this study a nonlinear model will be considered. To improve the plant performance, different controllers have been employed [1] including a Fractional PID, whose performance is evaluated in this paper.

As can be seen in Figure 1, in the hydro station the behavior of a single unit depends on the flow in the common tunnel, because its penstocks share a common conduit [4, 5]. The number of units in operation among the operating points determines the total flow. It is a common practice that only one unit operates at *part-load*.

Notwithstanding the advances in automatic control, the use of classical controllers is still very common in hydropower systems. In the literature there are many examples where industrial loops are controlled by these classical controllers, getting results that accomplish the requirements of the power systems [1, 6]. However, as was stated, the hydropower plant (Dinorwig) is a complex system and some of its characteristics make it difficult to obtain an appropriate performance by "only" using classical controllers.

For many years, different variations of PID that include nonlinear characteristics have been reported. In recent years, applications of PID controllers with integral and derivative parts of fractional order have been described. Those studies show an improvement of the performance of the controlled systems [7]. For instance, a generalization of the PID controller was proposed by Podlubny [8, 9]; that approach includes an integrator of order λ and a differentiator of order δ ($PI^{\lambda}D^{\delta}$ controller). In that work, the better response of this type of controller as compared with the classical PID controller was demonstrated. Frequency domain approaches

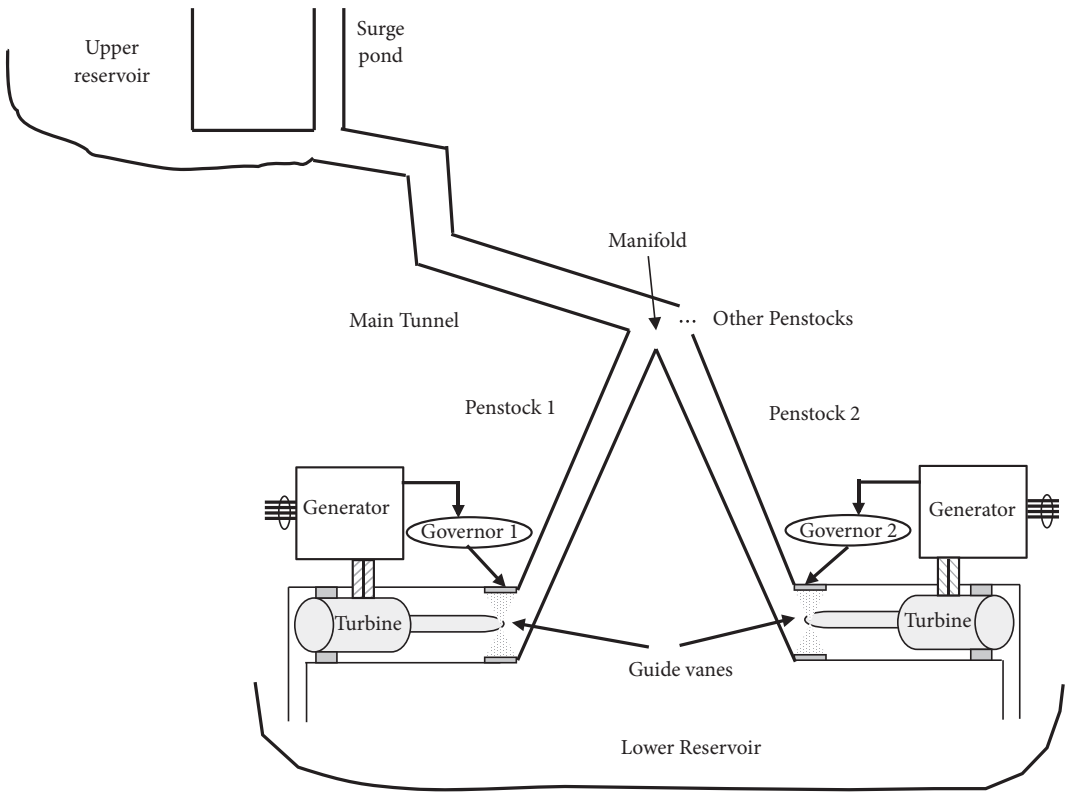

Figure 1: Dinorwig power station's representation showing only 2 of the 6 units.

for fractional order PID controllers have also been studied [10].

Several fractional order controller applications to hydropower plants have been published in recent years. Meng and Xue [11] have proposed, for example, a robust controller with fractional order for hydropower plants using automatic loop shaping to employ a Quantitative Feedback Theory (QFT) design. In that work, a flexible structure model is the main feature of this fractional order compensator. These authors have found that the fractional order controller is able to obtain a smaller high-frequency gain than the integer-order controller.

Chen et al. [12] have also described a fractional order PID controller (FOPID), whose parameters are calculated by means of a multiobjective optimization through a chaotic nondominated sorting genetic algorithm II (NSGAII). These authors used such a design to regulate a hydraulic turbine.

Xu et al. [13] have analyzed the dynamic stability of a mathematical model for a hydroturbine governing system using a fractional order regulator. The model includes a penstock system, a hydraulic servo-system, a generator, and a hydroturbine.

Wang et al. [14] have studied a finite time regulator when a hydroturbine is governed by using a fractional order nonlinear control. Their simulation results show that their proposed scheme is useful and robust.

Li et al. [15] have employed a fractional order regulator in a pumped storage unit. Their experimental results indicate that their proposal algorithm has shown excellent performance. Those results have also proved that the FOPID-CGGSA regulator presents superior benefits over other PID-type regulators with particular optimization proposals.

Xu et al. [16] have proposed a FOPID to control a reversible turbine. In their work, they use a combination of bacterial foraging (BFA) algorithm with a multiscenario functions set to select the controller's parameters.

Li, Yang, and Xia [17] have published a study that focused on the stability problems in a hydropower station, where a nonlinear hydropower generation system for the load rejection transient process was considered. They identified four critical variables of the system. Afterward, dynamic safety assessment based on the Fisher discriminant method was carried out. Their results demonstrate that the hydropower generation system in this study case can operate safely.

Fang, Yuan, and Liu [18] applied an approach based on active-disturbance-rejection-control fractional order PID to a hydroturbine speed governor system. Their proposed control has shown a strong ability of active disturbance rejection and more flexibility of nonlinear characteristics of hydroturbine speed governor system, which resolves the contradiction between fast response and small overshoot.

Nangrani and Bhat [19] have evaluated a Fractional Order Proportional Integrative Regulator for rotor angle control. Their results have shown that the proposed controller has improved the dynamic behavior of their power system.

Plant response optimization is significant for technical and economic reasons, and it is a priority for the company. Though many controllers have been applied to hydropower

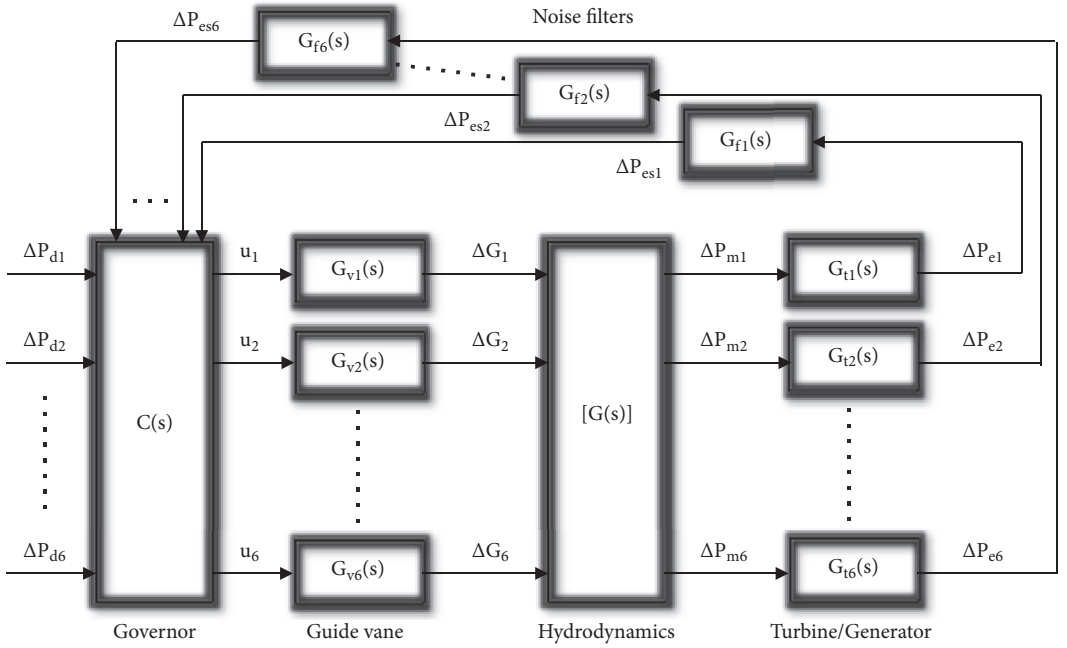

Figure 2: Subsystems of the power plant model.

systems, there are current opportunities. For example, Hote and Jain [20] recognized that the main challenge in Load Frequency Control is to develop a highly robust PID controller that maintains frequency deviation strictly in specified limits even in the presence of nonlinearities, physical constraints, and uncertain environment. For those reasons the main objective of the present paper is to increase power plants response in their precision and speed for short-term load perturbations and for frequency control using a nonlinear model to asset the performance of the proposed controller. To achieve this objective, a PID controller with fractional elements is deduced and evaluated as a proposed governor for a hydropower plant.

2. Hydropower Plant Model

In Dinorwig, the common tunnel produces an important cross-coupling effect; therefore the system is inherently multivariable [4]. This behavior has a contrary effect on the stability margin in closed loop. The units connected react modifying their control signals, via their governors, changing their operation points, while those units that are not connected have their valves closed in order to not "disturb" the flow. Consequently the number of active units determines the structure of the system. For this model all the variables are in per-unit (p.u.) form, standardized to 300MW and 50Hz; normally an electrical net with infinite busbars is assumed [21]; however, to simulate frequency control, a grid model is connected to the hydropower model. Figure 2 shows the 5 subsystems that compose the hydropower plant model. The governor is where the control signals are calculated; in this work a classical and a fractional order controller are evaluated; they are discussed in Sections 3 and 4. The guide vane model includes the valve dynamics and also the servo-mechanism for the six units; see (1). The hydrodynamics include the main tunnel and the six penstocks. Furthermore the turbine/generator is modeled, the outputs of this subsystem are filtrated before they are fed back; see (5).

For the guide vane subsystem, a hydraulic servo-system is employed to move the guide vanes in order to control the flow, represented by

$$\frac{\Delta G(s)}{u(s)} = \frac{1}{(\tau_1 s + 1)(\tau_2 s + 1)} \quad (1)$$

where u in (1) is the control signal [1, 2].

For the hydrodynamics subsystem, a nonlinear model that includes elastic characteristic is applied to simulate speed and power changes [4]. Figure 3 shows the interaction between the main tunnel and one penstock; the "surge tank and main tunnel" block will be connected to the other 5 penstocks in the complete hydraulic model.

In Figures 2 and 3, we have the following:

Surge impedance of the conduit, Z_0 (2)

Head loss coefficient in $m/(m^3/s)^2$, f_p

No load flow in m^3/s, q_{nl}

Turbine gain, A_t

Guide vane opening, ΔG

Mechanical power output of the turbine, ΔP_{mi}, i = 1, 2, . . ., 6

Electrical power alteration provided to the electrical net, ΔP_{ei}, i = 1, 2, . . ., 6

Length of penstocks in m, l

Water time constant in seconds, T_w [3, 22]

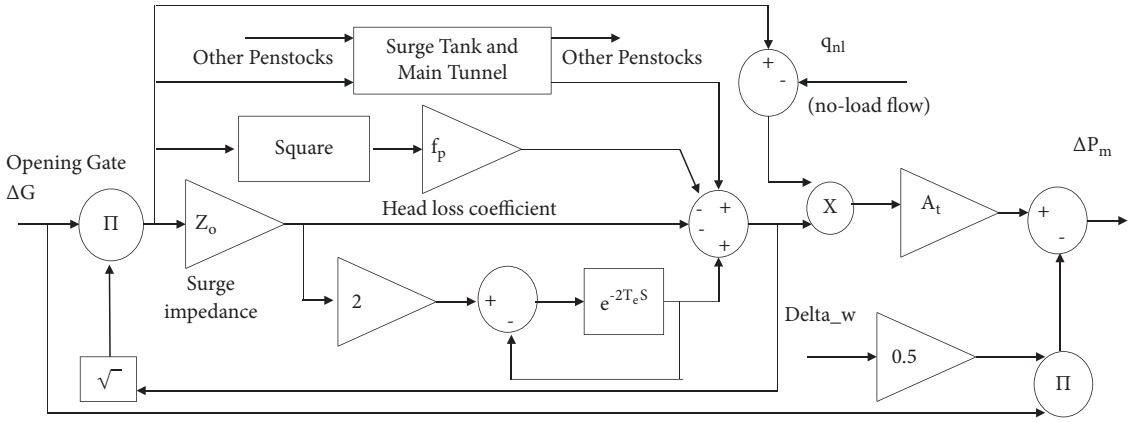

Figure 3: Hydraulic subsystem of the power plant.

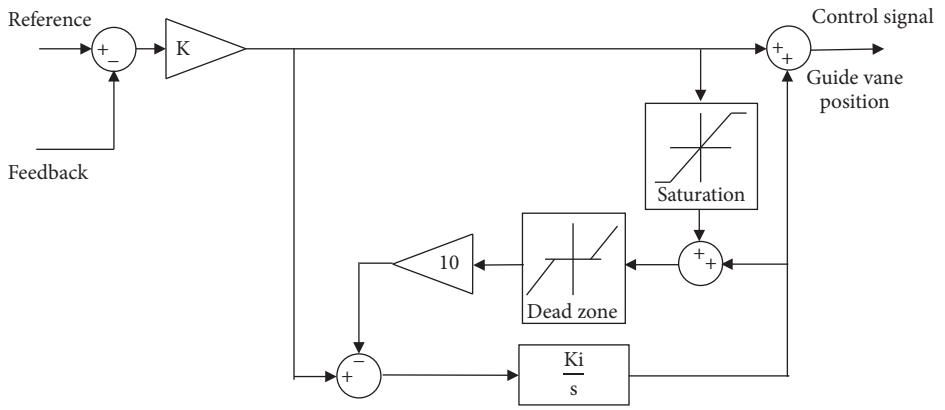

Figure 4: General scheme of PI antiwindup.

Wave travel time in seconds, T_e (3) [1, 3]

Velocity of sound in water in m/s, ν

$$Z_o = \frac{T_w}{T_e} \tag{2}$$

$$T_e = \frac{l}{\nu} \tag{3}$$

It is considered, for practical purposes, that the factors A_t, f_p, and q_{nl} are identical to simulate this system. Because the power plant has large penstocks, the water columns were modeled assuming elastic behavior [4]. The coupling effect is also modeled by including the main tunnel, which is represented as a penstock.

In Figures 2 and 3, the mechanical power ΔP_m is the input to the turbine-generator which is modeled for the turbine/generator subsystem, assuming a steady state by the "swing" equations [22] and

$$\Delta P_m - \Delta P_e = 2Hs\Delta\omega \tag{4}$$

where

ΔP_e is the alteration in electrical power contributed to the grid

H is the inertia constant of the electrical subsystem

$\Delta\omega$ is the alteration of the rotor's angular velocity

Finally, a first-order filter is used for noise reduction, indicated as noise filters subsystem in Figure 2, which has the transfer function:

$$\frac{\Delta P_{es}(s)}{\Delta P_e(s)} = \frac{1}{s+1} \tag{5}$$

3. Classical and Fractional PID

To regulate hydropower stations, classical controllers have been used for many years. Linear transfer functions are normally the basis to tune up these controllers. Nonetheless, as was stated before, hydropower plants are highly nonlinear, time variant, and multivariable. Therefore, it is difficult to have a good performance with a classical linear controller. As these controllers are, normally, the actual governors for many hydropower stations, it is important to conduct studies for improving the classical governor performance.

The performance of classical controllers depends strongly on their fixed value parameters. Generally, the main purpose of tuning is to have a suitable equilibrium among sensitivity, control effort, and fast response [23].

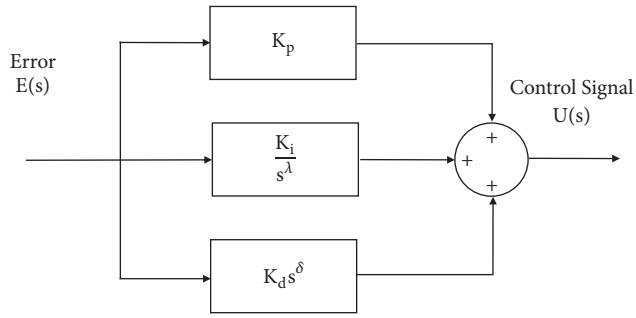

Figure 5: $PI^\lambda D^\delta$ controller (parallel general structure).

3.1. PI Antiwindup. A PI cautiously adjusted can offer suitable response although all processes are subjected to constraints. When constraints are activated, the performance of controllers can be significantly deteriorated. When the output of a system is saturated, making the error constant, an integral windup occurs. Because of a physical system, compared with an ideal one, it is physically impossible to reach the output in these conditions. This typically occurs when the output of the controller can no longer affect the controlled variable. To return the plant to stability, the control signal has to be of the contrary sign for a prolonged period, producing a longer settling time and a large overshoot [24–26].

A PI with antiwindup structure is showed in Figure 4. The PI controller contains an interior feedback track. To reduce the integrator input an internal saturation is employed. A value of 0.95 p.u. is usually employed for the saturation limit and the dead zone, both values selected manually. As was stated before, the hydropower model is in per-unit (p.u.) form, normalized to 300MW and 50Hz.

3.2. Fractional PID. The fractional order $PI^\lambda D^\delta$ (FOCPID controller) was first proposed by Podlubny [8, 9]. Figure 5 shows the internal structure of the fractional order controller [26]. In this controller, the λ-order integrator and the δ-order differentiator operators are real. The transfer function of such controller is represented by

$$C(s) = \frac{U(s)}{E(s)} = K_p + K_i s^{-\lambda} + K_d s^{\delta} \quad (6)$$

where (λ,$\delta > 0$)

K_p is the proportional constant

K_i is the integration constant

K_d is the differentiation constant

In discrete time the controller has the form:

$$C(z) = \frac{U(z)}{E(z)} = K_p + \frac{K_i}{(\omega(z^{-1}))^\lambda} + K_d\left(\omega\left(z^{-1}\right)\right)^\delta \quad (7)$$

In both (6) and (7) taking λ =1 and δ =1, a classical PID controller is obtained. If λ =0 and K_i =0, a PD^δ controller is found [7, 27].

4. Gain-Scheduled Antiwindup PID with Integral and Derivative of Fractional Order

Gain scheduling is a common method to control nonlinear systems since it is simple and employs linear design methods [29, 30]. Conventionally, gain-scheduled controllers are designed by carrying out a first linearization of the system to be regulated at certain scheduling operational points. Next, for each of these operational points, linear controllers are designed; each one is valid "only" near to that operational point. Then the regulator parameters are calculated at every operational point selected [31].

Figure 6 shows the general structure of the antiwindup fractional order PID controller with gain scheduling. As can be seen, the parameters K_p, K_i, and K_d can be adjusted depending on an external algorithm. Various algorithms have been published to tune up FOPID [32–35]. For this work a compromise between fast response and short overshoot was pursued, according to an Integral of Time Absolut Error (ITAE) index which was used to adjust the control parameters. The hydraulic head (h) was the station parameter used to retune the controller; therefore a different set of parameters was selected depending on the value of h. To reduce the ITAE index was the principal condition taking into account selecting those parameters. The method is based on the one described by Awouda and Mamat [36].

In some applications, it has been shown that calculating the control signal with the derivative of the output rather than the derivative of the error could help to improve the performance of the system. This structure, called Pseudo-Derivative Feedback (PDF) controller, provides all the control aspects of a PID, excluding the system zeros that are naturally introduced by this controller [37]. Figure 7 shows a diagram with the general structure of a fractional order controller with gain scheduling.

5. Evaluation of the Antiwindup PID with Fractional Order

The function of a hydropower system in frequency control mode is to deliver opportune and correct supply of its contribution objective to the total power to the net. The concrete form of the demanded power is associated with net frequency deviation; nevertheless it can be indicated as

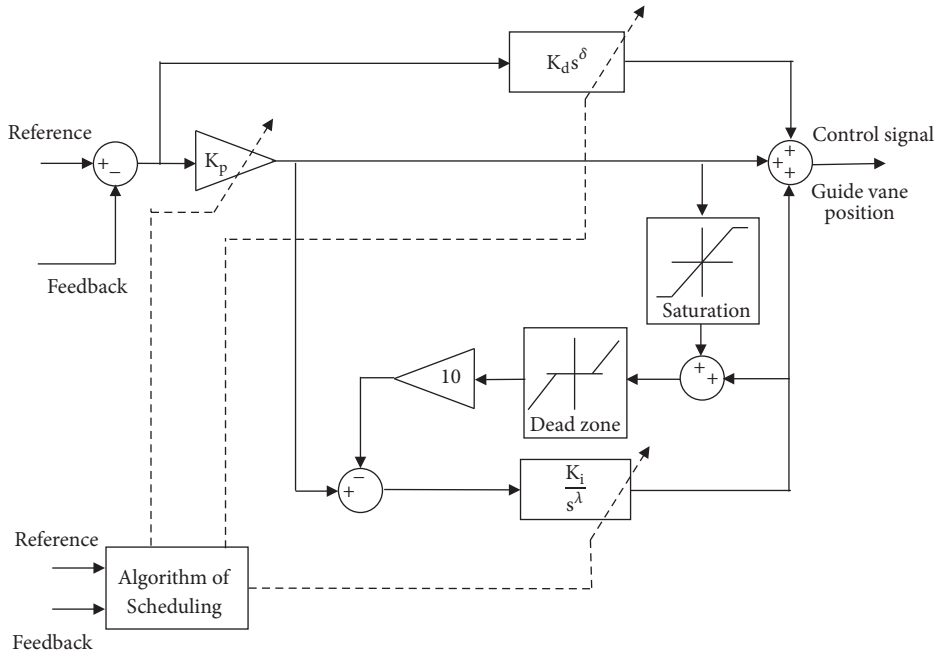

Figure 6: General structure of the antiwindup $PI^\lambda D^\delta$ gain scheduling controller.

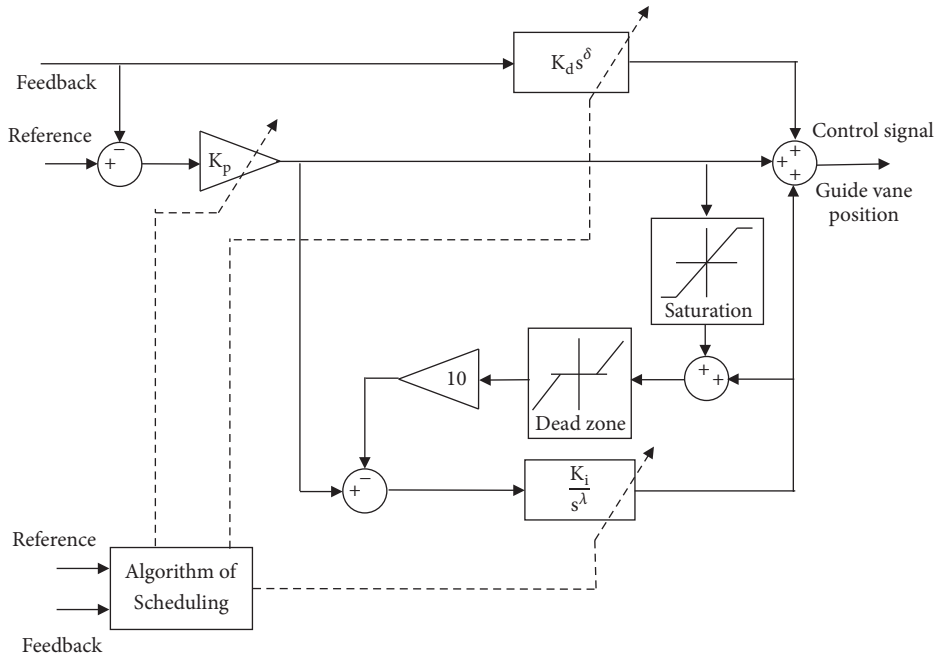

Figure 7: General structure of the antiwindup FO-PDF gain scheduling controller.

a relation of these input signals: step, ramp, and random [28, 38].

In this work some specifications are used to evaluate the hydroelectric station performance, which were proposed by Jones et al. [28]; those specifications represent an equilibrium between an important enhancement in speed and accuracy of response but are not so stressful that they result in impractical control activity and tunnel pressures.

The step response specification for one unit in operation is showed in Figure 8 [28]. Test P_1, *primary response* is usually the most significant criterion, which measures the time to accomplish a minimum 90% of the required step power change. Other important parameters are the overshoot (P_2) and the initial negative excursion (undershoot, P_6).

The Gain Scheduling Pseudo-Derivative Feedback Fractional Order with Antiwindup method (GS-PDF-AWU-FO)

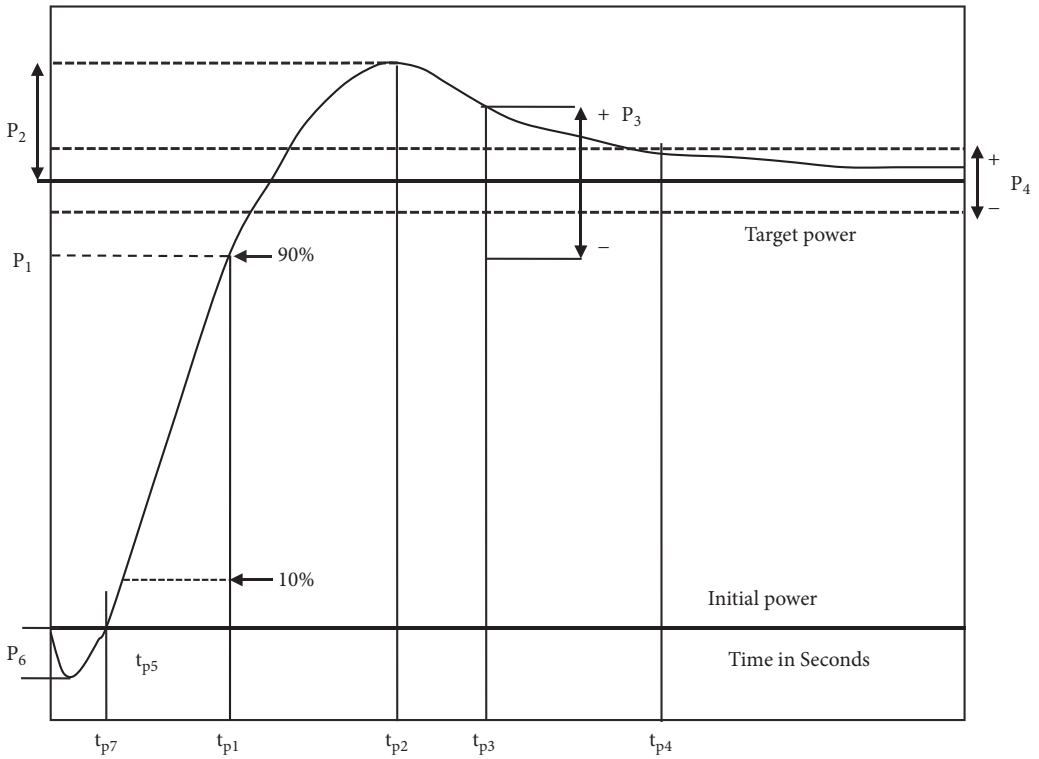

Figure 8: Specifications for a response to a step change in demanded power [1, 28].

was compared with an antiwindup PID controller (PID-AWU) with fix parameters (compromise to six operational units). Several simulations were run to assist the response of the two controllers. To evaluate the controllers an integral of time-weighted absolute error (ITAE) index was used. Both controllers were tuned for six operational units. However, the GS-PDF-AWU-FO has a different set of parameters depending on the value of the hydraulic head.

Adjusting a PID controller involves selecting the correct parameters that admit the controller to accomplish a required output specification. Mansoor [2] has presented a study with different sets of control parameters for Dinorwig's turbines in addition to the classical controller. The PI control with this set of parameters has a function that is a balance between one and six operational units. Hence, to optimize the functioning of the power system diverse groups of control constants were selected for different operational conditions, the extreme cases.

The PID-AWU parameter values were chosen as K = 0.16, K_i = 0.667, and K_d = 0 (working really as a PI controller), with a Rate Limit of 0.2 p.u. (Figure 3), in search of the best response when all units are in operation. The GS-PDF-AWU-FO was tuned for h=1 with λ= 0.95, δ= 0.6, K_p = 0.14, T_i = 0.85, and T_d = 0.025. For h=0.9 only two parameters were retuned: K_p = 0.16 and Ti=0.75 (Figure 7).

Figure 9 shows the reference values of the simulation; those values were selected because they represent "normal" changes when the frequency control mode is active. These references are also consistent with the ones reported by Munoz-Hernandez et al. [1], Mansoor [2], and Munoz-Hernandez [3]. The simulation begins with steps of 0.8 p.u. tested for the six units at time t = 0 for unit 1 and 0.5 for units 2-6. Formerly a 0.05 p.u. step is tested for unit 1 at t=100 s. Unit 2 was lifted to 0.8 p.u. and after that a step at 0.05 p.u. was tested only for unit 2 at t=500 s. At 600 s all units were fixed to 0.8 p.u. After that a 0.05 p.u. step was tested for all units at t=700 s. At t = 800 the value of the h is changed from 1 to 0.9 p.u. With this new value for h a 0.05 p.u. step was introduced to unit 1 at t = 900 s. Then unit 1 is getting back to 0.8 p.u. and then a step of 0.05 is applied at t= 1100 s to all units. Finally, at t=1200 s the unit 1 is connected in frequency control model using a model of the British Grid [1, 39].

Following the changes at the references specified before (Figure 9), the response produced by the Gain Scheduling Pseudo-Derivative Feedback Fractional Order with Anti-windup method (GS-PDF-AWU-FO) is compared with an antiwindup PID controller (PID-AWU). The results for one unit and six operational units, with h=1, are shown in Figures 10 and 11, respectively. In both cases the output under the GS-PDF-AWU-FO is faster than the one obtained under PID-AWU, although for six operational units the GS-PDF-AWU-FO produces an overshoot of less than 0.5%. As can be seen from Figure 10, one operational unit and h=1, the primary response of the system under the PID is higher (15.79 seconds) than the one obtained under the GS-PDF-FO (13.57 seconds). The result is similar to the system with six operational units and h=1 (Figure 11); in this case the primary response under the PID is 12.37 seconds and under the GS-PDF-AWU-FO is 10 seconds.

The cross-coupling responses for GS-PDF-AWU-FO and the modified PID-AWU are shown in Figure 12, where it is seen that although the GS-PDF-AWU-FO produces

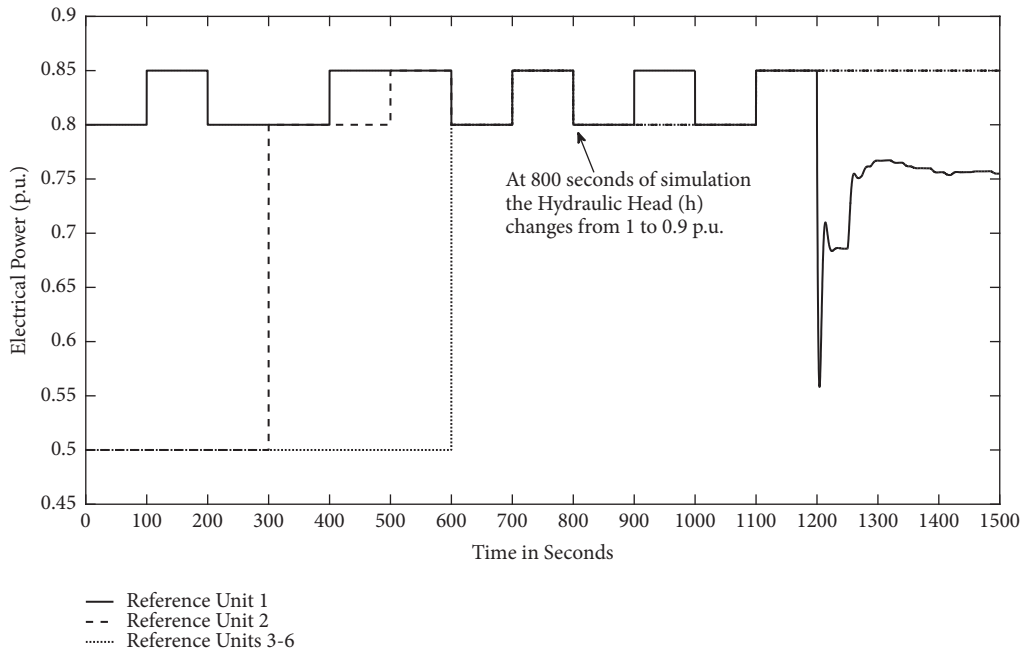

Figure 9: References used to simulate the hydropower plant.

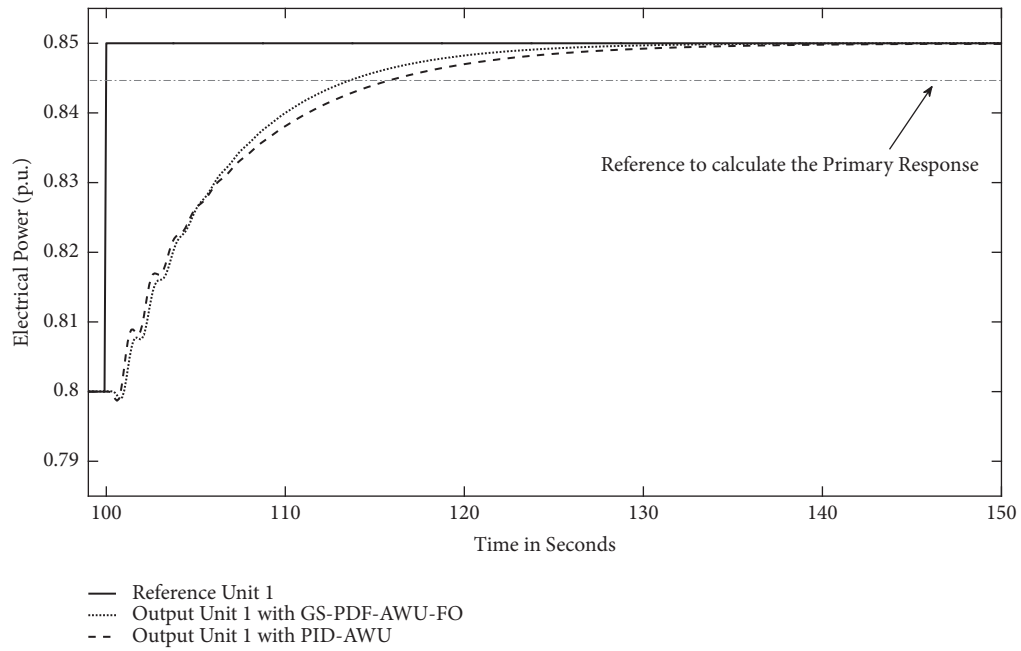

Figure 10: Step responses of PID and GS-PDF-FO, both with antiwindup, one operational unit, and h=1.

a bigger overshoot, it improves the nonminimum phase undershoot.

Following the sequence of the references indicated before (Figure 9), the outputs obtained by the GS-PDF-AWU-FO are compared with the ones from a PID -AWU. The results for one unit and six operational units, with h=0.9, are shown in Figures 13 and 14, respectively. As with h=1, in both cases the output under the GS-PDF-AWU-FO is faster than the one obtained under PID-AWU. Also for six operational units the GS-PDF-AWU-FO produces an overshoot, again less than 0.4%. As can be seen from Figure 13, one operational unit and h=1, the primary response of the system under the PID is higher (19.03 seconds) than the one obtained under the GS-PDF-FO (16.46 seconds). The result is similar to the system with six operational units and h=1 (Figure 13); in this case the primary response under the PID is 14.74 seconds and under the GS-PDF-AWU-FO is 12.37 seconds.

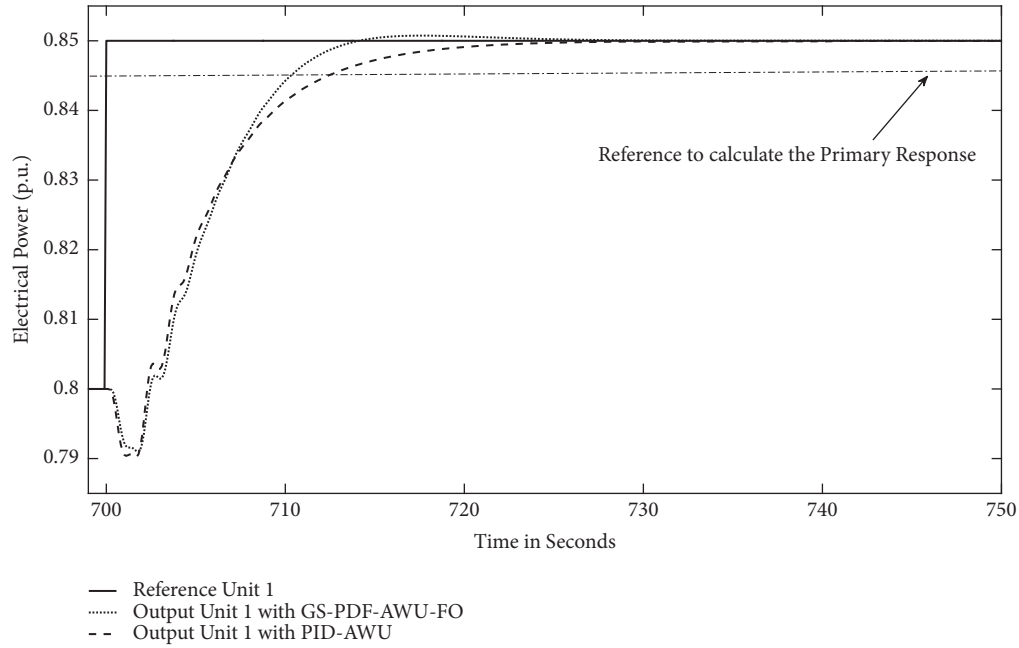

Figure 11: Step responses of PID and GS-PDF-FO, both with antiwindup, six operational units, and h=1.

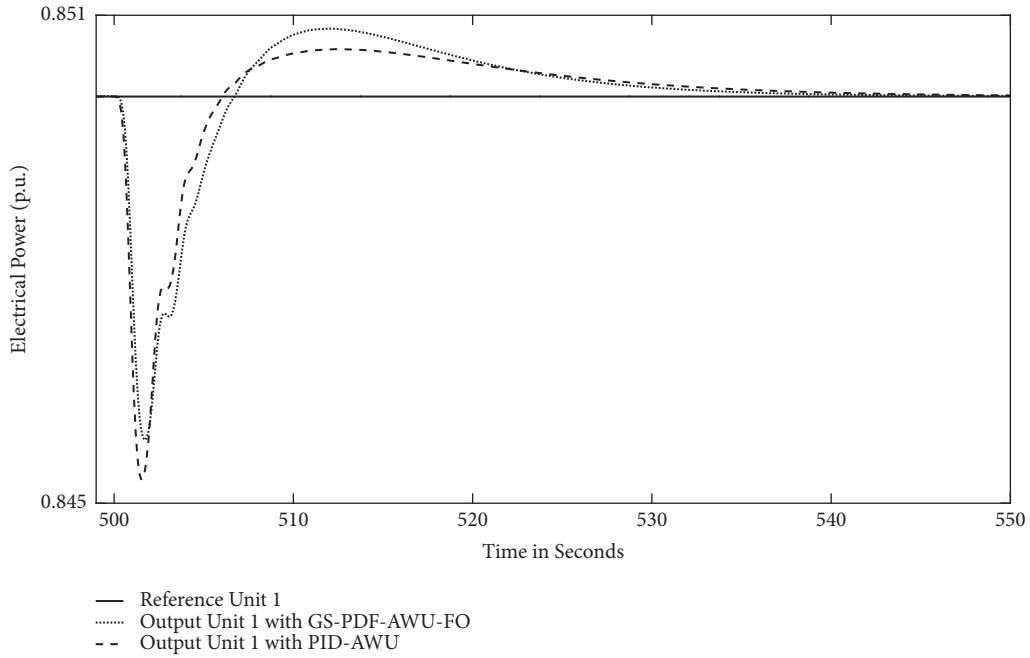

Figure 12: Cross-coupling reaction of unit 1 when unit 2 is under a step of 0.05 with 0.85 of operational point while h=1.

For both groups of simulation, one and six operational units, with different values of the hydraulic head (h=1 and h=0.9), ITAE indexes were calculated. For all cases, this index is lower when the system is controlled by the GS-PDF-AWU-FO rather than PID-AWU (Figure 15).

It is common that hydropower governors include a derivative term in the feedforward track from the reference for frequency control [22]. This produces a rapid change in power in response to rapidly changing frequency. A critical component of power systems is the model for the power network, because it is fundamental to assist or even to predict how the frequency will respond to power modifications. Evidently, the dynamic characteristics of a power network depend on its precise configuration at any instant. Nevertheless, studies have shown that a severe injection of power onto a network will often cause the frequency to increase, reaching a peak after some tens of seconds, after which it will fall back slightly.

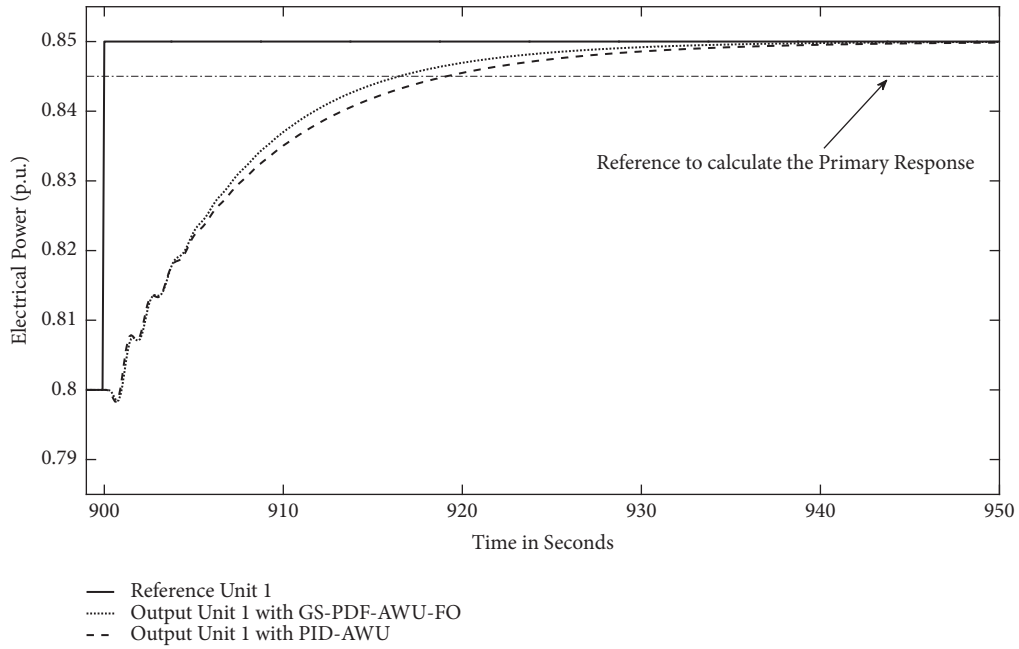

Figure 13: PID and GS-PDF-FO step responses, both with antiwindup, one operational unit, and h=0.9.

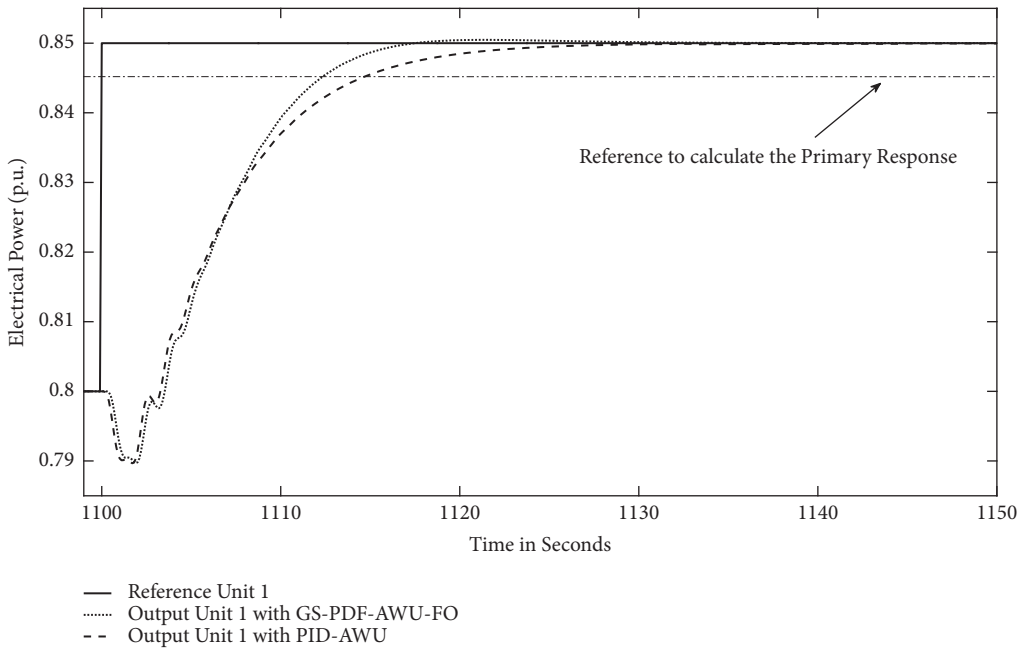

Figure 14: PID and GS-PDF-FO step responses, both with antiwindup, six operational units, and h=0.9.

In order to assist the system under frequency control it is essential to simulate the connection to the grid. For this purpose, a second-order transfer function is used in this work (8). This equation expresses fluctuations in grid frequency to load imbalance. The first time constant related to the addition of all the inertias of the rotating machines and the second time constant related to all governing mechanisms connected to the electrical net.

$$\Delta\omega_G = K\omega_n^2 T_R \left(\frac{s + 1/T_R}{s^2 + 2\zeta\omega_n s + \omega_n^2} \right) (\Delta P_e - \Delta P_L) \quad (8)$$

In this equation [1, 40]:

K is the grid "stiffness"

T_R is the time constant of the regulatory mechanisms

ω_n is the grid natural frequency

ζ is the grid damping factor

The grid works as a collector whose accumulated energy is proportional to the synchronous frequency of all the rotational equipment connected [22]. The total "amount"

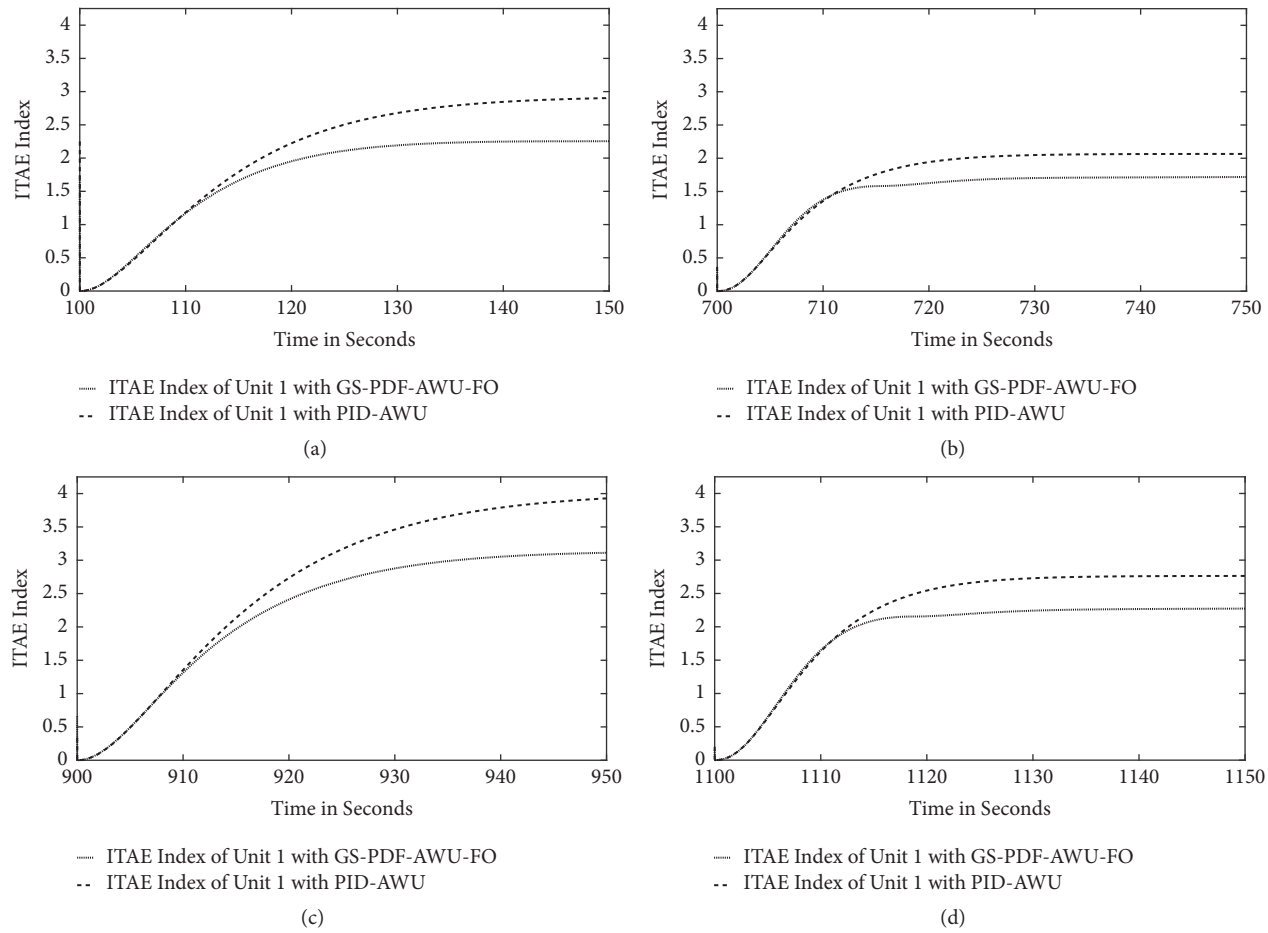

Figure 15: ITAE indexes. (a) One operational unit, h=1. (b) Six operational units, h=1. (c) One operational unit, h=0.9. (d) Six operational units, h=0.9.

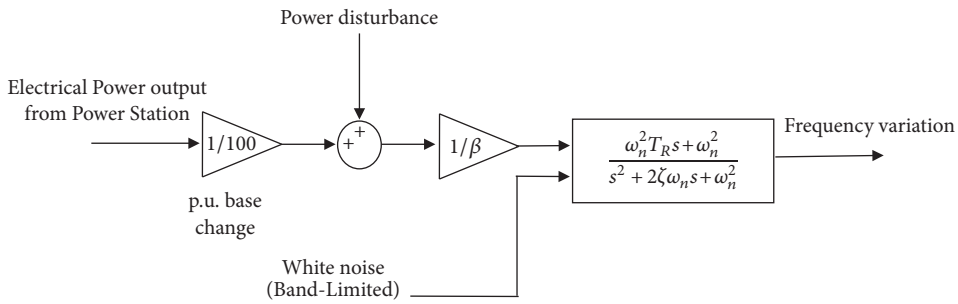

Figure 16: Grid model.

of the grid load (which ranges from 30 to 55GW in Great Britain) produces variations in the parameters K, T_R, ω_n, and ζ. Whereas ΔP_e is known, ΔP_L is the sum of a vast numbers of time-varying contributions, so ΔP_L is included in the model as an additive, random disturbance [1, 40].

In Figure 16 the net model, employed in this work, is showed [1]. This grid model simulates frequency variation. To introduce weak rapid variations a 0.003 p.u. white noise with limited band is included, as a disturbance element, in the net model. On the other hand, to introduce strong variations a high disturbance is included, using a step (in this case, 0.014 p.u. at t = 1250 s of simulation). The values of the parameters for the second-order model were $K = 0.089$, $T_R = 8$, $\omega_n = 0.37$, and $\zeta = 0.54$ [40]. The values of the second-order model and the disturbance elements are comparable with the ones reported by Munoz-Hernandez et al. [1, 30], Mansoor [2], and Jones [39].

A comparison of the responses produced by the hydropower station under PID-AWU and GS-PDF-AWU-FO controllers, with unit 1 in frequency variation and units 2-6 with a fix operational point at 0.85 p.u., was performed

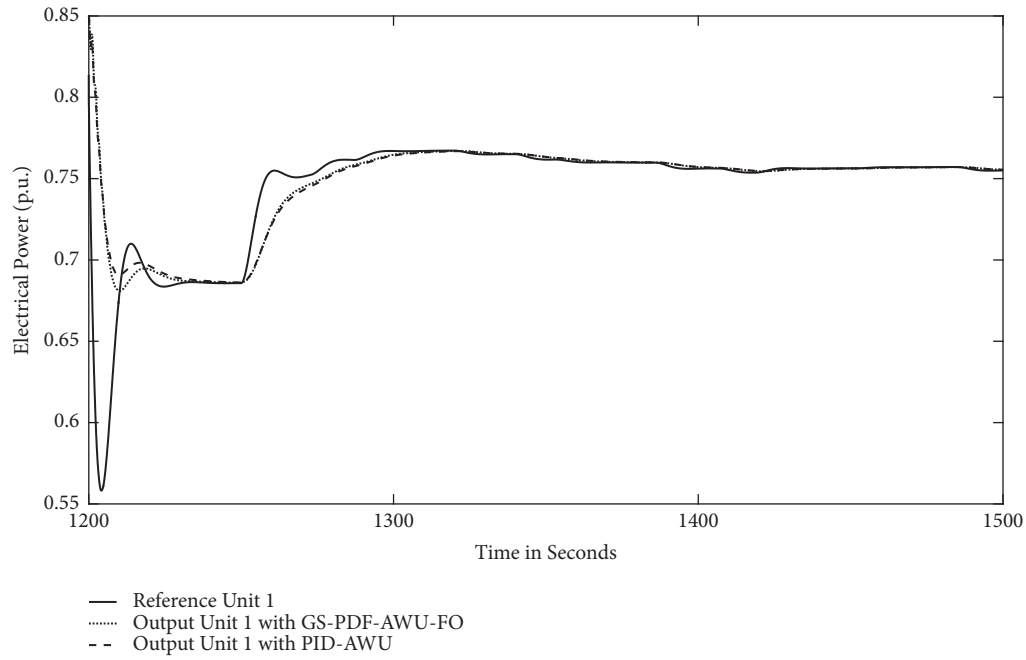

Figure 17: Evaluation of the responses produced by PID and GS-PDF-FO (both with antiwindup) with unit 1 in frequency variation (connected to the grid) and units 2-6 with 0.85 p.u. of fix operational point, h=0.9 p.u.

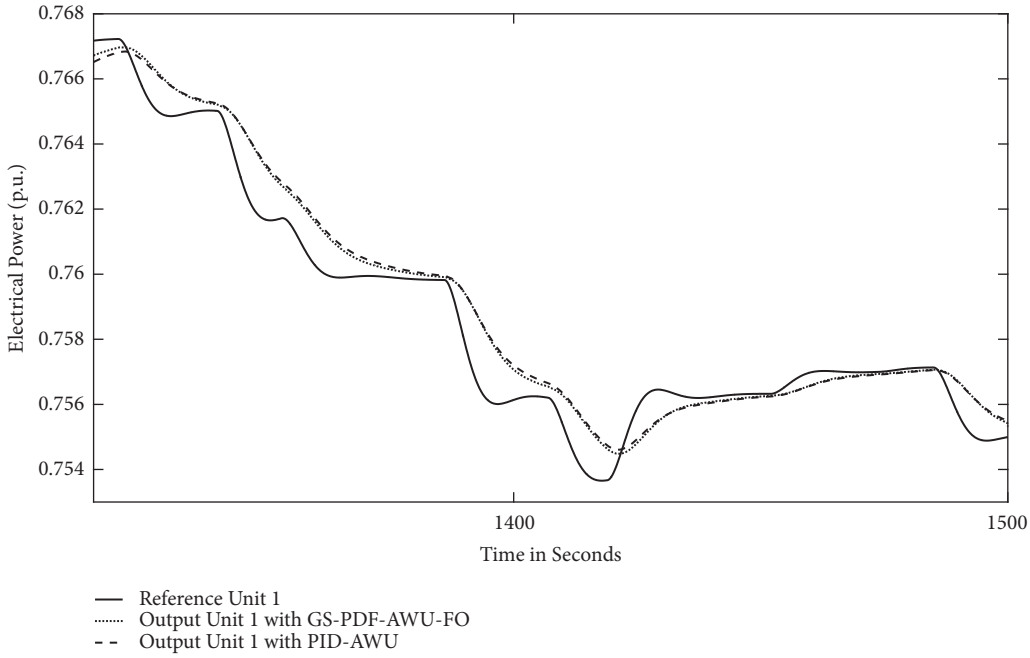

Figure 18: Evaluation of the responses produced by PID and GS-PDF-FO (both with antiwindup) with unit 1 in frequency variation (connected to the grid) and units 2-6 with 0.85 p.u. of fix operational point, h=0.9 p.u. (zoom).

using a hydraulic head equal to 0.9 p.u. (in Figure 9 with references shown). The reference value to units 2-6 was chosen close to the maximum power that is 0.95 [3]. As can be seen from Figures 17 and 18 both controllers produce responses that follow the input closely. However, the ITAE indexes, showed at Figure 19, indicate a better performance of the GS-PDF-AWU-FO.

The last analysis was developed to evaluate the performance of the GS-AWU-PDF-FO controller (with antiwindup) using the ITAE index as the way to select the tuning parameters. However, to compare the performance of GS-AWU-PDF-FO controller looking to fulfill the restrictions proposed by Jones et al. [28] this controller was retuned. Figures 20 and 21 show the specifications for single

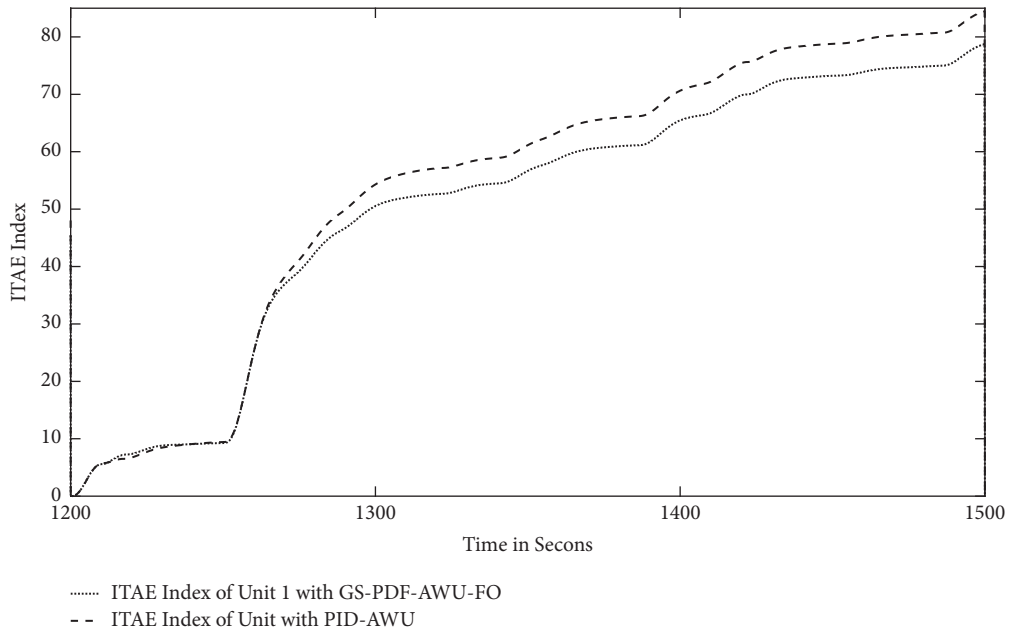

Figure 19: ITAE indexes of the comparison of the responses produced by PID and GS-PDF-FO (both with antiwindup) with unit 1 in frequency variation (connected to the grid) and units 2-6 with 0.85 p.u. of fix operational point, h=0.9 p.u.

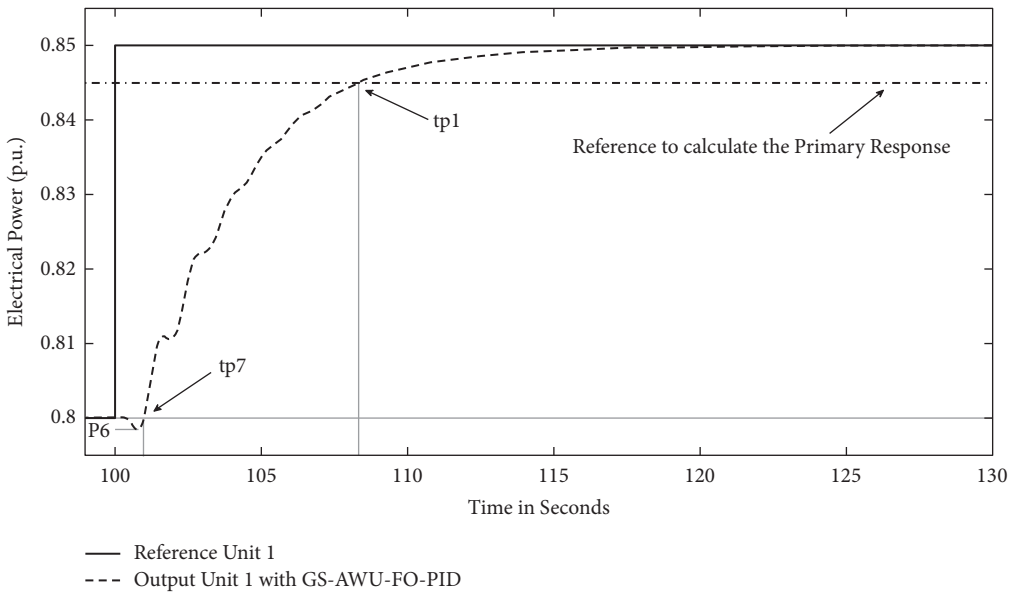

Figure 20: Step response of GS-PDF-FO with antiwindup, one operational unit, and h=1.

operational unit and also compares the parameters reported by [3] and the ones obtained using GS-AWU-PDF-FO as a controller. As can be seen in Table 1, all parameters are lower (or equal) than the ones from the standard when GS-AWU-PDF-FO is controlling the hydropower system.

6. Conclusions

The results from this study have shown that antiwindup GS-PDF-AWU with fractional order could be employed for a hydropower system to enhance its performance. When the nonlinear characteristic of the system is considered, as with GS-PDF-AWU, it is possible to improve the direct transient responses. The inclusion of adaptive characteristics, hydraulic head value, produces a rapid, well-damped response when the hydraulic head is at the maximum limit, without affecting the stability when this parameter has a lower value. Also the response of the hydropower plant under the GS-PDF-AWU-FO has a better performance when grid changes were evaluated. Finally, these results have showed that the anti-windup PDF controller with fractional order could produce

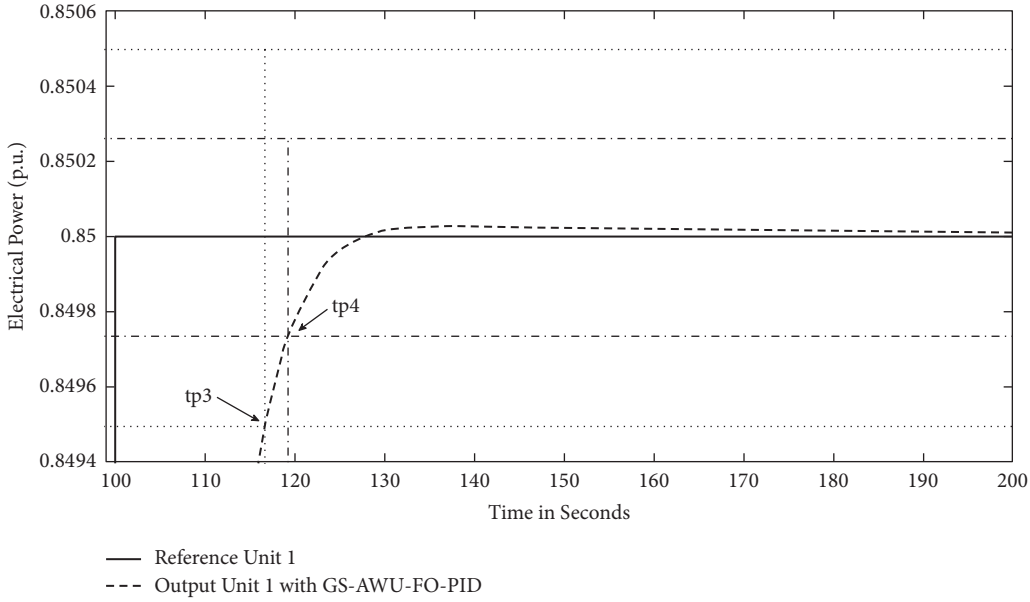

Figure 21: Step response of GS-PDF-FO with antiwindup, one operational unit, and h=1 (zoom).

Table 1: Specification of step response for advanced control design at Dinorwig [1, 3].

Test	Specification for single unit operation.	Single unit response with the governor reported in [3].	Single unit response with GS-AWU-PDF-FO.
P1	$P_1 \geq 90\%$ at $t_{p1} = 10s$	81% at 10s, 90% at 13.7 s	94.6 % at 10 s, 90% at 8.3 s
P2	$P_2 \leq 5\%$ and $t_{p2} \leq 20s$	No overshoot	No overshoot
P3	$t_{p3} = 25s$ for $P_3 \leq 1\%$	25.9 s	16.9 s
P4	$t_{p4} = 60s$ for $P_4 \leq 0.5\%$	29.2 s	19.3 s
P5	$t_{p5} = 8s$	12.1 s	7.64 s
P6	$P_6 = 2\%$	1.75%	2%
P7	$t_{p7} = 1.5s$	0.88 s	0.975 s

concrete advantages for hydroelectric systems operating in fast response.

Data Availability

The data used to support the findings of this study are available from the corresponding author upon request.

Additional Points

Highlights. (i) Nonlinear modeling of a hydropower station. (ii) Evaluation of the application of Fractional PID Controller to a hydroelectric station to increase the performance.

Conflicts of Interest

The authors declare that they have no conflicts of interest.

References

[1] G. A. Munoz-Hernandez, D. I. Jones, and S. P. Mansoor, *Modelling and Controlling Hydropower Plants*, Springer, London, UK, 2013.

[2] S. P Mansoor, *Thesis. Behaviour and Operation of Pumped Storage Hydro Plants [Ph.D. thesis]*, Bangor University, Gwynedd, UK, 2000.

[3] G. A. Munoz-Hernandez, *Application of Model Based Predictive Control to a Pumped Storage Hydroelectric Plant [Ph.D. thesis]*, Bangor University, Gwynedd, UK, 2005.

[4] IEEE Working Group, "Hydraulic turbine and turbine control models for system dynamic studies," *IEEE Transactions on Power Systems*, vol. 7, no. 1, pp. 167–179, 1992.

[5] L. Hannett, J. Feltes, B. Fardanesh, and W. Crean, "Modeling and control tuning of a hydro station with units sharing a common penstock section," *IEEE Transactions on Power Systems*, vol. 14, no. 4, pp. 1407–1414, 1999.

[6] M. Piovoso and J. Alpigini, "Visual tuning of controllers," *Computing and Control Engineering*, vol. 15, no. 3, pp. 34–39, 2004.

[7] C. A. Monje, Y. Chen, B. M. Vinagre, D. Xue, and V. Feliu, *Fractional Order Systems and Controls: Fundamentals*, J. Michael, Michael., and A. Johnson, Eds., Springer-Verlag, London, UK, 2010.

[8] L. Podlubny, Dorcak, and I. Kostial, "On Fractional Derivatives, Fractional-Order Dynamic Systems and PIlDu Controllers," in *Proceedings of the Conference on Decision and Control*, pp. 4985–4990, San Diego, Calif, USA, 1997.

[9] I. Podlubny, "Fractional-Order Systems and PILDu-Controllers," *IEEE Transactions on Automatic Control*, vol. 44, no. 1, pp. 208–214, 1999.

[10] B. Vinagre, I. Podlubny, L. Dorcak, and V. Feliu, "On fractional PID controllers: A frequency domain approach," in *Proceedings of the IFAC Digital Control: Past, Present and Future of PID Control*, pp. 51–56, Terrassa, Spain, 2000.

[11] M. Li and D. Xue, "Fractional order QFT controller for non-minimun phase hydro power plant," in *Proceedings of the Chinese Control and Decision Conference*, pp. 2796–2801, Taiyuan, China, May 2012.

[12] Z. Chen, X. Yuan, B. Ji, P. Wang, and H. Tian, "Design of a fractional order PID controller for hydraulic turbine regulating system using chaotic non-dominated sorting genetic algorithm II," *Energy Conversion and Management*, vol. 84, pp. 390–404, 2014.

[13] B. B. Xu, D. Y. Chen, H. Zhang, and F. F. Wang, "Modeling and stability analysis of a fractional-order Francis hydro-turbine governing system," *Chaos, Solitons & Fractals*, vol. 75, pp. 50–61, 2015.

[14] B. Wang, L. Yin, S. Wang, S. Miao, T. Du, and C. Zuo, "Finite Time Control for Fractional Order Nonlinear Hydroturbine Governing System via Frequency Distributed Model," *Advances in Mathematical Physics*, vol. 2016, Article ID 7345325, 9 pages, 2016.

[15] C. Li, N. Zhang, X. Lai, J. Zhou, and Y. Xu, "Design of a fractional-order PID controller for a pumped storage unit using a gravitational search algorithm based on the Cauchy and Gaussian mutation," *Information Sciences*, vol. 396, pp. 162–181, 2017.

[16] Y. Xu, J. Zhou, Y. Zhang, W. Fu, Y. Zheng, and X. Zhang, "Parameter Optimization of Robust Non-fragile Fractional Order PID Controller for Pump Turbine Governing System," in *Proceedings of the 2016 Sixth International Conference on Instrumentation & Measurement, Computer, Communication and Control (IMCCC)*, pp. 15–18, Harbin, China, July 2016.

[17] S. Li, Y. Yang, and Q. Xia, "Dynamic Safety Assessment in Nonlinear Hydropower Generation Systems," *Complexity*, vol. 2018, Article ID 5369253, 8 pages, 2018.

[18] H. Fang, X. Yuan, and P. Liu, "Active–disturbance–rejection–control and fractional order proportional integral derivative hybrid control for hydroturbine speed governor system," *Measurement and Control*, vol. 51, no. 5-6, pp. 192–201, 2018.

[19] S. P. Nangrani and S. S. Bhat, "Fractional order controller for controlling power system dynamic behavior," *Asian Journal of Control*, vol. 20, no. 1, pp. 403–414, 2018.

[20] Y. V. Hote and S. Jain, "PID controller design for load frequency control: Past, Present and future challenges," in *Proceedings of the 3rd IFAC Conference on Advances in Proportional- Integral-Derivative Control*, vol. 51, pp. 604–609, Ghent, Belgium, 2018.

[21] S. Mansoor, D. Jones, D. Bradley, F. Aris, and G. Jones, "Stability of a pump storage hydro-power station connected to a power system," in *Proceedings of the IEEE Power Engineering Society. 1999 Winter Meeting (Cat. No.99CH36233)*, pp. 646–650 vol.1, New York, NY, USA, Feburary 1999.

[22] P. Kundur, *Power System Stability and Control*, Mc Graw Hill, New York, NY, USA, 1994.

[23] J. Rossiter and J. Rossiter, *Model-Based Predictive Control*, CRC Press, Florida, Fl, USA, 2017.

[24] Y. Peng, D. Vrancic, and R. Hanus, "Anti-windup, bumpless, and conditioned transfer techniques for PID controllers," *IEEE Control Systems Magazine*, vol. 16, no. 4, pp. 48–57, 1996.

[25] C. Bohn and D. P. Atherton, "An analysis package comparing PID anti-windup strategies," *IEEE Control Systems Magazine*, vol. 15, no. 2, pp. 34–40, 1995.

[26] G. C. Goodwin, S. F. Graebe, and M. E. Salgado, *Control system design*, Prentice Hall, 2001.

[27] I. Petráš, *Fractional-Order Nonlinear Systems: Modeling, Analysis and Simulation*, A. C. J. Luo and N. H. Ibragimov, Eds., Springer, Beijing, China, 1st edition, 2011.

[28] D. Jones, S. Mansoor, F. Aris, G. Jones, D. Bradley, and D. King, "A standard method for specifying the response of hydroelectric plant in frequency-control mode," *Electric Power Systems Research*, vol. 68, no. 1, pp. 19–32, 2004.

[29] G. Orelind, L. Wozniak, J. Medanic, and T. Whittemore, "Optimal PID gain schedule for hydrogenerators-design and application," *IEEE Transactions on Energy Conversion*, vol. 4, no. 3, pp. 300–307, 1989.

[30] G. A. Munoz-Hernandez, C. A. Gracios-Marin, D. I. Jones, S. P. Mansoor, J. F. Guerrero-Castellanos, and E. A. Portilla-Flores, "Evaluation of gain scheduled predictive control in a nonlinear MIMO model of a hydropower station," *International Journal of Electrical Power & Energy Systems*, vol. 66, pp. 125–132, 2015.

[31] K. J. Astrom and B. Wittenmark, *Adaptive Control*, Addison-Wesley, 1989.

[32] C. A. Monje, B. M. Vinagre, V. Feliu, and Y. Q. Chen, "On Auto-Tuning of Fractional Order PIlDu Controllers," in *Proceedings of the 2nd IFAB Workshop on Fractional Differentiation and its Applications*, pp. 34–39, Porto, Portugal, 2006.

[33] C. A. Monje, B. M. Vinagre, V. Feliu, and Y. Chen, "Tuning and auto-tuning of fractional order controllers for industry applications," *Control Engineering Practice*, vol. 16, no. 7, pp. 798–812, 2008.

[34] I. Petráš, "Tuning and implementation methods for fractional-order controllers," *Fractional Calculus and Applied Analysis*, vol. 15, no. 2, pp. 282–303, 2012.

[35] F. J. Castillo-Garcia, A. San Millan-Rodriguez, V. Feliu-Batlle, and L. Sanchez-Rodriguez, "Fractional-Order PI control of first order plants with guaranteed time specifications," *Journal of Applied Mathematics*, vol. 10, Article ID 197186, 10 pages, 2013.

[36] A. E. Awouda and R. Bin Mamat, "Refine PID tuning rule using ITAE criteria," in *Proceedings of the 2nd International Conference on Computer and Automation Engineering (ICCAE 2010)*, pp. 171–176, Singapore, Feburary 2010.

[37] R. M. Phelan, *Automatic Control Systems*, Cornell University Press, Ithaca, NY, USA, 1st edition, 1977.

[38] D. Jones, "Multivariable control analysis of a hydraulic turbine," *Transactions of the Institute of Measurement and Control*, vol. 21, no. 2-3, pp. 122–136, 2016.

[39] D. Jones, "Estimation of Power System Parameters," *IEEE Transactions on Power Systems*, vol. 19, no. 4, pp. 1980–1989, 2004.

[40] P. Anderson and M. Mirheydar, "A low-order system frequency response model," *IEEE Transactions on Power Systems*, vol. 5, no. 3, pp. 720–729.

Hindawi
Complexity
Volume 2018, Article ID 8797314, 12 pages
https://doi.org/10.1155/2018/8797314

Research Article

Dynamics Feature and Synchronization of a Robust Fractional-Order Chaotic System

Xuan-Bing Yang,[1,2] Yi-Gang He ,[1] and Chun-Lai Li [2]

[1]*School of Electrical Engineering and Automation, Hefei University of Technology, Hefei 230009, China*
[2]*School of Information Science and Engineering, Hunan Institute of Science and Technology, Yueyang 414006, China*

Correspondence should be addressed to Yi-Gang He; 18655136887@163.com and Chun-Lai Li; hnistlichl@163.com

Received 20 September 2018; Accepted 6 November 2018; Published 2 December 2018

Guest Editor: Viet-Thanh Pham

Exploring the dynamics feature of robust chaotic system is an attractive yet recent topic of interest. In this paper, we introduce a three-dimensional fractional-order chaotic system. The important finding by analysis is that the position of signal x_3 descends at the speed of $1/c$ as the parameter b increases, and the signal amplitude of x_1, x_2 can be controlled by the parameter m in terms of the power function with the index $-1/2$. What is more, the dynamics remains constant with the variation of parameters b and m. Consequently, this system can provide rich encoding keys for chaotic communication. By considering the properties of amplitude and position modulation, the partial projective synchronization and partial phase synchronization are realized with linear control scheme. The distribution map of optimal synchronization region in the control-parameter space is charted by defining the power consumption of controller. Numerical simulations are executed to confirm the theoretical analysis.

1. Introduction

Over the past few decades, the dynamics and property of chaotic system have been extensively studied from different points of views as an active topic [1–4]. The investigation of chaos has benefited the exploration of the complex behavior, intrinsic nonlinear structure of natural system, and the construction of chaotic system, as well as practical applications such as secure communications and signal detection [5–9]. Robust chaotic system can usually provide signal-amplitude modulation by controlling one or some of the parameters in the dynamical equations yet keep the Lyapunov exponents and power spectral density invariable [10–14]. Therefore, it is a type of chaotic system with potential applications in synchronization, signal processing, image encryption, chaotic radar, and chaotic communication [10, 12]. However, according to what we know, there is little information and variety about such system reported in the present literatures.

Although fractional calculus has a history of more than 300 years, it was not really applied to physics, life sciences, and psychology until the last decade [15–18]. Fractional calculus can provide an excellent description of hereditary and memory properties in various materials and processes. The advantage of the fractional system is that it holds more degrees of freedom and that contains a "memory" in it. Therefore, it is of universal significance to study fractional dynamics and its applications [19–22]. Synchronization of integer-order chaotic system is investigated extensively and deeply, and many different types and methods have been presented since the landmark work by Pecora and Carroll [23–29]. However, due to the computational complexity of fractional systems, not all synchronization methods of the integer-order system are suitable for the fractional-order one [10]. In the existing synchronization types, projective synchronization can be interpreted as that the state trajectories of the drive and response systems synchronize to a constant proportion factor. This characteristic is usually used to extend binary digital communication to faster M-nary communication [30, 31]. Another synchronization type to be worth mentioning is phase synchronization, in which the controlled chaotic system adjusts the signal frequencies of dynamics to the rhythm of another chaotic system while the amplitudes go on varying in an irregular and uncorrelated fashion [32]. Phase synchronization has been observed in electrochemical oscillators [33], plasma discharge tubes [34], coupled HR neurons [35], fractional differential chaotic systems [36], etc.

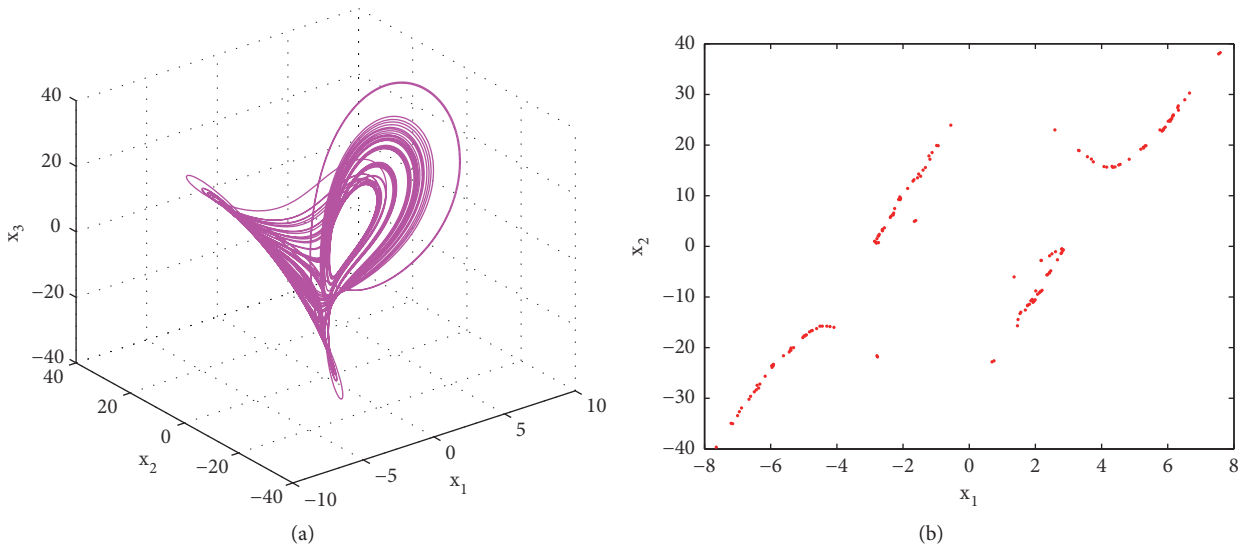

Figure 1: (a) 3D phase portrait; (b) Poincaré map with x_3=0.6.

In this paper, we attempt to explore some new dynamics properties of robust chaotic system by constructing a three-dimensional fractional chaotic system and to further consider the synchronization problem. Analysis of the derived system shows that the parameter m can control the signal amplitude of x_1, x_2 by the power function with the index −1/2 and that the parameter b can control the position of signal x_3 at the descent velocity of $1/c$. Then, by considering the vital property of amplitude and position modulation, a linear coupling scheme is designed to realize the partial projective synchronization and partial phase synchronization, respectively. Thus, the proportional factors in projective synchronization and the phase feature in phase synchronization are only determined by system parameters, which will improve the security of synchronous communication. The coupling-parameter range for synchronization is derived analytically and can be effectively narrowed down by appropriately selecting the auxiliary parameters. The distribution map of optimal synchronization region in the coupling-parameter space is further evaluated by defining the power consumption of controller. Numerical simulations are shown to further confirm the theoretical analysis.

2. Model of Fractional-Order Chaotic System

2.1. Model Description. The introduced fractional system is written in the form

$$\begin{aligned} D^q x_1 &= x_2 - a x_1 \\ D^q x_2 &= -b x_1 - c x_1 x_3 \\ D^q x_3 &= -n + m x_1 x_2 \end{aligned} \tag{1}$$

In system (1), $D^q x = d^q x/dt^q$ denotes the Caputo fractional derivative with the initial time $t = 0$ [37]. With the positive parameters a, b, c, n, and m, two equilibrium points of system (1) are obtained as

$$\begin{aligned} &E_+\left(\sqrt{\frac{n}{am}}, \sqrt{\frac{an}{m}}, -\frac{b}{c}\right), \\ &E_-\left(-\sqrt{\frac{n}{am}}, -\sqrt{\frac{an}{m}}, -\frac{b}{c}\right). \end{aligned} \tag{2}$$

The corresponding characteristic equation for any equilibrium point (x_{E1}, x_{E2}, x_{E3}) can be deduced as

$$\begin{aligned} \varphi(\lambda) = &-\lambda^3 - a\lambda^2 - \left(b + c x_{E3} + cm {x_{E1}}^2\right)\lambda \\ &- acm {x_{E1}}^2 - cm x_{E1} x_{E2} \end{aligned} \tag{3}$$

Specially, when selecting the parameter set $P = \{a = 2, b = 1, c = 1, n = 30, m = 1\}$, the corresponding equilibrium points and characteristic roots are

$$\begin{aligned} &E_+(3.873, 7.746, -1): \\ &\lambda_1 = -3.1912, \\ &\lambda_2 = 0.5956 + 4.2950i, \\ &\lambda_3 = 0.5956 - 4.2950i \\ &E_-(-3.873, -7.746, -1): \\ &\lambda_1 = -3.1912, \\ &\lambda_2 = 0.5956 + 4.2950i, \\ &\lambda_3 = 0.5956 - 4.2950i \end{aligned} \tag{4}$$

With the aid of stability theory of commensurate fractional system [38], the necessary condition for the chaos emergence is $q > (2/\pi)\text{atan}(|\text{Im}(\lambda*)|/\text{Re}(\lambda*)) = (2/\pi)\text{atan}(4.295/0.5956) = 0.9123$. For the parameter set P and the fractional order q=0.96, the 3D phase diagram and Poincaré map with dense dots are shown in Figure 1, revealing that system (1) is indeed chaotic.

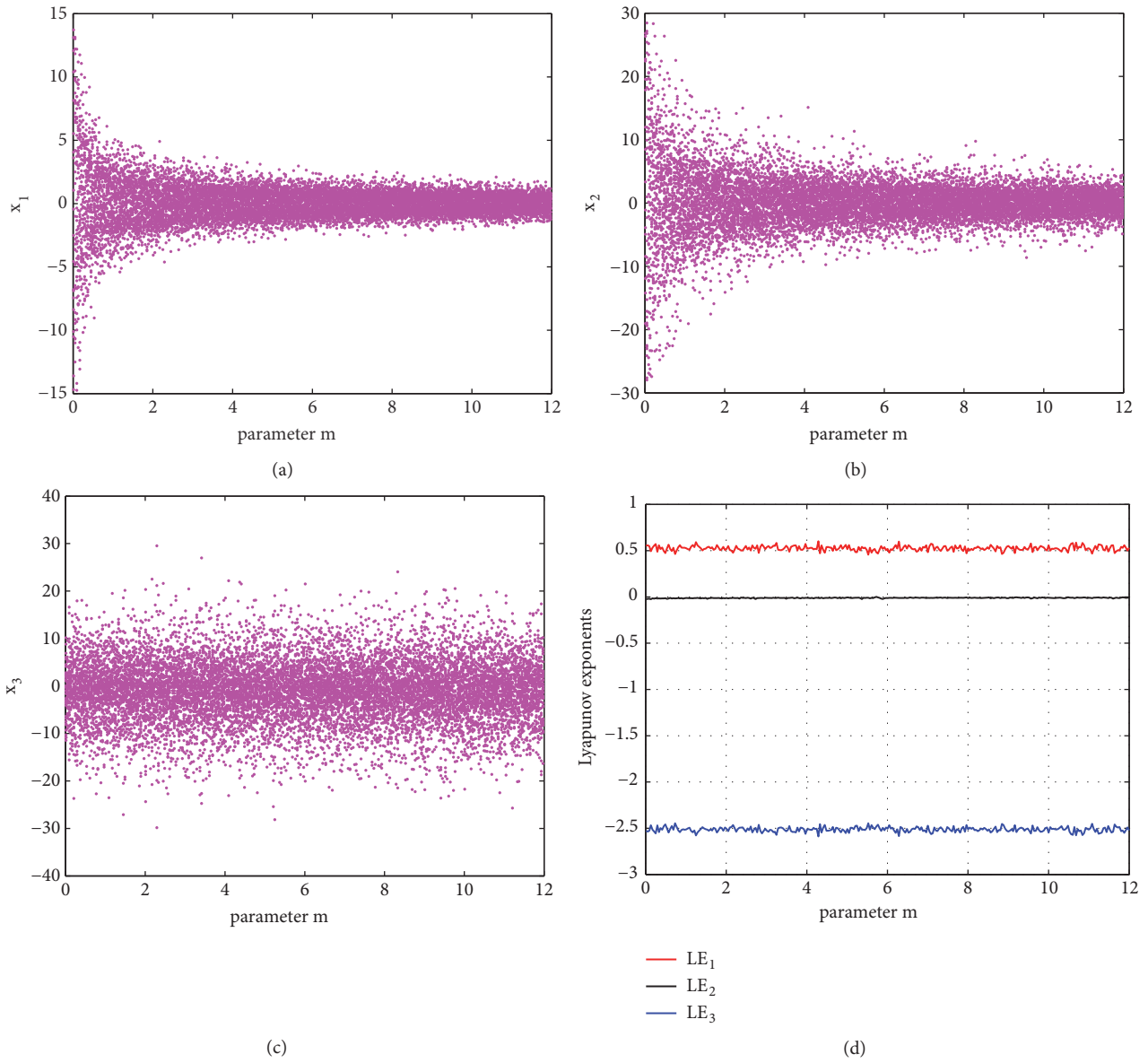

Figure 2: (a), (b), and (c) Bifurcation diagram and (d) Lyapunov exponent spectrum versus parameter m.

2.2. Dynamics Feature of Amplitude and Position Modulation. Our analysis found that the introduced system has the robust chaos of constant Lyapunov exponents with the variation of parameters m and b. More specifically, the parameter m can control some of the signal amplitude of state variables, and the parameter b can control the position of one of the variables with a certain speed. The revealed feature is rare in the current literature and we believe it will stimulate an exploration boom.

The linear transformation of $x_1 \longrightarrow x_1/\sqrt{m}$, $x_2 \longrightarrow x_2/\sqrt{m}$, and $x_3 \longrightarrow x_3$ is first considered to deduce system (1) to the normalized form about parameter m [12], as follows:

$$\begin{aligned} D^q x_1 &= x_2 - a x_1 \\ D^q x_2 &= -b x_1 - c x_1 x_3 \\ D^q x_3 &= -n + x_1 x_2 \end{aligned} \tag{5}$$

Therefore, the control parameter m can modulate the signal amplitude of variables x_1, x_2 according to $1/\sqrt{m}$, but the signal x_3 keeps its amplitude constant.

We substitute the nonzero equilibrium point E_+ or E_- into characteristic equation (3) to obtain

$$\varphi(\lambda) = -\lambda^3 - a\lambda^2 - \frac{cn}{a}\lambda - 2cn \tag{6}$$

Since (6) is irrespective to parameter m, the Lyapunov exponent spectrum remains invariable when m increases. The dynamics feature of amplitude modulation for system (1) is illustrated by bifurcation diagram and Lyapunov exponent spectrum, as shown in Figure 2. In the figure, the bifurcation diagrams are plotted with the local maxima of variables versus control parameter, and the spectrum of Lyapunov exponents is calculated by the wolf method.

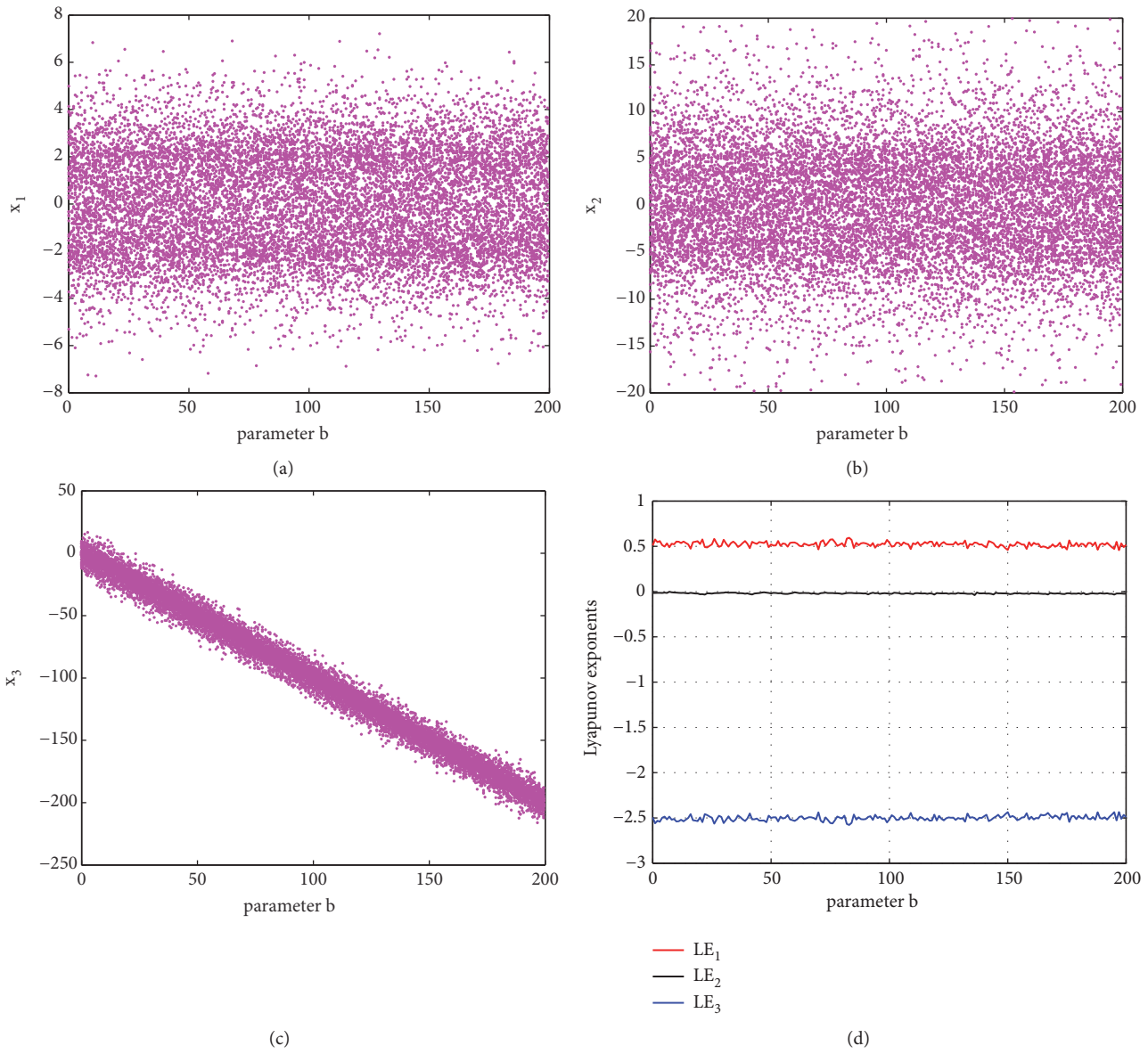

FIGURE 3: (a), (b), and (c) Bifurcation diagram and (d) Lyapunov exponent spectrum versus parameter b with the parameter set P except for b.

When introducing the linear transformation of $x_1 \longrightarrow x_1$, $x_2 \longrightarrow x_2$, and $x_3 \longrightarrow x_3 + k_p/c$, we then deduce system (1) to

$$\begin{aligned} D^q x_1 &= x_2 - a x_1 \\ D^q x_2 &= -\left(b + k_p\right) x_1 - c x_1 x_3 \\ D^q x_3 &= -n + m x_1 x_2 \end{aligned} \tag{7}$$

Therefore, the position of signal x_3 descends at the speed of $1/c$ as the parameter b increases, while the signals x_1, x_2 keep their amplitude invariable. Similarly, it is known that (6) is also irrespective to parameter b. Thus, the spectrum of Lyapunov exponent remains constant when b varies in field of real number. The phenomenon of position modulation for system (1) is described by bifurcation diagram and Lyapunov exponent spectrum, as shown in Figure 3. And the speed of position modulation influenced by parameter c is interpreted in Figure 4 by the bifurcation diagram and the maximal Lyapunov exponent spectrum, which signifies that a smaller c will give rise to a larger descent velocity.

3. Preliminaries for Synchronization of Fractional Chaotic System

In this section, some concepts and techniques are recalled for the stability analysis of fractional system.

Definition 1 (see [39]). When function $\alpha : R^+ \longrightarrow R^+$ is continuous, strictly increasing, and $\alpha(0) = 0$, it is said to be

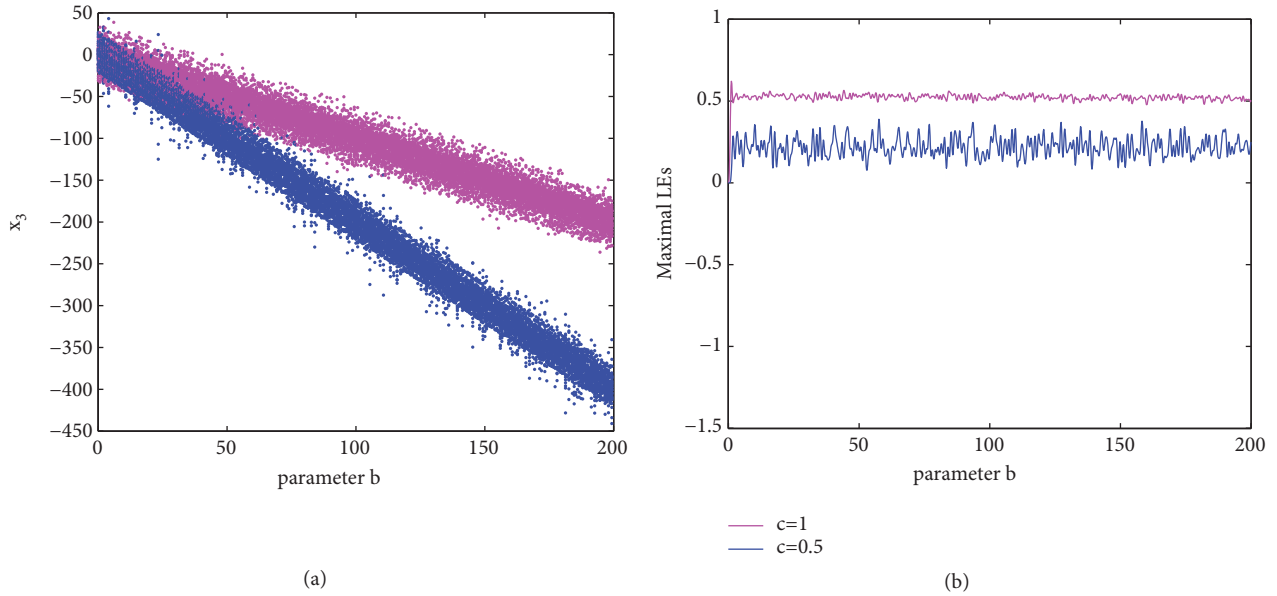

FIGURE 4: Influence of c on position modulation interpreted by (a) Bifurcation diagram and (b) Lyapunov exponent spectrum versus b with c=1 in magenta and c=0.5 in blue.

of class κ. If $\alpha \in \kappa$ and satisfies $\alpha(t) \longrightarrow \infty$ with $t \longrightarrow \infty$, it is said that α is of class κ_∞.

Lemma 2 (see [40, 41]). *Let $z(t) \in R$ be a continuous and derivable function. Then, for any time instant $t \geq 0$, it is held:*

$$0.5D^q z^2(t) \leq z(t) D^q z(t), \quad \forall q \in (0,1) \tag{8}$$

Lemma 3 (see [42, 43]). *Let $z(t) \in R^n$ be a real-valued continuous and derivable vector function. Then, for any time instant $t \geq 0$, one will always hold the following inequality:*

$$0.5D^q z^T(t) Pz(t) \leq z^T(t) PD^q z(t), \quad \forall q \in (0,1), \; P = \operatorname{diag}(p_1, p_2, \cdots, p_n) > 0 \tag{9}$$

Theorem 4 (Lyapunov stability and uniform stability of fractional system [42]). *Considering the following fractional-order system with the Caputo definition*

$$D^q z(t) = f(z,t), \quad q \in (0,1) \tag{10}$$

Let z=0 be an equilibrium point of system (10). If there exists a continuous Lyapunov function $V(z,t)$ and a scalar class-K function α_1 satisfying

$$V(z,t) \geq \alpha_1(\|z(t)\|) \tag{11}$$

and

$$D^q V(z,t) \leq 0, \quad q \in (0,1) \tag{12}$$

for any $z \neq 0$, then system (10) is Lyapunov stable at $z = 0$.

Furthermore, if there exists another scalar class-K function α_2 such that

$$V(z,t) \leq \alpha_2(\|z(t)\|) \tag{13}$$

then the origin of system (10) is said to be Lyapunov uniformly stable.

4. Partial Projective Synchronization of Fractional Chaotic System

4.1. Synchronization Scheme. The partial projective synchronization of the proposed system is studied here by taking the advantage of the property of amplitude modulation.

Let system (1) be as the drive system, and the response system is expressed as

$$\begin{aligned} D^q y_1 &= y_2 - a y_1 \\ D^q y_2 &= -b y_1 - c y_1 y_3 + u_2 \\ D^q y_3 &= -n + m_1 y_1 y_2 + u_3 \end{aligned} \tag{14}$$

where u_2 and u_3 are the controllers to be determined.

Assumption 5. The state variables of systems (1) and (14) are all bounded, and there exist three positive constants σ_1, σ_2, and σ_3, such that $|x_1|, |y_1| \leq \sigma_1$, $|x_2|, |y_2| \leq \sigma_2$, and $|x_3|, |y_3| \leq \sigma_3$.

The synchronization errors are set as $e_1 = y_1 - \sqrt{m/m_1}x_1$, $e_2 = y_2 - \sqrt{m/m_1}x_2$, and $e_3 = y_3 - x_3$, by taking the property of amplitude modulation considered. Then we obtain the error dynamical system

$$\begin{aligned} D^q e_1 &= e_2 - a e_1 \\ D^q e_2 &= -b e_1 - c y_1 e_3 - c e_1 x_3 + u_2 \\ D^q e_3 &= m_1 y_2 e_1 + m_1 \sqrt{\frac{m}{m_1}} x_1 e_2 + u_3 \end{aligned} \tag{15}$$

Theorem 6. *For the drive system (1) and response system (14), the controllers are designed as $u_2 = -k_2 e_2$ and $u_3 = -k_3 e_3$. If the coupling parameters k_2 and k_3 satisfy*

$$k_2 > \frac{\left(p_1 - bp_2 + cp_2\sigma_3\right)^2}{4ap_1p_2} \tag{16}$$

$$k_3 > \frac{m_1p_3\sigma_2\left(p_1 - bp_2 + cp_2\sigma_3\right)\left(m_1p_3\sqrt{m/m_1}\sigma_1 + cp_2\sigma_1\right) + k_2p_2\left(m_1p_3\sigma_2\right)^2 + ap_1\left(m_1p_3\sqrt{m/m_1}\sigma_1 + cp_2\sigma_1\right)^2}{p_3\left(4ap_1p_2k_2 - \left(p_1 - bp_2 + cp_2\sigma_3\right)^2\right)} \tag{17}$$

where p_1, p_2, and p_3 are positive auxiliary parameters to narrow down the values range of the coupling parameters, then the partial projective synchronization is realized with Lyapunov uniformly stability.

Proof. Let us propose the Lyapunov function $V(t) = 0.5(p_1{e_1}^2 + p_2{e_2}^2 + p_3{e_3}^2)$, which satisfies $\alpha_1(\|e\|) \le V(t) \le \alpha_2(\|e\|)$ for $\alpha_1(\|e\|) = \lambda_{\min}(P)\|e\|^2$, $\alpha_2(\|e\|) = \lambda_{\max}(P)\|e\|^2$, and $P = \mathrm{diag}(p_1, p_2, p_3)$. Taking q-order fractional derivative with respect to time t along the trajectories of (15), it yields

$$\begin{aligned}
D^qV(t) &= 0.5D^qp_1{e_1}^2 + 0.5D^qp_2{e_2}^2 + 0.5D^qp_3{e_3}^2 \\
&\le p_1e_1D^qe_1 + p_2e_2D^qe_2 + p_3e_3D^qe_3 \\
&= -ap_1{e_1}^2 - k_2p_2{e_2}^2 - k_3p_3{e_3}^2 \\
&\quad + \left(p_1 - bp_2 - cp_2x_3\right)e_1e_2 \\
&\quad + \left(m_1p_3\sqrt{\frac{m}{m_1}}x_1 - cp_2y_1\right)e_2e_3 \\
&\quad + m_1p_3y_2e_1e_3 \\
&\le -ap_1{e_1}^2 - k_2p_2{e_2}^2 - k_3p_3{e_3}^2 \\
&\quad + \left(p_1 - bp_2 + cp_2\sigma_3\right)|e_1||e_2| \\
&\quad + \left(m_1p_3\sqrt{\frac{m}{m_1}}\sigma_1 + cp_2\sigma_1\right)|e_2||e_3| \\
&\quad + m_1p_3\sigma_2|e_1||e_3| = |e|^T\,\Pi\,|e|
\end{aligned} \tag{18}$$

with

$$\begin{aligned}
|e| &= \left(|e_1|, |e_2|, |e_3|\right)^T, \\
\Pi &= \begin{pmatrix}
-ap_1 & \dfrac{p_1 - bp_2 + cp_2\sigma_3}{2} & \dfrac{m_1p_3\sigma_2}{2} \\
\dfrac{p_1 - bp_2 + cp_2\sigma_3}{2} & -p_2k_2 & \dfrac{m_1p_3\sqrt{m/m_1}\sigma_1 + cp_2\sigma_1}{2} \\
\dfrac{m_1p_3\sigma_2}{2} & \dfrac{m_1p_3\sqrt{m/m_1}\sigma_1 + cp_2\sigma_1}{2} & -p_3k_3
\end{pmatrix}.
\end{aligned} \tag{19}$$

It requires $\Pi \le 0$ for catering to $D^qV(t) \le 0$. Thus we have

$$\begin{aligned}
\Delta_1 &= -ap_1 \le 0 \\
\Delta_2 &= \det\begin{pmatrix}
-ap_1 & \dfrac{p_1 - bp_2 + cp_2\sigma_3}{2} \\
\dfrac{p_1 - bp_2 + cp_2\sigma_3}{2} & -p_2k_2
\end{pmatrix} \ge 0 \\
\Delta_3 &= \det\begin{pmatrix}
-ap_1 & \dfrac{p_1 - bp_2 + cp_2\sigma_3}{2} & \dfrac{m_1p_3\sigma_2}{2} \\
\dfrac{p_1 - bp_2 + cp_2\sigma_3}{2} & -p_2k_2 & \dfrac{m_1p_3\sqrt{m/m_1}\sigma_1 + cp_2\sigma_1}{2} \\
\dfrac{m_1p_3\sigma_2}{2} & \dfrac{m_1p_3\sqrt{m/m_1}\sigma_1 + cp_2\sigma_1}{2} & -p_3k_3
\end{pmatrix} \le 0
\end{aligned} \tag{20}$$

Therefore, we finally obtain inequalities (16) and (17). This completes the proof. □

4.2. Simulation Analysis. The appropriate selection of parameters p_1, p_2, and p_3 can effectively narrow down the values

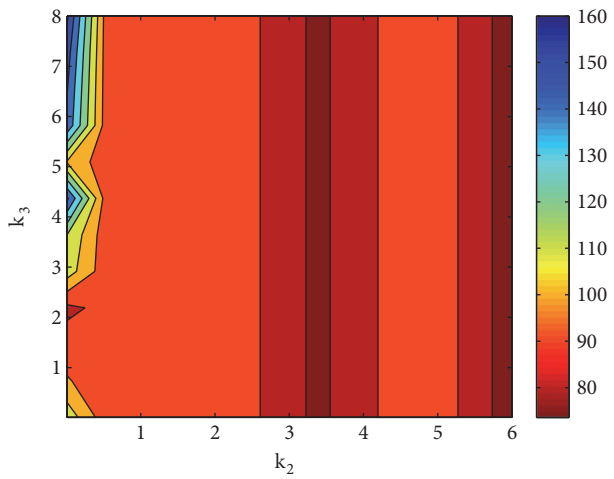

Figure 5: The distribution of the maximal power consumption of synchronous controller.

range of the coupling parameters, which is useful in actual synchronization process. However, it is a complicated relation between the coupling strengths (k_2, k_3) and (p_1, p_2, p_3). To optimize the synchronization scheme, we will evaluate the distribution map of optimal synchronization region in the coupling-parameter space, by coopting the idea introduced by Ma [44]. We first define the power consumption of the synchronous systems as $p_d = |x_1 x_3|$ and $p_r = |y_1 y_3|$, respectively. Thus, the power consumption for evaluating the synchronous controller can be defined as

$$p_{syn} = \left| |y_1 y_3| - \sqrt{\frac{m}{m_1}} |x_1 x_3| \right| \tag{21}$$

And for the sake of simplicity, we only consider the maximal power consumption of synchronous controller, as below

$$p_{msyn} = \max\left(p_{syn}\right) \tag{22}$$

Therefore, the optimal synchronization region will be the coupling-parameter region (k_2, k_3) with the minimum p_{msyn}.

In the numerical analysis, we choose the parameter values as a=2, b=1, c=1, n=30, m=1, m_1=16, and q=0.96 and set the initial values of drive system and the response system as $x(0)$=(-0.2, 0.1, 0.5), $y(0)$=(0.6, -0.5, -0.2). The distribution about the maximal power consumption of synchronous controller in the coupling-parameter space (k_2, k_3) is illustrated in Figure 5. It is known that the power consumption p_{msyn} is mainly determined by the coupling parameter k_2, and the optimal synchronization region appears alternately as k_2 increases. But to get shorter synchronous transition time, larger values of k_2 and k_3 are more appropriate.

The synchronization result with k_2=3.3, k_3=0.6 is depicted in Figure 6, which provides the proportional factors $\alpha_1 = \sqrt{m/m_1} = 0.25$, $\alpha_2 = \sqrt{m/m_1} = 0.25$, and $\alpha_3 = 1$. Figure 7 shows the synchronization result with the same proportional factors, when k_2=6, k_3=8. The comparative analysis shows that larger parameters k_2 and k_3 will lead to shorter synchronous transition time.

5. Partial Phase Synchronization of Fractional Chaotic System

5.1. Synchronization Scheme. Select the drive system (1) and the following response system:

$$\begin{aligned} D^q y_1 &= y_2 - a y_1 \\ D^q y_2 &= -b_1 y_1 - c y_1 y_3 + u_2 \\ D^q y_3 &= -n + m y_1 y_2 + u_3 \end{aligned} \tag{23}$$

And when considering the property of position modulation, the errors of partial phase synchronization are expressed as $e_1 = y_1 - x_1$, $e_2 = y_2 - x_2$, and $e_3 = y_3 - x_3 + (b_1 - b)/c$, then the error dynamical system is obtained as

$$\begin{aligned} D^q e_1 &= e_2 - a e_1 \\ D^q e_2 &= -b e_1 - c y_1 e_3 - c e_1 x_3 + u_2 \\ D^q e_3 &= m e_1 y_2 + m x_1 e_2 + u_3 \end{aligned} \tag{24}$$

Theorem 7. *For the drive system (1) and response system (23), the controllers are designed as $u_2 = -k_2 e_2$, $u_3 = -k_3 e_3$. If the coupling parameters k_2 and k_3 satisfy the condition*

$$k_2 > \frac{\left(p_1 - b p_2 + c p_2 \sigma_3\right)^2}{4 a p_1 p_2} \tag{25}$$

$$k_3 \geq \frac{m p_3 \sigma_2 \left(m p_3 \sigma_1 + c p_2 \sigma_1\right)\left(p_1 - b p_2 + c p_2 \sigma_3\right) + k_2 p_2 \left(m p_3 \sigma_2\right)^2 + a p_1 \left(m p_3 \sigma_1 + c p_2 \sigma_1\right)^2}{4 a p_1 p_2 p_3 k_2 - p_3 \left(p_1 - b p_2 + c p_2 \sigma_3\right)^2} \tag{26}$$

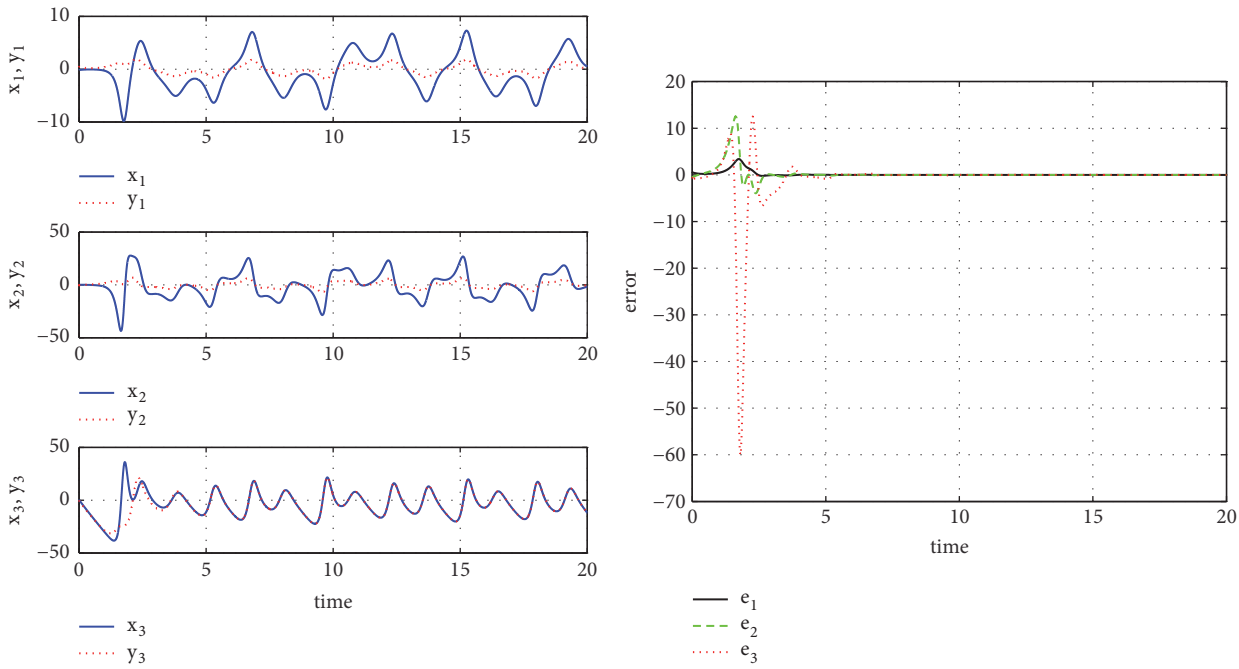

FIGURE 6: Partial projective synchronization with k_2=3.3; k_3=0.6: (a) time response; (b) synchronization error.

where p_1, p_2, and $p_3$are positive constants, then the partial phase synchronization is realized with Lyapunov uniformly stability.

Here we skip the proof process for brevity since it resembles the one of Theorem 6.

5.2. Simulation Analysis. Likewise, to effectively evaluate the optimal synchronization region, we consider the distribution of coupling parameters by defining the maximal power consumption of synchronous controller, as follows:

$$p_{msyn} = \max\left(\left|\left|y_1 y_3\right| - \left|x_1\left(x_3 - \frac{(b_1 - b)}{c}\right)\right|\right) \quad (27)$$

In the numerical analysis, we choose the parameter values as a=2, b=1, c=1, n=30, m=1, b_1=12, and q=0.96 and set the initial values of drive system and the response system as $x(0)$=(-0.2, 0.1, 0.5), $y(0)$=(0.6, -0.5, -0.2). The distribution map about the maximal power consumption of synchronous controller in the coupling-parameter space (k_2, k_3) is illustrated in Figure 8. It is found that the distribution of p_{msyn} is complicated when k_2 is less than 4, and there exists an optimized coupling-parameter region near k_2=1. When k_2 continues to increase with the condition of $k_3 > 1$, the value of p_{msyn} gradually decreases, and finally it keeps in the optimal synchronization region with $k_2 > 9$.

As the examples to explain our analysis, we select two sets of coupling parameters (k_2=1, k_3=4) and (k_2=10, k_3=4) to realize the optimal synchronization. It can be found that we can realize the partial phase synchronization of fractional chaotic system with the selected coupling parameters, but larger parameters k_2 and k_3 will lead to shorter synchronous transition time, as illustrated in Figures 9 and 10. Further, to analyze the influence of c on the difference between various states of synchronized systems, the representative process of phase synchronization when k_2=10, k_3=4, and c=0.5 is considered, as shown in Figure 11. The graphs in Figures 10 and 11 signify that a smaller c will lead to a larger difference between the system variables of the phase synchronization.

6. Conclusion

Robust chaotic system is a recent research interest yet a promising candidate for signal processing, image encryption, chaotic radar, and chaotic communication. Therefore, it is worthwhile to explore the dynamics feature of robust chaotic system. In this paper, we introduced a robust fractional-order chaotic system and revealed the significant dynamics of position modulation and amplitude modulation.

The linear control scheme is designed to realize the partial projective synchronization and partial phase synchronization, by considering the property of amplitude and position modulation. The distribution of optimal synchronization region in the control-parameter space is evaluated by searching the minimum power consumption of the linear controller. Numerical experiments are executed to confirm the theoretical analysis. Since the relation of synchronization

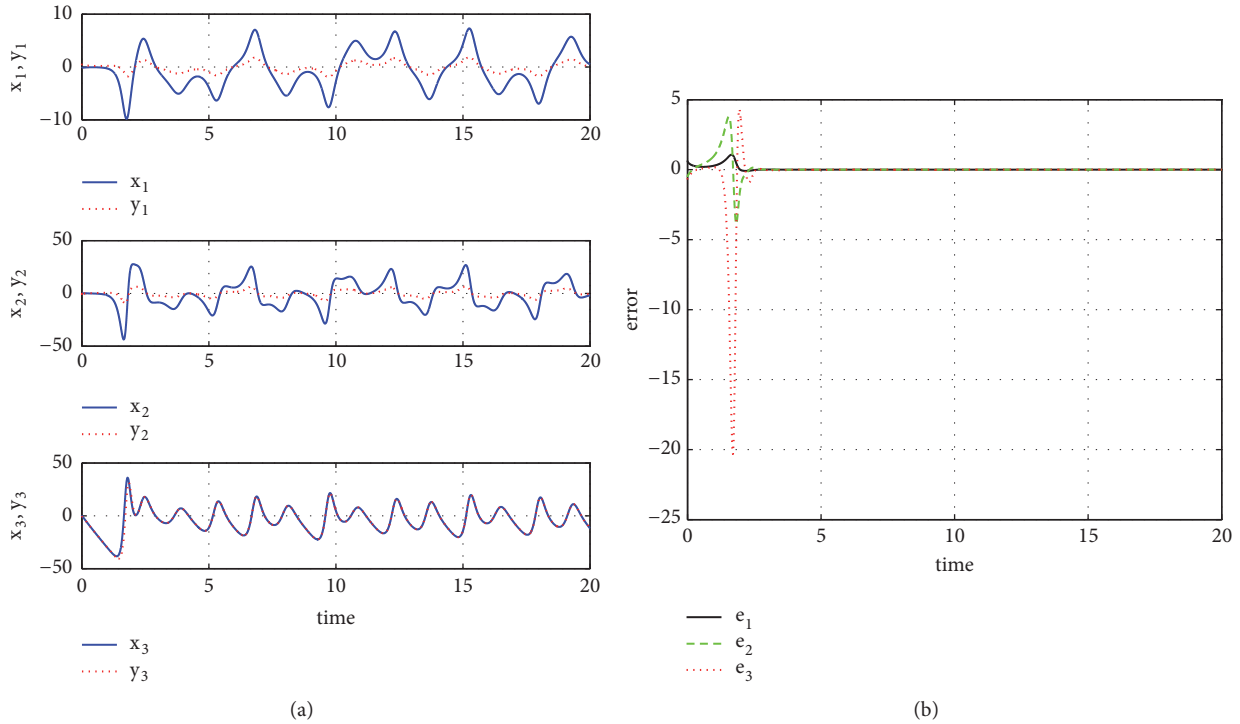

Figure 7: Partial projective synchronization with k_2=6; k_3=8: (a) time response; (b) synchronization error.

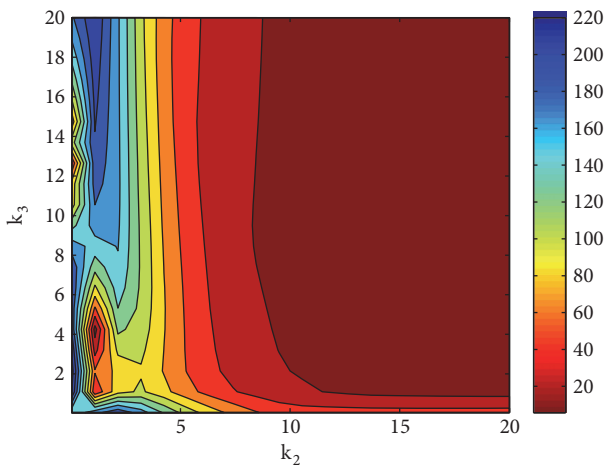

Figure 8: The distribution of the maximal power consumption of synchronous controller.

variables only depends on the system parameters, it is not easy to attack and accurately reconstruct the drive system. Therefore, it could be significant in secure communication for masking signals.

Data Availability

The data used to support the findings of this study are included within the article.

Conflicts of Interest

The authors declare that there are no conflicts of interest regarding the publication of this paper.

Acknowledgments

This work was supported by the National Natural Science Foundation of China under Grant no. 51577046, the

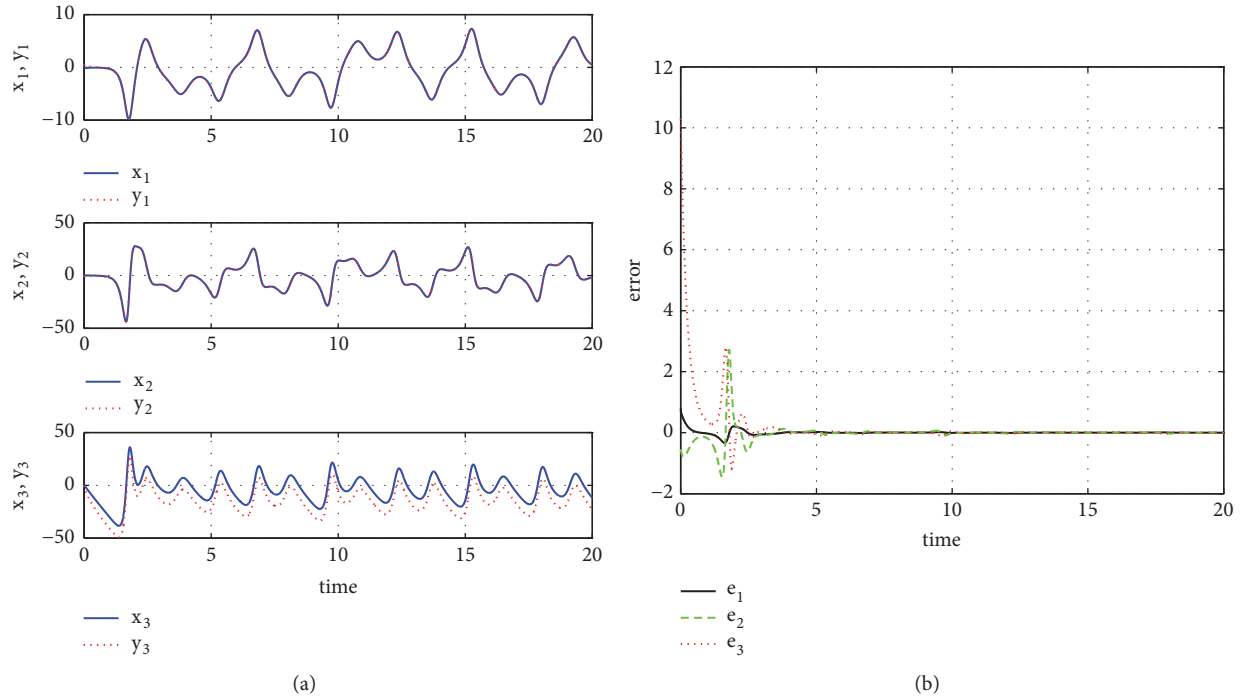

Figure 9: Partial phase synchronization with k_2=1; k_3=4: (a) time response; (b) synchronization error.

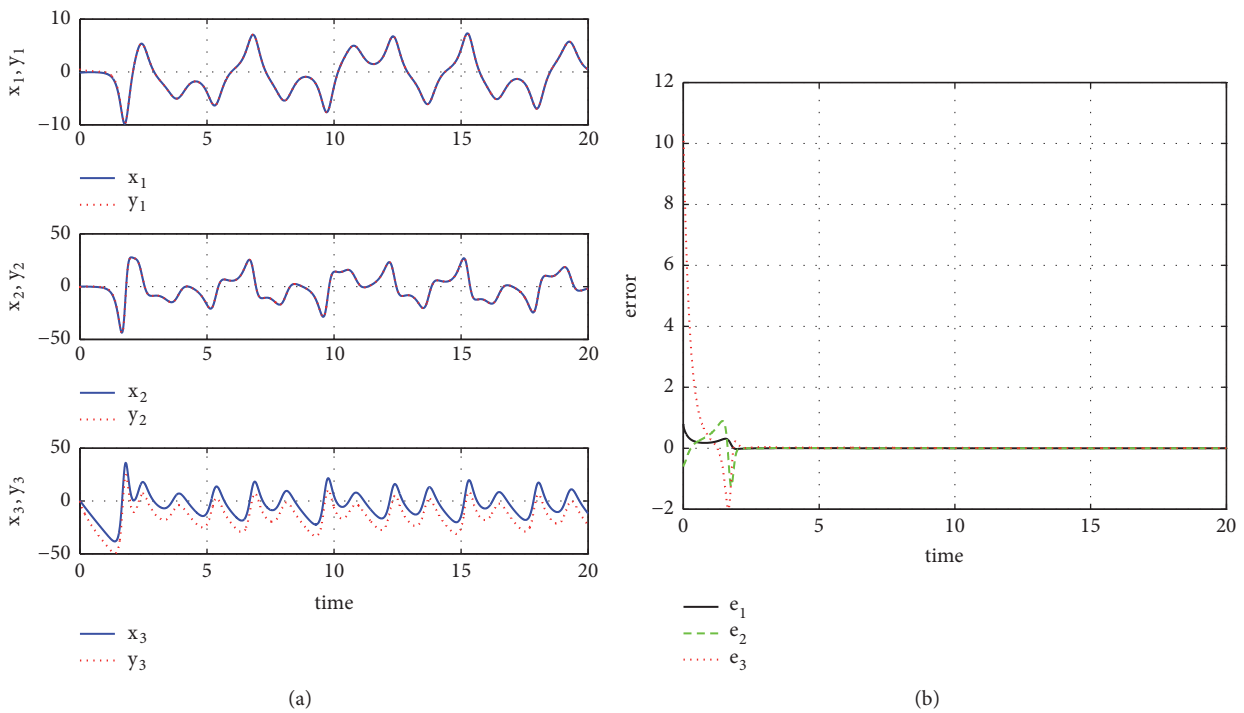

Figure 10: Partial phase synchronization with k_2=10, k_3=4, and c=1: (a) time response; (b) synchronization error.

State Key Program of National Natural Science Foundation of China under Grant no. 51637004, the National Key Research and Development Plan "Important Scientific Instruments and Equipment Development" under Grant no. 2016YFF0102200, Equipment Research Project in Advance under Grant no. 41402040301, the Research Foundation of Education Bureau of Hunan Province of China under Grant no. 16B113, and Hunan Provincial Natural Science Foundation of China under Grant no. 2016JJ4036.

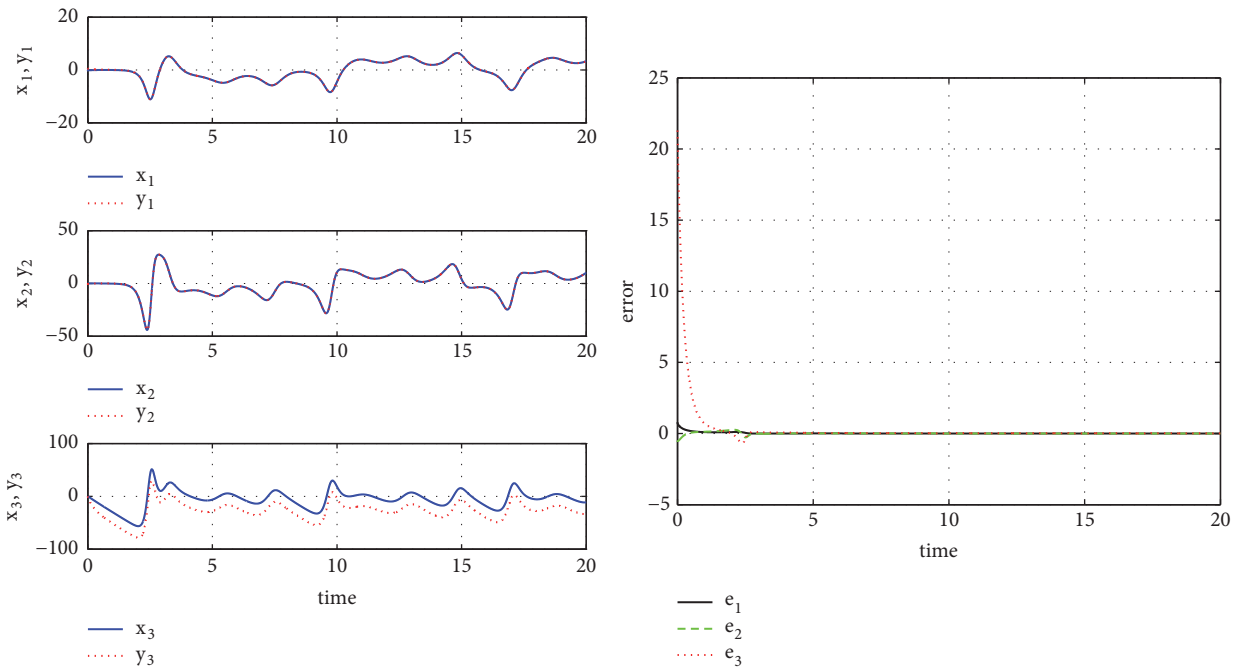

FIGURE 11: Partial phase synchronization with k_2=10, k_3=4, and c=0.5: (a) time response; (b) synchronization error.

References

[1] D. Kim, R. B. Gillespie, and P. H. Chang, "Simple, robust control and synchronization of the Lorenz system," *Nonlinear Dynamics*, vol. 73, no. 1-2, pp. 971–980, 2013.

[2] F. Peng, D.-L. Zhou, M. Long, and X.-M. Sun, "Discrimination of natural images and computer generated graphics based on multi-fractal and regression analysis," *AEUE - International Journal of Electronics and Communications*, vol. 71, pp. 72–81, 2017.

[3] Y. Li, D. Xu, Y. Fu, and J. Zhang, "Dynamic effects of delayed feedback control on nonlinear vibration isolation floating raft systems," *Journal of Sound and Vibration*, no. 13, pp. 2665–2676, 2014.

[4] L. Zhang, G. Cai, and X. Fang, "Stability for a novel time-delay financial hyperchaotic system by adaptive periodically intermittent linear control," *Journal of Information and Computing Science*, vol. 10, no. 3, pp. 189–198, 2015.

[5] Y. Zhao, X. Zhang, J. Xu, and Y. Guo, "Identification of chaotic memristor systems based on piecewise adaptive Legendre filters," *Chaos, Solitons & Fractals*, vol. 81, no. part A, pp. 315–319, 2015.

[6] H. Saberi Nik, S. Effati, and M. Shirazian, "An approximate-analytical solution for the Hamilton-Jacobi-Bellman equation via homotopy perturbation method," *Applied Mathematical Modelling*, vol. 36, no. 11, pp. 5614–5623, 2012.

[7] Y. Ji, X. Liu, and F. Ding, "New criteria for the robust impulsive synchronization of uncertain chaotic delayed nonlinear systems," *Nonlinear Dynamics*, vol. 79, no. 1, pp. 1–9, 2015.

[8] Y. Luo, M. Du, and J. Liu, "A symmetrical image encryption scheme in wavelet and time domain," *Communications in Nonlinear Science and Numerical Simulation*, vol. 20, no. 2, pp. 447–460, 2015.

[9] X. Xiang and B. Shi, "Weak signal detection based on the information fusion and chaotic oscillator," *Chaos: An Interdisciplinary Journal of Nonlinear Science*, vol. 20, no. 1, pp. 135–138, 2010.

[10] C. Li and J. Zhang, "Synchronisation of a fractional-order chaotic system using finite-time input-to-state stability," *International Journal of Systems Science*, vol. 47, no. 10, pp. 2440–2448, 2016.

[11] X. Y. Zhou, "A chaotic system with invariable Lyapunov exponent and its circuit simulation," *Acta Physica Sinica*, vol. 60, no. 10, Article ID 100503, 2011.

[12] C. Li, K. Su, and J. Zhang, "Amplitude control and projective synchronization of a dynamical system with exponential nonlinearity," *Applied Mathematical Modelling: Simulation and Computation for Engineering and Environmental Systems*, vol. 39, no. 18, pp. 5392–5398, 2015.

[13] J. Jiang and Q. Qing Wu, "A New Three-Dimensional Chaotic System with Constant Exponent Spectrum: Analysis, Synchronization and Circuit Implementation," *Journal of Software* , vol. 11, no. 5, pp. 494–511, 2016.

[14] C. Li, L. Wu, H. Li, and Y. Tong, "A novel chaotic system and its topological horseshoe," *Nonlinear Analysis: Modelling and Control*, vol. 18, no. 1, pp. 66–77, 2013.

[15] L. Pan, W. Zhou, L. Zhou, and K. Sun, "Chaos synchronization between two different fractional-order hyperchaotic systems," *Communications in Nonlinear Science and Numerical Simulation*, vol. 16, no. 6, pp. 2628–2640, 2011.

[16] J. He, S. Yu, and J. Cai, "A method for image encryption based on fractional-order hyperchaotic systems," *Journal of Applied Analysis and Computation*, vol. 5, no. 2, pp. 197–209, 2015.

[17] M. P. Aghababa, "Fractional modeling and control of a complex nonlinear energy supply-demand system," *Complexity*, vol. 20, no. 6, pp. 74–86, 2015.

[18] Y. Wang, K. Sun, S. He, and H. Wang, "Dynamics of fractional-order sinusoidally forced simplified Lorenz system and its synchronization," *The European Physical Journal Special Topics*, vol. 223, no. 8, pp. 1591–1600, 2014.

[19] S. He, K. Sun, and H. Wang, "Complexity analysis and DSP implementation of the fractional-order Lorenz hyperchaotic system," *Entropy*, vol. 17, no. 12, pp. 8299–8311, 2015.

[20] J. Ruan, K. Sun, J. Mou, S. He, and L. Zhang, "Fractional-order simplest memristor-based chaotic circuit with new derivative," *The European Physical Journal Plus*, vol. 133, no. 1, 2018.

[21] V.-T. Pham, S. T. Kingni, C. Volos, S. Jafari, and T. Kapitaniak, "A simple three-dimensional fractional-order chaotic system without equilibrium: Dynamics, circuitry implementation, chaos control and synchronization," *AEÜ - International Journal of Electronics and Communications*, vol. 78, pp. 220–227, 2017.

[22] L. Zhang, K. Sun, W. Liu, and S. He, "A novel color image encryption scheme using fractional-order hyperchaotic system and DNA sequence operations," *Chinese Physics B*, vol. 26, no. 10, p. 100504, 2017.

[23] L. M. Pecora and T. L. Carroll, "Synchronization in chaotic systems," *Physical Review Letters*, vol. 64, no. 8, pp. 821–824, 1990.

[24] D. Xu and C. Y. Chee, "Controlling the ultimate state of projective synchronization in chaotic systems of arbitrary dimension," *Physical Review E: Statistical, Nonlinear, and Soft Matter Physics*, vol. 66, no. 4, 2002.

[25] M. G. Rosenblum, A. S. Pikovsky, and J. Kurths, "Phase synchronization of chaotic oscillators," *Physical Review Letters*, vol. 76, no. 11, pp. 1804–1807, 1996.

[26] A. Tayebi, S. Berber, and A. Swain, "Performance analysis of chaotic DSSS-CDMA synchronization under jamming attack," *Circuits, Systems and Signal Processing*, vol. 35, no. 12, pp. 4350–4371, 2016.

[27] A. Kajbaf, M. A. Akhaee, and M. Sheikhan, "Fast synchronization of non-identical chaotic modulation-based secure systems using a modified sliding mode controller," *Chaos, Solitons & Fractals*, vol. 84, pp. 49–57, 2016.

[28] I. Ahmad, A. Bin Saaban, A. B. Ibrahim, and M. Shahzad, "Global chaos synchronization of new chaotic system using linear active control," *Complexity*, vol. 21, no. 1, pp. 379–386, 2015.

[29] H. Saberi Nik, S. Effati, and J. Saberi-Nadjafi, "New ultimate bound sets and exponential finite-time synchronization for the complex Lorenz system," *Journal of Complexity*, vol. 31, no. 5, pp. 715–730, 2015.

[30] D. Ghosh and S. Bhattacharya, "Projective synchronization of new hyperchaotic system with fully unknown parameters," *Nonlinear Dynamics*, vol. 61, no. 1-2, pp. 11–21, 2010.

[31] S. Zheng, "Impulsive complex projective synchronization in drive-response complex coupled dynamical networks," *Nonlinear Dynamics*, vol. 79, no. 1, pp. 147–161, 2015.

[32] E. E. Mahmoud, "Modified projective phase synchronization of chaotic complex nonlinear systems," *Mathematics and Computers in Simulation*, vol. 89, pp. 69–85, 2013.

[33] W. Wang, I. Z. Kiss, and J. L. Hudson, "Experiments on arrays of globally coupled chaotic electrochemical oscillators: Synchronization and clustering," *Chaos: An Interdisciplinary Journal of Nonlinear Science*, vol. 10, no. 1, pp. 248–256, 2000.

[34] J. E. Rosa, W. B. Pardo, C. M. Ticos, J. A. Walkenstein, and M. Monti, "Phase synchronization of chaos in a plasma discharge tube," *International Journal of Bifurcation and Chaos*, vol. 10, no. 11, pp. 2551–2563, 2000.

[35] H. Wang, Q. Wang, Q. Lu, and Y. Zheng, "Equilibrium analysis and phase synchronization of two coupled HR neurons with gap junction," *Cognitive Neurodynamics*, vol. 7, no. 2, pp. 121–131, 2013.

[36] Z. Odibat, "A note on phase synchronization in coupled chaotic fractional order systems," *Nonlinear Analysis: Real World Applications*, vol. 13, no. 2, pp. 779–789, 2012.

[37] M. Caputo, "Linear models of dissipation whose Q is almost frequency independent-II," *Annals of Geophysics*, vol. 19, no. 4, pp. 529–539, 1966.

[38] K. Diethelm and N. J. Ford, "Analysis of fractional differential equations," *Journal of Mathematical Analysis and Applications*, vol. 265, no. 2, pp. 229–248, 2002.

[39] C. Li and H. Li, "Robust control for a class of chaotic and hyperchaotic systems via linear state feedback," *Physica Scripta*, vol. 85, no. 2, p. 025007, 2012.

[40] N. Aguila-Camacho, M. A. Duarte-Mermoud, and J. A. Gallegos, "Lyapunov functions for fractional order systems," *Communications in Nonlinear Science and Numerical Simulation*, vol. 19, no. 9, pp. 2951–2957, 2014.

[41] P. Zhou, H. Cai, and C. D. Yang, "Stabilization of the unstable equilibrium points of the fractional-order BLDCM chaotic system in the sense of Lyapunov by a single-state variable," *Nonlinear Dynamics*, vol. 84, no. 4, pp. 2357–2361, 2016.

[42] M. A. Duarte-Mermoud, N. Aguila-Camacho, J. A. Gallegos, and R. Castro-Linares, "Using general quadratic LYApunov functions to prove LYApunov uniform stability for fractional order systems," *Communications in Nonlinear Science and Numerical Simulation*, vol. 22, no. 1-3, pp. 650–659, 2015.

[43] Q. Wang, D. Ding, and D. Qi, "Mittag–Leffler synchronization of fractional-order uncertain chaotic systems," *Chinese Physics B*, vol. 24, no. 6, p. 060508, 2015.

[44] F. Li, W. Y. Jin, and J. Ma, "Modulation of nonlinear coupling on the synchronization induced by linear coupling," *Acta Physica Sinica*, vol. 61, no. 24, Article ID 240501, 2012.

Hindawi
Complexity
Volume 2018, Article ID 4019749, 13 pages
https://doi.org/10.1155/2018/4019749

Research Article

Complex Dynamics of the Fractional-Order Rössler System and Its Tracking Synchronization Control

Huihai Wang, Shaobo He, and Kehui Sun

School of Physics and Electronics, Central South University, Changsha 410083, China

Correspondence should be addressed to Shaobo He; heshaobo_123@163.com

Received 22 September 2018; Accepted 5 November 2018; Published 2 December 2018

Guest Editor: Viet-Thanh Pham

Numerical analysis of fractional-order chaotic systems is a hot topic of recent years. The fractional-order Rössler system is solved by a fast discrete iteration which is obtained from the Adomian decomposition method (ADM) and it is implemented on the DSP board. Complex dynamics of the fractional-order chaotic system are analyzed by means of Lyapunov exponent spectra, bifurcation diagrams, and phase diagrams. It shows that the system has rich dynamics with system parameters and the derivative order q. Moreover, tracking synchronization controllers are theoretically designed and numerically investigated. The system can track different signals including chaotic signals from the fractional-order master system and constant signals. It lays a foundation for the application of the fractional-order Rössler system.

1. Introduction

Some studies have shown that fractional-order chaotic systems have more complex dynamic properties than the corresponding integer-order systems. The differential order q of the fractional-order chaotic system equation is one of the bifurcation parameters of the system [1, 2]. It is necessary to study the corresponding fractional-order chaotic system based on the existing integer-order chaotic system. Since the well-known Rössler system was derived in 1976 [3], it has been studied as one of typical chaotic systems [4–6]. The properties and characteristics of its attractor depend on the control parameters a, b, and c. Some researchers investigated the chaotic dynamics of fractional-order Rössler systems [7–9]. In [7], Li and Chen analyzed the dynamics of fractional-order Rössler systems by employing frequency-domain method [10] based on the approximation of the transition function $1/s^q$ and discussed only cases of q=0.7, 0.8, 0.9. For this approximation, in general, $q \in [0.1, 0.9]$ with the step size of 0.1 is considered because of complicated mathematical transformations [11]. Obviously, the step size of order is too large. So, it is not competent when q changes continuously. In addition, whether this approximation accurately reflects the chaos characteristics of a fractional-order nonlinear system was questioned in [12, 13]. The Adams-Bashforth-Moulton predictor-corrector approaches [14–16] were used to solve the fractional-order Rössler systems in [8, 9]. However, along with the computation, the algorithm consumes too much computer resources, and the speed of calculation is very slow. So, this algorithm is not suitable for engineering applications.

Adomian decomposition method (ADM) [17] is capable of dealing with linear and nonlinear problems in time domain. In [18], the fractional-order Chen system was investigated, and it shows that ADM provides the solution in a closed form and preserves the system nonlinearity. In [19], the fractional-order Lorenz system, the fractional-order Chua-Hartley system, and the fractional-order Lü system are analyzed by using ADM, and the results reveal that the method is very effective, and it leads to accurate, approximately convergent solutions. The fractional-order Lorenz-Stenflo system was analyzed by adopting ADM, and some different dynamics were provided with different order q compared with its integer-order counterpart [1]. The chaos range of the fractional-order simplified Lorenz system solved by adopting ADM is wider than that by using Adams-Bashforth-Moulton predictor-corrector approach [2]. Further, the two fractional-order chaotic systems in [1, 2] are implemented on DSP platform. He *et al.* [20] concluded the characteristics of ADM which has the advantages of high accuracy, fast convergence, and less computer resource consumption. So, it is worth

studying whether the fractional-order Rössler system solved by employing ADM provides different dynamics compared with its integrate-order counterpart and by using others methods.

On the other hand, the synchronization of chaotic systems has always been a hot topic [21–23]. The synchronization of the fractional-order chaotic systems has just begun to attract some attentions due to its potential applications in secure communications and control processing [24]. A variety of approaches have been proposed for the synchronization of fractional-order chaotic systems [25–28]. However, numerical solutions of the above reports are obtained by employing the Adams-Bashforth-Moulton algorithm and the frequency-domain method. As far as we know, there are no articles dealing with synchronization of fractional-order Rössler systems based on ADM. Thus, it is still a novel topic to investigate the synchronization of fractional-order Rössler systems by employing ADM.

The outline of this paper is as follows. In Section 2, the ADM is introduced briefly, and the iterative algorithm and Lyapunov exponent spectra algorithm of the fractional-order Rössler system are presented. In Section 3, the dynamics of this fractional-order chaotic system are analyzed by Lyapunov exponent spectra and bifurcation diagram. In Section 4, the synchronization of fractional-order Rössler systems is investigated theoretically and numerically. It includes tracking constant signals and tracking chaotic signal from the master system. Finally, the results are summarized.

2. Numerical Analysis Methods Based on ADM

2.1. The Adomian Decomposition Method. For a given fractional-order differential equation ${}^{*}D_{t_0}^{q}\mathbf{x}(t) = f(\mathbf{x}(t)), f(\mathbf{x}(t))$ can be separated into three terms [29, 30],

$$ {}^{*}D_{t_0}^{q}\mathbf{x}(t) = L\mathbf{x}(t) + N\mathbf{x}(t) + \mathbf{g}(t). \tag{1} $$

Here, ${}^{*}D_{t_0}^{q}$ is the Caputo derivative operator of order q (m-1<q ≤m, m∈N) [31], and t_0 represents the starting time, t>t_0. $\mathbf{x}(t) = [x_1(t), x_2(t), \ldots, x_n(t)]^{\mathrm{T}}$ are state variables. L and N represent linear and nonlinear operator, respectively, and $\mathbf{g}(t)$=$[g_1(t), g_2(t), \ldots, g_n(t)]^{\mathrm{T}}$ are constants in the autonomous system. $\mathbf{x}^{(k)}(t_0^{+}) = \mathbf{b}_k$, $k = 0, \cdots, m-1$, are initial states of the equation. $J_{t_0}^{q}$ is R-L fractional integral operator with order q.

Definition 1 (see [31]). The Caputo definition is defined as

$$ {}^{*}D_{t_0}^{q}f(t) = \frac{1}{\Gamma(1-q)}\int_{t_0}^{t}\frac{\dot{f}(\tau)}{(t-\tau)^{q}}d\tau, \tag{2} $$

where 0<q≤1 and $\Gamma(\cdot)$ is the gamma function.

The fundamental properties of the integral operator $J_{t_0}^{q}$ are described by [31]

$$ {}^{*}D_{t_0}^{q}J_{t_0}^{q}\mathbf{x}(t) = \mathbf{x}(t), \tag{3} $$

$$ J_{t_0}^{q}\left({}^{*}D_{t_0}^{q}\right)\mathbf{x}(t) = \mathbf{x}(t) - \sum_{k=0}^{m-1}\mathbf{x}^{(k)}(t_0^{+})\frac{(t-t_0)^{k}}{k!}, \tag{4} $$

$$ J_{t_0}^{q}(t-t_0)^{\gamma} = \frac{\Gamma(\gamma+1)}{\Gamma(\gamma+1+q)}(t-t_0)^{\gamma+q}, \tag{5} $$

$$ J_{t_0}^{q}C = \frac{C}{\Gamma(q+1)}(t-t_0)^{q}, \tag{6} $$

$$ J_{t_0}^{q}J_{t_0}^{r}x(t) = J_{t_0}^{q+r}x(t). \tag{7} $$

Here, r≥0, γ >-1, and C is a real constant. According to (4), the following equation is obtained by applying the operator $J_{t_0}^{q}$ to both sides of (1) [32]:

$$ \mathbf{x} = J_{t_0}^{q}L\mathbf{x} + J_{t_0}^{q}N\mathbf{x} + J_{t_0}^{q}\mathbf{g} + \sum_{k=0}^{m-1}\mathbf{b}_k\frac{(t-t_0)^{k}}{k!}. \tag{8} $$

Based on ADM, the nonlinear terms in (8) are expressed by Adomian polynomials [32]

$$ N\mathbf{x} = \sum_{i=0}^{\infty}\mathbf{A}^{i}\left(\mathbf{x}^{0}, \mathbf{x}^{1}, \cdots, \mathbf{x}^{i}\right). \tag{9} $$

Here, $\mathbf{x}^{i}$ is the No. i (i = 0, 1, …, ∞) of Adomian polynomials, and A_j^{i} is obtained according to

$$ \begin{aligned} A_j^{i} &= \frac{1}{i!}\left[\frac{d^{i}}{d\lambda^{i}}N\left(\nu_j^{i}(\lambda)\right)\right]_{\lambda=0} \\ \nu_j^{i}(\lambda) &= \sum_{k=0}^{i}(\lambda)^{k}x_j^{k}, \end{aligned} \tag{10} $$

where j = 1, 2, …, n (the system dimension). Then, the solution of (1) is expressed as $\mathbf{x} = \sum_{i=0}^{\infty}\mathbf{x}^{i}$, where $\mathbf{x}^{i}$ is derived from

$$ \begin{aligned} \mathbf{x}^{0} &= J_{t_0}^{q}\mathbf{g} + \sum_{k=0}^{m-1}\mathbf{b}_k\frac{(t-t_0)^{k}}{k!} \\ \mathbf{x}^{1} &= J_{t_0}^{q}L\mathbf{x}^{0} + J_{t_0}^{q}\mathbf{A}^{0}\left(\mathbf{x}^{0}\right) \\ \mathbf{x}^{2} &= J_{t_0}^{q}L\mathbf{x}^{1} + J_{t_0}^{q}\mathbf{A}^{1}\left(\mathbf{x}^{0}, \mathbf{x}^{1}\right) \\ &\vdots \\ \mathbf{x}^{i} &= J_{t_0}^{q}L\mathbf{x}^{i-1} + J_{t_0}^{q}\mathbf{A}^{i-1}\left(\mathbf{x}^{0}, \mathbf{x}^{1}, \cdots, \mathbf{x}^{i-1}\right) \\ &\vdots. \end{aligned} \tag{11} $$

2.2. Numerical Solution of Fractional-Order Rössler System. The fractional-order Rössler system is [7]

$$ \begin{aligned} {}^{*}D_{t_0}^{q}x &= -y - z \\ {}^{*}D_{t_0}^{q}y &= x + ay \\ {}^{*}D_{t_0}^{q}z &= b + z(x-c), \end{aligned} \tag{12} $$

where a, b, and c are the control parameters. By employing ADM and according to (5)-(7), the exact numerical solution

of fractional-order Rössler system can be obtained, but it is an infinite length iteration. Considering the fast convergence performance of ADM [33], the first five terms of the iteration are truncated as approximate solution as shown in (13)-(18).

$$\begin{bmatrix} x_{m+1} \\ y_{m+1} \\ z_{m+1} \end{bmatrix} = \begin{bmatrix} x_{10} + x_{11} + x_{12} + x_{13} + x_{14} \\ y_{10} + y_{11} + y_{12} + y_{13} + y_{14} \\ z_{10} + z_{11} + z_{12} + z_{13} + z_{14} \end{bmatrix}, \tag{13}$$

where

$$\begin{aligned} x_{10} &= x_m \\ y_{10} &= y_m \\ z_{10} &= z_m + b\frac{h^q}{\Gamma(q+1)} \\ C_{10} &= x_{10} \\ C_{20} &= y_{10} \\ C_{30} &= z_0, \end{aligned} \tag{14}$$

$$\begin{aligned} C_{11} &= -C_{20} - C_{30} \\ C_{110} &= -b \\ x_{11} &= C_{11}\frac{h^q}{\Gamma(q+1)} + C_{110}\frac{h^{2q}}{\Gamma(2q+1)} \\ C_{21} &= C_{10} + aC_{20} \\ y_{11} &= C_{21}\frac{h^q}{\Gamma(q+1)} \\ C_{31} &= C_{10}C_{30} - cC_{30} \\ C_{310} &= bC_{10} - bc \\ z_{11} &= C_{31}\frac{h^q}{\Gamma(q+1)} + C_{310}\frac{h^{2q}}{\Gamma(2q+1)}, \end{aligned} \tag{15}$$

$$\begin{aligned} C_{12} &= -C_{21} - C_{31} \\ C_{120} &= -C_{310} \\ x_{12} &= C_{12}\frac{h^{2q}}{\Gamma(2q+1)} + C_{120}\frac{h^{3q}}{\Gamma(3q+1)} \\ C_{22} &= C_{11} + aC_{21} \\ C_{220} &= C_{110} \\ y_{12} &= C_{22}\frac{h^{2q}}{\Gamma(2q+1)} + C_{220}\frac{h^{3q}}{\Gamma(3q+1)} \\ C_{32} &= C_{11}C_{30} + C_{10}C_{31} - cC_{31} \\ C_{320} &= bC_{11}\frac{\Gamma(2q+1)}{\Gamma^2(q+1)} + C_{30}C_{10} + C_{10}C_{310} - cC_{310} \\ C_{321} &= bC_{110}\frac{\Gamma(3q+1)}{\Gamma(q+1)\Gamma(2q+1)} \\ z_{12} &= C_{32}\frac{h^{2q}}{\Gamma(2q+1)} + C_{320}\frac{h^{3q}}{\Gamma(3q+1)} \\ &\quad + C_{321}\frac{h^{4q}}{\Gamma(4q+1)}, \end{aligned} \tag{16}$$

$$\begin{aligned} C_{13} &= -C_{22} - C_{32} \\ C_{130} &= -C_{120} - C_{320} \\ C_{131} &= -C_{321} \\ x_{13} &= C_{13}\frac{h^{3q}}{\Gamma(3q+1)} + C_{130}\frac{h^{4q}}{\Gamma(4q+1)} \\ &\quad + C_{131}\frac{h^{5q}}{\Gamma(5q+1)} \\ C_{23} &= C_{12} + aC_{22} \\ C_{230} &= C_{120} + aC_{220} \\ y_{13} &= C_{23}\frac{h^{3q}}{\Gamma(3q+1)} + C_{230}\frac{h^{4q}}{\Gamma(4q+1)} \\ C_{33} &= C_{12}C_{30} + C_{10}C_{32} - cC_{32} + C_{11}C_{31}\frac{\Gamma(2q+1)}{\Gamma^2(q+1)} \\ C_{330} &= C_{30}C_{120} + C_{10}C_{320} \\ &\quad + \left(bC_{12} + C_{11}C_{310} + C_{31}C_{110}\right)\frac{\Gamma(3q+1)}{\Gamma(2q+1)\Gamma(q+1)} \\ &\quad - cC_{320} \\ C_{331} &= bC_{120}\frac{\Gamma(4q+1)}{\Gamma(3q+1)\Gamma(q+1)} + C_{10}C_{321} \\ &\quad + C_{110}C_{310}\frac{\Gamma(4q+1)}{\Gamma^2(2q+1)} - cC_{321} \\ z_{13} &= C_{33}\frac{h^{3q}}{\Gamma(3q+1)} + C_{330}\frac{h^{4q}}{\Gamma(4q+1)} \\ &\quad + C_{331}\frac{h^{5q}}{\Gamma(5q+1)}, \end{aligned} \tag{17}$$

$$\begin{aligned} C_{14} &= -C_{23} - C_{33} \\ C_{140} &= -C_{230} - C_{330} \\ C_{141} &= -C_{331} \\ x_{14} &= C_{14}\frac{h^{4q}}{\Gamma(4q+1)} + C_{140}\frac{h^{5q}}{\Gamma(5q+1)} \\ &\quad + C_{141}\frac{h^{6q}}{\Gamma(6q+1)} \end{aligned}$$

$$
\begin{aligned}
C_{24} &= C_{13} + aC_{23} \\
C_{240} &= C_{130} + aC_{230} \\
y_{14} &= C_{24}\frac{h^{4q}}{\Gamma(4q+1)} + C_{240}\frac{h^{5q}}{\Gamma(5q+1)} \\
&\quad + C_{131}\frac{h^{6q}}{\Gamma(6q+1)} \\
C_{340} &= C_{13}C_{30} + C_{10}C_{33} \\
&\quad + (C_{11}C_{32} + C_{12}C_{31})\frac{\Gamma(3q+1)}{\Gamma(2q+1)\Gamma(q+1)} - cC_{33} \\
C_{341} &= C_{30}C_{130} + C_{10}C_{330} - cC_{330} \\
&\quad + (bC_{13} + C_{11}C_{320} + C_{31}C_{120})\frac{\Gamma(4q+1)}{\Gamma(3q+1)\Gamma(q+1)} \\
&\quad + (C_{110}C_{32} + C_{12}C_{310})\frac{\Gamma(4q+1)}{\Gamma^2(2q+1)} \\
C_{342} &= C_{30}C_{331} + C_{10}C_{331} - cC_{331} \\
&\quad + (bC_{130} + C_{11}C_{321})\frac{\Gamma(5q+1)}{\Gamma(4q+1)\Gamma(q+1)} \\
&\quad + (C_{110}C_{320} + C_{120}C_{310})\frac{\Gamma(5q+1)}{\Gamma(3q+1)\Gamma(2q+1)} \\
C_{343} &= bC_{131}\frac{\Gamma(6q+1)}{\Gamma(5q+1)\Gamma(q+1)} \\
&\quad + C_{110}C_{321}\frac{\Gamma(6q+1)}{\Gamma(2q+1)\Gamma(4q+1)} \\
z_{14} &= C_{340}\frac{h^{4q}}{\Gamma(4q+1)} + C_{341}\frac{h^{5q}}{\Gamma(5q+1)} \\
&\quad + C_{342}\frac{h^{6q}}{\Gamma(6q+1)} + C_{343}\frac{h^{7q}}{\Gamma(7q+1)}.
\end{aligned}
\tag{18}
$$

Here h is iteration step size. In this paper, we set h=0.01.

2.3. Lyapunov Exponent Spectra. According to (13)-(18), the chaotic sequences of the fractional-order Rössler system are obtained with initial values $[x_0, y_0, z_0]$, q, and appropriate parameters a, b, c. So, the bifurcation diagrams of the fractional-order chaotic system are plotted. In addition, if we obtain the solution of the fractional-order chaotic system, the Lyapunov exponent spectra can be calculated by adopting QR-factorization [34]

$$
\begin{aligned}
&qr\left[\mathbf{J}_m\mathbf{J}_{m-1}\cdots\mathbf{J}_1\right] = qr\left[\mathbf{J}_m\mathbf{J}_{m-1}\cdots\mathbf{J}_2\left(\mathbf{J}_1\mathbf{Q}_0\right)\right] \\
&\quad = qr\left[\mathbf{J}_m\mathbf{J}_{m-1}\cdots\mathbf{J}_3\left(\mathbf{J}_2\mathbf{Q}_1\right)\right]\left[\mathbf{R}_1\right] \\
&\quad = qr\left[\mathbf{J}_m\mathbf{J}_{m-1}\cdots\left(\mathbf{J}_3\mathbf{Q}_2\right)\right]\left[\mathbf{R}_2\mathbf{R}_1\right] = \cdots \\
&\quad = qr\left[\mathbf{J}_m\mathbf{J}_{m-1}\cdots\left(\mathbf{J}_i\mathbf{Q}_{i-1}\right)\right]\left[\mathbf{R}_{i-1}\mathbf{R}_{i-2}\cdots\mathbf{R}_2\mathbf{R}_1\right] = \cdots \\
&\quad = \mathbf{Q}_m\left[\mathbf{R}_m\cdots\mathbf{R}_2\mathbf{R}_1\right] = \mathbf{Q}_m\mathbf{R}.
\end{aligned}
\tag{19}
$$

Here, $qr[.]$ denotes the QR-factorization process. $\mathbf{J}$ is the Jacobin matrix of the iteration (13). $\mathbf{Q}$ is the orthogonal matrix, and $\mathbf{R}$ are the diagonal elements. m is the iteration number. Then, the Lyapunov exponent spectra are calculated by

$$
\lambda_k = \frac{1}{mh}\sum_{i=1}^{m}\ln\left|\mathbf{R}_i(k,k)\right|, \tag{20}
$$

where the system dimension k = 1, 2, …, n. Dynamics of system (12) are investigated with the variation of derivative q and system parameter a.

3. Numerical Analysis of the Fractional-Order Rössler System

3.1. Dynamics with Variation of Derivative q. For a=0.55, b=2, and c=4, the bifurcation diagrams versus $q\in[0.2, 1]$ and the corresponding Lyapunov exponent spectra are shown in Figure 1. The bifurcation diagram is consistent with the Lyapunov exponent spectra. As q increases, the system is periodic at q=0.268, and it gradually enters chaotic state by period-doubling bifurcations. The first pitchfork bifurcation occurs at q=0.346. The lowest order at which the chaos exists is about 3 (the dimension of the system) ×0.346=1.119 when q=0.373, and the corresponding phase portrait is shown in Figure 2(a). However, in [7], the lowest order obtained is about q=0.7-0.8. For $q\in$[0.346, 1], the system maintains the chaotic state in most regions except for some periodic windows. The phase portrait when q=0.564 is plotted as shown in Figure 2(b). Figure 1 indicates that the differential order q is another bifurcation parameter except for the system parameters a, b, and c in the fractional-order Rössler system.

Compared with q=1, the system has different dynamic characteristics when q is fractional, including chaotic, periodic, period-doubling, and tangent bifurcations. In Figure 1, the step size of q is 0.001 when the fractional-order chaotic system is analyzed. In theory, the step size of q will be smaller, and it is not limited according to the iteration.

3.2. Dynamics with Variation of Parameter a. Let b=2 and c=4; the dynamics are investigated versus $a\in[0.2, 0.6]$ with the step sizes of 0.001. Figures 3(a), 3(b), and 3(c) are the bifurcation diagrams for q=1, q=0.8, and q=0.6, respectively. Their bifurcation structures are similar. However, the first pitchfork bifurcations occur at different positions, located at a=0.330, a=0.339, and a=0.366 for q=1, q=0.8, and q=0.6, respectively. The maximum a at which the chaos exists are also different, and they are at a=0.556, a=0.560, and a=0.572 for q=1, q=0.8, and q=0.6, respectively. The chaotic regions of the system move to the right along with the decreasing q. Figure 3(d) shows the maximum Lyapunov exponent spectra versus a with different q. Obviously, the smaller q is, the larger the maximum Lyapunov exponent is. It illustrates that

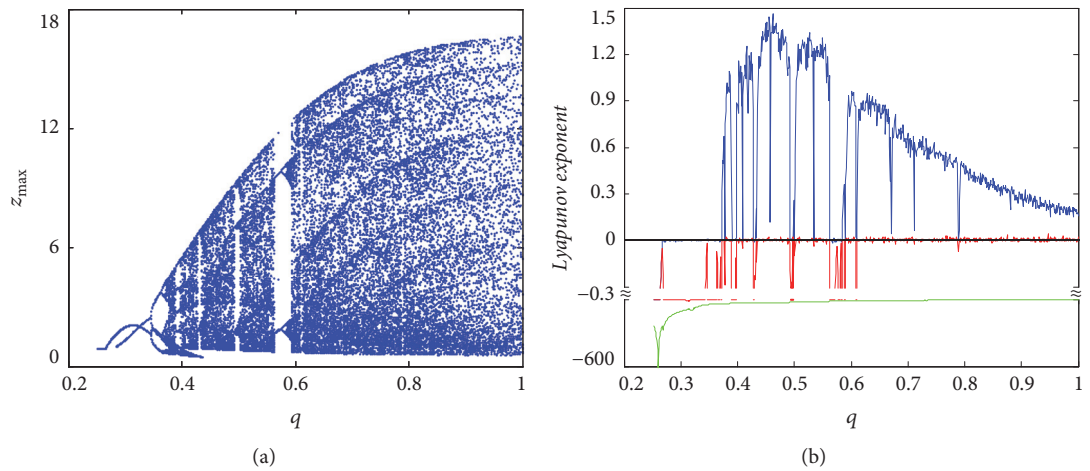

FIGURE 1: Bifurcation diagram and Lyapunov exponent spectra for fractional-order Rössler system with a=0.55, b=2, and c=4. (a) Bifurcation diagram. (b) Lyapunov exponent spectra.

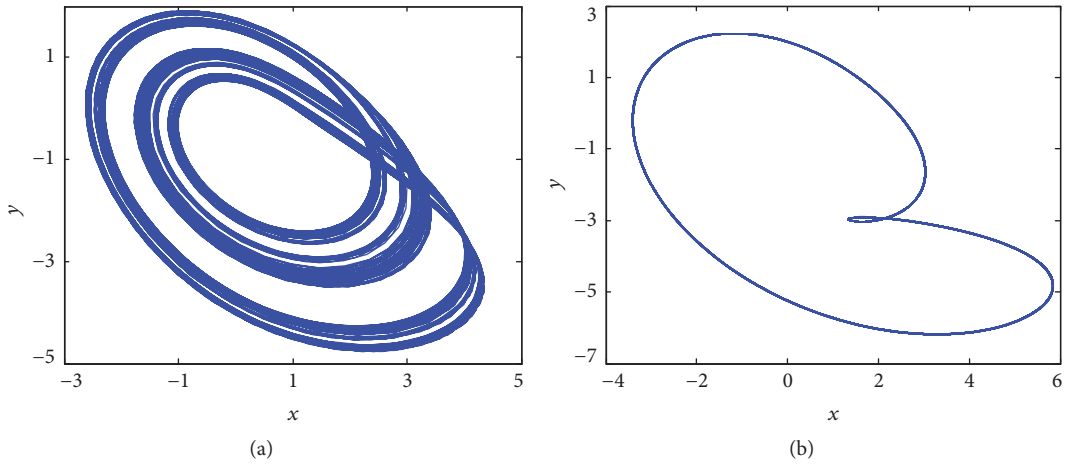

FIGURE 2: Phase portraits on x-y plane of attractor obtained by simulation. (a) q=0.373. (b) q=0.564.

the smaller the differential order q is, the more complex the fractional-order chaotic system is. This result indicates that the fractional-order Rössler system has broader applications than its integer-order counterpart. Figure 3 verifies that the differential order q affects the dynamic characteristics of the fractional-order Rössler system. Figure 4 shows phase portraits on x-y plane of attractor obtained by simulation for different q and a. It illustrates that the other conditions are the same, but q is different, and the phase portraits of the system are different. When a=0.504, the system is periodic for q=1, and it is chaotic for q=0.8 and q=0.6. However, when a=0.441, the system is periodic for q=0.6, and in the other two cases, the system is chaotic. Figure 4 also verifies that the dynamic characteristics of the fractional-order Rössler system are affected by q.

3.3. Implementation on DSP. The realization of fractional-order chaotic system is an important part of its application. We implement the fractional-order Rössler system on DSP platform. In [2], we realized the fractional-order simplified Lorenz system in the DSP board based on Adomian decomposition method, and the same technique is employed in this paper. For hardware design, the block diagram of the working principle is shown in Figure 5. In the experiments, the Texas Instrument DSP device TMS320F2812 is employed. TMS320F2812 is a 32-bit DSP running at 150MHz with fixed point operation. Such a high-speed clock rate is considered to be sufficient for our experiments. It can easily interface with a 16-bit dual channels digital-to-analog converter DAC8552 by SPI (serial peripheral interface). Phase portraits of the system are captured randomly by oscilloscope (Tektronix MSO 4102B-L).

For software design, the operational procedure is shown in Figure 6. It is based on the discrete iterative equations (13)-(18). The initial values, including h, q, $[x_0, y_0, z_0]$, parameters and iteration number are set after initializing DSP. To improve the calculation speed, all $\Gamma(\cdot)$ and h^{nq} are calculated before iterative computation. According to (13)-(18), some sequences are negative, and input data of DAC8552 must be integers in $[0, 2^{16}-1]$. Thus, to display the attractors of the fractional-order chaotic system, the data processing includes three steps. Firstly, a positive integer A is added

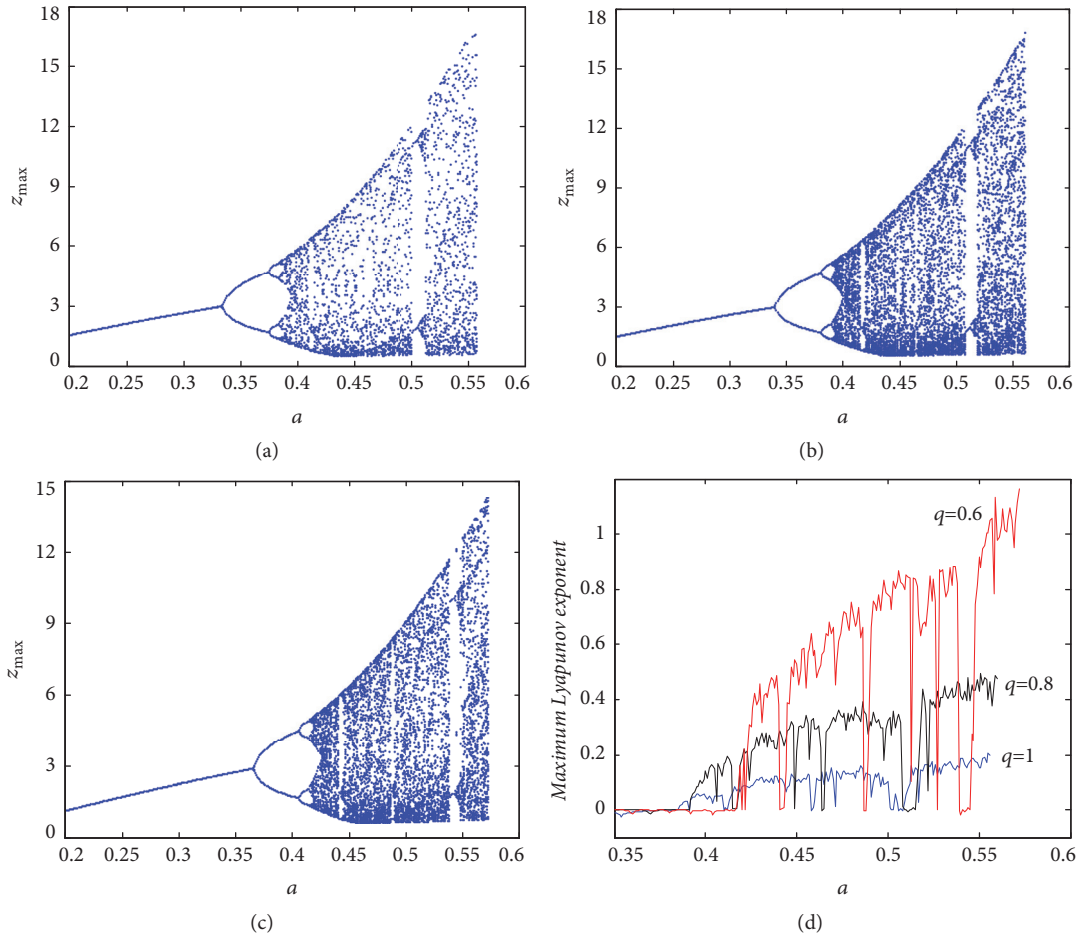

FIGURE 3: Bifurcation diagrams and Lyapunov exponent spectra for fractional-order Rössler system with b=2 and c=4. (a) Bifurcation diagram with q=1. (b) Bifurcation diagram with q=0.8. (c) Bifurcation diagram with q=0.6. (d) Maximum Lyapunov exponent spectra.

to all sequences. It makes sure that each dataset is positive. Secondly, a scaling process is carried out by multiplying a positive integer B. Finally, the above results are rounded up. A and B are different for the sequences with different parameters and q. In addition, the iterative computation is not affected by data processing by employing the operation of pushing and popping [2].

We set $h = 0.01$, initial values $[x_0, y_0, z_0] = [2, -3, 2]$, and the parameters a, b, c are the same as those in Section 3.3; $A = 15$ and $B = 1400$. Phase portraits of the system are captured by the oscilloscope as shown in Figure 7. The experimental results qualify the simulation analysis, as shown in Figure 2. It indicates that the fractional-order Rössler system is realized successfully on DSP platform. For the DSP implementation of the fractional-order Rössler system, the number of variations is not changed in the calculation. So, it is not worrisome that the computer resources will be exhausted, and ADM is suitable for engineering applications.

4. Tracking Synchronization

Synchronization control of fractional-order chaotic system is one of the main aspects of its applications. In practical applications, we need to eliminate the chaos or transform it into some useful signals. Therefore, tracking control, which transforms the chaos signal into desired bounded signal, is significant in practice. We investigate the tracking synchronization of fractional-order Rössler systems based on ADM.

The tracking system with controllers is defined as

$$\begin{aligned} {}^{*}D_{t_0}^{q} x' &= -y' - z' + u_1 \\ {}^{*}D_{t_0}^{q} y' &= x' + ay' + u_2 \\ {}^{*}D_{t_0}^{q} z' &= b - cz' + x'z' + u_3, \end{aligned} \tag{21}$$

where $\mathbf{u}=[u_1, u_2, u_3]^{\mathrm{T}}$ are the controllers. By designing proper controllers, variable states x', y', and z' in system (21) track the signals φ_1, φ_2, and φ_3, respectively. Here we define the error between variable states and target signals as follows:

$$\begin{aligned} e_1(t) &= x'(t) - \varphi_1(t) \\ e_2(t) &= y'(t) - \varphi_2(t) \\ e_3(t) &= z'(t) - \varphi_3(t). \end{aligned} \tag{22}$$

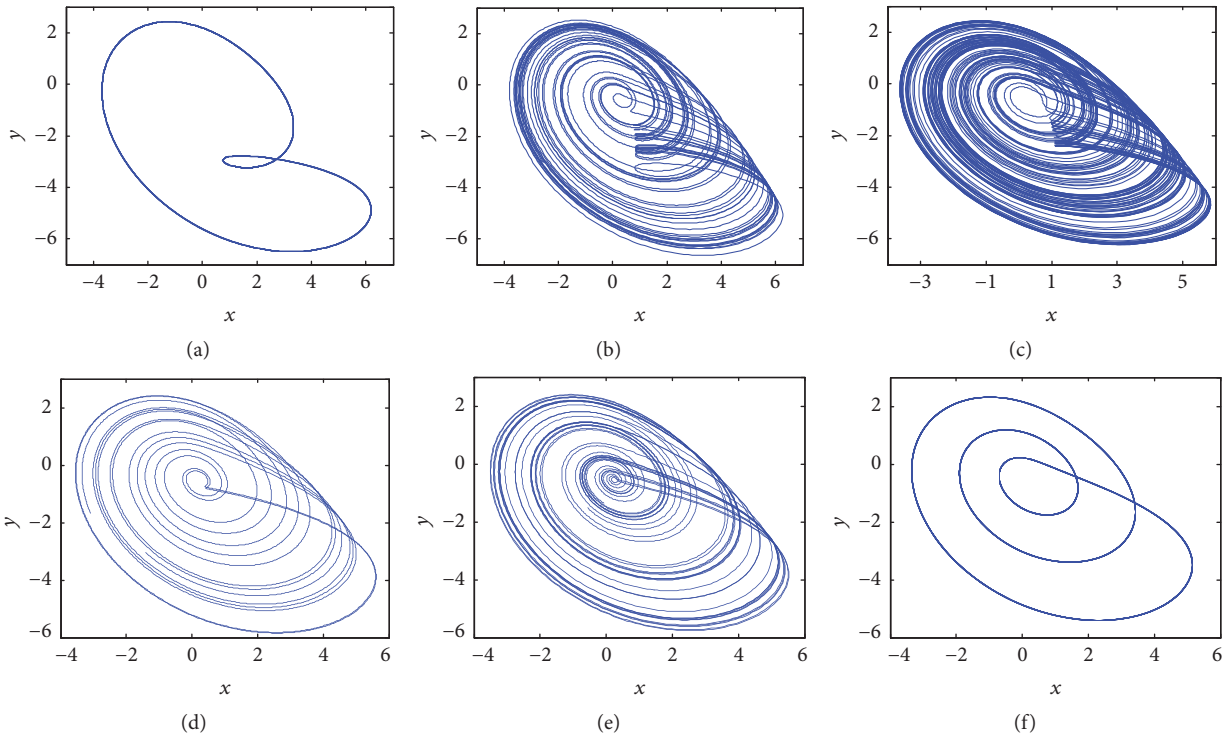

FIGURE 4: Phase portraits on x-y plane of attractor obtained by simulation. (a) q=1, a=0.504. (b) q=0.8, a=0.504. (c) q=0.6, a=0.504. (d) q=1, a=0.441. (e) q=0.8, a=0.441. (f) q=0.6, a=0.441.

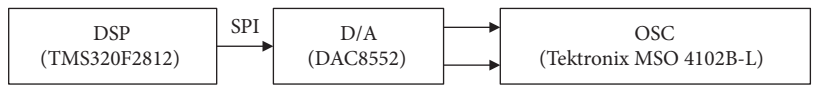

FIGURE 5: Simplified block diagram for DSP implementation of a fractional-order chaotic system.

Definition 2. For the tracking system (21), if there is a controller $\mathbf{u}$ making $e_i(t) \longrightarrow 0$, $(i = 1, 2, 3)$, then variable states x', y', and z' of the system are synchronized with the signals φ_1, φ_2, and φ_3, respectively.

For a fractional-order linear system given by ${}^{*}D_{t_0}^{q} x'(t) = -kx'(t)$, where k is a real constant, if $k>0$, then $x(t)$ convergences to zero with the increase of time t. In this paper, the obtained error system ${}^{*}D_{t_0}^{q} e_i(t) = -k_i e_i(t)$ $(i$=1, 2, 3) will satisfy this property.

4.1. Tracking the Constant Signals. Let variable states x', y', and z' in system (21) track the constants φ_1, φ_2, and φ_3, respectively. It means that the system will be controlled to a fixed point. Suppose that we have the following controllers:

$$\begin{aligned} u_1 &= -k_1\left(x' - \varphi_1\right) + y' + z' \\ u_2 &= -k_2\left(y' - \varphi_2\right) - x' - ay' \\ u_3 &= -k_3\left(z' - \varphi_3\right) - b + cz' - x'z'. \end{aligned} \tag{23}$$

By subtracting (11) from (21), we have

$$\begin{aligned} {}^{*}D_{t_0}^{q} e_1 &= {}^{*}D_{t_0}^{q} x' = -k_1\left(x' - \varphi_1\right) = -k_1 e_1 \\ {}^{*}D_{t_0}^{q} e_2 &= {}^{*}D_{t_0}^{q} y' = -k_2\left(y' - \varphi_2\right) = -k_2 e_2 \\ {}^{*}D_{t_0}^{q} e_3 &= {}^{*}D_{t_0}^{q} z' = -k_3\left(z' - \varphi_3\right) = -k_3 e_3. \end{aligned} \tag{24}$$

Linearizing error system (24) at its equilibrium point e_1=e_2=e_3=0 yields the Jacobin matrix $\mathbf{J}$ as shown in (25). The eigenvalues of $\mathbf{J}$ are $\lambda_1 = \lambda_2 = \lambda_3 = -1$, and they satisfy $|\arg(\lambda_i)| > q\pi/2$. So, the error system (24) is asymptotically stable at its equilibrium point.

$$\mathbf{J} = \begin{bmatrix} -k_1 & 0 & 0 \\ 0 & -k_2 & 0 \\ 0 & 0 & -k_3 \end{bmatrix}. \tag{25}$$

The error system (24) with controller is solved by adopting ADM, too. The obtained approximate solution is shown in (26)-(31).

$$\begin{bmatrix} x'_{m+1} \\ y'_{m+1} \\ z'_{m+1} \end{bmatrix} = \begin{bmatrix} x'_{10} + x'_{11} + x'_{12} + x'_{13} + x'_{14} \\ y'_{10} + y'_{11} + y'_{12} + y'_{13} + y'_{14} \\ z'_{10} + z'_{11} + z'_{12} + z'_{13} + z'_{14} \end{bmatrix}, \tag{26}$$

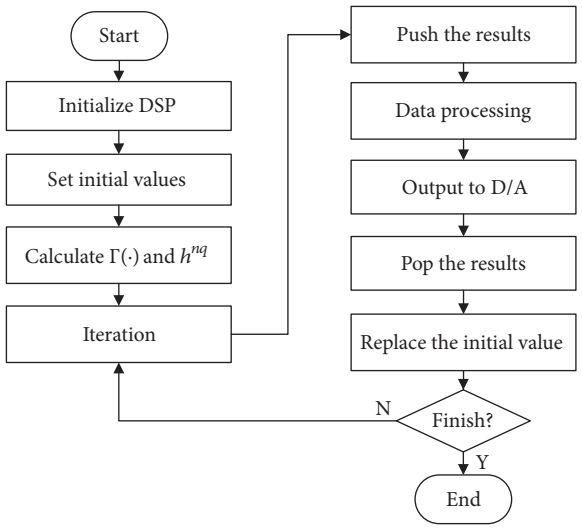

Figure 6: Flow chart for DSP implementation of a fractional-order chaotic system.

where

$$
\begin{aligned}
C_{10} &= x'_m \\
C_{20} &= y'_m \\
C_{30} &= z'_m \\
C_{100} &= k_1\varphi_1 \\
C_{200} &= k_2\varphi_2 \\
C_{300} &= k_3\varphi_3 \\
x'_{10} &= C_{10} + C_{100}\frac{h^q}{\Gamma(q+1)} \\
y'_{10} &= C_{20} + C_{200}\frac{h^q}{\Gamma(q+1)} \\
z'_{10} &= C_{30} + C_{300}\frac{h^q}{\Gamma(q+1)},
\end{aligned}
\tag{27}
$$

$$
\begin{aligned}
C_{11} &= -k_1C_{10} \\
C_{110} &= -k_1C_{100} \\
C_{21} &= -k_2C_{20} \\
C_{210} &= -k_2C_{200} \\
C_{31} &= -k_3C_{30} \\
C_{310} &= -k_3C_{300} \\
x'_{11} &= C_{11}\frac{h^q}{\Gamma(q+1)} + C_{110}\frac{h^{2q}}{\Gamma(2q+1)} \\
y'_{11} &= C_{21}\frac{h^q}{\Gamma(q+1)} + C_{210}\frac{h^{2q}}{\Gamma(2q+1)} \\
z'_{11} &= C_{31}\frac{h^q}{\Gamma(q+1)} + C_{310}\frac{h^{2q}}{\Gamma(2q+1)},
\end{aligned}
\tag{28}
$$

$$
\begin{aligned}
C_{12} &= -k_1C_{11} \\
C_{120} &= -k_1C_{110} \\
C_{22} &= -k_2C_{21} \\
C_{220} &= -k_2C_{210} \\
C_{32} &= -k_3C_{31} \\
C_{320} &= -k_3C_{310} \\
x'_{12} &= C_{12}\frac{h^{2q}}{\Gamma(2q+1)} + C_{120}\frac{h^{3q}}{\Gamma(3q+1)} \\
y'_{12} &= C_{22}\frac{h^{2q}}{\Gamma(2q+1)} + C_{220}\frac{h^{3q}}{\Gamma(3q+1)} \\
z'_{12} &= C_{32}\frac{h^{2q}}{\Gamma(2q+1)} + C_{320}\frac{h^{3q}}{\Gamma(3q+1)},
\end{aligned}
\tag{29}
$$

$$
\begin{aligned}
C_{13} &= -k_1C_{12} \\
C_{130} &= -k_1C_{120} \\
C_{23} &= -k_2C_{22} \\
C_{230} &= -k_2C_{220} \\
C_{33} &= -k_3C_{32} \\
C_{330} &= -k_3C_{320} \\
x'_{13} &= C_{13}\frac{h^{3q}}{\Gamma(3q+1)} + C_{130}\frac{h^{4q}}{\Gamma(4q+1)} \\
y'_{13} &= C_{23}\frac{h^{3q}}{\Gamma(3q+1)} + C_{230}\frac{h^{4q}}{\Gamma(4q+1)} \\
z'_{13} &= C_{33}\frac{h^{3q}}{\Gamma(3q+1)} + C_{330}\frac{h^{4q}}{\Gamma(4q+1)},
\end{aligned}
\tag{30}
$$

$$
\begin{aligned}
C_{14} &= -k_1C_{13} \\
C_{140} &= -k_1C_{130} \\
C_{24} &= -k_2C_{23} \\
C_{240} &= -k_2C_{230} \\
C_{34} &= -k_3C_{33} \\
C_{340} &= -k_3C_{330} \\
x'_{14} &= C_{14}\frac{h^{4q}}{\Gamma(4q+1)} + C_{140}\frac{h^{5q}}{\Gamma(5q+1)} \\
y'_{14} &= C_{24}\frac{h^{4q}}{\Gamma(4q+1)} + C_{240}\frac{h^{5q}}{\Gamma(5q+1)}
\end{aligned}
$$

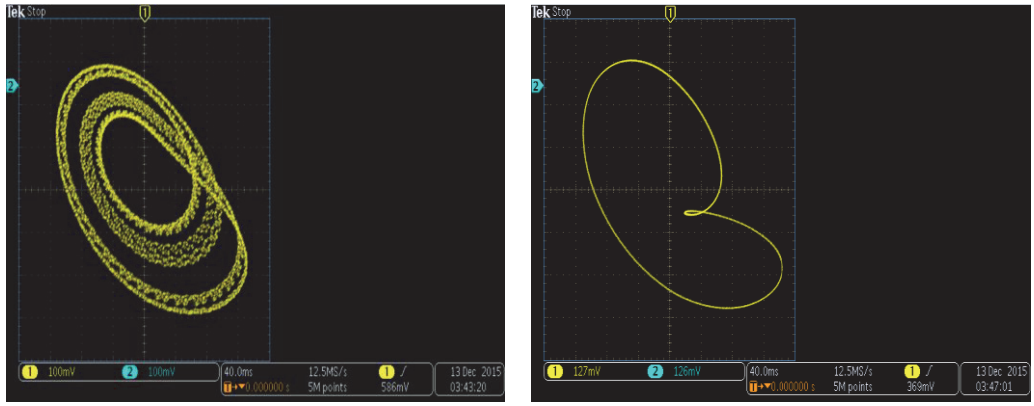

(a) (b)

Figure 7: Phase portraits on x-y plane of attractor displayed on oscilloscope. (a) q=0.373. (b) q=0.564.

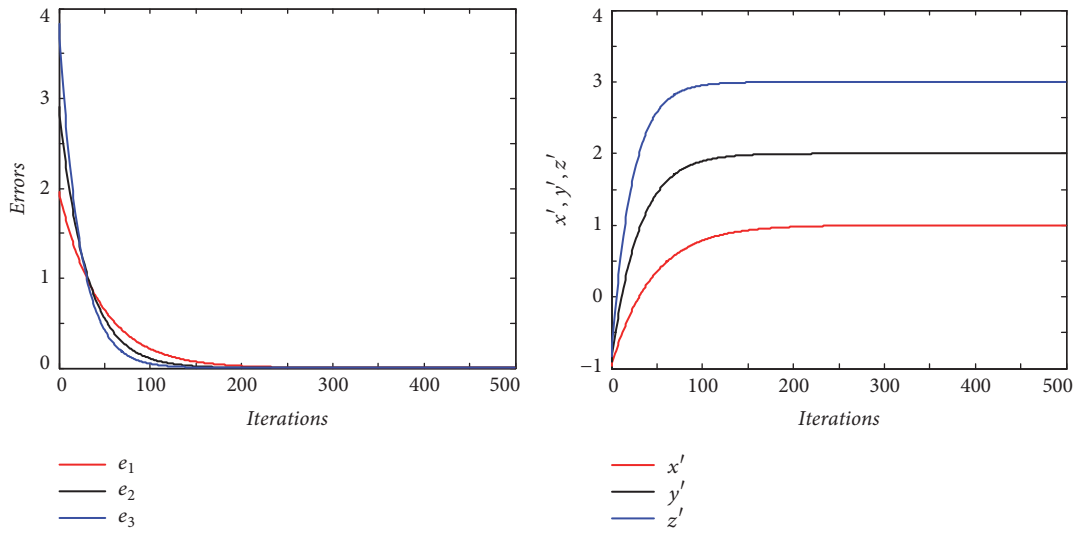

(a) (b)

Figure 8: Tracking constant signals. (a) Error curves of synchronization system. (b) Tracked variable states.

$$z'_{14} = C_{340}\frac{h^{4q}}{\Gamma(4q+1)} + C_{341}\frac{h^{5q}}{\Gamma(5q+1)} \tag{31}$$

Setting q=0.98, $[k_1, k_2, k_3]$=[2, 3, 4], and $[\varphi_1, \varphi_2, \varphi_3]$=[1, 2, 3] in (24), respectively, the synchronizations of fractional-order Rössler systems are simulated. The error curves of simulation results are displayed in Figure 8(a). It shows that the evolution of the synchronization errors asymptotically converges to zero. Eventually $[x', y'z']$= $[\varphi_1, \varphi_2, \varphi_3]$=[1, 2, 3] as shown in Figure 8(b). The results verify that the variable states x', y', and z' in system (21) track the constants φ_1, φ_2, and φ_3, successfully.

4.2. Tracking the Fractional-Order Chaotic Signals. In this case, φ_1, φ_2, and φ_3 are fractional q-order differentiable function signals. Suppose that $\varphi_1(t) = x(t)$, $\varphi_2(t) = y(t)$, and $\varphi_3(t) = z(t)$, from the driving system given by

$$\begin{aligned} {}^{*}D^{q}_{t_0}x &= -y - z \\ {}^{*}D^{q}_{t_0}y &= x + ay \\ {}^{*}D^{q}_{t_0}z &= b - cz + xz. \end{aligned} \tag{32}$$

The controller's equations are as given as follows:

$$\begin{aligned} u_1 &= -k_1\left(x' - \varphi_1\right) + y' + z' + {}^{*}D^{q}_{t_0}\varphi_1(t) \\ u_2 &= -k_2\left(y' - \varphi_2\right) - x' - ay' + {}^{*}D^{q}_{t_0}\varphi_2(t) \\ u_3 &= -k_3\left(z' - \varphi_3\right) - b + cz' - x'z' + {}^{*}D^{q}_{t_0}\varphi_3(t). \end{aligned} \tag{33}$$

Now system (21) is denoted as

$$\begin{aligned} {}^{*}D^{q}_{t_0}x' &= -k_1\left(x' - \varphi_1\right) + {}^{*}D^{q}_{t_0}\varphi_1(t) \\ {}^{*}D^{q}_{t_0}y' &= -k_2\left(y' - \varphi_2\right) + {}^{*}D^{q}_{t_0}\varphi_2(t) \end{aligned}$$

$$
{}^{*}D_{t_0}^{q} z' = -k_3 \left(z' - \varphi_3\right) + {}^{*}D_{t_0}^{q} \varphi_3 (t), \tag{34}
$$

Obviously,

$$
\begin{aligned}
{}^{*}D_{t_0}^{q} x' - {}^{*}D_{t_0}^{q} \varphi_1 (t) &= {}^{*}D_{t_0}^{q} e_1 = -k_1 \left(x' - \varphi_1\right) \\
&= -k_1 e_1 \\
{}^{*}D_{t_0}^{q} y' - {}^{*}D_{t_0}^{q} \varphi_2 (t) &= {}^{*}D_{t_0}^{q} e_2 = -k_2 \left(y' - \varphi_2\right) \\
&= -k_2 e_2 \\
{}^{*}D_{t_0}^{q} z' - {}^{*}D_{t_0}^{q} \varphi_3 (t) &= {}^{*}D_{t_0}^{q} e_3 = -k_3 \left(z' - \varphi_3\right) \\
&= -k_3 e_3,
\end{aligned} \tag{35}
$$

and system (21) can be synchronized with the driving signals. Moreover, since $\varphi_1(t) = x(t)$, $\varphi_2(t) = y(t)$, and $\varphi_3(t) = z(t)$, system (21) is given by

$$
\begin{aligned}
{}^{*}D_{t_0}^{q} x' &= -k_1 \left(x' - x\right) + {}^{*}D_{t_0}^{q} x (t) \\
&= -k_1 \left(x' - x\right) - y - z \\
{}^{*}D_{t_0}^{q} y' &= -k_2 \left(y' - y\right) + {}^{*}D_{t_0}^{q} y (t) \\
&= -k_2 \left(y' - y\right) + x + ay \\
{}^{*}D_{t_0}^{q} z' &= -k_3 \left(z' - z\right) + {}^{*}D_{t_0}^{q} z (t) \\
&= -k_3 \left(z' - z\right) + b - cz + xz,
\end{aligned} \tag{36}
$$

System (36) is solved by adopting ADM, and the solution is as follows:

$$
\begin{bmatrix} x'_{m+1} \\ y'_{m+1} \\ z'_{m+1} \end{bmatrix} = \begin{bmatrix} x'_{10} + x'_{11} + x'_{12} + x'_{13} + x'_{14} \\ y'_{10} + y'_{11} + y'_{12} + y'_{13} + y'_{14} \\ z'_{10} + z'_{11} + z'_{12} + z'_{13} + z'_{14} \end{bmatrix}, \tag{37}
$$

where

$$
\begin{aligned}
x'_{10} &= x'_{m} \\
y'_{10} &= y'_{m} \\
z'_{10} &= z'_{m} + b \frac{h^q}{\Gamma (q+1)} \\
G_{10} &= x'_{10} \\
G_{20} &= y'_{10} \\
G_{30} &= z'_{0},
\end{aligned} \tag{38}
$$

$$
\begin{aligned}
G_{11} &= -k_1 \left(G_{10} - C_{10}\right) + C_{11} \\
G_{110} &= C_{110} \\
x'_{11} &= G_{11} \frac{h^q}{\Gamma (q+1)} + G_{110} \frac{h^{2q}}{\Gamma (2q+1)} \\
G_{21} &= -k_2 \left(G_{20} - C_{20}\right) + C_{21} \\
y'_{11} &= G_{21} \frac{h^q}{\Gamma (q+1)} \\
G_{31} &= -k_3 \left(G_{30} - C_{30}\right) + C_{31} \\
G_{310} &= C_{310} - k_3 b \\
z_{11} &= G_{31} \frac{h^q}{\Gamma (q+1)} + G_{310} \frac{h^{2q}}{\Gamma (2q+1)},
\end{aligned} \tag{39}
$$

$$
\begin{aligned}
G_{12} &= -k_1 \left(G_{11} - C_{11}\right) + C_{12} \\
G_{120} &= -k_1 \left(G_{110} - C_{110}\right) + C_{120} \\
x'_{12} &= G_{12} \frac{h^{2q}}{\Gamma (2q+1)} + G_{120} \frac{h^{3q}}{\Gamma (3q+1)} \\
G_{22} &= -k_2 \left(G_{21} - C_{21}\right) + C_{22} \\
G_{220} &= C_{220} \\
y'_{12} &= G_{22} \frac{h^{2q}}{\Gamma (2q+1)} + G_{220} \frac{h^{3q}}{\Gamma (3q+1)} \\
G_{32} &= -k_3 \left(G_{31} - C_{31}\right) + C_{32} \\
G_{320} &= -k_2 \left(G_{310} - C_{320}\right) + C_{320} \\
G_{321} &= C_{321} \\
z'_{12} &= G_{32} \frac{h^{2q}}{\Gamma (2q+1)} + G_{320} \frac{h^{3q}}{\Gamma (3q+1)} \\
&\quad + G_{321} \frac{h^{4q}}{\Gamma (4q+1)},
\end{aligned} \tag{40}
$$

$$
\begin{aligned}
G_{13} &= -k_1 \left(G_{12} - C_{12}\right) + C_{13} \\
G_{130} &= -k_1 \left(G_{120} - C_{120}\right) + C_{130} \\
G_{131} &= C_{131} \\
x'_{13} &= G_{13} \frac{h^{3q}}{\Gamma (3q+1)} + G_{130} \frac{h^{4q}}{\Gamma (4q+1)} \\
&\quad + G_{131} \frac{h^{5q}}{\Gamma (5q+1)} \\
G_{23} &= -k_2 \left(G_{22} - C_{22}\right) + C_{23} \\
G_{230} &= -k_2 \left(G_{220} - C_{220}\right) + C_{230} \\
y'_{13} &= G_{23} \frac{h^{3q}}{\Gamma (3q+1)} + G_{230} \frac{h^{4q}}{\Gamma (4q+1)}
\end{aligned}
$$

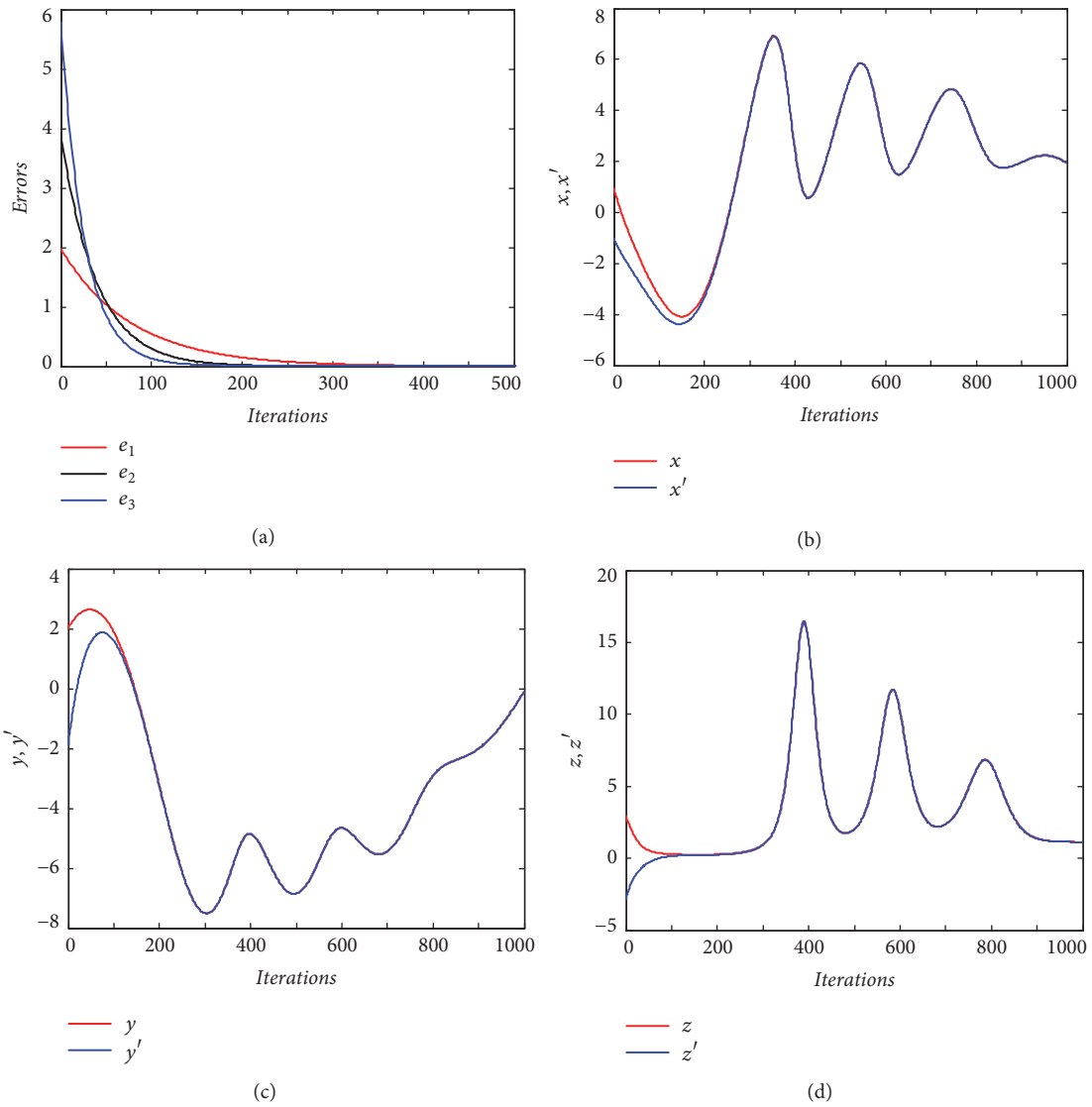

FIGURE 9: Tracking chaotic signal from the master system. (a) Error curves of synchronization system. (b) Tracked variable state (x and x'). (c) Tracked variable state (y and y'). (d) Tracked variable state (z and z').

$$
\begin{aligned}
G_{33} &= -k_3\left(G_{32} - C_{32}\right) + C_{33}\\
G_{330} &= -k_3\left(G_{320} - C_{320}\right) + C_{330}\\
G_{331} &= C_{331}\\
z'_{13} &= G_{33}\frac{h^{3q}}{\Gamma\left(3q+1\right)} + G_{330}\frac{h^{4q}}{\Gamma\left(4q+1\right)}\\
&\quad + G_{331}\frac{h^{5q}}{\Gamma\left(5q+1\right)},\\
G_{14} &= -k_1\left(G_{13} - C_{13}\right) + C_{14}\\
G_{140} &= -k_1\left(G_{130} - C_{130}\right) + C_{140}\\
G_{141} &= -k1\left(G_{131} - C_{131}\right) + C_{141}
\end{aligned}
\tag{41}
$$

$$
\begin{aligned}
x'_{14} &= G_{14}\frac{h^{4q}}{\Gamma\left(4q+1\right)} + G_{140}\frac{h^{5q}}{\Gamma\left(5q+1\right)}\\
&\quad + G_{141}\frac{h^{6q}}{\Gamma\left(6q+1\right)}\\
G_{24} &= -k_2\left(G_{23} - C_{23}\right) + C_{24}\\
G_{240} &= -k_2\left(G_{230} - C_{230}\right) + C_{240}\\
G_{241} &= C_{131}\\
y'_{14} &= G_{24}\frac{h^{4q}}{\Gamma\left(4q+1\right)} + G_{240}\frac{h^{5q}}{\Gamma\left(5q+1\right)}\\
&\quad + G_{241}\frac{h^{6q}}{\Gamma\left(6q+1\right)}\\
G_{340} &= -k_3\left(G_{33} - C_{33}\right) + C_{340}
\end{aligned}
$$

$$G_{341} = -k_3\left(G_{330} - C_{330}\right) + C_{341}$$

$$G_{342} = -k_3\left(G_{331} - C_{331}\right) + C_{342}$$

$$G_{343} = C_{343}$$

$$z'_{14} = G_{340}\frac{h^{4q}}{\Gamma\left(4q+1\right)} + G_{341}\frac{h^{5q}}{\Gamma\left(5q+1\right)} + G_{342}\frac{h^{6q}}{\Gamma\left(6q+1\right)} + G_{343}\frac{h^{7q}}{\Gamma\left(7q+1\right)} \tag{42}$$

In (37)-(42), C is the same as that in the solution (see (13)-(18)) of the driving system.

In (36), let a=0.55, b=2, c=4, q=0.95, and $[k_1, k_2, k_3]$=[1, 2, 3]. The simulation results are shown in Figure 9. Figure 9(a) demonstrates that synchronization between two fractional-order Rössler systems with the designed controller is achieved by employing ADM. Figures 9(b), 9(c), and 9(d) illustrate the changes of the tracked variable states, and they show that the system can track the chaotic signals from master system successfully.

5. Conclusions

The fractional-order Rössler system is solved by adopting Adomian decomposition method, and the numerical solution is presented. Based on the given iteration, dynamics and synchronizations of the fractional-order Rössler system are investigated.

(1) Compared with its integer-order counterpart, the fractional-order Rössler system shows different dynamics. q affects the dynamic characteristics of the fractional-order chaotic system, and it is another bifurcation parameter except for the system parameters a, b, and c.

(2) When the fractional-order Rössler system is solved by employing ADM, the lowest order at which the chaos exists is about 1.119 when q=0.373 with a=0.55, b=2, c=4, and h=0.01. The results are more accurate than that by adopting frequency-domain method.

(3) Based on ADM, the tracking synchronization of fractional-order Rössler systems is realized. It lays the foundation for the extensive applications research of the fractional-order chaotic system.

Data Availability

The data used to support the findings of this study are included within the article.

Conflicts of Interest

The authors declare that there are no conflicts of interest regarding the publication of this paper.

Acknowledgments

This work was supported by the Postdoctoral Innovative Talents Support Program [No. BX20180386] and the National Natural Science Foundation of China (Grant Nos. 11747150, 61161006, and 61573383).

References

[1] H. H. Wang, K. H. Sun, and S. B. He, "Dynamic analysis and implementation of a digital signal processor of a fractional-order Lorenz-Stenflo system based on the Adomian decomposition method," *Physica Scripta*, vol. 90, no. 1, Article ID 015206, 2015.

[2] H. H. Wang, K. H. Sun, and S. B. He, "Characteristic analysis and DSP realization of fractional-order simplified Lorenz system based on Adomian decomposition method," *International Journal of Bifurcation and Chaos*, vol. 25, no. 6, Article ID 1550085, 2015.

[3] O. E. Rössler, "An equation for continuous chaos," *Physics Letters A*, vol. 57, no. 5, pp. 397-398, 1976.

[4] C. Letellier, P. Dutertre, and B. Maheu, "Unstable periodic orbits and templates of the Rössler system: Toward a systematic topological characterization," *Chaos: An Interdisciplinary Journal of Nonlinear Science*, vol. 5, no. 1, pp. 271–282, 1995.

[5] R. M. Tudoran and A. Gîrban, "On the completely integrable case of the Rössler system," *Journal of Mathematical Physics*, vol. 53, no. 5, Article ID 052701, 2012.

[6] N. V. Kuznetsov, T. N. Mokaev, and P. A. Vasilyev, "Numerical justification of Leonov conjecture on LYApunov dimension of Rossler attractor," *Communications in Nonlinear Science and Numerical Simulation*, vol. 19, no. 4, pp. 1027–1034, 2014.

[7] C. Li and G. Chen, "Chaos and hyperchaos in the fractional-order Rössler equations," *Physica A: Statistical Mechanics and Its Applications*, vol. 341, no. 1–4, pp. 55–61, 2004.

[8] S. Wang, Y.-G. Yu, H. Wang, and A. Rahmani, "Function projective lag synchronization of fractional-order chaotic systems," *Chinese Physics B*, vol. 23, no. 4, Article ID 040502, 2014.

[9] A. Razminia, V. J. Majd, and D. Baleanu, "Chaotic incommensurate fractional order Rössler system: active control and synchronization," *Advances in Difference Equations*, vol. 2011, no. 1, pp. 1–12, 2011.

[10] H. H. Sun, A. A. Abdelwahab, and B. Onaral, "Linear approximation of transfer function with a pole of fractional order," *IEEE Transactions on Automatic Control*, vol. 29, no. 5, pp. 441–444, 1984.

[11] W. M. Ahmad and J. C. Sprott, "Chaos in fractional-order autonomous nonlinear systems," *Chaos, Solitons & Fractals*, vol. 16, no. 2, pp. 339–351, 2003.

[12] M. S. Tavazoei and M. Haeri, "Unreliability of frequency-domain approximation in recognising chaos in fractional-order systems," *IET Signal Processing*, vol. 1, no. 4, pp. 171–181, 2007.

[13] M. S. Tavazoei and M. Haeri, "Limitations of frequency domain approximation for detecting chaos in fractional order systems," *Nonlinear Analysis: Theory, Methods & Applications*, vol. 69, no. 4, pp. 1299–1320, 2008.

[14] K. Diethelm, "An algorithm for the numerical solution of differential equations of fractional order," *Electronic Transactions on Numerical Analysis*, vol. 5, pp. 1–6, 1997.

[15] K. Diethelm, N. J. Ford, and A. D. Freed, "A predictor-corrector approach for the numerical solution of fractional differential equations," *Nonlinear Dynamics*, vol. 29, no. 1–4, pp. 3–22, 2002.

[16] Y. Wang, K. Sun, S. He, and H. Wang, "Dynamics of fractional-order sinusoidally forced simplified Lorenz system and its

synchronization," *The European Physical Journal Special Topics*, vol. 223, no. 8, pp. 1591–1600, 2014.

[17] G. Adomian, "A new approach to nonlinear partial differential equations," *Journal of Mathematical Analysis and Applications*, vol. 102, no. 2, pp. 420–434, 1984.

[18] D. Cafagna and G. Grassi, "Bifurcation and chaos in the fractional-order Chen system via a time-domain approach," *International Journal of Bifurcation and Chaos*, vol. 18, no. 7, pp. 1845–1863, 2008.

[19] R. Caponetto and S. Fazzino, "An application of Adomian decomposition for analysis of fractional-order chaotic systems," *International Journal of Bifurcation and Chaos*, vol. 23, no. 3, Article ID 1350050, 2013.

[20] S. B. He, K. H. Sun, and H. H. Wang, "Solution of the fractional-order chaotic system based on Adomian decomposition algorithm and its complexity analysis," *Acta Physica Sinica*, vol. 63, no. 3, Article ID 030502, 2014 (Chinese).

[21] S. Liu, Y. Yu, and S. Zhang, "Robust synchronization of memristor-based fractional-order Hopfield neural networks with parameter uncertainties," *Neural Computing and Applications*, vol. 1, pp. 1–10, 2017.

[22] L. Zhou, C. Wang, S. Du, and L. Zhou, "Cluster synchronization on multiple nonlinearly coupled dynamical subnetworks of complex networks with nonidentical nodes," *IEEE Transactions on Neural Networks and Learning Systems*, vol. 28, no. 3, pp. 570–583, 2017.

[23] L. Zhou and C. Wang, "Hybrid combinatorial synchronization on multiple sub-networks of complex network with unknown boundaries of uncertainties," *Optik - International Journal for Light and Electron Optics*, vol. 127, no. 22, pp. 11037–11048, 2016.

[24] K. H. Sun, Y. Wang, and Y. L. Wang, "Hyperchaos behaviors and chaos synchronization of two unidirectional coupled simplified Lorenz systems," *Journal of Central South University*, vol. 21, no. 3, pp. 948–955, 2014.

[25] D. Chen, W. Zhao, J. C. Sprott, and X. Ma, "Application of Takagi-Sugeno fuzzy model to a class of chaotic synchronization and anti-synchronization," *Nonlinear Dynamics*, vol. 73, no. 3, pp. 1495–1505, 2013.

[26] S. Zhang, Y. Yu, G. Wen, and A. Rahmani, "Lag-generalized synchronization of time-delay chaotic systems with stochastic perturbation," *Modern Physics Letters B. Condensed Matter Physics, Statistical Physics, Applied Physics*, vol. 30, no. 1, Article ID 1550263, 2016.

[27] S. Bhalekar and V. Daftardar-Gejji, "Synchronization of different fractional order chaotic systems using active control," *Communications in Nonlinear Science and Numerical Simulation*, vol. 15, no. 11, pp. 3536–3546, 2010.

[28] I. El Gammoudi and M. Feki, "Synchronization of integer order and fractional order Chua's systems using robust observer," *Communications in Nonlinear Science and Numerical Simulation*, vol. 18, no. 3, pp. 625–638, 2013.

[29] S. Momani and K. Al-Khaled, "Numerical solutions for systems of fractional differential equations by the decomposition method," *Applied Mathematics and Computation*, vol. 162, no. 3, pp. 1351–1365, 2005.

[30] V. Daftardar-Gejji and H. Jafari, "Adomian decomposition: a tool for solving a system of fractional differential equations," *Journal of Mathematical Analysis and Applications*, vol. 301, no. 2, pp. 508–518, 2005.

[31] A. Carpinteri and F. Mainardi, *Fractal and Fractional Calculus in Continuum Mechanics*, Springer-Verlag, Wien, Austria, 1997.

[32] N. T. Shawagfeh, "Analytical approximate solutions for nonlinear fractional differential equations," *Applied Mathematics and Computation*, vol. 131, no. 2-3, pp. 517–529, 2002.

[33] K. Abbaoui and Y. Cherruault, "Convergence of Adomian's method applied to differential equations," *Computers & Mathematics with Applications*, vol. 28, no. 5, pp. 103–109, 1994.

[34] H. F. von Bremen, F. E. Udwadia, and W. Proskurowski, "An efficient QR based method for the computation of Lyapunov exponents," *Physica D: Nonlinear Phenomena*, vol. 101, no. 1-2, pp. 1–16, 1997.

Hindawi
Complexity
Volume 2018, Article ID 1872943, 12 pages
https://doi.org/10.1155/2018/1872943

Research Article

Adaptive Inverse Control Based on Kriging Algorithm and Lyapunov Theory of Crawler Electromechanical System

Guanyu Zhang[1,2], **Yitian Wang**[1,2], **Yiyao Fan**[1,2] and **Chen Chen**[1,2]

[1] *College of Instrumentation & Electrical Engineering, Jilin University, Changchun 130061, China*
[2] *Key Laboratory of Geo-Exploration Instruments, Ministry of Education of China, Jilin University, Changchun 130061, China*

Correspondence should be addressed to Chen Chen; cchen@jlu.edu.cn

Received 17 September 2018; Accepted 1 November 2018; Published 2 December 2018

Guest Editor: Viet-Thanh Pham

The electromechanical system of a crawler is a multi-input, multioutput strongly coupled nonlinear system. In this study, an adaptive inverse control method based on kriging algorithm and Lyapunov theory is proposed to improve control accuracy during adaptive driving. The electromechanical coupling model of the electromechanical system is established on the basis of the dynamic analysis of the crawler. In accordance with the kriging algorithm, the inverse model of the electromechanical system of the crawler is established by offline data. The adaptive travel control law of the crawler is obtained on the basis of Lyapunov theory. Combined with the kriging algorithm, the adaptive driving reverse control method is designed, and the online system is used to update and perfect the inverse system model in real time. Finally, the virtual prototype model of the crawler is established, and the control effect of the adaptive inverse control method is verified by theoretical analysis and virtual prototype simulation.

1. Introduction

As the most common construction machinery traveling device used in engineering applications, the crawler mechanism incurs increasing requirements on the driving force due to the trend of large-scale construction vehicles. Therefore, increasing crawler-type construction vehicles use a motor as their driving mode. On the basis of the characteristics of the motor itself, the electromechanical system of a crawler has become a typical multi-input, multioutput (MIMO) strong coupling and nonlinear dynamic model. Hence, with the development of intelligent control technology, intelligent modeling technologies have been applied extensively to the inverse system control for this complex MIMO system, which provides the possibility of precise control of the adaptive travel process of a crawler. Among these technologies, inverse system control is a control strategy based on feedback linearization method. The basic idea is as follows. First, the inverse system model of the controlled object is established, and the inverse system model and the controlled object are connected in series to form the pseudolinear compound method, thereby realizing the approximate linearization and basic decoupling of the controlled object. Additional controllers are then designed for each subsystem after linearization and decoupling using various mature controller design methods to control the multivariable nonlinear system effectively [1–3].

In the existing inverse control research, neural network algorithm is the most commonly used method in inverse modeling [4, 5]. Alexandridis, Stogiannos, and Kyriou presented a novel control scheme based on the approximation of the inverse process dynamics with a radial basis function (RBF) neural network model trained with the fuzzy means algorithm [6]. Imtiaz, Assadzadeh, and Jamuar investigated the approximation capability of a neural network model. Inverse neural networks (INNs) were used to control the temperature of a biochemical reactor and its effect on ethanol production. An INN trained using the backpropagation learning algorithm from data sets of a fundamental model provided an artificial neural network application of the recognition and control of nonlinear systems [7]. Alanis, Ornelas-Tellez, and Sanchez presented a robust inverse optimal neural control approach to stabilize a discrete-time uncertain nonlinear system while simultaneously minimizing a meaningful

cost function, thereby improving the adaptability of a neural network by introducing an optimization algorithm [8]. Singh, Vinoth, and Kiran addressed the inverse dynamics of a three-degrees-of-freedom U-shaped planar parallel manipulator with three legs consisting of prismatic–prismatic–revolute joint arrangement, in which each leg has one active prismatic joint; they also proposed a proportional–derivative-like adaptive sliding mode control combined with a disturbance observer for the motion control of the proposed manipulator [9, 10]. Bilello proposed the recursive neural network theory to establish positive and inverse models simultaneously with a recurrent neural network, in which the nonlinear object can show good adaptivity under a control system [11]. J. Li, S. Li, and Chen developed an adaptive control strategy that combined a neural network inverse controller with an RBF network disturbance observer for a MIMO system with non-minimum phase and internal and external disturbances [12]. In electronic systems, Aravind and Alexander explored the inverse control effect of a neural network on an H-bridge inverter [13]. The aforementioned studies reveal that inverse control systems with a neural network have a good effect in many industrial fields. However, realizing real-time tracking control is difficult because of low training efficiency.

In addition, foreign scholars have worked on other algorithms with considerable experimentation and research to improve the performance of inverse control systems. In the optimal control aspect, Ornelas-Tellez, Sanchez, and Loukianov presented an inverse optimal control approach to prevent solving the associated Hamilton–Jacobi–Bellman equation and minimize the cost function in stabilizing discrete-time nonlinear systems [14]. El-Hussieny, Abouelsoud, and Assal used particle swarm optimization to retrieve the unknown cost in their proposed ILQR problem; they proposed an evolving ILQR algorithm in refining the learned cost once new unseen demonstrations exist to overcome the overfitting problem [15]. In the fuzzy control aspect, Boukezzoula et al. applied the Takagi–Sugeno fuzzy model and the fuzzy mathematical model to identify the inverse model of nonlinear systems [16]. Chen, Zhang, and Zhao et al. proposed an independent adaptive fuzzy control system of nominal dynamics and uncertain parts to control an underactuated underwater vehicle with uncertainties based on a computed torque controller [17]. In the aspect of adaptive control, Rahideh, Bajodah, and Shaheed investigated the development and experimental implementation of an adaptive dynamic nonlinear model inversion control law for a twin rotor MIMO system using artificial neural networks; they used a highly nonlinear aerodynamic test rig with complex cross-coupled dynamics to represent the control challenges of modern air vehicles [18]. Wang, Chen, and Jian et al. proposed a new adaptive inverse control method based on a recently developed maximum correntropy criterion algorithm to improve the robustness of the adaptive inverse control against impulsive noises [19]. To some extent, the aforementioned algorithms improve the effectiveness of the inverse control. However, in a complex environment, the inverse modeling accuracy of the algorithms is extremely low.

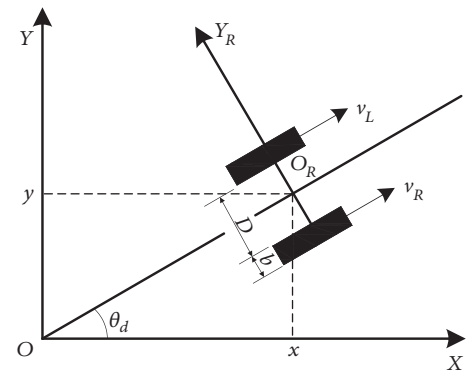

Figure 1: Kinematics analysis diagram of double crawlers.

Thus, the present study focuses on improving the inverse modeling precision and efficiency.

In this study, a kriging algorithm is used for the inverse modeling of complicated nonlinear MIMO systems to realize accurate online control. In comparison with other traditional function-modeling technologies, the kriging algorithm presents two advantages. First, instead of using all information, a kriging model uses only some data near the estimated point based on the known information of dynamic construction to simulate the unknown. Second, this model has local and global statistical features, which allow the analysis of the known trend and information dynamics [20].

In this study, it is assumed that the crawler can be unmanned in a complex environment. Because the electromechanical coupling model of crawler is a nonlinear system with multiple parameters and strong coupling, the problem of control precision is more difficult. In order to improve control accuracy during adaptive driving, a Lyapunov adaptive control algorithm, a kriging algorithm modeling, an adaptive inverse control design, and an inverse control in the application of the crawler, we analyze the control performance of adaptive inverse control algorithm through theoretical calculation and virtual prototype simulation. The control method provides a theoretical basis for the practical application of the crawler in the unmanned driving situation.

2. Modeling of the Crawler

2.1. Kinematics Analysis of the Crawler. As shown in Figure 1, a global coordinate system XOY and a moving coordinate system $X_RO_RY_R$ are established, where O_R is the geometric center of the crawler; O_RX_R points to the track; O_RY_R points to the track side and is perpendicular to O_RX_R; v_R and v_L are located on both sides of the crawler forward speed and direction, respectively; and O_RX_R is consistent. θ_d is the included angle between the global and moving coordinate systems; it is positive when deflected counterclockwise and negative when clockwise. D denotes the body width. In the course of driving, the crawler mainly relies on both sides of the track to achieve the speed difference. In the steering movement, the inner and outer crawlers undergo some side

slip. The sliding movement of the crawler belts on both sides is consistent, and the wheel displacement and tracks of the track internal mechanism will not occur because the crawler frame is an entirely rigid structure.

Figure 1 shows the crawler movement to t at the moment. The state equation of motion can be expressed as

$$\dot{W} = \begin{bmatrix} \dot{x} \\ \dot{y} \\ \dot{\theta}_d \end{bmatrix} = \begin{bmatrix} \frac{1}{2}\cos\theta_d & \frac{1}{2}\cos\theta_d \\ \frac{1}{2}\sin\theta_d & \frac{1}{2}\sin\theta_d \\ -\frac{1}{D+2b} & \frac{1}{D+2b} \end{bmatrix} \begin{bmatrix} v_L \\ v_R \end{bmatrix} \tag{1}$$

where W is the current travel position and attitude equation of the crawler. According to the structural characteristics and geometric center of the track O_R, linear velocity v_O and angular velocity ω_O determine the current left track speed v_L and the right track speed v_R.

$$\begin{bmatrix} v_L \\ v_R \end{bmatrix} = \begin{bmatrix} 1 & -\frac{D+2b}{2} \\ 1 & \frac{D+2b}{2} \end{bmatrix} \begin{bmatrix} v_O \\ \omega_O \end{bmatrix} \tag{2}$$

Substituting (2) into (1) yields

$$\dot{W} = \begin{bmatrix} \dot{x} \\ \dot{y} \\ \dot{\theta}_d \end{bmatrix} = \begin{bmatrix} \cos\theta_d & 0 \\ \sin\theta_d & 0 \\ 0 & 1 \end{bmatrix} \begin{bmatrix} v_O \\ \omega_O \end{bmatrix} = H_1 \begin{bmatrix} v_O \\ \omega_O \end{bmatrix} \tag{3}$$

where H_1 is the velocity state matrix of the crawler in the global coordinate system. On the basis of $v = R{\cdot}\omega$ and (2), the crawler radius during steering can be calculated as follows:

$$R = \frac{v_O}{\omega_O} = \frac{D+2b}{2} \cdot \frac{v_L + v_R}{v_L - v_R} \tag{4}$$

When $v_L = v_R$, both sides of the crawler speed are equal to the straight crawler line; that is, $R = \infty$; when $v_L \neq v_R$ and $v_L \neq -v_R$, the crawler is in the course of steering.

2.2. Kinetic Analysis of the Crawler. Figure 2 shows the process of driving the crawler to overcome the operational, wind, and steering resistance.

Figure 3 shows the crawler used for speed analysis. r_{Si} is the distance from the longitudinal axis of the track to the steering center, ω is the steering angular velocity of the vehicle, O_i is the geometric center of the track ground plane, O_i' is the intersection of the steering center with the vertical line and longitudinal axis of the track, O_{Si} is the instantaneous center of the track speed, b denotes the track width, and A_i represents the distance from O_i to O_{Si}.

The speed analysis indicates that, for the driving side of the crawler, the instantaneous center of the speed is away from the steering center position. For the brake side of the crawler, the instantaneous speed is in the center of the steering center position. The magnitude of the force acting

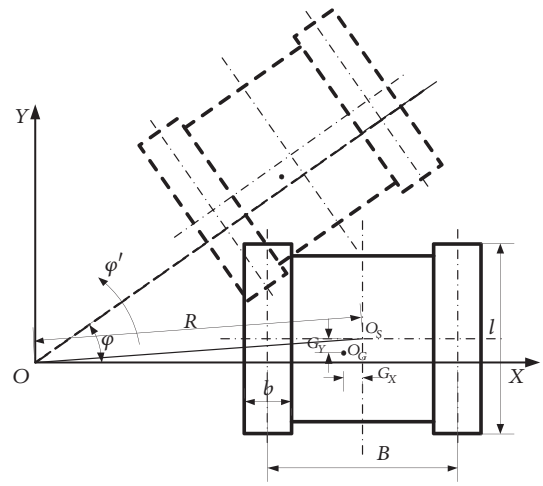

Figure 2: Turning diagram.

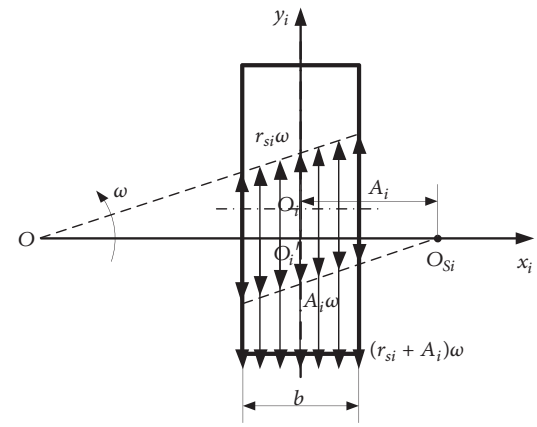

Figure 3: Velocity analysis of the crawlers.

on the track by the ground is related to the vertical load, and the direction is opposite to the absolute speed. Therefore, the speed of the crawler surface can be subjected to stress analysis after the evaluation.

The crawler ground is used for dxdy force analysis, as shown in Figure 4. A right-angle scale is constructed by taking the crawler center O_i as the origin, the longitudinal axis of the track as the Y_i-axis, and the straight line that crosses the center and perpendicular to the Y_i-axis as the X_i-axis. To withstand the role of trace friction dF_i, the direction and the absolute speed of the opposite for each dxdy crawler surface are expressed as follows:

$$\mathrm{d}F_i = \mu p(x, y)\,\mathrm{d}x\mathrm{d}y, \tag{5}$$

where $p(x, y)$ is the ground pressure ratio function and μ is the steering resistance coefficient, the value of which is correlated to the turning radius.

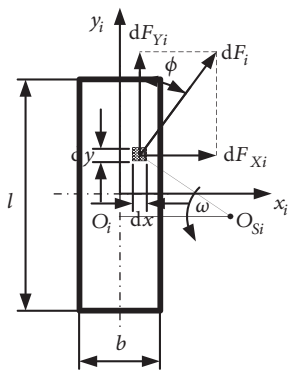

Figure 4: Force analysis of the crawler.

The component of dF_i in the direction of the X_i- and Y_i-axes is

$$dF_{Xi} = dF_i \sin\phi = dF_i \frac{y - D_i}{\sqrt{(x - A_i)^2 + (y - D_i)^2}} \quad (6)$$

$$dF_{Yi} = dF_i \cos\phi = dF_i \frac{x - A_i}{\sqrt{(x - A_i)^2 + (y - D_i)^2}} \quad (7)$$

When the crawler ground pressure is uniform, the available ground facing the track resistance torque (crawler ground geometric center O_i) is as follows:

$$\begin{aligned} M_{Oi} &= \iint y dF_{Xi} - \iint x dF_{Yi} \\ &= \int_{-l/2}^{l/2} \int_{-b/2}^{b/2} \left[\frac{y(y - D_i) + x(x - A_i)}{\sqrt{(x - A_i)^2 + (y - D_i)^2}} \right] \\ &\quad \cdot \mu p(x, y)\, dx dy \end{aligned} \quad (8)$$

where $p(x, y) = F_{Zi}/bl$, $i = 1, 2$, and D_i is the vertical offset of the instantaneous center.

After the integration obtains the single crawler on the longitudinal friction, lateral force and steering resistance torque occur. Figure 5 shows the crawler walking device balance analysis of stress. The overall force of the vehicle can be listed in a balance equation.

$$\begin{aligned} F_{X1} + F_{X2} &= 0 \\ F_{Y1} + F_{Y2} + F_{R1} + F_{R2} - F_{Q1} - F_{Q2} &= 0 \\ M_{O1} + M_{O2} - F_{Y1} r_{S1} - F_{Y2} r_{S2} + F_{X1} D_1 + F_{X2} D_2 &= 0 \end{aligned} \quad (9)$$

Steering or braking force is required to obtain the solution equilibrium equation. Thus, we can list the crawler travel device steering dynamic equation as

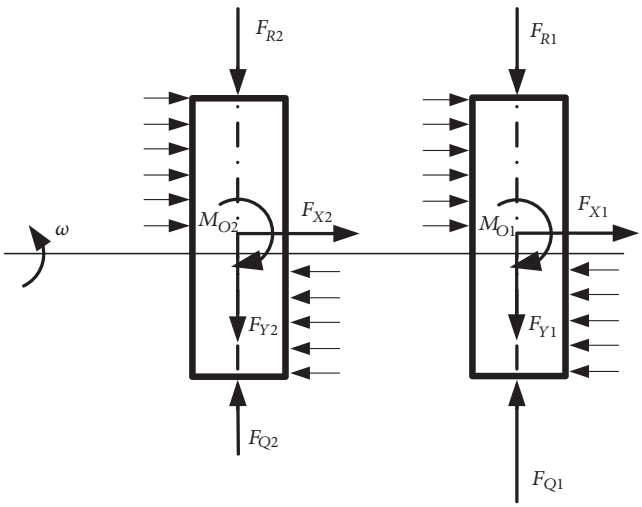

Figure 5: Force equilibrium diagram of the crawler.

$$\begin{aligned} \dot{v}_c &= \frac{F_{Q1} + F_{Q2} - (F_{R1} + F_{R2})}{m} \\ \dot{\omega}_c &= \frac{B[-F_{Q1} + F_{Q2} - (-F_{R1} + F_{R2})] - 2M}{J_O}. \end{aligned} \quad (10)$$

2.3. Electromechanical Coupling Modeling of the Crawler. The symmetrical three-phase asynchronous motor electric current oscillations in its windings are described by the six circuit voltage equations transformed next into the system of four Park's equations in the so-called "$\alpha\beta$–dq" reference system. We obtain the state equation of the induction motor, as shown as follows:

$$\begin{aligned} \frac{d\omega}{dt} &= \frac{n_p^2 L_m}{J L_r} \left(i_{sq} \psi_{rd} - i_{sd} \psi_{rq} \right) - \frac{n_p}{J} T_L \\ \frac{d\psi_{rd}}{dt} &= -\frac{1}{T_r} \psi_{rd} + (\omega_n - \omega) \psi_{rq} + \frac{L_m}{T_r} i_{sd} \\ \frac{d\psi_{rq}}{dt} &= -\frac{1}{T_r} \psi_{rq} - (\omega_n - \omega) \psi_{rd} + \frac{L_m}{T_r} i_{sq} \\ \frac{di_{sd}}{dt} &= \frac{L_m}{\sigma L_s L_r T_r} \psi_{rd} + \frac{L_m}{\sigma L_s L_r} \omega \psi_{rq} \\ &\quad - \frac{R_s L_r^2 + R_r L_m^2}{\sigma L_s L_r^2} i_{sd} + \omega_n i_{sq} + \frac{u_{sd}}{\sigma L_s} \\ \frac{di_{sq}}{dt} &= \frac{L_m}{\sigma L_s L_r T_r} \psi_{rq} + \frac{L_m}{\sigma L_s L_r} \omega \psi_{rd} \\ &\quad - \frac{R_s L_r^2 + R_r L_m^2}{\sigma L_s L_r^2} i_{sq} - \omega_n i_{sd} + \frac{u_{sq}}{\sigma L_s} \end{aligned} \quad (11)$$

where u_{sd} and u_{sq} are the stator voltages; R_s and R_r are the stator and rotor winding resistance, respectively; i_{sd} and i_{sq}

are the stator currents; Ψ_{rd} and Ψ_{rq} are the rotor fluxes; L_s and L_r are the self-inductance of the equivalent two-phase winding of the stator and the rotor, respectively; L_m is the mutual inductance between the equivalent windings when the stator and rotor are coaxial; n_p is the number of pole pairs; J is the motor's moment of inertia; T_L is the load torque; ω_n is the rotating magnetic field speed; ω is the rotor speed; $\sigma = 1 - L_m^2/(L_s \cdot L_r)$ is the flux leakage factor of the motor; and $T_r = L_r/R_r$ is the rotor's electromagnetic time constant.

The torque and motion are expressed as

$$T_e = n_P L_m \left(i_{sq} i_{rd} - i_{sd} i_{rq}\right) \tag{12}$$

$$\frac{J}{n_P}\frac{d\omega}{dt} = T_e - T_L. \tag{13}$$

Substituting (10) into (13) yields

$$\begin{aligned} Te_1 &= \left[F_{R1} - \frac{M}{B} - \frac{J_O r}{B^2 i}\left(\frac{d\omega_2}{dt} - \frac{d\omega_1}{dt}\right) + \frac{mr}{4i}\left(\frac{d\omega_2}{dt} + \frac{d\omega_1}{dt}\right)\right]\frac{r}{i} + \frac{J}{n_p}\frac{d\omega_1}{dt} \\ Te_2 &= \left[F_{R2} + \frac{M}{B} + \frac{J_O r}{B^2 i}\left(\frac{d\omega_2}{dt} - \frac{d\omega_1}{dt}\right) + \frac{mr}{4i}\left(\frac{d\omega_2}{dt} + \frac{d\omega_1}{dt}\right)\right]\frac{r}{i} + \frac{J}{n_p}\frac{d\omega_2}{dt}. \end{aligned} \tag{14}$$

According to the kinematic characteristics of the crawler, the dynamic equation of motion is expressed by combining (11) and (14), as shown as follows:

$$\begin{aligned}
&\frac{d\omega_1}{dt} \\
&= \frac{\left(J_O r^2/B^2 i^2 + (1/4)\left(mr^2/i^2\right) + J/n_p\right)\left\{\left(n_p L_m/L_r\right)\left(i_{sq1}\psi_{rd1} - i_{sd1}\psi_{rq1}\right) - \left[F_{R1} - mgl\mu_{\max}\left(2R_k\omega_2 - 2R_k\omega_1 - B\omega_2 - B\omega_1\right)/2R_k\left(2\omega_2\right)^{n_k}\left(\omega_2 - \omega_1\right)^{1-n_k} B\right](r/i)\right\}}{\left(J_O r^2/B^2 i^2 + (1/4)\left(mr^2/i^2\right) + J/n_p\right)^2 - \left(-J_O r^2/B^2 i^2 + (1/4)\left(mr^2/i^2\right)\right)^2} \\
&\quad - \cdots - \frac{\left(-J_O r^2/B^2 i^2 + (1/4)\left(mr^2/i^2\right)\right)\left\{\left(n_p L_m/L_r\right)\left(i_{sq2}\psi_{rd2} - i_{sd2}\psi_{rq2}\right) - \left[F_{R2} + mgl\mu_{\max}\left(2R_k\omega_2 - 2R_k\omega_1 - B\omega_2 - B\omega_1\right)/2R_k\left(2\omega_2\right)^{n_k}\left(\omega_2 - \omega_1\right)^{1-n_k} B\right](r/i)\right\}}{\left(J_O r^2/B^2 i^2 + (1/4)\left(mr^2/i^2\right) + J/n_p\right)^2 - \left(-J_O r^2/B^2 i^2 + (1/4)\left(mr^2/i^2\right)\right)^2} \\
&\frac{d\psi_{rd1}}{dt} = -\frac{1}{T_r}\psi_{rd1} + \left(\omega_{n1} - \omega_1\right)\psi_{rq1} + \frac{L_m}{T_r} i_{sd1} \\
&\frac{d\psi_{rq1}}{dt} = -\frac{1}{T_r}\psi_{rq1} - \left(\omega_{n1} - \omega_1\right)\psi_{rd1} + \frac{L_m}{T_r} i_{sq1} \\
&\frac{di_{sd1}}{dt} = \frac{L_m}{\sigma L_s L_r T_r}\psi_{rd1} + \frac{L_m}{\sigma L_s L_r}\omega_1\psi_{rq1} - \frac{R_s L_r^2 + R_r L_m^2}{\sigma L_s L_r^2} i_{sd1} + \omega_{n1} i_{sq1} + \frac{u_{sd1}}{\sigma L_s} \\
&\frac{di_{sq1}}{dt} = \frac{L_m}{\sigma L_s L_r T_r}\psi_{rq1} + \frac{L_m}{\sigma L_s L_r}\omega_1\psi_{rd1} - \frac{R_s L_r^2 + R_r L_m^2}{\sigma L_s L_r^2} i_{sq1} - \omega_{n1} i_{sd1} + \frac{u_{sq1}}{\sigma L_s} \\
&\frac{d\omega_2}{dt} = \frac{\left(-J_O r^2/B^2 i^2 + (1/4)\left(mr^2/i^2\right)\right)\left\{\left(n_p L_m/L_r\right)\left(i_{sq1}\psi_{rd1} - i_{sd1}\psi_{rq1}\right) - \left[F_{R1} - mgl\mu_{\max}\left(2R_k\omega_2 - 2R_k\omega_1 - B\omega_2 - B\omega_1\right)/2R_k\left(2\omega_2\right)^{n_k}\left(\omega_2 - \omega_1\right)^{1-n_k} B\right](r/i)\right\}}{\left(-J_O r^2/B^2 i^2 + (1/4)\left(mr^2/i^2\right)\right)^2 - \left(\left(J_O r^2/B^2 i^2\right) + (1/4)\left(mr^2/i^2\right) + J/n_p\right)^2} \\
&\quad - \cdots \\
&\quad - \frac{\left(J_O r^2/B^2 i^2 + (1/4)\left(mr^2/i^2\right) + J/n_p\right)\left\{\left(n_p L_m/L_r\right)\left(i_{sq2}\psi_{rd2} - i_{sd2}\psi_{rq2}\right) - \left[F_{R2} + mgl\mu_{\max}\left(2R_k\omega_2 - 2R_k\omega_1 - B\omega_2 - B\omega_1\right)/2R_k\left(2\omega_2\right)^{n_k}\left(\omega_2 - \omega_1\right)^{1-n_k} B\right](r/i)\right\}}{\left(-J_O r^2/B^2 i^2 + (1/4)\left(mr^2/i^2\right)\right)^2 - \left(J_O r^2/B^2 i^2 + (1/4)\left(mr^2/i^2\right) + J/n_p\right)^2} \\
&\frac{d\psi_{rd2}}{dt} = -\frac{1}{T_r}\psi_{rd2} + \left(\omega_{n2} - \omega_2\right)\psi_{rq2} + \frac{L_m}{T_r} i_{sd2} \\
&\frac{d\psi_{rq2}}{dt} = -\frac{1}{T_r}\psi_{rq2} - \left(\omega_{n2} - \omega_2\right)\psi_{rd2} + \frac{L_m}{T_r} i_{sq2} \\
&\frac{di_{sd2}}{dt} = \frac{L_m}{\sigma L_s L_r T_r}\psi_{rd2} + \frac{L_m}{\sigma L_s L_r}\omega_2\psi_{rq2} - \frac{R_s L_r^2 + R_r L_m^2}{\sigma L_s L_r^2} i_{sd2} + \omega_{n2} i_{sq2} + \frac{u_{sd2}}{\sigma L_s} \\
&\frac{di_{sq2}}{dt} = \frac{L_m}{\sigma L_s L_r T_r}\psi_{rq2} + \frac{L_m}{\sigma L_s L_r}\omega_2\psi_{rd2} - \frac{R_s L_r^2 + R_r L_m^2}{\sigma L_s L_r^2} i_{sq2} - \omega_{n2} i_{sd2} + \frac{u_{sq2}}{\sigma L_s}.
\end{aligned} \tag{15}$$

3. Controller Design

3.1. Approximate Inversion Modeling Based on Kriging. As a semiparametric interpolation method, the kriging model contains polynomials and random parts [20], as shown as follows:

$$Y(X) = f^T(x)\,\beta_k + z_k(x), \tag{16}$$

where $f(x) = [f_1(x), \ldots, f_m(x)]^T$ and $\beta_k = [\beta_{k1}, \ldots, \beta_{km}]^T$, in which m is the number of basis functions of the regression model. $Y(x)$ is the response to be measured; and $f(x)$ is a polynomial for x, which provides a simulated global approximation. Normally, $f(x)$ can take a constant value without affecting the accuracy of the simulation, and it does not play a decisive role in the accuracy of the simulation. β_k is

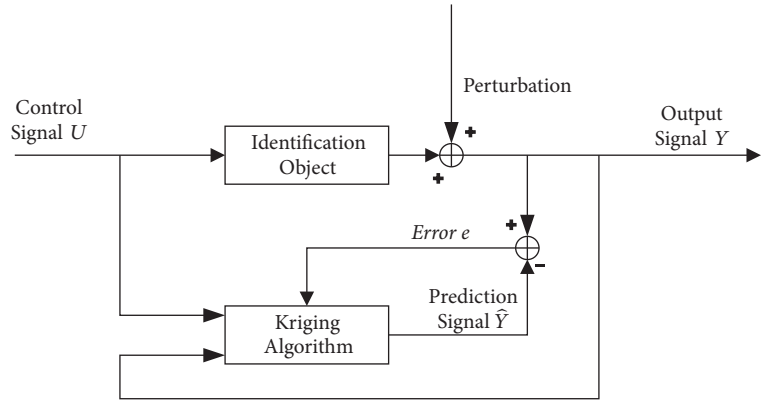

Figure 6: Inverse system modeling.

a vector of regression coefficients, and $z_k(x)$ is a random error function whose mean is zero but the variance is not zero.

$z_k(x)$ is not independent and identically distributed to provide a simulated local error approximation. Specifically, the covariance is not zero, and its covariance matrix is

$$\operatorname{cov}\left(x_i, x_j\right) = \sigma^2 R\left(x_i, x_j\right), \quad i, j = 1 \ldots n_k, \tag{17}$$

where x_i is the known sample point, n_k is the sample point, $R(\ldots)$ is the correlation equation, and σ^2 is the process variance.

In the kriging model, the random error function is dependent, and the associated correlation function $R(x_i, x_j)$ plays a decisive role in the accuracy of the simulation.

$$R\left(\theta_k, x_i, x_j\right) = \prod_{k=1}^{n} R\left(\theta_k, x_i^k - x_j^k\right), \tag{18}$$

where θ_k is a relative coefficient and x_i^k is the nth component of x_i.

3.2. Adaptive Control Law Design. On the basis of Lyapunov theory, we construct a scalar function that can satisfy its stability condition as follows:

$$\begin{aligned} E\left(x_e, y_e, \theta_e\right) = {} & \frac{1}{2}\left[x_e^2 + \left(y_e + k_\theta \theta_e\right)^2\right] \\ & + k_y\left(1 - \cos\theta_e\right). \end{aligned} \tag{19}$$

The differential equation (see (19)) combined with the system error formula is expressed as follows:

$$\begin{aligned} & \dot{E}\left(x_e, y_e, \theta_e\right) \\ & \quad = x_e\left(\omega y_e - v + v_r \cos\theta_e\right) \\ & \qquad + \left(y_e + k_\theta \theta_e\right)\left(-\omega x_e + v_r \sin\theta_e + k_\theta \omega_r - k_\theta \omega\right) \\ & \qquad + k_y \sin\left(\theta_e\right)\left(\omega_r - \omega\right). \end{aligned} \tag{20}$$

We obtain the control law $U = [v, \omega]$ as

$$\begin{aligned} v &= v_r \cos\theta_e + k_x x_e - k_\theta \theta_e \omega \\ \omega &= \omega_r + v_r\left[\frac{1}{k_y}\alpha_c\left(y_e + k_\theta \theta_e\right) + \frac{\beta_c}{k_\theta}\sin\theta_e\right]. \end{aligned} \tag{21}$$

Substituting (21) into (20) yields

$$\begin{aligned} \dot{E}\left(x_e, y_e, \theta_e\right) = {} & -k_x x_e^2 - \frac{k_\theta v_r \alpha_c}{k_y}\left(y_e + k_\theta \theta_e\right)^2 \\ & - \frac{k_y \beta_c v_r}{k_\theta}\sin^2\theta_e \\ & + \left(1 - \alpha_c - \beta_c\right)\left(y_e + k_\theta \theta_e\right) v_r \sin\theta_e, \end{aligned} \tag{22}$$

where k_x, k_y, k_θ, α_c, and β_c are constants greater than zero. When $\alpha_c + \beta_c = 1$, (22) must be negatively definite.

Therefore, on the basis of Lyapunov theory, the crawler walking device can achieve the effect of stable tracking control under the control of the law $U = [v, \omega]$.

3.3. Inverse Controller Design with Kriging Model. As shown in Figure 6, on the basis of the characteristics of the electromechanical system of the crawler, the input parameters include the supply voltage of the drive motor on both sides of the crawler U_L, U_R, drive motor supply frequencies f_L, f_R, and the crawler load torque on both sides TL_L, TL_R. The output parameters include both sides of the crawler driving speed V_L, V_R. The function mapping relationship between the input and output parameters of the electromechanical system of the crawler is approximated by the kriging algorithm to establish the black box model.

In this system, the control and output signals are $U = [U_L, U_R, f_L, f_R, TL_L, TL_R]$ and $Y = [V_L, V_R]$, respectively. The corresponding output signal is obtained by inputting the control signal into the system of the identification object. The input and output signals are taken as samples, and the kriging algorithm is used for modeling and training. The inverse model parameters established by the kriging algorithm are adjusted using the deviation signal between the output signals

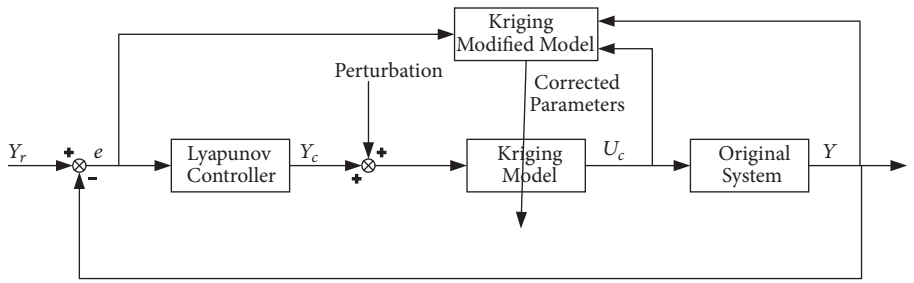

Figure 7: Adaptive inverse control approach.

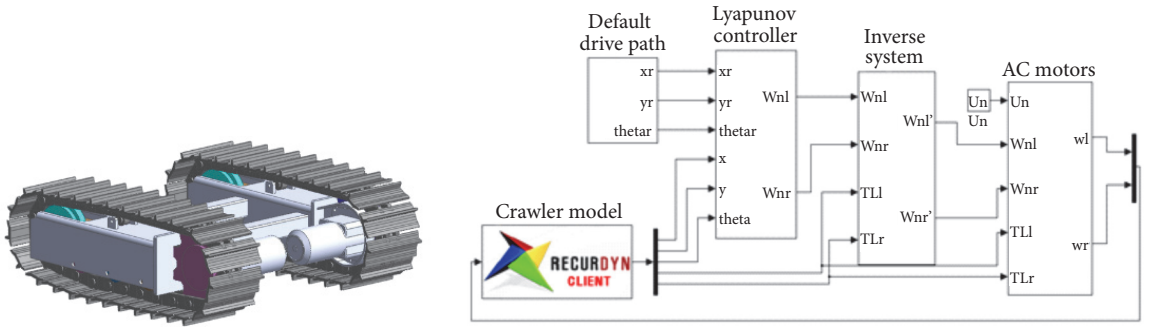

(a) (b)

Figure 8: Virtual prototype model of the crawlers.

of the identification object and the inverse model to improve the modeling accuracy of the inverse system.

Figure 7 shows the complete block diagram of the developed adaptive nonlinear model using the inverse control approach based on the kriging model. The concrete realization process is as follows.

(1) $t = 0$. The online learning kriging inverse system is initialized, and the modeling coefficient of the offline training kriging inverse system is taken as the initial value of the adaptive inverse control of online learning.

(2) In the adaptive control process, the error $e(t)$ between the ideal output signal and the output of the controlled system is calculated at time t. The deviation is taken as the controller input to calculate the theoretical control signal. The theoretical control signal is disturbed by external disturbances. The signal is inputted as an inverse system model.

(3) The inverse system model outputs U_c input to the original system and the inverse system correction model. The parameters of the kriging inverse system and the model are corrected on the basis of the error e, inverse system output U_c, and original system output Y.

(4) The parameters obtained in the modified model are inputted to the kriging inverse system. Moreover, the inverse system is modified to improve its control accuracy.

4. Simulation Analysis and Discussions

The test crawler design dimensions are used to establish the dynamic simulation model shown in Figure 8, and the road surface is a hard pavement.

The input and output parameters of the range are shown in

$$\begin{aligned} U_L &= U_R = 380\text{V} \\ 0 &\le f_L, f_R \le 50\text{Hz} \\ 0 &\le V_L, V_R \le 0.4\text{m/s} \end{aligned} \tag{23}$$

Figure 9 shows the designed trajectory. After traveling at a linear velocity of 0.3 m/s at a centroid of 0.3 m/s, the trajectory turns to the right at an angular velocity of 0.1 rad/s, turns to the left, and then stops for a while after traveling in a straight line.

The preset travel path indicates that this study uses neural network, fuzzy, and kriging algorithms to establish the inverse control system of the tracked mobile device and simulates the crawler walking device. The simulation results are as mentioned in Figures 10, 11, and 12.

Figure 10 indicates that the inverse control system based on kriging, neural network, and fuzzy algorithms shows a good control effect. However, the adaptive inverse control system based on the kriging algorithm indicates the best control effect. The robustness based on the kriging algorithm is the strongest during the two steering operations and can follow the reference path better. The same course angle deviation is set during the start of the crawler travel. In the first straight-line phase (Figure 11), the control system based on the kriging algorithm allows the crawler to track the upper reference path considerably faster. The deviation of the X- and Y-axes and heading angle θ is maintained at 0 m and 0

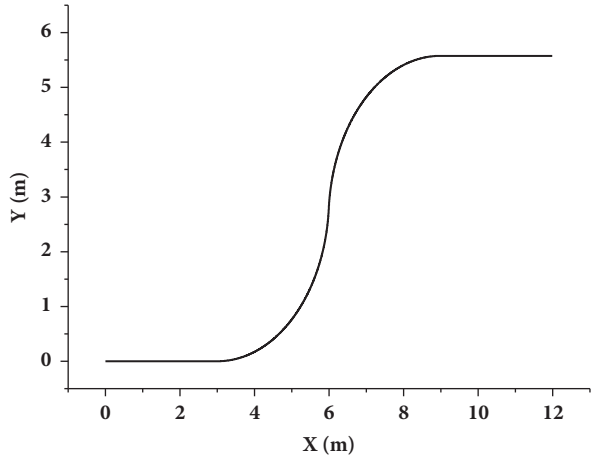

Figure 9: Reference trajectory of the crawlers.

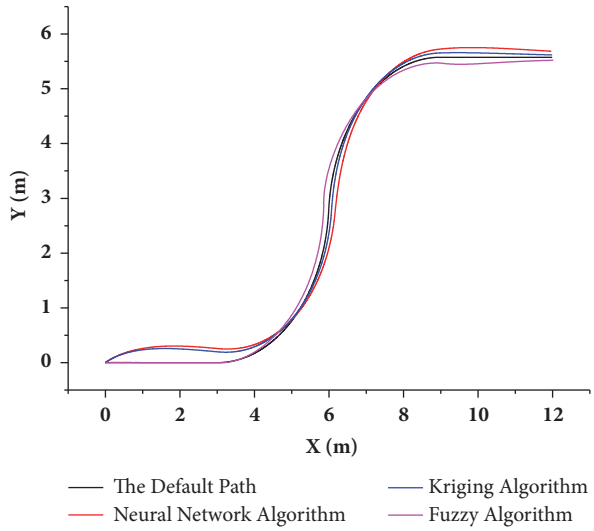

Figure 10: Result analysis of travel path.

rad, respectively. Fuzzy control and neural network control effects are relatively close. From the analysis of the results of the crawler walking speed on both sides in Figure 12, the outputs of the kriging and neural network algorithms are closer to a given ideal traveling speed under the three inverse control systems. Among them, the fuzzy inverse control system presents a relatively large deviation, especially in the steering of the moment. A larger deviation gain will occur when the maximum error is up to 50%. Therefore, the results suggest that, on the basis of the same training samples, the kriging algorithm indicates better training efficiency and training effect and shows the best control effect in the classical inverse control algorithm.

The inverse control system is based on the kriging algorithm in the control of the driving process of the crawler walking device. The electromechanical coupling performance analysis results are as mentioned in Figures 13, 14, and 15.

In the course of traveling, the crawler initially runs through a straight line and then goes through two turns, such that it travels straight to the final point. Therefore, the load on the crawler drive motor is nearly the same as that of the crawler on both sides while traveling straight (Figure 13(b)). The effective value fluctuates at approximately 30 N·m. During the driving process, the crawler walking device receives the ground and the load of the machine itself and will also be turned to the driving torque. Therefore, the load on the inner track decreases, and that on the outer track increases. Finally, a straight-line driving process is resumed.

On the basis of the above variation of load torque, the input voltage of the driving motor on both sides of the crawler is consistently kept at 380 V, and the change of the driving power of the motor directly influences the load torque (Figures 14 and 15). Therefore, during the entire driving process, the change of the output current of the driving motor

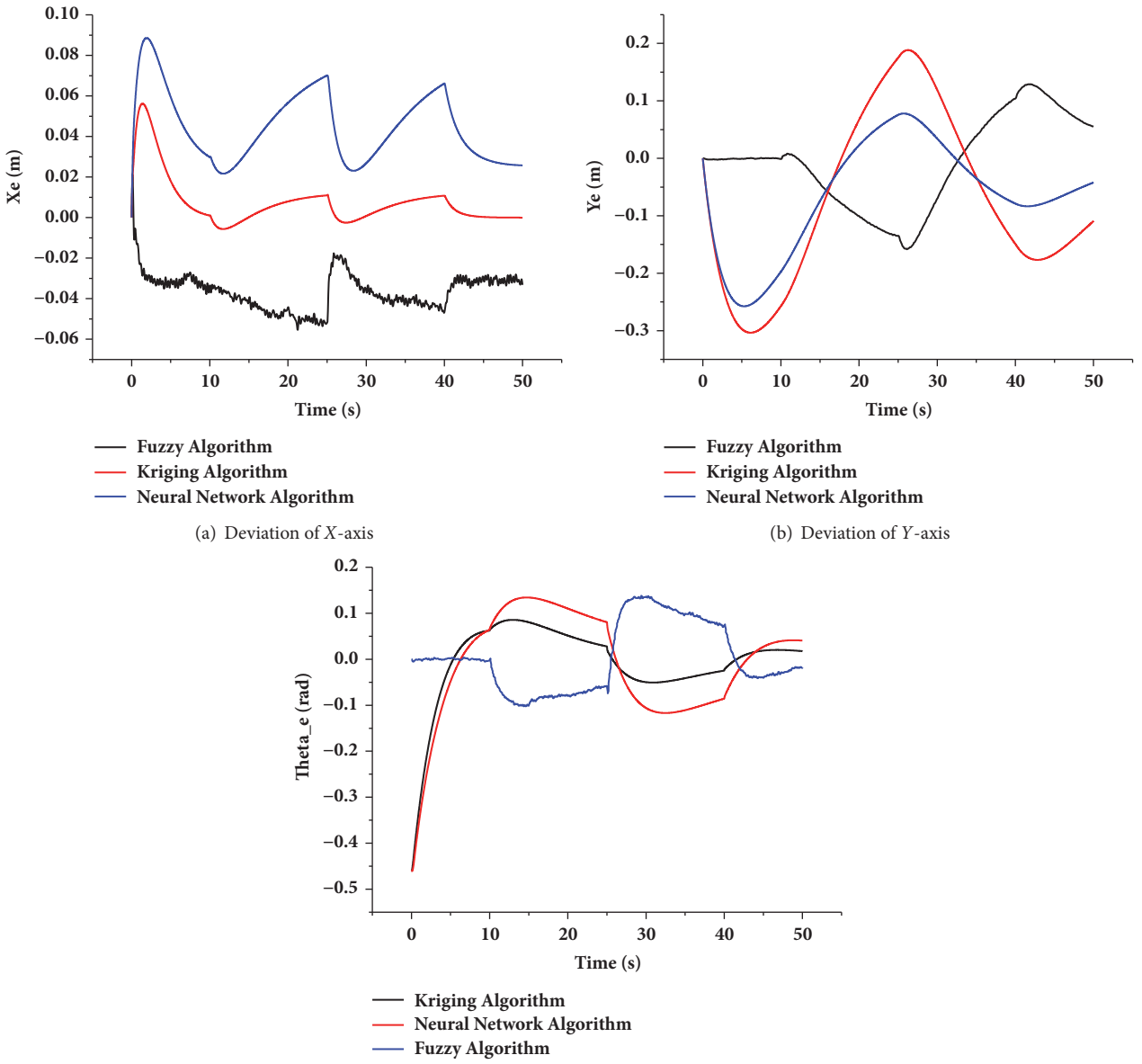

(a) Deviation of X-axis

(b) Deviation of Y-axis

(c) Deviation of θ

FIGURE 11: Result analysis of deviation.

is consistent with the load torque, and the output power of the driving motor is approximately 750 W when traveling in a straight line. When steering, the output power values of the outer and inner track drive motors are approximately 1 kW and 550 W, respectively.

5. Conclusion

An adaptive inverse control algorithm based on kriging algorithm is proposed in this study, and the control algorithm is applied to the adaptive control of the crawler. First, an inverse modeling system based on the kriging algorithm and an online adaptive inverse control system are established. Second, taking the crawler as an example, the electromechanical coupling model of the crawler is established. Moreover, the inverse model of the electromechanical system is developed by the kriging algorithm. Finally, the virtual prototyping cosimulation is used to set a specific driving path. Furthermore, the control effects of the classical inverse modeling method neural network and fuzzy and kriging algorithms are compared. The simulation results show that the adaptive inverse control method based on the kriging algorithm has better control accuracy and robustness. The robustness based on kriging algorithm is the strongest during the two steering operations and can better follow the reference path, compared with neural network and fuzzy algorithm, thereby establishing a foundation for the adaptive walking function of a crawler in driverless situations.

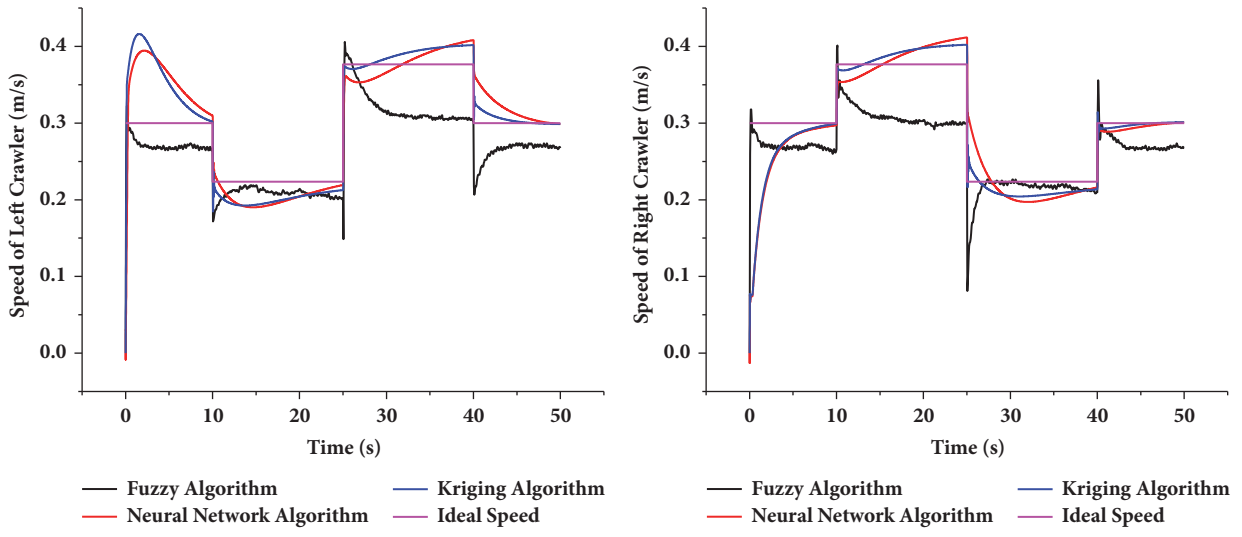

(a) Left crawler (b) Right crawler

Figure 12: Velocity analysis of the crawlers.

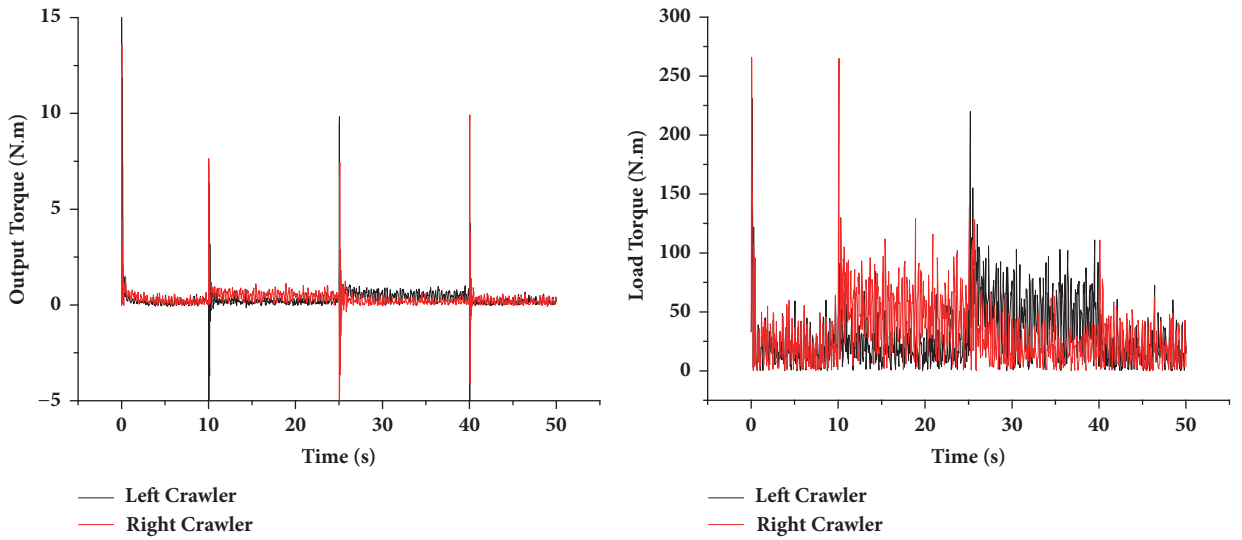

(a) Output torque of motors (b) Load torque of the crawlers

Figure 13: Result analysis of torques of the crawlers.

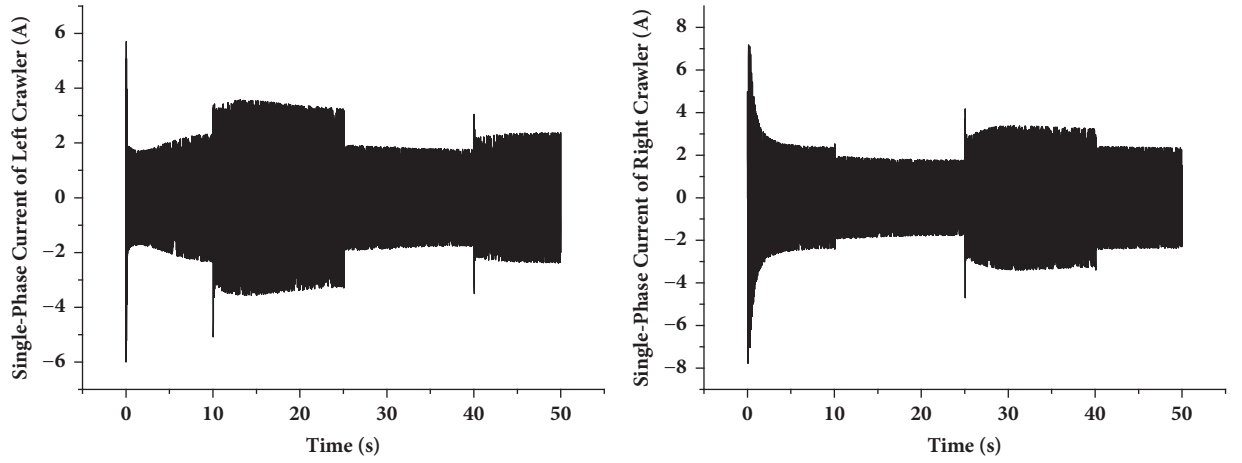

(a) Left (b) Right

Figure 14: Single-phase current analysis of crawler motors.

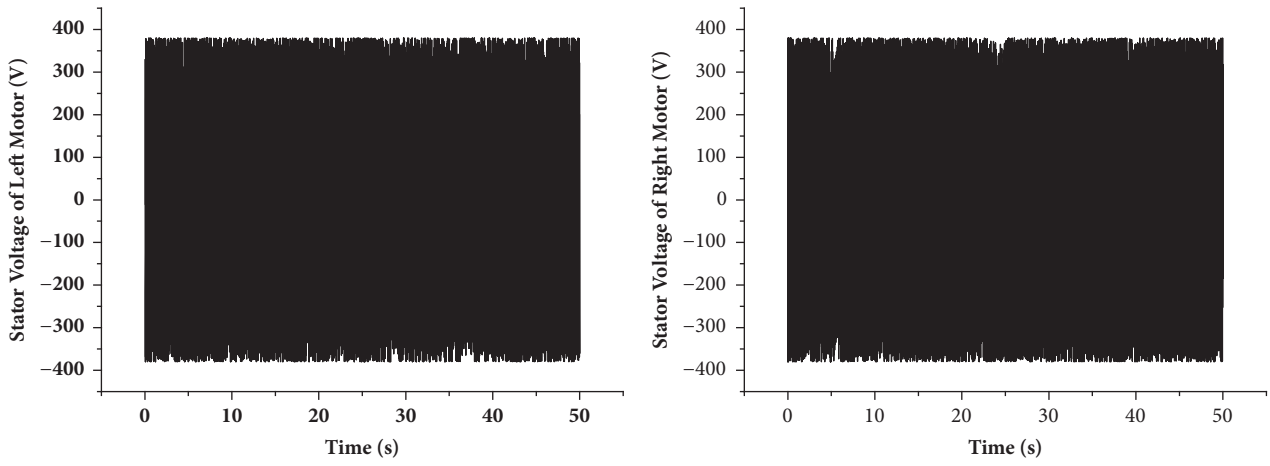

(a) Left (b) Right

Figure 15: Single-phase voltage analysis of crawler motors.

Data Availability

The process details of how experimental data was achieved need to be kept confidential, because this manuscript got the support from a confidential project.

Conflicts of Interest

The authors declare that they have no conflicts of interest.

Acknowledgments

This work is supported by National Natural Science Foundation of China (Project Nos. 51705187, 61871199), the Postdoctoral Science Foundation of China (Grant No. 2017M621202), and the National Key R&D Program of China (No. 2016YFC0303902).

References

[1] K. M. Vu, "A model predictive controller for inverse response control systems," *IFAC-PapersOnLine*, vol. 28, no. 8, pp. 562–567, 2015.

[2] Y. Su and C. Zheng, "Global finite-time inverse tracking control of robot manipulators," *Robotics and Computer-Integrated Manufacturing*, vol. 27, no. 3, pp. 550–557, 2011.

[3] M. Galicki, "Inverse-free control of a robotic manipulator in a task space," *Robotics and Autonomous Systems*, vol. 62, no. 2, pp. 131–141, 2014.

[4] H.-G. Han and J.-F. Qiao, "Adaptive dissolved oxygen control based on dynamic structure neural network," *Applied Soft Computing*, vol. 11, no. 4, pp. 3812–3820, 2011.

[5] H.-G. Han, J.-F. Qiao, and Q.-L. Chen, "Model predictive control of dissolved oxygen concentration based on a self-organizing RBF neural network," *Control Engineering Practice*, vol. 20, no. 4, pp. 465–476, 2012.

[6] A. Alexandridis, M. Stogiannos, A. Kyriou, and H. Sarimveis, "An offset-free neural controller based on a non-extrapolating scheme for approximating the inverse process dynamics," *Journal of Process Control*, vol. 23, no. 7, pp. 968–979, 2013.

[7] U. Imtiaz, A. Assadzadeh, S. S. Jamuar, and J. N. Sahu, "Bioreactor temperature profile controller using inverse neural network (INN) for production of ethanol," *Journal of Process Control*, vol. 23, no. 5, pp. 731–742, 2013.

[8] A. Y. Alanis, F. Ornelas-Tellez, and E. N. Sanchez, "Discrete-time inverse optimal neural control for synchronous generators," *Engineering Applications of Artificial Intelligence*, vol. 26, no. 2, pp. 697–705, 2013.

[9] Y. Singh, V. Vinoth, Y. R. Kiran, J. K. Mohanta, and S. Mohan, "Inverse dynamics and control of a 3-DOF planar parallel (U-shaped 3-PPR) manipulator," *Robotics and Computer-Integrated Manufacturing*, vol. 34, pp. 164–179, 2015.

[10] Y. Singh and M. Santhakumar, "Inverse dynamics and robust sliding mode control of a planar parallel (2-PRP and 1-PPR) robot augmented with a nonlinear disturbance observer," *Mechanism and Machine Theory*, vol. 92, pp. 29–50, 2015.

[11] Y. Kim, Y. Choi, and J. Lee, "Speed-sensorless vector control for permanent-magnet synchronous motors based on instantaneous reactive power in the wide-speed region," *IEE Proceedings - Electric Power Applications*, vol. 152, no. 5, p. 1343, 2005.

[12] J. Li, S. Li, X. Chen, and J. Yang, "RBFNDOB-based neural network inverse control for non-minimum phase MIMO system with disturbances," *ISA Transactions®*, vol. 53, no. 4, pp. 983–993, 2014.

[13] P. Shanmuga Aravind and S. Albert Alexander, "Harmonic minimization of a solar fed cascaded H Bridge inverter using Artificial Neural Network," in *Proceedings of the 2013 International Conference on Energy Efficient Technologies for Sustainability, ICEETS 2013*, pp. 163–167, India, April 2013.

[14] F. Ornelas-Tellez, E. N. Sanchez, A. G. Loukianov, and J. J. Rico, "Robust inverse optimal control for discrete-time nonlinear system stabilization," *European Journal of Control*, vol. 20, no. 1, pp. 38–44, 2014.

[15] H. El-Hussieny, A. A. Abouelsoud, S. F. M. Assal, and S. M. Megahed, "Adaptive learning of human motor behaviors: An evolving inverse optimal control approach," *Engineering Applications of Artificial Intelligence*, vol. 50, pp. 115–124, 2016.

[16] R. Boukezzoula, S. Galichet, and L. Foulloy, "Nonlinear internal model control: application of inverse model based fuzzy control," *IEEE Transactions on Fuzzy Systems*, vol. 11, no. 6, pp. 814–829, 2003.

[17] Y. Chen, R. Zhang, X. Zhao, and J. Gao, "Adaptive fuzzy inverse trajectory tracking control of underactuated underwater vehicle with uncertainties," *Ocean Engineering*, vol. 121, pp. 123–133, 2016.

[18] A. Rahideh, A. H. Bajodah, and M. H. Shaheed, "Real time adaptive nonlinear model inversion control of a twin rotor MIMO system using neural networks," *Engineering Applications of Artificial Intelligence*, vol. 25, no. 6, pp. 1289–1297, 2012.

[19] R. Wang, X. Chen, T. Jian, and B. Chen, "Robust Adaptive Inverse Control Based on Maximum Correntropy Criterion," *IFAC-PapersOnLine*, vol. 48, no. 28, pp. 285–290, 2015.

[20] G. Zhang, G. Wang, X. Li, and Y. Ren, "Global optimization of reliability design for large ball mill gear transmission based on the Kriging model and genetic algorithm," *Mechanism and Machine Theory*, vol. 69, pp. 321–336, 2013.

Hindawi
Complexity
Volume 2018, Article ID 7941012, 12 pages
https://doi.org/10.1155/2018/7941012

Research Article

The Unique Existence of Weak Solution and the Optimal Control for Time-Fractional Third Grade Fluid System

Guangming Shao,[1] **Biao Liu**,[2] **and Yueying Liu**[3]

[1]*Anhui University of Chinese Medicine, Hefei 230012, China*
[2]*School of Mathematical Sciences, Anhui University, Hefei 230601, China*
[3]*College of Mathematics and Systems Science, Shandong University of Science and Technology, Qingdao 266590, China*

Correspondence should be addressed to Yueying Liu; yyliu0823@163.com

Received 10 June 2018; Revised 11 October 2018; Accepted 22 October 2018; Published 13 November 2018

Guest Editor: Viet-Thanh Pham

The paper concerns the third grade fluid system with the time-fractional derivative of the order $\alpha \in (0,1)$. We first establish unique existence criterion of weak solutions in the case that the dimension $n = 3$. Then we prove the sufficient condition of optimal pairs.

1. Introduction

We consider the significant case of the fluids of grade n introduced by Rivlin-Ericksen [1] in a bounded domain $\Omega \subset \mathbb{R}^3$

$$\begin{aligned} &\frac{\partial v}{\partial t} - \nu\Delta u + (u\cdot\nabla)\, v + \sum_j v_j \nabla u_j \\ &\quad - (\sigma_1 + \sigma_2)\, \mathrm{div}\left(A^2(u)\right) \\ &- \beta \mathrm{div}\left(|A(u)|^2 A(u)\right) + \nabla p = f, \\ &v = u - \sigma_1 \Delta u, \end{aligned} \tag{1}$$

where $\nu > 0$ is the constant kinematic viscosity, σ_1, σ_2, and β are material constants, and $\beta > 0$. The unknown functions u, p are the fluid velocity and the scalar pressure, respectively. The given functions u_0, f represent the initial fluid velocity and the forcing term, respectively. In fact, A is the tensor whose component is

$$A(u) = \nabla u + (\nabla u)^T. \tag{2}$$

Here, $(\nabla u)^T$ is the transposition of the Jacobian matrix ∇u, and $|A(u)|^2$ denotes $tr(A^2(u))$.

In [2], Ladyzhenskaya studied a particular case of the third grade fluids (1) in $\mathbb{R}^3$, where they assumed $\sigma_1 = 0$. In this case, system (1) becomes

$$\begin{aligned} &\partial_t u - \nu\Delta u + u\cdot\nabla u - \sigma \mathrm{div}\left(A^2(u)\right) \\ &\quad - \beta \mathrm{div}\left(|A(u)|^2 A(u)\right) + \nabla p = f, \\ &\mathrm{div} u = 0, \\ &\qquad u = 0,\ x \in \partial\Omega,\ t > 0,\ u(x,0) = u_0,\ x \in \Omega. \end{aligned} \tag{3}$$

In the past years, some nice works on the third grade fluid system have already been available. We refer to Fosdick and Rajagopal [3], Amrouche and Cioranescu [4], Sequeira and Videman [5], Busuioc and Iftimie [6], Paicu [7], Hamza and Paicu [8], Zhao et al. [9], and Chai et al. [10]; much is yet to be carried out.

Unlike the boundary value problems of the classical third grade fluid system, the theoretical analysis of time-fractional third grade fluid system is not so rich, so we need to develop many aspects of these problems. It is significant to study this type of system when it is recognized that the time-fractional third grade fluid system can be used to describe diffusion phenomenon in fractal media. So the scholars have been more and more interested in investigating the fractional calculus.

The fractional calculus was introduced by Herrmann [11] and Hilfer [12], especially for the classical time-fractional Navier-Stokes equations

$$\begin{aligned} \partial_t^\alpha u - \nu\Delta u + (u\cdot\nabla)\,u + \nabla p &= f, \\ \operatorname{div} u &= 0, \end{aligned} \tag{4}$$

where ∂_t^α is the Caputo fractional derivative of order $\alpha \in (0,1)$.

For some recent work on analytical solutions of these systems, we refer to El-Shahed et al. [13], Ganji et al. [14], Zhou [15], Momani and Zaid [16], Carvalho-Neto and Gabriela [17], Zhou and Peng [18, 19], Zhou et al. [20], Al-Mdallal et al. [21], Jarad [22–25], and further papers cited therein.

In this paper, we consider mainly the weak solutions of the time-fractional third grade fluid system and optimal control in an open set $\Omega \subset \mathbb{R}^3$ with smooth boundary $\partial\Omega$

$$\begin{aligned} &\partial_t^\alpha u - \nu\Delta u + u\cdot\nabla u - \sigma\operatorname{div}\left(A^2(u)\right) \\ &\quad - \beta\operatorname{div}\left(|A(u)|^2 A(u)\right) + \nabla p = f, \\ &\operatorname{div} u = 0, \end{aligned} \tag{5}$$

with the initial and boundary value conditions

$$\begin{aligned} u &= 0, \\ x &\in \partial\Omega, \\ t &> 0, \\ u(x,0) &= u_0, \quad x \in \Omega. \end{aligned} \tag{6}$$

Noting that the system converges formally to the well-known time-fractional Navier-Stokes equations when the material constants σ, β in (5) tend to zero. So it is reasonable to propose the time-fractional third grade fluid system.

In this paper, we firstly investigate the existence and uniqueness of solutions for the time-fractional third grade fluid equations (5) (associated with appropriate initial and boundary conditions). Then we proceed the systems with control in $\Omega \in \mathbb{R}^3$

$$\begin{aligned} &\partial_t^\alpha u - \nu\Delta u + (u\cdot\nabla)\,u - \sigma\operatorname{div}\left(A^2(u)\right) \\ &\quad - \beta\operatorname{div}\left(|A(u)|^2 A(u)\right) = -\nabla p + c_0\omega + f, \\ &\nabla\cdot u = 0, \\ &\qquad u = 0,\ x \in \partial\Omega;\ u(x,0) = u_0,\ x \in \Omega, \end{aligned} \tag{7}$$

where U is a real Hilbert space, $\omega : [0,T] \longrightarrow U$, and the operator $c_0 : U \longrightarrow \mathbb{H}$ is linear continuous.

Now let us talk about the organization of this paper. In Section 2, we provide some preliminaries about the function spaces. In Section 3, we prove the existence of solutions for system (5). The uniqueness of solutions is established in Section 4, while in Section 5 we show the existence of the optimal control of system (7).

2. Preliminaries

In this section, for convenience, we mainly introduce some notions, operators, definitions, and lemmas, which are useful in the sequel.

Let $\Omega \subset \mathbb{R}^3$ be an open bounded smooth domain; we define

$$\begin{aligned} \mathscr{V} &= \left\{u \in C_0^\infty(\Omega)\times C_0^\infty(\Omega)\times C_0^\infty(\Omega)\right\}, \operatorname{div} u = 0\}, \\ \mathbb{H} &= \mathscr{V}^{\mathbb{L}^2(\Omega)}, \text{with norm } \|\cdot\| \\ &= \|\cdot\|_{\mathbb{L}^2}\left(\text{the usual } \mathbb{L}^2 \text{ norm}\right), \\ \mathbb{H}_0^s &= \mathscr{V}^{\mathbb{H}^2(\Omega)}, \text{with norm } \|\cdot\| \\ &= \|\cdot\|_{\mathbb{H}^2}\left(\text{the usual } \mathbb{H}^2 \text{ norm}\right), \\ \mathbb{V} &= \mathscr{V}^{\mathbb{H}_0^1(\Omega)}, \text{with norm } \|\cdot\|_{\mathbb{V}} \\ &= \|\nabla\cdot\|, \text{and the dual space } \mathbb{V}^*, \\ \mathbb{W} &= \mathscr{V}^{\mathbb{W}_0^{1,4}(\Omega)}, \text{with norm } \|\cdot\|_{\mathbb{W}} \\ &= \|\nabla\cdot\|_{\mathbb{L}^4}, \text{and the dual space } \mathbb{W}^*. \end{aligned} \tag{8}$$

Define the linear "Stokes operator" $\mathscr{A} = -\triangle$ from $\mathbb{V}$ to $\mathbb{V}^*$ by

$$\langle \mathscr{A}u, v\rangle_{\mathbb{V}^*,\mathbb{V}} = \sum_{i,j=1}^{3}\int_\Omega \partial_j u_i \partial_j v_i\,dx, \quad \forall u, v \in \mathbb{V}, \tag{9}$$

and the bilinear operator $\mathscr{B}(u,v)$ from $\mathbb{V}\times\mathbb{V}$ into $\mathbb{V}^*$ as

$$\begin{aligned} \langle \mathscr{B}(u,v), w\rangle_{\mathbb{V}^*,\mathbb{V}} &= \sum_{i,j=1}^{3}\int_\Omega u_i \frac{\partial v_j}{\partial x_i} w_j\,dx, \\ &\forall u, v, w \in \mathbb{V}. \end{aligned} \tag{10}$$

We also introduce the operators $\mathscr{K}(u), \mathscr{J}(u)$ from $\mathbb{W}$ into $\mathbb{W}^*$ as

$$\begin{aligned} &\left\langle \mathscr{K}(u), \phi\right\rangle_{\mathbb{W}^*,\mathbb{W}} \\ &\quad = \alpha\int_\Omega A^2(u)\cdot\nabla\phi\,dx \left(\le C\|A(u)\|_{\mathbb{L}^4}^2 \left\|\nabla\phi\right\|_{\mathbb{L}^4}\right), \\ &\qquad\qquad \forall u, \phi \in \mathbb{W}, \end{aligned} \tag{11}$$

$$\begin{aligned} \left\langle \mathscr{J}(u), \phi\right\rangle_{\mathbb{W}^*,\mathbb{W}} &= \beta\int_\Omega |A(u)|^2 A(u)\cdot\nabla\phi\,dx, \\ &\forall u, \phi \in \mathbb{W}. \end{aligned}$$

Let $|\alpha| < \sqrt{2\nu\beta}$. We denote $\mathscr{T}(u)$ from $\mathbb{W}$ into $\mathbb{W}^*$ as

$$\begin{aligned} \mathscr{T}(u) &= \left(\nu - \nu\delta_0\right)\mathscr{A}u + \left(1-\delta_0\right)\mathscr{J}(u) + \mathscr{K}(u), \\ \delta_0 &= 1 - \sqrt{\frac{\alpha^2}{2\nu\beta}} \in (0,1). \end{aligned} \tag{12}$$

Note that (see, e.g., [26–28])

$$\mathscr{A}u = -\Delta u \text{ for } u \in D(\mathscr{A}) = \left\{u \in \mathbb{H}_0^2(\Omega), \operatorname{div} u = 0\right\}. \quad (13)$$

By the Hilbert-Schmidt theorem, one can deduce that $\mathscr{A}$ has a sequence of orthonormal eigenfunctions w_j, belonging to $C_p^\infty(\Omega)$ with zero mean in Ω. Since $\mathscr{A}$ is a self-adjoint positive operator with compact inverse, $\{\omega_j\}_{j=1}^\infty$ forms a basis of the space $\mathbb{H}$. Moreover, $\{\omega_j\}_{j=1}^\infty$ also forms a basis of the space $D(\mathscr{A}^{s/2}) = \{\mathbb{H}_0^s(\Omega), \operatorname{div} u = 0\}$, for any positive integer s [28].

Next, we will introduce some definitions and lemmas, which are used throughout this paper.

Definition 1 (see [18, 29]). Let X be a Banach space, $v : [0,T] \longrightarrow X$; the left and right Riemann-Liouville fractional integrals ${}_0I_t^\alpha v(t)$ and ${}_tI_T^\alpha v(t)$ of order $\alpha \in (0,1]$ are defined by

$$\begin{aligned} {}_0I_t^\alpha v(t) &= \int_0^t g_\alpha(t-s)\, v(s)\, ds, \\ {}_tI_T^\alpha v(t) &= \int_t^T g_\alpha(s-t)\, v(s)\, ds, \\ & \qquad t > 0, \end{aligned} \quad (14)$$

provided the integrals are point-wise defined on $[0,\infty)$, where g_α denotes the Riemann-Liouville kernel

$$g_\alpha(t) = \frac{t^{\alpha-1}}{\Gamma(\alpha)}, \quad t > 0. \quad (15)$$

Definition 2 (see [29]). The left Caputo and right Riemann-Liouville fractional derivative ${}_0^cD_t^\alpha v(t)$ and ${}_tD_T^\alpha v(t)$ of order are defined by

$$\begin{aligned} {}_0^cD_t^\alpha v(t) &= \int_0^t g_{1-\alpha}(t-s)\frac{d}{ds}v(s)\, ds, \\ {}_tD_T^\alpha v(t) &= -\frac{d}{dt}\left(\int_t^T g_{1-\alpha}(s-t)\, v(s)\, ds\right), \\ & \qquad t > 0. \end{aligned} \quad (16)$$

More generally, for $v : [0,\infty) \times \mathbb{R}^n \longrightarrow \mathbb{R}^n$, the left Caputo fractional derivative with respect to time can be defined by

$$\partial_t^\alpha u(x,t) = \int_0^t g_{1-\alpha}(t-s)\frac{\partial}{\partial s}v(x,s)\, ds, \quad t > 0. \quad (17)$$

For more detail, we can refer to [30].

Definition 3 (see [18, 29]). Let $v : \mathbb{R} \longrightarrow X$; the Liouville-Weyl fractional integral and the Caputo fractional derivative on the real axis are defined, respectively, as follows:

$$\begin{aligned} {}_{-\infty}I_t^\alpha v(t) &= \int_{-\infty}^t g_\alpha(t-s)\, v(s)\, ds, \\ {}_{-\infty}{}^cD_t^\alpha v(t) &= \int_{-\infty}^t g_{1-\alpha}(t-s)\frac{d}{ds}v(s)\, ds. \end{aligned} \quad (18)$$

Lemma 4 (see [8]). *The operator $\mathscr{J}$ is a monotone operator; that is, for any $u, v \in \mathbb{W}$, we have*

$$\langle \mathscr{J}(u) - \mathscr{J}(v), u - v\rangle_{\mathbb{W}^*,\mathbb{W}} \geq 0. \quad (19)$$

Lemma 5 (see [8]). *The operator $\mathscr{T}$ is a monotone operator; that is, for any $u, v \in \mathbb{W}$, we have*

$$\langle \mathscr{T}(u) - \mathscr{T}(v), u - v\rangle_{\mathbb{W}^*,\mathbb{W}} \geq 0. \quad (20)$$

Let $\mathscr{T}_1 : \mathbb{W} \longrightarrow \mathbb{W}^*$ be defined as

$$\mathscr{T}_1(v) = \mathscr{A}v + \mathscr{K}(v) + \mathscr{J}(v). \quad (21)$$

Thanks to the above lemmas, $\mathscr{T}_1$ is also a monotone operator.

Lemma 6 (see [31]). *The fractional integration by parts in the formula*

$$\begin{aligned} \int_0^T \left(\partial_t^\alpha v(t), \varphi(t)\right) &= \int_0^t \left(v(t),\, {}_tD_T^\alpha \varphi(t)\right) dt \\ &\quad + \left(v(t),\, {}_tI_T^{1-\alpha}\varphi(t)\right)\Big|_0^T. \end{aligned} \quad (22)$$

Since $\lim_{t\longrightarrow T}\, {}_tI_T^{1-\alpha}\varphi(t) = 0$ *for* $\varphi \in C_0^\infty(0,T;X)$, *then*

$$\begin{aligned} \int_0^T \left(\partial_t^\alpha v(t), \varphi(t)\right) &= \int_0^T \left(v(t),\, {}_tD_T^\alpha \varphi(t)\right) dt \\ &\quad - \left(v(0),\, {}_tI_T^{1-\alpha}\varphi(t)\right). \end{aligned} \quad (23)$$

For more details, we refer to relations (16)-(21) in [31].

Lemma 7 (see [19]). $\partial_t^\alpha(u(t), v) = \langle \partial_t^\alpha u(t), v\rangle$ *in* $\mathscr{L}(C_0^\infty(0,T;\Omega))$ *for* $u \in W^\alpha([0,T],V,V')$, $v \in V$, *where* $W^\alpha([[0,T],V,V') := \{u \in L^2([0,T],V) : \partial_t^\alpha u \in L^2([0,T],V')\}$.

Lemma 8 (see [32]). *Suppose that X is a real Hilbert space and $v : [0,T] \longrightarrow X$ have a derivative, then there holds*

$$\left(v(t), {}_0^cD_t^\alpha v(t)\right) \geq \frac{1}{2}\, {}_0^cD_t^\alpha |v(t)|^2. \quad (24)$$

Lemma 9 (see [19]). *Suppose that a nonnegative function $v(t)$ satisfies*

$$ {}_0^cD_t^\alpha v(t) + c_1 v(t) \leq c_2(t) \quad (25)$$

for almost all $t \in [0,T]$, where $c_1 > 0$ and the function c_2 is nonnegative and integrable for $t \in [0,T]$. Then

$$v(t) \leq v(0) + \frac{1}{\Gamma(\alpha)}\int_0^t (t-s)^{\alpha-1} c_2(s)\, ds. \quad (26)$$

We need the compactness theorem [26] involving fractional derivative.

Assume X_0, X, X_1 are Hilbert spaces with

$$X_0 \hookrightarrow X \hookrightarrow X_1, \quad (27)$$

being continuous, and

$$X_0 \hookrightarrow X \text{ is compact.} \tag{28}$$

Let $\psi(t)$ be a function from $\mathbb{R}$ to X_1; we denote by $\widehat{\psi}(\tau)$ its Fourier transform

$$\widehat{\psi}(\tau) = \int_{-\infty}^{+\infty} \exp(-2\pi i t\tau)\, \psi(t)\, dt. \tag{29}$$

The derivative in t of order γ is the inverse Fourier transform of $(2i\pi\tau)^{\gamma}\widehat{\psi}(\tau)$; that is,

$$\widehat{D_t^{\gamma}\psi(t)} = (2i\pi\tau)^{\gamma}\,\widehat{\psi}(\tau). \tag{30}$$

For given $\gamma > 0$, define the space

$$\begin{aligned} M^{\gamma} &= M^{\gamma}(\mathbb{R}; X_0, X_1) \\ &= \left\{\psi \in L^2(\mathbb{R}; X_0), D_t^{\gamma}\psi \in L^2(\mathbb{R}; X_1)\right\}. \end{aligned} \tag{31}$$

Then, M^{γ} is a Hilbert space with the norm

$$\|\psi\|_{M^{\gamma}} = \left\{\|\psi\|^2_{L^2(\mathbb{R};X_0)} + \left\||\tau|^{\gamma}\,\widehat{\psi}(\tau)\right\|^2_{L^2(\mathbb{R};X_1)}\right\}^{1/2}. \tag{32}$$

For any set $K \subset \mathbb{R}$, the subspace M_K^{γ} of M^{γ} is defined as the set of functions $u \in M^{\gamma}$ with support contained in K:

$$M_K^{\gamma} = M_K^{\gamma}(\mathbb{R}; X_0, X_1) = \{\psi \in M^{\gamma}, \operatorname{supp}\psi \subseteq K\}. \tag{33}$$

Lemma 10 (see [26]). *Assume X_0, X, X_1 are Hilbert spaces satisfying (27) and (28). Then, for any bounded set K and $\forall\gamma > 0$, we have following compact embedding:*

$$M_K^{\gamma}(\mathbb{R}; X_0, X_1) \hookrightarrow L^2(\mathbb{R}; X). \tag{34}$$

The following Korn's inequality plays an essential role in our analysis.

Lemma 11 (see [33]). *Assume that $1 < q < \infty$ and $\Omega \in \mathbb{R}^n$, $n = 2, 3$. Let $v \in \mathbb{W}_0^{1,q}(\Omega)$. Then there exist two positive constants $c_0 = c_0(q, \Omega)$, $c_1 = c_1(q, \Omega)$ such that*

$$c_0 \|\nabla v\|_{L^q} \le \|A(v)\|_{L^q} \le c_1 \|\nabla v\|_{L^q}. \tag{35}$$

Using the notation and operators introduced earlier, we can express the weak formulation of the time-fractional third grade fluid system (5) in the solenoidal vector fields as follows.

Definition 12. Let $u_0 \in \mathbb{H}$ and $f \in L^{2/\alpha_1}(0, T; \mathbb{V}^*)$ $(\alpha_1 \in (0, \alpha))$ be given. A weak solution of system (5) is a function $u \in L^2(0, T; \mathbb{V}) \cap L^{\infty}(0, T; \mathbb{H}) \cap L^4(0, T; \mathbb{W})$ such that for any $v \in \mathbb{W}$

$$\begin{aligned} &\partial_t^{\alpha}(u, v) + \nu((u, v)) + b(u, u, v) \\ &\quad - \left\langle \sigma\operatorname{div}\left(A^2(u)\right) + \beta\operatorname{div}\left(|A(u)|^2 A(u)\right), v\right\rangle \\ &\quad = \langle f, v\rangle, \\ &u(x, 0) = u_0. \end{aligned} \tag{36}$$

Now we give the equivalent form of the first equality of (36) as follows:

$$\begin{aligned} \partial_t^{\alpha}(u, v) = \Big\langle & f - \nu\mathscr{A}u - \mathscr{B}(u, u) + \sigma\operatorname{div}\left(A^2(u)\right) \\ & + \beta\operatorname{div}\left(|A(u)|^2 A(u)\right), v\Big\rangle, \quad \forall v \in \mathbb{W}. \end{aligned} \tag{37}$$

Since $\mathscr{A}u \in L^2(0, T; \mathbb{V}^*) \hookrightarrow L^{4/3}(0, T; \mathbb{W}^*)$, then $f - \nu\mathscr{A}u - \mathscr{B}(u, u) + \sigma\operatorname{div}(A^2(u)) + \beta\operatorname{div}(|A(u)|^2 A(u)) \in \mathbb{W}^*$. Thus

$$\begin{aligned} \partial_t^{\alpha} u = & f - \nu\mathscr{A}u - \mathscr{B}(u, u) + \sigma\operatorname{div}\left(A^2(u)\right) \\ & + \beta\operatorname{div}\left(|A(u)|^2 A(u)\right). \end{aligned} \tag{38}$$

An equivalent form of (36) is as follows:

$$\begin{aligned} &{}_0^c D_t^{\alpha} u + \nu\mathscr{A}u + \mathscr{B}(u, u) - \sigma\operatorname{div}\left(A^2(u)\right) \\ &\quad - \beta\operatorname{div}\left(|A(u)|^2 A(u)\right) = f, \\ &u(x, 0) = u_0. \end{aligned} \tag{39}$$

3. Existence for Time-Fractional Third Grade Fluid System

In this section, we prove the existence of solutions for time-fractional third grade fluid system.

Theorem 13. *Let $u_0 \in \mathbb{H}$ and $f \in L^{2/\alpha_1}(0, T; \mathbb{V}^*)$, $\beta > 0, |\sigma| < \sqrt{2\nu\beta}$. Then there exists at least one solution $u \in L^2(0, T; \mathbb{V}) \cap L^{\infty}(0, T; \mathbb{H}) \cap L^4(0, T; \mathbb{W})$.*

Proof. In order to apply the Galerkin procedure. We consider a basis of $\mathbb{H}_0^1(\Omega)$ constituted of elements ω_i of $\mathscr{D}(\Omega)$ and set $P_m : \mathbb{H} \longrightarrow \mathbb{H}_m$ be the corresponding projection operators. For each m, we define u_m by

$$u_m(t) = \sum_{i=1}^{m} g_{im}(t)\,\omega_i. \tag{40}$$

Applying P_m to (39), we can obtain

$$\begin{aligned} &{}_0^c D_t^{\alpha} u_m + \nu\mathscr{A}u_m + P_m\mathscr{B}(u_m, u_m) \\ &\quad - \sigma P_m\operatorname{div}\left(A^2(u_m)\right) \\ &\quad - \beta P_m\operatorname{div}\left(|A(u_m)|^2 A(u_m)\right) = f_m, \\ &u_m(0) = u_{0m}, \end{aligned} \tag{41}$$

where u_{0m} is the orthogonal projection of u_0 onto the space spanned by $\omega_1, \ldots, \omega_m$ in $\mathbb{H}$.

Taking the scalar product of (41) $_1$ with ω_k, we have

$$\begin{aligned} &\left({}_0^c D_t^{\alpha} u_m, \omega_k\right) + \nu\left((u_m, \omega_k)\right) + \left(P_m\mathscr{B}(u_m, u_m), \omega_k\right) \\ &\quad - \left\langle \sigma P_m\operatorname{div}\left(A^2(u_m)\right)\right. \\ &\quad \left. + \beta P_m\operatorname{div}\left(|A(u_m)|^2 A(u_m)\right), \omega_k\right\rangle = \langle f_m, \omega_k\rangle. \end{aligned} \tag{42}$$

Equations (42) form a nonlinear differential system for the functions $g_{1m}, \ldots, g_{mm}$. By the standard theory of ODE, we have the existence of a solution defined at least on some interval $[0, t_m)$, $0 < t_m \leq T$. Moreover, if $t_m < T$, then $\lim_{t \longrightarrow t_m} \|u_m\| \longrightarrow +\infty$. Otherwise, the following a priori estimates show that in fact $t_m = T$.

Indeed, if we multiply (42) by $g_{km}(t)$ and add all these equations for $k = 1, \ldots, m$,

$$\begin{aligned} &\left({}_0^c D_t^\alpha u_m, u_m\right) + \nu\left(\left(u_m, u_m\right)\right) + b\left(u_m, u_m, u_m\right) \\ &- \left\langle \sigma \operatorname{div}\left(A^2\left(u_m\right)\right) + \beta \operatorname{div}\left(\left|A\left(u_m\right)\right|^2 A\left(u_m\right)\right), u_m \right\rangle \\ &= \left(f_m, u_m\right). \end{aligned} \tag{43}$$

Since $b(u_m, u_m, u_m) = 0$, according to Lemma 5 and Young's inequality, we have

$$\begin{aligned} &{}_0^c D_t^\alpha \left|u_m\right|^2 + 2\nu \left\|u_m\right\|^2 \\ &\quad + 2\int_\Omega \left(\sigma A^2\left(u_m\right) + \beta \left|A\left(u_m\right)\right|^2 A\left(u_m\right)\right) \\ &\quad \cdot \nabla u_m dx \leq \frac{1}{\nu}\left|f\right|^2 + \nu \left\|u_m\right\|^2. \end{aligned} \tag{44}$$

Note that $A(u_m)$ is symmetric; we get

$$\int_\Omega \left|A\left(u_m\right)\right|^2 A\left(u_m\right) \cdot \nabla u_m dx = \frac{1}{2}\left\|A\left(u_m\right)\right\|_{\mathbb{L}^4}^4. \tag{45}$$

From the Cauchy-Schwartz inequality and the fact that

$$\left|A^2\left(u_m\right)\right| = \left|A\left(u_m\right) A\left(u_m\right)\right| \leq \left|A\left(u_m\right)\right|^2, \tag{46}$$

we deduce that

$$\begin{aligned} &\left|\sigma \int_\Omega A^2\left(u_m\right) \cdot \nabla u_m dx\right| \\ &\quad \leq \frac{|\sigma|\,\delta}{2}\left\|A\left(u_m\right)\right\|_{\mathbb{L}^4}^4 + \frac{|\sigma|}{2\delta}\left\|u_m\right\|^2. \end{aligned} \tag{47}$$

Since $|\sigma| < \sqrt{2\beta\nu}$, we can choose $\delta = (2\beta\nu + \sigma^2)/4|\sigma|\nu$, such that

$$\begin{aligned} &\frac{|\sigma|\,\delta}{2} < \frac{\beta}{2} \\ &\text{and } \frac{|\sigma|}{2\delta} < \nu. \end{aligned} \tag{48}$$

We deduce that

$${}_0^c D_t^\alpha \left|u_m\right|^2 + C_0\left\|u_m\right\|^2 + C_1\left\|A\left(u_m\right)\right\|_{\mathbb{L}^4}^4 \leq \frac{1}{\nu}\left|f\right|^2. \tag{49}$$

Integration of (49) from 0 to t shows that

$$\begin{aligned} &\left|u_m(t)\right|^2 + C_0\int_0^t (t-s)^{\alpha-1}\left\|u_m\right\|^2 ds \\ &\quad + C_1\int_0^t (t-s)^{\alpha-1}\left\|A\left(u_m\right)\right\|_{\mathbb{L}^4}^4 ds \leq \left|u_{0m}\right|^2 \\ &\quad + \frac{1}{\nu}\int_0^t (t-s)^{\alpha-1}\left|f\right|^2 ds \leq \left|u_{0m}\right|^2 + \frac{1}{\nu}\int_0^t \left|f\right|^{2/\alpha_1} ds \\ &\quad + \frac{1}{\nu}\int_0^t (t-s)^{(\alpha-1)/(1-\alpha_1)} ds \leq \left|u_{0m}\right|^2 \\ &\quad + \frac{1}{\nu}\int_0^t \left|f(t)\right|^{2/\alpha_1} ds + \frac{1-\alpha_1}{\nu(\alpha-\alpha_1)} T^{(\alpha-1)/(1-\alpha_1)} \\ &\quad \leq \left|u_0\right|^2 + \frac{1}{\nu}\int_0^T \left|f(t)\right|^{2/\alpha_1} ds \\ &\quad + \frac{1-\alpha_1}{\nu(\alpha-\alpha_1)} T^{(\alpha-1)/(1-\alpha_1)}. \end{aligned} \tag{50}$$

Hence $t_m = T$ and

$$\sup_{t\in[0,T]} \left|u_m(t)\right| \leq d_3, \tag{51}$$

$$\int_0^t (t-s)^{\alpha-1}\left\|u_m\right\|^2 ds \leq \frac{d_3}{C_0}, \tag{52}$$

$$\int_0^t (t-s)^{\alpha-1}\left\|A\left(u_m\right)\right\|_{\mathbb{L}^4}^4 ds \leq \frac{d_3}{C_1}, \tag{53}$$

where

$$\begin{aligned} d_3 &= \left|u_0\right|^2 + \frac{1}{\nu}\int_0^T \left|f(t)\right|^{2/\alpha_1} ds \\ &\quad + \frac{1-\alpha_1}{\nu(\alpha-\alpha_1)} T^{(\alpha-1)/(1-\alpha_1)}. \end{aligned} \tag{54}$$

Moreover

$$T^{\alpha-1}\int_0^T \left\|u_m\right\|^2 ds \leq \int_0^t (t-s)^{\alpha-1}\left\|u_m\right\|^2 ds \leq \frac{d_3}{C_0}, \tag{55}$$

$$\begin{aligned} T^{\alpha-1}\int_0^T \left\|A\left(u_m\right)\right\|_{\mathbb{L}^4}^4 ds &\leq \int_0^t (t-s)^{\alpha-1}\left\|A\left(u_m\right)\right\|_{\mathbb{L}^4}^4 ds \\ &\leq \frac{d_3}{C_1}. \end{aligned} \tag{56}$$

Hence, $\{u_m\}$ is bounded in $L^2(0,T;\mathbb{V}) \cap L^\infty(0,T;\mathbb{H}) \cap L^4(0,T;\mathbb{W})$.

As done several times before, we extend all functions by 0 outside the interval $[0,T]$ and consider the Fourier transform of the different equations. The following relations then hold on $\mathbb{R}$.

$$\begin{aligned} {}_0^c D_t^\alpha\left(\widetilde{u}_m(t), \omega_k\right) &= \left\langle \widetilde{\phi}_m(t), \omega_k \right\rangle \\ &\quad + \left(u_{0m}, \omega_k\right)\, {}_{-\infty}I_t^{1-\alpha}\,\delta_{(0)} \\ &\quad - \left(u_m(T), \omega_k\right)\, {}_{-\infty}I_t^{1-\alpha}\,\delta_{(T)}, \end{aligned} \tag{57}$$

where

$$\phi_m = f - \nu \mathcal{A} u_m - \mathcal{B}(u_m) + \sigma \operatorname{div}\left(A^2(u_m)\right) + \beta \operatorname{div}\left(\left|A(u_m)\right|^2 A(u_m)\right). \tag{58}$$

After taking Fourier transforms, (57) yields

$$\begin{aligned}(2i\pi\tau)^{\alpha}(\widehat{u}_m, \omega_k) &= \left\langle \widehat{\phi}_m, \omega_k \right\rangle + (u_{0m}, \omega_k)(2i\pi\tau)^{\alpha-1} \\ &\quad - (u_m(T), \omega_k)(2i\pi\tau)^{\alpha-1}\exp(-2i\pi\tau T),\end{aligned} \tag{59}$$

where $\widehat{u}_m$ and $\widehat{\phi}_m$ represent, respectively, the Fourier transforms of $\widetilde{u}_m$ and $\widetilde{\phi}_m$.

We multiply (59) by $\widehat{g}_k(\tau)$ ($\widehat{g}_k$ = Fourier transform of $\widetilde{g}_k$) and then add these relations for $k = 1, \ldots, m$; we obtain

$$\begin{aligned}(2i\pi\tau)^{\alpha}\left|\widehat{u}_m(\tau)\right|^2 &= \left\langle \widehat{\phi}_m(\tau), \widehat{u}_m(\tau) \right\rangle + (u_{0m}, \widehat{u}_m(\tau))(2i\pi\tau)^{\alpha-1} \\ &\quad - (u_m(T), \widehat{u}_m(\tau))(2i\pi\tau)^{\alpha-1}\exp(-2i\pi\tau T).\end{aligned} \tag{60}$$

In view of the inequality

$$\|\mathcal{B}(u)\|_{\mathbb{V}^*} \le C\|u\|^2, \quad \text{for all } u \in \mathbb{V}. \tag{61}$$

We can obtain

$$\begin{aligned}\int_0^T \|\phi_m\|_{\mathbb{V}^*}\, dt &\le \int_0^T \left(\|f\|_{\mathbb{V}^*} + C_0\|u_m\| + C_1\|u_m\|^2 \right. \\ &\quad \left. + C_2\|A(u_m)\|_{\mathbb{L}^4}^4\right) dt \le \int_0^T \left(\|f\|_{\mathbb{V}^*} + C_0\|u_m\| \right. \\ &\quad \left. + C_1\|u_m\|^2 + C_{2'}\|u_m\|_{\mathbb{W}}^4\right) dt \le C.\end{aligned} \tag{62}$$

Therefore

$$\begin{aligned}\sup_{\tau\in\mathbb{R}} \left\|\widehat{\phi}_m(\tau)\right\|_{\mathbb{V}^*} &\le C, \\ |u_{0m}| &\le C, \\ |u_m(T)| &\le C, \\ &\text{for all } m.\end{aligned} \tag{63}$$

And we can conclude from (60) that

$$|\tau|^{\alpha}\left|\widehat{u}_m(\tau)\right|^2 \le C_3\left\|\widehat{u}_m(\tau)\right\| + C_4|\tau|^{\alpha-1}\left|\widehat{u}_m(\tau)\right|; \tag{64}$$

namely

$$|\tau|^{\alpha}\left|\widehat{u}_m(\tau)\right|^2 \le C_5 \max\left\{1, |\tau|^{\alpha-1}\right\}\left\|\widehat{u}_m(\tau)\right\|. \tag{65}$$

For some fixed $\gamma \in (0, 1/4)$, we have $|\tau|^{2\gamma} \le C_6(\gamma)((1 + |\tau|^{\alpha})/(1 + |\tau|^{\alpha-2\gamma}))$, $\forall \tau \in \mathbb{R}$. Thus

$$\begin{aligned}&\int_{-\infty}^{+\infty} |\tau|^{2\gamma}\left|\widehat{u}_m(\tau)\right|^2 d\tau \\ &\quad \le C_6(\gamma)\int_{-\infty}^{+\infty} \frac{1 + |\tau|^{\alpha}}{1 + |\tau|^{\alpha-2\gamma}}\left|\widehat{u}_m(\tau)\right|^2 d\tau \\ &\quad = C_6(\gamma)\int_{-\infty}^{+\infty} \frac{\left|\widehat{u}_m(\tau)\right|^2}{1 + |\tau|^{\alpha-2\gamma}} d\tau \\ &\qquad + C_6(\gamma)\int_{-\infty}^{+\infty} \frac{|\tau|^{\alpha}\left|\widehat{u}_m(\tau)\right|^2}{1 + |\tau|^{\alpha-2\gamma}} d\tau \\ &\quad \le C_6(\gamma)\int_{-\infty}^{+\infty} \left|\widehat{u}_m(\tau)\right|^2 d\tau \\ &\qquad + C_6(\gamma)\int_{-\infty}^{+\infty} \frac{|\tau|^{\alpha}\left|\widehat{u}_m(\tau)\right|^2}{1 + |\tau|^{\alpha-2\gamma}} d\tau.\end{aligned} \tag{66}$$

By Parseval equality and Poincaré inequality, we have

$$\begin{aligned}C_6(\gamma)\int_{-\infty}^{+\infty} \left|\widehat{u}_m(\tau)\right|^2 d\tau &= C_6(\gamma)\int_{-\infty}^{+\infty} \left|\widetilde{u}_m(t)\right|^2 dt \\ &= C_6(\gamma)\int_0^T |u_m(t)|^2 dt \\ &\le \lambda_1^{-2} C_6(\gamma)\int_0^T \|u_m(t)\|^2 dt \le C(C_0, \gamma, d_3),\end{aligned} \tag{67}$$

and

$$\begin{aligned}&C_6(\gamma)\int_{-\infty}^{+\infty} \frac{|\tau|^{\alpha}\left|\widehat{u}_m(\tau)\right|^2}{1 + |\tau|^{\alpha-2\gamma}} d\tau \le C_7(\gamma) \\ &\quad \cdot \int_{-\infty}^{+\infty} \frac{|\tau|^{\alpha-1}\left\|\widehat{u}_m(\tau)\right\|}{1 + |\tau|^{\alpha-2\gamma}} d\tau + C_8(\gamma) \\ &\quad \cdot \int_{-\infty}^{+\infty} \frac{\left\|\widehat{u}_m(\tau)\right\|}{1 + |\tau|^{\alpha-2\gamma}} d\tau \le C_7(\gamma) \\ &\quad \cdot \left(\int_{-\infty}^{+\infty} \frac{d\tau}{\left(1 + |\tau|^{\alpha-2\gamma}\right)^2}\right)^{1/2} \\ &\quad \cdot \left(\int_{-\infty}^{+\infty} |\tau|^{2\alpha-2}\left\|\widehat{u}_m(\tau)\right\|^2 d\tau\right)^{1/2} + C_8(\gamma) \\ &\quad \cdot \left(\int_{-\infty}^{+\infty} \left\|\widehat{u}_m(\tau)\right\|^2 d\tau\right)^{1/2} \\ &\quad \cdot \left(\int_{-\infty}^{+\infty} \frac{d\tau}{\left(1 + |\tau|^{\alpha-2\gamma}\right)^2}\right)^{1/2} = C_7(\gamma) \\ &\quad \cdot \left(\int_{-\infty}^{+\infty} \frac{d\tau}{\left(1 + |\tau|^{\alpha-2\gamma}\right)^2}\right)^{1/2}\end{aligned}$$

$$\cdot\left(\int_{-\infty}^{+\infty}|\tau|^{2\alpha-2}\left\|\widehat{u}_m(\tau)\right\|^2 d\tau\right)^{1/2}+C_8(\gamma)$$
$$\cdot\left(\int_{-\infty}^{+\infty}\frac{d\tau}{\left(1+|\tau|^{\alpha-2\gamma}\right)^2}\right)^{1/2}\left(\int_0^T\left\|u_m(t)\right\|^2 dt\right)^{1/2}$$
$$=C_7(\gamma)\left(\int_{-\infty}^{+\infty}\frac{d\tau}{\left(1+|\tau|^{\alpha-2\gamma}\right)^2}\right)^{1/2}$$
$$\cdot\left(\int_{-\infty}^{+\infty}\left\|{}_{-\infty}I_t^{1-\alpha}\widetilde{u}_m(t)\right\|^2 dt\right)^{1/2}+C_8(\gamma)$$
$$\cdot\left(\int_{-\infty}^{+\infty}\frac{d\tau}{\left(1+|\tau|^{\alpha-2\gamma}\right)^2}\right)^{1/2}\left(\int_0^T\left\|u_m(t)\right\|^2 dt\right)^{1/2}$$
$$=C_7(\gamma)\left(\int_{-\infty}^{+\infty}\frac{d\tau}{\left(1+|\tau|^{\alpha-2\gamma}\right)^2}\right)^{1/2}$$
$$\cdot\left(\int_0^T\left\|{}_0I_t^{1-\alpha}u_m(t)\right\|dt\right)^{1/2}+C_8(\gamma)$$
$$\cdot\left(\int_{-\infty}^{+\infty}\frac{d\tau}{\left(1+|\tau|^{\alpha-2\gamma}\right)^2}\right)^{1/2}\left(\int_0^T\left\|u_m(t)\right\|^2 dt\right)^{1/2}$$
$$=C_7(\gamma)\left(\int_{-\infty}^{+\infty}\frac{d\tau}{\left(1+|\tau|^{\alpha-2\gamma}\right)^2}\right)^{1/2}$$
$$\cdot\int_0^T\left(\left\|u_m(t)\right\|^2 dt\right)^{1/2}+C_8(\gamma)$$
$$\cdot\left(\int_{-\infty}^{+\infty}\frac{d\tau}{\left(1+|\tau|^{\alpha-2\gamma}\right)^2}\right)^{1/2}\left(\int_0^T\left\|u_m(t)\right\|^2 dt\right)^{1/2}. \tag{68}$$

We have also used the convergence of the infinite integral in the above integral

$$\left(\int_{-\infty}^{+\infty}\frac{d\tau}{\left(1+|\tau|^{\alpha-2\gamma}\right)^2}\right)^{1/2},\quad for\ some\ \gamma\in\left(0,\frac{1}{4}\right). \tag{69}$$

We can conclude that

$$\int_{-\infty}^{+\infty}|\tau|^{2\gamma}\left|\widehat{u}_m(\tau)\right|^2 d\tau\le C.\quad for\ some\ \gamma\in\left(0,\frac{1}{4}\right). \tag{70}$$

Next, we want to pass to the limit as $m\longrightarrow\infty$ in (42) using the estimates (51), (55)-(56), and (70). We are only concerned with a passage to the limit as $m\longrightarrow\infty$.

Considering the Lemma 7, there exist a sequence $m'\longrightarrow\infty$, and one function $\{u\}$ such that

$$\begin{aligned}
&u_{m'}\rightharpoonup u\ in\ L^2(0,T;\mathbb{V})\ \ weakly,\\
&u_{m'}\longrightarrow u\ in\ L^\infty(0,T;\mathbb{H})\ \ weak-star,\\
&u_{m'}\longrightarrow u\ in\ L^2(0,T;\mathbb{H})\ \ strongly,\\
&u_{m'}\rightharpoonup u\ in\ L^4(0,T;\mathbb{W})\ \ weakly.
\end{aligned} \tag{71}$$

Taking $v\in\mathscr{V}$, we multiply (41) by v, integrate over $[t_0,t]$, and we have

$$\begin{aligned}
\left(u_{m'}(t),v\right)-\left(u_{m'}(t_0),v\right)&=\int_0^{t_0}\left(\left(t_0-s\right)^{\alpha-1}-(t\right.\\
&-s)^{\alpha-1}\left.\right)\left[\nu\left(\left(u_{m'}(s),v\right)\right)\right.\\
&+b\left(u_{m'}(s),u_{m'}(s),P_{m'}v\right)-\left\langle\sigma\mathrm{div}\left(A^2\left(u_{m'}\right)\right)\right.\\
&+\left.\beta\mathrm{div}\left(\left|A\left(u_{m'}\right)\right|^2A\left(u_{m'}\right)\right),P_{m'}v\right\rangle\\
&-\left\langle f_{m'},v\right\rangle\Big]ds-\int_{t_0}^t(t-s)^{\alpha-1}\left[\nu\left(\left(u_{m'}(s),v\right)\right)\right.\\
&+b\left(u_{m'}(s),u_{m'}(s),P_{m'}v\right)-\left\langle\sigma\mathrm{div}\left(A^2\left(u_{m'}\right)\right)\right.\\
&+\left.\beta\mathrm{div}\left(\left|A\left(u_{m'}\right)\right|^2A\left(u_{m'}\right)\right),P_{m'}v\right\rangle\\
&-\left\langle f_{m'},v\right\rangle\Big]ds.
\end{aligned} \tag{72}$$

In view of $u_{m'}\rightharpoonup u$ in $L^2(0,T;\mathbb{V})$, we can assume that $u_{m'}(t_0)\rightharpoonup u(t_0)$ in $\mathbb{V}$ for all $t_0\in[0,T]\backslash K$, where $\mathrm{mes}(K)=0$. Therefore, $\lim_{m'\longrightarrow\infty}u_{m'}(t_0)=u(t_0)$ in $\mathbb{H}$ for $t_0\notin K$.

Finally, we look at the convergence of the nonlinear terms in (72).

By (55)-(56) and using Lebesgue's dominated convergence theorem, we have

$$\begin{aligned}
&\lim_{m'\longrightarrow\infty}\int_{t_0}^t(t-s)^{\alpha-1}b\left(u_{m'}(s),u_{m'}(s),P_{m'}v\right)ds\\
&\quad=\int_{t_0}^t(t-s)^{\alpha-1}b\left(u(s),u(s),Pv\right)ds,\\
&\lim_{m'\longrightarrow\infty}\int_0^{t_0}\left(\left(t_0-s\right)^{\alpha-1}-(t-s)^{\alpha-1}\right)\\
&\quad\cdot b\left(u_{m'}(s),u_{m'}(s),P_{m'}v\right)ds=\int_0^{t_0}\left(\left(t_0-s\right)^{\alpha-1}\right.\\
&\quad\left.-(t-s)^{\alpha-1}\right)b\left(u(s),u(s),v\right)ds.
\end{aligned} \tag{73}$$

Next, let $\mathscr{T}_1:\mathbb{W}\longrightarrow\mathbb{W}^*$ be defined as

$$\begin{aligned}
\mathscr{T}_1(v)=&-\nu\triangle v-\sigma\mathrm{div}\left(A^2(v)\right)\\
&-\beta\mathrm{div}\left(|A(v)|^2A(v)\right).
\end{aligned} \tag{74}$$

It is clear that $\mathscr{T}_1$ is a monotone operator. We show that

$$\begin{aligned}(\mathrm{I})\ &\lim_{m'\longrightarrow\infty}\int_0^{t_0}\left((t_0-s)^{\alpha-1}-(t-s)^{\alpha-1}\right)\left\langle\mathscr{T}_1\left(u_{m'}(t)\right),v\right\rangle ds\\&=\int_0^{t_0}\left((t_0-s)^{\alpha-1}-(t-s)^{\alpha-1}\right)\left\langle\mathscr{T}_1\left(u(s)\right),v\right\rangle ds.\end{aligned}\tag{75}$$

This can be achieved by the monotony method as in [8, 34]; see also [35, 36]. Indeed, since $\mathscr{T}_1(u_{m'})$ is uniformly (in m') bounded in $L^{4/3}(0,T;\mathbb{W}^*)$, we may assume that

$$\mathscr{T}_1\left(u_{m'}\right)\longrightarrow\Xi\ \textit{weak-star in}\ L^{4/3}\left(0,T;\mathbb{W}^*\right).\tag{76}$$

Due to (43) and taking a sequence $\{m'\mid m'\longrightarrow\infty\}$, we have

$$\left({}_0^cD_t^\alpha u_{m'},u_{m'}\right)+\left\langle\mathscr{T}_1\left(u_{m'}\right),u_{m'}\right\rangle=\left\langle f,u_{m'}\right\rangle,\tag{77}$$

and integration of (77) from 0 to t_0 red shows that

$$\begin{aligned}&\int_0^{t_0}(t-s)^{\alpha-1}\left\langle\mathscr{T}_1\left(u_{m'}\right),u_{m'}\right\rangle_1 ds\\&\le\frac{1}{2}\left|u_{m'}(0)\right|^2-\frac{1}{2}\left|u_{m'}(t_0)\right|^2\\&\quad+\int_0^{t_0}(t-s)^{\alpha-1}\left\langle f,u_{m'}\right\rangle_1 ds,\end{aligned}\tag{78}$$

where $\langle,\rangle_1$ is the duality product between the spaces $L^{4/3}(0,T;\mathbb{W}^*)$ and $L^4(0,T;\mathbb{W})$.

By (42), we have

$$\begin{aligned}&\left({}_0^cD_t^\alpha u_{m'},\omega\psi\right)+\left\langle\mathscr{B}\left(u_{m'},u_{m'}\right),\omega\psi\right\rangle\\&\quad-\left\langle\mathscr{T}_1\left(u_{m'}\right),\omega\psi\right\rangle=\left\langle f,\omega\psi\right\rangle.\end{aligned}\tag{79}$$

Passing to the limit in (79),

$$\left({}_0^cD_t^\alpha u,\omega\psi\right)+\left\langle\mathscr{B}(u,u),\omega\psi\right\rangle-\left\langle\Xi,\omega\psi\right\rangle=\left\langle f,\omega\psi\right\rangle.\tag{80}$$

Taking $\omega\psi=u$, we can obtain

$$\begin{aligned}&\int_0^{t_0}(t-s)^{\alpha-1}\left\langle\Xi,u\right\rangle_1 ds\\&\le\frac{1}{2}\left|u(0)\right|^2-\frac{1}{2}\left|u(t_0)\right|^2\\&\quad+\int_0^{t_0}(t-s)^{\alpha-1}\left\langle f,u_{m'}\right\rangle_1 ds.\end{aligned}\tag{81}$$

Due to the monotonicity of $\mathscr{T}_1$, we have for any $\varphi\in L^4(0,T;\mathbb{W})$

$$\begin{aligned}\left\langle\mathscr{T}_1\left(u_{m'}\right),u_{m'}\right\rangle_1&\ge\left\langle\mathscr{T}_1\left(u_{m'}\right),\varphi\right\rangle_1\\&\quad+\left\langle\mathscr{T}_1(\varphi),u_{m'}-\varphi\right\rangle_1.\end{aligned}\tag{82}$$

Combining (78), (81), and (82), we obtain by passing to the limit in m'

$$\begin{aligned}&\int_0^{t_0}(t-s)^{\alpha-1}\left\langle\Xi-\mathscr{T}_1(\varphi),u_\epsilon-\varphi\right\rangle_1 ds\ge0,\\&\qquad\text{for any }\varphi\in L^4(0,T;\mathbb{W}).\end{aligned}\tag{83}$$

Take $\varphi=u-\delta\phi$ for $\delta>0$ and $\phi\in L^4(0,T;\mathbb{W})$. Then after division by δ and tending δ to 0, we deduce that

$$\begin{aligned}&\int_0^{t_0}(t-s)^{\alpha-1}\left\langle\Xi-\mathscr{T}_1(u),\phi\right\rangle_1 ds\ge0,\\&\qquad\text{for any }\phi\in L^4(0,T;\mathbb{W}).\end{aligned}\tag{84}$$

Hence, $\Xi=\mathscr{T}_1(u)$. Then

$$\begin{aligned}&\lim_{m'\longrightarrow\infty}\int_0^{t_0}\left((t_0-s)^{\alpha-1}-(t-s)^{\alpha-1}\right)\\&\quad\cdot\left\langle\mathscr{T}_1\left(u_{m'}(t)\right),v\right\rangle ds=\int_0^{t_0}\left((t_0-s)^{\alpha-1}\right.\\&\quad\left.-(t-s)^{\alpha-1}\right)\left\langle\mathscr{T}_1\left(u(s)\right),v\right\rangle ds.\end{aligned}\tag{85}$$

A simple argument shows that

$$\begin{aligned}&\lim_{m'\longrightarrow\infty}\int_{t_0}^{t}(t-s)^{\alpha-1}\left\langle\mathscr{T}_1\left(u_{m'}(t)\right),v\right\rangle ds\\&\quad=\int_{t_0}^{t}(t-s)^{\alpha-1}\left\langle\mathscr{T}_1\left(u(s)\right),v\right\rangle ds.\end{aligned}\tag{86}$$

Taking the limit of (72) as $m'\longrightarrow\infty$, we find that

$$\begin{aligned}&\left(u(t),v\right)-\left(u(t_0),v\right)=\int_0^{t_0}\left((t_0-s)^{\alpha-1}-(t-s)^{\alpha-1}\right)\\&\quad\cdot\left[\nu\left(\left(u(s),v\right)\right)+b\left(u(s),u(s),v\right)\right.\\&\quad-\left\langle\sigma\mathrm{div}\left(A^2(u)\right)+\beta\mathrm{div}\left(\left|A(u)\right|^2A(u)\right),v\right\rangle\\&\quad\left.-\left\langle f,v\right\rangle\right]ds-\int_{t_0}^{t}(t-s)^{\alpha-1}\left[\nu\left(\left(u(s),v\right)\right)\right.\\&\quad+b\left(u(s),u(s),v\right)\\&\quad-\left\langle\sigma\mathrm{div}\left(A^2(u)\right)+\beta\mathrm{div}\left(\left|A(u)\right|^2A(u)\right),v\right\rangle\\&\quad\left.-\left\langle f,v\right\rangle\right]ds.\end{aligned}\tag{87}$$

It is clear that $(u(t),v)-(u(t_0),v)\longrightarrow0$, as $t\longrightarrow t_0$.

Set $t_0=0$ in (87); we can obtain (36). The proof is complete. □

4. Uniqueness of Solutions for the Time-Fractional Third Grade Fluid System

In this section, we prove the uniqueness of solutions of problem (39).

Theorem 14. *The solution u of problems (39) given by Theorem 13 is unique.*

Proof. We denote by u_1, u_2 two solutions of problem (39) and set $u = u_1 - u_2$, by subtracting the relation (39) satisfied by u_1 and u_2; we obtain

$$\begin{aligned} &{}_0^cD_t^\alpha u - \nu \triangle u + \mathcal{J}(u_1) - \mathcal{J}(u_2) + \mathcal{K}(u_1) - \mathcal{K}(u_2) \\ &\quad = \mathcal{B}(u_2) - \mathcal{B}(u_1), \\ &\nabla \cdot u = 0. \end{aligned} \tag{88}$$

Taking the inner product of (88) with u, it yields

$$\begin{aligned} &\left\langle {}_0^cD_t^\alpha u, u \right\rangle + \nu \|u(t)\|^2 \\ &\quad = -\left\langle \mathcal{J}(u_1) - \mathcal{J}(u_2), u \right\rangle \\ &\qquad - \left\langle \mathcal{K}(u_1) - \mathcal{K}(u_2), u \right\rangle - b(u, u_2, u). \end{aligned} \tag{89}$$

Since $b(v, w, w) = 0$, then

$$\begin{aligned} &{}_0^cD_t^\alpha |u(t)|^2 + 2\nu \|u(t)\|^2 \\ &\quad = -2\left\langle \mathcal{J}(u_1) - \mathcal{J}(u_2), u \right\rangle \\ &\qquad - 2\left\langle \mathcal{K}(u_1) - \mathcal{K}(u_2), u \right\rangle - 2b(u, u_2, u). \end{aligned} \tag{90}$$

Bear in mind that

$$\begin{aligned} &\mathcal{T}(u) = -(\nu - \nu\delta_0) \triangle u + (1 - \delta_0)\mathcal{J}(u) + \mathcal{K}(u), \\ &\delta_0 = 1 - \sqrt{\frac{\alpha^2}{2\nu\beta}} \in (0, 1). \end{aligned} \tag{91}$$

We deduce that

$${}_0^cD_t^\alpha |u(t)|^2 + 2\nu\delta_0 \|u(t)\|^2 \le 2\left|b(u, u_2, u)\right|. \tag{92}$$

Noting that $H_0^1 \hookrightarrow L^6$ and

$$\left|b(u, u_2, u)\right| \le C\|u\|_{L^6} \left\|\nabla u_2\right\|_{L^3} |u| \tag{93}$$

implies that

$$\begin{aligned} 2\left|b(u, u_2, u)\right| &\le C\|u\| \left\|\nabla u_2\right\|_{L^3} |u| \\ &\le 2\nu\delta_0 \|u\|^2 + C_9 |u|^2 \left\|\nabla u_2\right\|_{L^3}^2. \end{aligned} \tag{94}$$

Thus

$${}_0^cD_t^\alpha |u(t)|^2 \le C_9 |u|^2 \left\|\nabla u_2\right\|_{L^3}^2. \tag{95}$$

By Gronwall inequality and (51), (53), we have

$$\begin{aligned} &|u(t)|^2 \\ &\le |u(0)|^2 \exp\left(\frac{C_9}{\Gamma(\alpha)} \int_0^t (t-s)^{\alpha-1} \left\|\nabla u_2\right\|_{L^3}^2 ds\right) \\ &\le |u(0)|^2 \exp\left(\frac{C_9}{\Gamma(\alpha)} \int_0^t (t-s)^{\alpha-1} \left\|Au_2\right\|_{L^4}^4 ds\right) \\ &\le |u(0)|^2 \exp\left(\frac{C_9 d_3}{\Gamma(\alpha) C_1}\right). \end{aligned} \tag{96}$$

Since $u(0) = 0$, the last relation can imply that

$$|u(t)|^2 = 0, \quad 0 \le t \le T, \tag{97}$$

and the uniqueness is proved. □

5. Optimal Control

In this section, we will consider the optimal control problems

$$\begin{aligned} \text{minimize} \quad &\frac{1}{2} \int_0^T \int_\Omega (u(x,t) - z(x,t))^2 \, dx \, dt \\ &+ \int_0^T h(\omega(t)) \, dt, \end{aligned} \tag{98}$$

where $\omega \in L^{2/\alpha_1}(0, T; U)$.

We will consider the systems with control in $\Omega \subset \mathbb{R}^3$

$$\begin{aligned} &\partial_t^\alpha u - \nu\Delta u + (u \cdot \nabla) u - \sigma \mathrm{div}\left(A^2(u)\right) \\ &\quad - \beta \mathrm{div}\left(|A(u)|^2 A(u)\right) = -\nabla p + c_0\omega + f, \\ &\nabla \cdot u = 0, \\ &\qquad u = 0, \ x \in \partial\Omega; \ u(x, 0) = u_0, \ x \in \Omega. \end{aligned} \tag{99}$$

Definition 15. Let $u_0 \in \mathbb{H}, f \in L^{2/\alpha_1}(0, T; \mathbb{V}^*)$ and $\omega \in L^{2/\alpha_1}(0, T; U)$; a function $u \in L^2(0, T; \mathbb{V}) \cap L^\infty(0, T; \mathbb{H}) \cap L^4(0, T; \mathbb{W})$ is called a weak solution of system (7) if

$$\begin{aligned} &\partial_t^\alpha (u, v) + \nu((u, v)) + b(u, u, v) \\ &\quad - \left\langle \sigma \mathrm{div}\left(A^2(u)\right) + \beta \mathrm{div}\left(|A(u)|^2 A(u)\right), v \right\rangle \\ &\quad = \left\langle c_0\omega + f, v \right\rangle, \\ &u(0) = u_0. \end{aligned} \tag{100}$$

Similarly we give the equivalent form as follows:

$$\begin{aligned} &{}_0^cD_t^\alpha u + \nu\mathcal{A}u + \mathcal{B}(u, u) + \mathcal{K}(u) + \mathcal{J}(u) = C\omega + f, \\ &\qquad u(0) = u_0. \end{aligned} \tag{101}$$

If $z \in L^2(0, T; \mathbb{H})$, rewriting problem (98) in the abstract form, we have

$$\begin{aligned} \text{(P)} \ \text{minimize} \quad &J(u, \omega) \\ &= \frac{1}{2} \int_0^T (u(x,t) - z(x,t))^2 \, dt \\ &\quad + \int_0^T h(\omega(t)) \, dt \end{aligned} \tag{102}$$

over $(u, \omega) \in (L^2(0, T; \mathbb{V}) \cap L^\infty(0, T; \mathbb{H}) \cap L^4(0, T; \mathbb{W})) \times L^{2/\alpha_1}(0, T; U)$ subject to (101).

We assume that

(i) $z \in L^2(0, T; \mathbb{H})$;

(ii) the function $h : U \longrightarrow \mathbb{R}$ is convex and lower semicontinuous and satisfies

$$h(\omega) \ge b_1 |\omega|_U^{2/\alpha_1} + b_2 \tag{103}$$

for some $b_1 > 0, b_2 \in \mathbb{R}$.

Theorem 16. *If hypotheses (i) and (ii) hold, then problem (P) has at least one solution* $(u^*, \omega^*) \in (L^2(0,T;\mathbb{V}) \cap L^\infty(0,T;\mathbb{H}) \cap L^4(0,T;\mathbb{W})) \times L^{2/\alpha_1}(0,T;U)$.

Proof. Replacing f with $C\omega + f$ in Theorems 13 and 14, we show that system (101) has an weak solution corresponding to ω. Suppose that (u_m, ω_m) are a minimizing sequence of problem (P); namely,

$$\begin{aligned} &J(u_m,\omega_m) \longrightarrow \inf J(u,\omega), \\ &{}_0^c D_t^\alpha u_m + \nu \mathscr{A} u_m + \mathscr{B}(u_m,u_m) + \mathscr{K}(u_m) + \mathscr{J}(u_m) \\ &\quad = C\omega_m + f, \\ &u_m(0) = u_0. \end{aligned} \tag{104}$$

According to hypothesis (ii), we can conclude that $\{\omega_m\}$ is bounded in $L^{2/\alpha_1}(0,T;U)$. Thus, there exists $\omega^* \in L^{2/\alpha_1}(0,T;U)$ such that

$$\omega_m \rightharpoonup \omega^* \text{ in } L^{2/\alpha_1}(0,T;U) \text{ weakly}. \tag{105}$$

Similar to (49), we obtain

$$\begin{aligned} &{}_0^c D_t^\alpha |u_m|^2 + C_0 \|u_m\|^2 + C_1 \|A(u_m)\|_{\mathbb{L}^4}^4 \\ &\quad \le \frac{1}{\nu} |f + C\omega_m|^2. \end{aligned} \tag{106}$$

This yields

$$\begin{aligned} &|u_m(t)|^2 + C_0 \int_0^t (t-s)^{\alpha-1} \|u_m\|^2 \, ds \\ &\quad + C_1 \int_0^t (t-s)^{\alpha-1} \|A(u_m)\|_{\mathbb{L}^4}^4 \, ds \\ &\le |u_m(0)|^2 + \frac{1}{\nu} \int_0^T |f(t) + C\omega_m|^{2/\alpha_1} \, ds \\ &\quad + \frac{1-\alpha_1}{\nu(\alpha-\alpha_1)} T^{(\alpha-1)/(1-\alpha_1)}. \end{aligned} \tag{107}$$

Hence

$$\begin{aligned} &C_0 T^{\alpha-1} \int_0^t \|u_m(s)\|^2 \, ds \\ &\le C_0 \int_0^t (t-s)^{\alpha-1} \|u_m(s)\|^2 \, ds \\ &\le |u_m(0)|^2 + \frac{1}{\nu} \int_0^T |f(t) + C\omega_m(s)|^{2/\alpha_1} \, ds \\ &\quad + \frac{1-\alpha_1}{\nu(\alpha-\alpha_1)} T^{(\alpha-1)/(1-\alpha_1)}, \end{aligned} \tag{108}$$

$$\begin{aligned} &C_1 T^{\alpha-1} \int_0^t \|A(u_m(s))\|_{\mathbb{L}^4}^4 \, ds \\ &\le C_1 \int_0^t (t-s)^{\alpha-1} \|A(u_m(s))\|_{\mathbb{L}^4}^4 \, ds \\ &\le |u_m(0)|^2 + \frac{1}{\nu} \int_0^T |f(t) + C\omega_m(s)|^{2/\alpha_1} \, ds \\ &\quad + \frac{1-\alpha_1}{\nu(\alpha-\alpha_1)} T^{(\alpha-1)/(1-\alpha_1)}. \end{aligned} \tag{109}$$

Therefore, $\{u_m\}$ is bounded in $L^\infty(0,T;\mathbb{H}) \cap L^2(0,T;\mathbb{V}) \cap L^4(0,T;\mathbb{W})$. Thus, there exists an element $u^* \in L^2(0,T;\mathbb{V}) \cap L^\infty(0,T;\mathbb{H}) \cap L^4(0,T;\mathbb{W})$ such that

$$\begin{aligned} &u_m \longrightarrow u^* \text{ in } L^\infty(0,T;\mathbb{H}) \text{ weak} - \text{star}, \\ &u_m \rightharpoonup u^* \text{ in } L^2(0,T;\mathbb{V}) \text{ weakly}, \\ &u_m \longrightarrow u^* \text{ in } L^2(0,T;\mathbb{H}) \text{ strongly}, \\ &u_m \rightharpoonup u^* \text{ in } L^4(0,T;\mathbb{W}) \text{ weakly}. \end{aligned} \tag{110}$$

We need to have some uniform bound on $\mathscr{A}u_m, \mathscr{B}(u_m,u_m)$, $\mathscr{K}(u_m)$, and $\mathscr{J}(u_m)$.

We firstly estimate the term $\mathscr{B}(u_m,u_m)$. In fact

$$|\mathscr{B}(u_m,u_m),v| = C|u_m|\|u_m\|\|v\|, \quad \forall v \in \mathbb{V}. \tag{111}$$

Then

$$|\mathscr{B}(u_m,u_m)|_{\mathbb{V}^*} \le C|u_m|\|u_m\|. \tag{112}$$

Therefore

$$\begin{aligned} &\int_0^t |\mathscr{B}(u_m(s),u_m(s))|_{\mathbb{V}^*}^2 \, ds \\ &\quad \le C \int_0^t |u_m(s)|^2 \|u_m(s)\|^2 \, ds \\ &\quad \le C \sup |u_m(s)|^2 \int_0^t \|u_m(s)\|^2 \, ds < \infty. \end{aligned} \tag{113}$$

This implies that there exists η^* such that

$$\mathscr{B}(u_m,u_m) \rightharpoonup \mathscr{B}(u^*,u^*) \text{ in } L^2(0,T;\mathbb{V}^*) \text{ weakly}. \tag{114}$$

For the similar derivations of relation (I), we deduce that

$$\begin{aligned} &\nu \mathscr{A} u_m + \mathscr{K}(u_m) + \mathscr{J}(u_m) = \mathscr{T}_1(u_m) \rightharpoonup \mathscr{T}_1(u^*) \\ &\quad = \nu \mathscr{A} u^* + \mathscr{K}(u^*) + \mathscr{J}(u^*) \text{ in } L^{4/3}(0,T;\mathbb{W}^*). \end{aligned} \tag{115}$$

Now let $v \in \mathscr{V}$; take the scalar product of (104) with v and integrate; it follows

$$\begin{aligned}
&(u_m(t), v) - (u_m(t_0), v) = \int_0^{t_0} \left((t_0 - s)^{\alpha-1}\right. \\
&\left. - (t-s)^{\alpha-1}\right) [b(u_m(s), u_m(s), v) \\
&+ \langle v\mathscr{A}u_m + \mathscr{K}(u_m) + \mathscr{J}(u_m), v\rangle \\
&- \langle C\omega_m(s) + f(s), v\rangle] ds - \int_{t_0}^{t} (t-s)^{\alpha-1} \\
&\cdot [b(u_m(s), u_m(s), v) \\
&+ \langle v\mathscr{A}u_m + \mathscr{K}(u_m) + \mathscr{J}(u_m), v\rangle \\
&- \langle C\omega_m(s) + f(s), v\rangle] ds.
\end{aligned} \tag{116}$$

By similar arguments in Theorem 13 and taking the limits as $m \longrightarrow \infty$, we can conclude

$$\begin{aligned}
&(u^*(t), v) - (u^*(t_0), v) = \int_0^{t_0} \left((t_0 - s)^{\alpha-1}\right. \\
&\left. - (t-s)^{\alpha-1}\right) [b(u^*(s), u^*(s), v) \\
&+ \langle v\mathscr{A}u^* + \mathscr{K}(u^*) + \mathscr{J}(u^*), v\rangle \\
&- \langle C\omega^*(s) + f(s), v\rangle] ds - \int_{t_0}^{t} (t-s)^{\alpha-1} \\
&\cdot [b(u^*(s), u^*(s), v) \\
&+ \langle v\mathscr{A}u^* + \mathscr{K}(u^*) + \mathscr{J}(u^*), v\rangle \\
&- \langle C\omega^*(s) + f(s), v\rangle] ds.
\end{aligned} \tag{117}$$

Applying the Caputo fractional derivative of order α on the sides of the above equality for $t_0 = 0$, we obtain

$$\begin{aligned}
&\left\langle {}_0^c D_t^{\alpha} u^*, v\right\rangle + \langle v\mathscr{A}u^* + \mathscr{K}(u^*) + \mathscr{J}(u^*), v\rangle \\
&\quad + b(u^*, u^*, v) = \langle C\omega^* + f, v\rangle, \\
&u^*(0) = u_0.
\end{aligned} \tag{118}$$

Namely, an equivalent form of the last equality is

$$\begin{aligned}
&{}_0^c D_t^{\alpha} u^* + v\mathscr{A}u^* + \mathscr{K}(u^*) + \mathscr{J}(u^*) + \mathscr{B}(u^*, u^*) \\
&\quad = C\omega^* + f, \\
&u^*(0) = u_0.
\end{aligned} \tag{119}$$

Hence, we can see that (u^*, ω^*) satisfies system (104).

From weak lower semicontinuity of function $(u, \omega) \longrightarrow J(u, \omega)$, we deduce

$$J(u^*, \omega^*) = \inf J(u, \omega). \tag{120}$$

Then (u^*, ω^*) is an optimal pair for problem (P). The proof of Theorem 16 is complete. □

Data Availability

No data were used to support this study.

Conflicts of Interest

The authors declare that there are no conflicts of interest regarding the publication of this article.

Acknowledgments

This work was partially supported by the Scientific Research Project of Anhui University of Chinese Medicine (no. 2018zryb04).

References

[1] R. S. Rivlin and J. L. Ericksen, "Stress-deformation relations for isotropic materials," *Journal of Rational Mechanics and Analysis*, vol. 4, pp. 323–425, 1955.

[2] O. A. Ladyzhenskaya, "New equations for the description of the motions of viscous incompressible fluids, and global solvability for their boundary value problems," *Trudy Matematicheskogo Instituta Imeni V. A. Steklova*, vol. 102, pp. 85–104, 1967.

[3] R. L. Fosdick and K. R. Rajagopal, "Anomalous features in the model of 'second order fluids'," *Archive for Rational Mechanics and Analysis*, vol. 70, no. 2, pp. 145–152, 1979.

[4] C. Amrouche and D. Cioranescu, "On a class of fluids of grade 3," *International Journal of Non-Linear Mechanics*, vol. 32, no. 1, pp. 73–88, 1997.

[5] A. Sequeira and J. Videman, "Global existence of classical solutions for the equations of third grade fluids," *Journal of Mathematical and Physical Sciences*, vol. 29, no. 2, pp. 47–69, 1995.

[6] V. Busuioc and D. Iftimie, "Global existence and uniqueness of solutions for the equations of third grade fluids," *International Journal of Non-Linear Mechanics*, vol. 39, no. 1, pp. 1–12, 2004.

[7] M. Paicu, "Global existence in the energy space of the solutions of a non-Newtonian fluid," *Physica D: Nonlinear Phenomena*, vol. 237, no. 10-12, pp. 1676–1686, 2008.

[8] M. Hamza and M. Paicu, "Global existence and uniqueness result of a class of third-grade fluids equations," *Nonlinearity*, vol. 20, no. 5, pp. 1095–1114, 2007.

[9] C. Zhao, Y. Liang, and M. Zhao, "Upper and lower bounds of time decay rate of solutions to a class of incompressible third grade fluid equations," *Nonlinear Analysis: Real World Applications*, vol. 15, pp. 229–238, 2014.

[10] X. Chai, Z. Chen, and W. Niu, "Large time behavior of a third grade fluid system," *Acta Mathematica Scientia B*, vol. 36, no. 6, pp. 1590–1608, 2016.

[11] R. Herrmann, *Fractional Calculus: An Introduction for Physicists*, World Scientific, Singapore, 2nd edition, 2014.

[12] R. Hilfer, *Applications of Fractional Calculus in Physics*, World Scientific, Singapore, 2000.

[13] M. El-Shahed and A. Salem, "On the generalized Navier-Stokes equations," *Applied Mathematics and Computation*, vol. 156, no. 1, pp. 287–293, 2004.

[14] Z. Z. Ganji, D. D. Ganji, A. D. Ganji, and M. Rostamian, "Analytical solution of time-fractional Navier-Stokes equation in polar coordinate by homotopy perturbation method,"

Numerical Methods for Partial Differential Equations, vol. 26, no. 1, pp. 117–124, 2010.

[15] L. Peng, Y. Zhou, B. Ahmad, and A. Alsaedi, "The Cauchy problem for fractional Navier–Stokes equations in Sobolev spaces," *Chaos, Solitons & Fractals*, vol. 102, pp. 218–228, 2017.

[16] S. Momani and Z. Odibat, "Analytical solution of a time-fractional Navier-Stokes equation by Adomian decomposition method," *Applied Mathematics and Computation*, vol. 177, no. 2, pp. 488–494, 2006.

[17] P. M. de Carvalho-Neto and G. Planas, "Mild solutions to the time fractional Navier-Stokes equations in RN," *Journal of Differential Equations*, vol. 259, no. 7, pp. 2948–2980, 2015.

[18] Y. Zhou and L. Peng, "On the time-fractional Navier—Stokes equations," *Computers & Mathematics with Applications*, vol. 73, no. 6, pp. 874–891, 2017.

[19] Y. Zhou and L. Peng, "Weak solutions of the time-fractional Navier—Stokes equations and optimal control," *Computers & Mathematics with Applications*, vol. 73, no. 6, pp. 1016–1027, 2017.

[20] Y. Zhou, L. Peng, B. Ahmad, and A. Alsaedi, "Energy methods for fractional Navier–Stokes equations," *Chaos, Solitons & Fractals*, vol. 102, pp. 78–85, 2017.

[21] Q. Al-Mdallal, K. Abro, and I. Khan, "Analytical Solutions of Fractional Walter's B Fluid with Applications," *Complexity*, vol. 2018, Article ID 8131329, 10 pages, 2018.

[22] T. A. Maraaba, F. Jarad, and D. Baleanu, "On the existence and the uniqueness theorem for fractional differential equations with bounded delay within Caputo derivatives," *Science China Mathematics*, vol. 51, no. 10, pp. 1775–1786, 2008.

[23] T. Maraaba, D. Baleanu, and F. Jarad, "Existence and uniqueness theorem for a class of delay differential equations with left and right Caputo fractional derivatives," *Journal of Mathematical Physics*, vol. 49, no. 8, 083507, 11 pages, 2008.

[24] Y. Adjabi, F. Jarad, D. Baleanu, and T. Abdeljawad, "On Cauchy problems with CAPuto Hadamard fractional derivatives," *Journal of Computational Analysis and Applications*, vol. 21, no. 4, pp. 661–681, 2016.

[25] Y. Y. Gambo, R. Ameen, F. Jarad, and T. Abdeljawad, "Existence and uniqueness of solutions to fractional differential equations in the frame of generalized Caputo fractional derivatives," *Advances in Difference Equations*, Paper No. 134, 13 pages, 2018.

[26] R. Temam, *Navier-Stokes Equations*, North-Holland, Amsterdam, The Netherlands, 1984.

[27] R. Temam, *Navier-Stokes equations and nonlinear functional analysis*, vol. 66 of *CBMS-NSF Regional Conference Series in Applied Mathematics*, Society for Industrial and Applied Mathematics (SIAM), Philadelphia, Pa, USA, 2nd edition, 1995.

[28] J. C. Robinson, *Infinite-Dimensional Dynamical Systems: An Introduction to Dissipative parabolic PDEs and the Theory Of Global Attractors*, Cambridge Texts in Applied Mathematics, Cambridge University Press, Cambridge, UK, 2001.

[29] Y. Zhou, *Basic Theory of Fractional Differential Equations*, World Scientific, Singapore, 2014.

[30] A. A. Kilbas, H. M. Srivastava, and J. J. Trujillo, *Theory and Applications of Fractional Differential Equations*, New York, NY, USA, Elsevier, 2006.

[31] O. P. Agrawal, "Fractional variational calculus in terms of Riesz fractional derivatives," *Journal of Physics A: Mathematical and Theoretical*, vol. 40, no. 24, pp. 6287–6303, 2007.

[32] A. A. Alikhanov, "A priori estimates for solutions of boundary value problems for equations of fractional order," *Differentsial'nye Uravneniya*, vol. 46, no. 5, pp. 658–664, 2010.

[33] H. Bellout and F. Bloom, *Incompressible bipolar and non-Newtonian viscous fluid flow*, Advances in Mathematical Fluid Mechanics, Birkhäuser/ Springer, Cham, switzerland, 2014.

[34] O. A. Ladyzhenskaya, *Mathematical problems of the dynamics of a viscous incompressible liquid*, Second revised and supplemented edition, Nauka, Moscow, Russia, 1970.

[35] A. V. Busuioc, D. Iftimie, and M. Paicu, "On steady third grade fluids equations," *Nonlinearity*, vol. 21, no. 7, pp. 1621–1635, 2008.

[36] J. L. Lions, *Quelques Méthodes de Résolution des Problèmes aux Limites Non Linéaires*, Dunod, Paris, Farnce, 1969.

Hindawi
Complexity
Volume 2018, Article ID 8154230, 24 pages
https://doi.org/10.1155/2018/8154230

Research Article

Consensus of Multi-Integral Fractional-Order Multiagent Systems with Nonuniform Time-Delays

Jun Liu[1,2] **Wei Chen**[1] **Kaiyu Qin**[2] **and Ping Li**[1]

[1]*School of Control Engineering, Chengdu University of Information Technology, Chengdu 610225, China*
[2]*School of Aeronautics and Astronautics, University of Electronic Science and Technology of China, Chengdu 611731, China*

Correspondence should be addressed to Jun Liu; liujun@cuit.edu.cn

Received 2 June 2018; Revised 15 August 2018; Accepted 17 October 2018; Published 1 November 2018

Guest Editor: Christos K. Volos

Consensus of fractional-order multiagent systems (FOMASs) with single integral has been wildly studied. However, the dynamics with multiple integral (especially double integral to sextuple integral) also exist in FOMASs, and they are rarely studied at present. In this paper, consensus problems for multi-integral fractional-order multiagent systems (MIFOMASs) with nonuniform time-delays are addressed. The consensus conditions for MIFOMASs are obtained by a novel frequency-domain method which properly eliminates consensus problems of the systems associated with nonuniform time-delays. Besides, the method revealed in this paper is applicable to classical high-order multiagent systems which is a special case of MIFOMASs. Finally, several numerical simulations with different parameters are performed to validate the correctness of the results.

1. Introduction

The research related to multiagent systems (MASs) has been going on for decades, due to its many meaningful applications, e.g., sweep coverage control of MASs [1], flocking behavior of mobile robots [2], and coordinated attitude control of a formation of satellites [3]. Consensus is an agreement on the quality of certain concerns about the specific states of all agents, which is one of the most fundamental requirements for the research on MASs.

Up to now, numerous studies have been conducted to resolve the problems about consensus of MASs with different dynamics. During the past decades, a lot of results have been accomplished about consensus of first-order MASs [4–11]. In [4], a simple model was presented for the phase transition of a set of self-driven particle, and it was demonstrated that the headings of all agents in MASs converged to a common value by simulation. In [5], authors provided some theoretical explanations for Vicsek's linearized model and analyzed the alignment of undirected switching topologies of agents that were regularly connected. Based on the research works of [5], more relaxed consensus conditions over dynamic switching topologies were given in [6, 7]. Authors in [8] put forward a framework about consensus theory of MASs with directed information flow, link/node failures, time-delays, and so on. Robust H_∞ control about consensus problems for MASs with parameter uncertainties, external disturbances, nonidentical state, and time-delays was discussed in [9]. In recent years, more and more researchers have paid more attention to consensus of second-order MASs [12–16]. For instance, authors in [12] investigated consensus problems for second-order continuous-time MASs in the presence of jointly connected topologies and time-delay. In [13], two types of consensus problems for second-order MASs with and without delay over switching topology and directed topology were studied. In [14], the local consensus problem for second-order MASs whose dynamics were nonlinear dynamics under directed and switching random topology was discussed, and several sufficient conditions were derived to ensure the MASs reach consensus. Furthermore, taking into account the fact that high-order MASs were widely used, consensus problems for high-order MASs have been studied in [17–21]. In particular, the output consensus problem in [17] was addressed for high-order MASs with external disturbances,

and some conditions were derived to ensure consensus for the MASs. The consensus problems in [18] were considered for a class of high-order MASs with time-delays and switching networks, and a nearest-neighbour rule was designed and some conditions were derived to guarantee consensus for the systems with time-delays. The conditions of consensus in [21] for high-order MASs with nonuniform time-delays were proposed by a novel frequency-domain approach which properly resolved the challenges associated with multiple time-delays.

It is worth noting that many results above about MASs were based on the integer-order dynamics. In fact, many scholars have declared that the essential characteristic or behavior of an object in the complex environment could be better revealed by adopting fractional-order dynamics. Examples include unmanned aerial vehicles operating in an environment with the impacts of rain and wind [22], food searching with the help of the individual secretions and microbial [23], and submarine robots in the bottom of the sea with large amounts of microorganisms and viscous substances [24]. Compared to integer-order dynamics, fractional-order dynamics provided an excellent tool in the description of memory and hereditary properties [25, 26]. Moreover, authors in [27, 28] indicated that the integer-order systems were only the special examples of the fractional-order systems. Based on these facts, the research results on consensus of FOMASs with single integral in [29–34] have been continuously springing up in recent years. As we know, consensus problem of FOMASs was first proposed and investigated by Cao *et al.* [29]. Next, consensus control of FOMASs with time-delays was studied by Yang *et al.* [30, 31], where homogeneous dynamics and heterogeneous dynamics were used to illustrate the agent of system. In [32], consensus problem of linear FOMASs with input time-delay and the consensus problem of nonlinear FOMASs with input time-delay were investigated, respectively. In [33], consensus problems were studied for FOMASs with nonuniform time-delays. Meanwhile, by means of matrix theory tool, Laplace transform and graph theory tool, two delay margins were obtained as the consensus conditions. Lately, consensus of FOMASs with double integral was proposed in [35–39]. The consensus problem of FOMASs with double integral over fixed topology was studied in [35]. By applying Mittag-Leffler function, Laplace transform, and dwell time technique, consensus for FOMASs with double integral over switching topology was investigated in [36]. Based on the sliding mode estimator, consensus problem for FOMASs with double integral was studied in [37]. By means of matrix theory tool, Laplace transform, and graph theory tool, consensus problems for a FOMAS with double integral and time-delay were studied in [38]. Nevertheless, the above research results on the consensus problems of FOMASs with or without time-delays were based on the single-integral fractional-order or double-integral fractional-order dynamics. To this day, there is almost no research on consensus problems of MIFOMASs with time-delays, especially nonuniform time-delays.

Motivated by above analysis, we extend FOMASs from single-integral fractional-order dynamics to multi-integral fractional-order ones in this paper. Consensus problems of FOMASs with multiple integral in the presence of nonuniform time-delays are studied. The main idea of this paper is to first obtain the characteristic polynomial of a MIFOMAS with imaginary eigenvalues through the model transformation of the system and then determine the stability conditions of the system according to this characteristic polynomial, so as to determine the consensus conditions of the system according to the stability conditions of the system. The consensus conditions of the MIFOMAS with nonuniform time-delays can be obtained by inequalities.

The main contributions of this paper are as follows. Firstly, we consider multi-integral fractional-order dynamics. As far as we know, this paper is the first paper that studies consensus of MIFOMASs. Just as integer-order MASs have first-order (single-integral) MASs [4–11], second-order (double-integral) MASs [12–16], and high-order (multi-integral) MASs [17–21], FOMASs also have single-integral FOMASs [29–34], double-integral FOMASs [35–39], and MIFOMASs, which makes the overall theory of FOMASs perfect from single-integral to multi-integral FOMASs. In addition, single-integral and double-integral FOMASs are the special cases of MIFOMASs. Secondly, we consider symmetric and asymmetric time-delays. The symmetric time-delays contain up to $n(n-1)/2$ different values and the asymmetric time-delays contain up to $n(n-1)$ different values when the MIFOMAS consists of n agents. Thirdly, we consider the dynamics of each agent containing multiple state variables with different fractional orders. The MIFOMAS with nonuniform time-delays consists of some agents, and each agent contains multiple state variables with different fractional orders. Finally, we derive the consensus conditions for a MIFOMAS with nonuniform time-delays.

The remainder of this article is organized as follows. In Section 2, fractional calculus and its Laplace transform are given. In Section 3, the knowledge about graph theory is shown out. In Sections 4 and 5, consensus algorithms for a MIFOMAS in the presence of nonuniform time-delays are studied. In Section 6, some numerical examples with different parameters are simulated to verify the results. Finally, conclusions are drawn out in Section 7.

2. Fractional Calculus

In [40], several different definitions of fractional calculus have been proposed, in which the Caputo fractional derivative played an important role in fractional-order systems. Because the initial value of Caputo fractional derivative has practical signification in many problems, which is commonly used in the variety of physical fields. Ergo, this paper will model the system dynamical characteristics by using Caputo derivative which is defined by

$$ {}_{a}^{C}D_{t}^{\alpha}x(t) = \frac{1}{\Gamma(m-\alpha)}\int_{a}^{t}\frac{x^{(m)}(\eta)}{(t-\eta)^{1+\alpha-m}}d\eta, \tag{1} $$

where $a \in \mathbb{R}$ denotes the initial value, α represents the order of the Caputo derivative, and $m-1 < \alpha \le m (m \in z^+)$. $\Gamma(\cdot)$ is given by

$$\Gamma(y) = \int_0^{+\infty} e^{-t} t^{y-1} dt. \tag{2}$$

If ${}_a^C D_t^\alpha x(t)$ is replaced by $x^{(\alpha)}(t)$, and the Laplace transform of $x(t)$ is represented by $X(s) = \mathscr{L}\{x(t)\} = \int_{0^-}^{\infty} e^{-st} x(t) dt$, then the following equation can be used to denote Laplace transform of the Caputo derivative.

$$\mathscr{L}\left\{x^{(\alpha)}(t)\right\} = \begin{cases} s^\alpha X(s) - s^{\alpha-1} x\left(0^-\right), & \alpha \in (0,1] \\ s^\alpha X(s) - s^{\alpha-1} x\left(0^-\right) - s^{\alpha-2} x'\left(0^-\right), & \alpha \in (1,2] \end{cases} \tag{3}$$

where $x(0^-) = \lim_{t \longrightarrow 0^-} x(t)$ and $x'(0^-) = \lim_{t \longrightarrow 0^-} x'(t)$.

3. Graph Theory

For a MAS with n agents, the network topology can be denoted by a graph $\mathscr{G} = (\mathscr{V}, \mathscr{E})$, where $\mathscr{V} = \{s_1, \ldots, s_n\}$ and $\mathscr{E} \subseteq \mathscr{V}^2$, respectively, represent the set of nodes and the set of edges. The node indices belong to a finite index set $\mathscr{I} = \{1, 2, \ldots, n\}$. The weighted adjacency matrix is denoted by $\mathscr{A} = [a_{ij}]_{n \times n}$. The element of the i-th row and the j-th column in matrix $\mathscr{A}$ indicates the connection state between agents s_i and s_j. If nodes s_i and s_j are connected, i.e., $e_{ij} \in \mathscr{E}$, then $a_{ij} > 0$, and s_j is called a neighbor of node s_i. $N_i = \{j \in \mathscr{I}, j \ne i\}$ denotes the index set of all neighbors of agent i. If nodes s_i and s_j are connected and $a_{ij} = a_{ji}$, then $\mathscr{G}$ is an undirected graph; otherwise the $\mathscr{G}$ is a directed graph. In a directed graph, a directed path is a sequence of edges by $(s_1, s_2), (s_2, s_3), \ldots$, where $(s_j, s_i) \in \mathscr{E}$. The directed graph has a directed spanning tree if all other nodes have directional paths from the same node. The Laplacian matrix of the graph $\mathscr{G}$ is defined by $L = \Delta - \mathscr{A} \in \mathbb{R}^{n \times n}$, where $\Delta \triangleq \text{diag}\{deg_{out}(s_1), deg_{out}(s_2), \ldots, deg_{out}(s_i), \ldots, deg_{out}(s_n)\}$ is a diagonal matrix with $deg_{out}(s_i) = \sum_{j=1}^{n} a_{ij}$. Supposing some graphs $\mathscr{G}_1, \mathscr{G}_2, \ldots, \mathscr{G}_M$ and graph $\mathscr{G}$ consist of the same nodes, and the edge set of graph $\mathscr{G}$ is the sum of the edge sets of other graphs $\mathscr{G}_1, \mathscr{G}_2, \ldots, \mathscr{G}_M$, then there is $L = \sum_{m=1}^{M} L_m$, which means the Laplacian matrix of graph $\mathscr{G}$ is the sum of other graphs' Laplacian matrix.

4. Problem Statement

There are two lemmas [41] for the later analysis.

Lemma 1. *If graph $\mathscr{G}$ is an undirected and connected graph, then its Laplacian matrix L has one singleton zero eigenvalue and other eigenvalues are all positive; i.e., $0 = \lambda_1 < \lambda_2 \le \lambda_3 \le \cdots \le \lambda_n$.*

Lemma 2. *If graph $\mathscr{G}$ is a directed graph with a spanning tree, then its Laplacian matrix L has one singleton zero eigenvalue and other eigenvalues have a positive real part; i.e., $\lambda_1 = 0, \text{Re}(\lambda_i) > 0$ $(i = 2, 3, \ldots, n)$.*

Consider a MIFOMAS composed of n agents. Each node in graph $\mathscr{G}$ corresponds to each agent of the MIFOMAS. If $a_{ij} > 0$, we can think that the i-th agent can get state information from the j-th agent. The dynamics of the i-th agent of the MIFOMAS are represented by

$$\begin{aligned} x_{i_1}^{(\alpha_1)}(t) &= x_{i_2}(t), \\ x_{i_2}^{(\alpha_2)}(t) &= x_{i_3}(t), \\ &\vdots \\ x_{i_{(l-1)}}^{(\alpha_{l-1})}(t) &= x_{i_l}(t), \\ x_{i_l}^{(\alpha_l)}(t) &= u_i(t), \\ & i \in \mathscr{I}, \end{aligned} \tag{4}$$

where $x_{i_1}(t), x_{i_2}(t), \ldots, x_{i_l}(t) \in \mathbb{R}$, respectively, represent l different states of the i-th agent, $x_{i_1}^{(\alpha_1)}(t)$ is the α_1-order Caputo derivative of $x_{i_1}(t)$, $x_{i_2}^{(\alpha_2)}(t)$ is the α_2-order Caputo derivative of $x_{i_2}(t), \ldots, x_{i_l}^{(\alpha_l)}(t)$ is the α_l-order Caputo derivative of $x_{i_l}(t)$ $(\alpha_1, \alpha_2, \ldots, \alpha_l \in (0,1])$, and $u_i(t) \in \mathbb{R}$ is the control input.

Definition 3. If and only if the states of all agents in MIFOMAS (4) satisfy

$$\begin{aligned} \lim_{t \longrightarrow +\infty} \left(x_{i_1}(t) - x_{j_1}(t)\right) &= 0, \\ \lim_{t \longrightarrow +\infty} \left(x_{i_2}(t) - x_{j_2}(t)\right) &= 0, \\ &\vdots \\ \lim_{t \longrightarrow +\infty} \left(x_{i_l}(t) - x_{j_l}(t)\right) &= 0, \\ & i, j \in \mathscr{I}, \end{aligned} \tag{5}$$

then MIFOMAS (4) can reach consensus. In (5), $x_{i_1}(t), x_{i_2}(t), \ldots, x_{i_l}(t) \in \mathbb{R}$, respectively, represent l different states of the i-th agent, and $x_{j_1}(t), x_{j_2}(t), \ldots, x_{j_l}(t) \in \mathbb{R}$, respectively, represent l different states of the j-th agent.

In this paper, the control protocol for MIFOMAS (4) will be given by

$$\begin{aligned} u_i(t) = &-\sum_{k=1}^{l-1} P_{k+1} x_{i_{k+1}}(t) \\ &+ \sum_{j \in N_i} a_{ij} \left[x_{j_1}\left(t - \tau_{ij}\right) - x_{i_1}\left(t - \tau_{ij}\right)\right], \end{aligned} \tag{6}$$

where N_i denotes the neighbors index collection of the agent i, a_{ij} is the (i,j)-th element of $\mathscr{A}$, $\tau_{ij} > 0$ is the time-delay which is from the j-th agent to the i-th agent, and $P_{k+1} > 0$ are scale coefficients. If all $\tau_{ij} = \tau_{ji}$, then the time-delays are symmetrical; else the time-delays are asymmetrical. The symmetric time-delays and the asymmetric time-delays are two different forms of nonuniform time-delays. For ease of analysis, we define that τ_m denote M different time-delays of MIFOMAS (4); i.e., $\tau_m \in \{\tau_{ij} : i,j \in \mathscr{I}\}$ $(m = 1,2,\ldots,M)$. Then the following control protocol is provided to resolve consensus problems of MIFOMAS (4):

$$u_i(t) = -\sum_{k=1}^{l-1} P_{k+1} x_{i_{k+1}}(t) + \sum_{j\in N_i} a_{ij}\left[x_{j_1}(t-\tau_m) - x_{i_1}(t-\tau_m)\right]. \tag{7}$$

Assume the state vector of the i-th agent is $\xi_i(t) = [x_{i_1}(t), x_{i_2}(t), \ldots, x_{i_l}(t)]^T \in \mathbb{R}^l$, and the joint state vector of MIFOMAS (4) consisting of n agents is $\psi(t) = [\xi_1^T(t), \xi_2^T(t), \ldots, \xi_n^T(t)]^T \in \mathbb{R}^{ln}$.

If we define two matrices as follows,

$$A = \begin{bmatrix} 0 & 1 & 0 & \cdots & 0 & 0 \\ 0 & 0 & 1 & \cdots & 0 & 0 \\ \vdots & \vdots & \vdots & \ddots & \vdots & \vdots \\ 0 & 0 & 0 & \cdots & 1 & 0 \\ 0 & 0 & 0 & \cdots & 0 & 1 \\ 0 & -P_2 & -P_3 & \cdots & -P_{l-1} & -P_l \end{bmatrix} \in \mathbb{R}^{l\times l}, \tag{8}$$

and

$$B = \begin{bmatrix} 0 & 0 & \cdots & 0 \\ \vdots & \vdots & \ddots & \vdots \\ 0 & 0 & \cdots & 0 \\ 1 & 0 & \cdots & 0 \end{bmatrix} \in \mathbb{R}^{l\times l}, \tag{9}$$

then under the control protocol given by (7), the closed-loop dynamics of MIFOMAS (4) can be described as

$$\left[x_{1_1}^{(\alpha_1)}(t), x_{1_2}^{(\alpha_2)}(t), \ldots, x_{1_l}^{(\alpha_l)}(t), x_{2_1}^{(\alpha_1)}(t), x_{2_2}^{(\alpha_2)}(t), \ldots, x_{2_l}^{(\alpha_l)}(t), \ldots, x_{n_1}^{(\alpha_1)}(t), x_{n_2}^{(\alpha_2)}(t), \ldots, x_{n_l}^{(\alpha_l)}(t)\right]^T = (I_n \otimes A)\psi(t) - \sum_{m=1}^{M}(L_m \otimes B)\cdot\psi(t-\tau_m). \tag{10}$$

5. Main Results

Theorem 4. *Suppose that a FOMAS with multiple integral is given by MIFOMAS (4) whose corresponding network topology $\mathscr{G}$ satisfies Lemma 1. Define the following functions:*

$$\begin{aligned} F_l(\omega) &= -\sum_{k=1}^{l}(-j\omega)^{\sum_{i=1}^{k}\alpha_i} P_{k+1}, \\ \theta_l(\omega) &= \arg\left[F_l(\omega)\right] = \arg\left[-\sum_{k=1}^{l}(-j\omega)^{\sum_{i=1}^{k}\alpha_i} P_{k+1}\right] \\ &= \arctan R_l(\omega), \\ T_l(\omega) &= \frac{1}{\omega}\theta_l(\omega), \end{aligned} \tag{11}$$

where $l \in \{1,2,3,4,5,6\}$, $R_l(\omega) \triangleq \mathrm{Im}[F_l(\omega)]/\mathrm{Re}[F_l(\omega)] = \tan[\theta_l(\omega)]$, and $\mathrm{Re}[F_l(\omega)]$ and $\mathrm{Im}[F_l(\omega)]$, respectively, denote the real part and the imaginary part of $F_l(\omega)$.

If all $\tau_m < \overline{\tau} = T_l(\overline{\omega}) = (1/\overline{\omega})\theta_l(\overline{\omega})$ for the MIFOMAS (10) with symmetric time-delays, then the control protocol (7) can resolve the consensus problem of the MIFOMAS (10) with symmetric time-delays, and on the contrary, then the control protocol (7) can not resolve the consensus problem of the MIFOMAS (10) with symmetric time-delays. The value of $\overline{\omega}$ corresponding to l in $T_l(\overline{\omega})$ is determined by the following equation:

$$\left|F_l(\overline{\omega})\right| = \lambda_n, \quad l \in \{1,2,3,4,5,6\}, \tag{12}$$

where $|F_l(\omega)|$ is the modulus of $F_l(\omega)$ and λ_n is the maximum eigenvalue of L.

Proof. We shall apply the frequency-domain method to analyze the MIFOMAS (10) with symmetric time-delays, and we can get

$$\left\{I_n \otimes \begin{bmatrix} s^{\alpha_1} & 0 & \cdots & 0 & 0 \\ 0 & s^{\alpha_2} & \cdots & 0 & 0 \\ \vdots & \vdots & \ddots & \vdots & \vdots \\ 0 & 0 & \cdots & s^{\alpha_{l-1}} & 0 \\ 0 & 0 & \cdots & 0 & s^{\alpha_l} \end{bmatrix}\right\}\Psi(s) - \left\{I_n \otimes \begin{bmatrix} s^{\alpha_1-1} & 0 & \cdots & 0 & 0 \\ 0 & s^{\alpha_2-1} & \cdots & 0 & 0 \\ \vdots & \vdots & \ddots & \vdots & \vdots \\ 0 & 0 & \cdots & s^{\alpha_{l-1}-1} & 0 \\ 0 & 0 & \cdots & 0 & s^{\alpha_l-1} \end{bmatrix}\right\}\psi(0^-)$$

$$
\begin{aligned}
&-\left(I_n \otimes A\right)\Psi\left(s\right) + \sum_{m=1}^{M}\left(L_m \otimes B\right)e^{-s\tau_m}\Psi\left(s\right) = 0,\\
&\Psi\left(s\right) = \mathscr{R}\psi\left(0^-\right)G_{\tau_m}^{-1}\left(s\right),
\end{aligned}
\tag{13}
$$

where $\Psi(s)$ is the Laplace transform of $\psi(t)$, $\psi(0^-)$ is the initial value of $\psi(t)$,

$$
\mathscr{R} = I_n \otimes \begin{bmatrix}
s^{\alpha_1-1} & 0 & \cdots & 0 & 0\\
0 & s^{\alpha_2-1} & \cdots & 0 & 0\\
\vdots & \vdots & \ddots & \vdots & \vdots\\
0 & 0 & \cdots & s^{\alpha_{l-1}-1} & 0\\
0 & 0 & \cdots & 0 & s^{\alpha_l-1}
\end{bmatrix},
\tag{14}
$$

and

$$
\begin{aligned}
G_{\tau_m}\left(s\right) = \Bigg\{ & I_n \otimes \Bigg\{ \begin{bmatrix}
s^{\alpha_1} & 0 & \cdots & 0 & 0\\
0 & s^{\alpha_2} & \cdots & 0 & 0\\
\vdots & \vdots & \ddots & \vdots & \vdots\\
0 & 0 & \cdots & s^{\alpha_{l-1}} & 0\\
0 & 0 & \cdots & 0 & s^{\alpha_l}
\end{bmatrix}\\
& - \begin{bmatrix}
0 & 1 & 0 & \cdots & 0\\
0 & 0 & 1 & \cdots & 0\\
\vdots & \vdots & \vdots & \ddots & \vdots\\
0 & 0 & 0 & \cdots & 1\\
0 & -P_2 & -P_3 & \cdots & -P_l
\end{bmatrix} \Bigg\}\\
& + \sum_{m=1}^{M}\left(L_m \otimes B\right)e^{-s\tau_m} \Bigg\}.
\end{aligned}
\tag{15}
$$

Motivated by the stability analysis of a fractional-order system in [42], we can study consensus of the MIFOMAS (10) with symmetric time-delays by analyzing the characteristic eigenvalues' position of the characteristic polynomial $\det[G_{\tau_m}(s)]$ of the MIFOMAS (10) with symmetric time-delays. Specifically, consensus of the MIFOMAS (10) without delays (all $\tau_m = 0$) is necessary for consensus of the MIFOMAS (10) with symmetric time-delays; that is to say, in this case the characteristic eigenvalues of $\det[G_{\tau_m}(s)]$ of the MIFOMAS (10) with symmetric time-delays are all situated in the left half plane (LHP) of the complex plane, and as τ_m increases continuously from zero, the characteristic eigenvalue of $\det[G_{\tau_m}(s)]$ of the MIFOMAS (10) with symmetric time-delays will change continuously from the LHP to the right half plane (RHP) of the complex plane. Once the characteristic eigenvalue of $\det[G_{\tau_m}(s)]$ of the MIFOMAS (10) with symmetric time-delays reaches the RHP of the complex plane through the imaginary axis, the MIFOMAS (10) with symmetric time-delays will be unstable and can not achieve consensus. Ergo, we only need to consider the critical time-delay when the nonzero characteristic eigenvalue of $\det[G_{\tau_m}(s)]$ of the MIFOMAS (10) with symmetric time-delays is just situated on the imaginary axis for the first time as τ_m increases continuously from zero, and the corresponding time-delay is just the delay margin $\overline{\tau}$ of the MIFOMAS (10) with symmetric time-delays.

Assume $s = -j\omega \neq 0$ is the characteristic eigenvalue of $\det[G_{\tau_m}(s)]$ of the MIFOMAS (10) with symmetric time-delays on the imaginary axis, $u = u_1 \otimes [1,0,\ldots,0,0]^T + u_2 \otimes [0,1,0,\ldots,0]^T + \cdots + u_{l-1} \otimes [0,\ldots,0,1,0]^T + u_l \otimes [0,\ldots,0,0,1]^T$ is the corresponding eigenvector, and $\|u\| = \mathbf{1}$, $u_1, u_2, \ldots, u_{l-1}, u_l \in \mathbb{C}^n$; we have the following equations:

$$
\begin{aligned}
\Bigg\{ & I_n \\
& \otimes \Bigg\{ \begin{bmatrix}
(-j\omega)^{\alpha_1} & 0 & \cdots & 0 & 0\\
0 & (-j\omega)^{\alpha_2} & \cdots & 0 & 0\\
\vdots & \vdots & \ddots & \vdots & \vdots\\
0 & 0 & \cdots & (-j\omega)^{\alpha_{l-1}} & 0\\
0 & 0 & \cdots & 0 & (-j\omega)^{\alpha_l}
\end{bmatrix}\\
& - \begin{bmatrix}
0 & 1 & 0 & \cdots & 0\\
0 & 0 & 1 & \cdots & 0\\
\vdots & \vdots & \vdots & \ddots & \vdots\\
0 & 0 & 0 & \cdots & 1\\
0 & -P_2 & -P_3 & \cdots & -P_l
\end{bmatrix} \Bigg\}\\
& + \sum_{m=1}^{M}\left(L_m \otimes B\right)e^{-s\tau_m} \Bigg\} u = 0,
\end{aligned}
$$

$$\left\{ I_n \otimes \left\{ \begin{bmatrix} (-j\omega)^{\alpha_1} & -1 & 0 & \cdots & 0 \\ 0 & (-j\omega)^{\alpha_2} & -1 & \cdots & 0 \\ \vdots & \vdots & \vdots & \ddots & \vdots \\ 0 & 0 & 0 & \cdots & -1 \\ 0 & P_2 & P_3 & \cdots & P_l + (-j\omega)^{\alpha_l} \end{bmatrix} \right\} + \sum_{m=1}^{M} (L_m \otimes B) e^{-s\tau_m} \right\} u = 0,$$

$$\underbrace{\{I_n \otimes \Omega\} u}_{(1)} + \underbrace{\left\{ \sum_{m=1}^{M} (L_m \otimes B) e^{j\omega\tau_m} \right\} u}_{(2)} = 0, \tag{16}$$

$$\begin{aligned}
(1) &= \{I_n \otimes \Omega\} u = I_n u_1 \otimes \left(\Omega [1, 0, \ldots, 0]^T\right) + I_n u_2 \\
&\otimes \left(\Omega [0, 1, 0, \ldots, 0]^T\right) + I_n u_3 \\
&\otimes \left(\Omega [0, 0, 1, 0, \ldots, 0]^T\right) + \cdots + I_n u_{l-1} \\
&\otimes \left(\Omega [0, 0, \cdots, 0, 1, 0]^T\right) + I_n u_l \\
&\otimes \left(\Omega [0, \ldots, 0, 1]^T\right) = I_n u_1 \otimes \left[(-j\omega)^{\alpha_1}, 0, \ldots, 0\right]^T \\
&+ I_n u_2 \otimes \left[-1, (-j\omega)^{\alpha_2}, 0, \ldots, 0, P_2\right]^T + I_n u_3 \otimes \left[0, \right. \\
&\left. -1, (-j\omega)^{\alpha_3}, 0, \ldots, 0, P_3\right]^T + \cdots + I_n u_{l-1} \otimes \left[0, \ldots, \right. \\
&\left. 0, -1, (-j\omega)^{\alpha_{l-1}}, P_{l-1}\right]^T + I_n u_l \otimes \left[0, \ldots, 0, -1, \right. \\
&\left. (-j\omega)^{\alpha_l} + P_l\right]^T = I_n \otimes \left[(-j\omega)^{\alpha_1} u_1, 0, \ldots, 0\right]^T + I_n \\
&\otimes \left[-u_2, (-j\omega)^{\alpha_2} u_2, 0, \ldots, 0, P_2 u_2\right]^T + I_n \otimes \left[0, \right. \\
&\left. - u_3, (-j\omega)^{\alpha_3} u_3, 0, \ldots, 0, P_3 u_3\right]^T + \cdots + I_n \otimes \left[0, \right. \\
&\left. \ldots, 0, -u_{l-1}, (-j\omega)^{\alpha_{l-1}} u_{l-1}, P_{l-1} u_{l-1}\right]^T + I_n \otimes \left[0, \ldots, \right. \\
&\left. 0, -u_l, \left((-j\omega)^{\alpha_l} + P_l\right) u_l\right]^T = I_n \otimes \left[(-j\omega)^{\alpha_1} u_1 \right. \\
&\left. - u_2, (-j\omega)^{\alpha_2} u_2 - u_3, \ldots, (-j\omega)^{\alpha_{l-1}} u_{l-1} - u_l, P_2 u_2 \right. \\
&\left. + P_3 u_3 + \cdots + P_{l-1} u_{l-1} + P_l u_l + (-j\omega)^{\alpha_l} u_l\right]^T, \\
&= \left[I_n \left((-j\omega)^{\alpha_1} u_1 - u_2\right), I_n \left((-j\omega)^{\alpha_2} u_2 - u_3\right), \ldots, \right. \\
&\left. I_n \left((-j\omega)^{\alpha_{l-1}} u_{l-1} - u_l\right), I_n \left(P_2 u_2 + P_3 u_3 + \cdots \right. \right. \\
&\left. \left. + P_{l-1} u_{l-1} + P_l u_l + (-j\omega)^{\alpha_l} u_l\right)\right]^T,
\end{aligned} \tag{17}$$

$$\begin{aligned}
(2) &= \left\{ \sum_{m=1}^{M} (L_m \otimes B) e^{j\omega\tau_m} \right\} u = \sum_{m=1}^{M} (L_m \otimes B) u e^{j\omega\tau_m} \\
&= \sum_{m=1}^{M} \left\{ (L_m u_1) \otimes \left(B [1, 0, \ldots, 0]^T\right) + (L_m u_2) \right. \\
&\otimes \left(B [0, 1, 0, \ldots, 0]^T\right) + \cdots + (L_m u_{l-1}) \\
&\otimes \left(B [0, 0, \ldots, 0, 1, 0]^T\right) + (L_m u_l) \\
&\left. \otimes \left(B [0, \ldots, 0, 1]^T\right)\right\} e^{j\omega\tau_m} = \sum_{m=1}^{M} \left\{ (L_m u_1) \right. \\
&\otimes \left([0, 0, \ldots, 0, 1]^T\right) + (L_m u_2) \otimes \left([0, 0, 0, \ldots, 0]^T\right) \\
&+ \cdots + (L_m u_{l-1}) \otimes \left([0, 0, \ldots, 0, 0, 0]^T\right) + (L_m u_l) \\
&\left. \otimes \left([0, \ldots, 0, 0]^T\right)\right\} e^{j\omega\tau_m} = \sum_{m=1}^{M} (L_m \otimes I_l) \left[\left(u_1 \right. \right. \\
&\otimes [0, 0, \ldots, 0, 1]^T\Big) + \left(u_2 \otimes [0, 0, \ldots, 0, 0]^T\right) + \cdots \\
&+ \left(u_{l-1} \otimes [0, 0, \ldots, 0, 0]^T\right) + \left(u_l \right. \\
&\left. \left. \otimes [0, 0, \ldots, 0, 0]^T\right)\right] e^{j\omega\tau_m} = \sum_{m=1}^{M} (L_m \otimes I_l) \\
&\cdot [0, 0, \ldots, 0, u_1]^T e^{j\omega\tau_m} = \left[0, 0, \ldots, 0, \right. \\
&\left. \sum_{m=1}^{M} (L_m \otimes I_l) u_1 e^{j\omega\tau_m}\right]^T.
\end{aligned} \tag{18}$$

Because of (1) + (2) = 0, we have

$$I_n \left((-j\omega)^{\alpha_1} u_1 - u_2\right) = 0,$$

$$I_n \left((-j\omega)^{\alpha_2} u_2 - u_3\right) = 0,$$

$$\vdots$$

$$I_n\left(\left(-j\omega\right)^{\alpha_{l-1}}u_{l-1}-u_l\right)=0,$$

$$I_n\left[P_2u_2+P_3u_3+\cdots+P_{l-1}u_{l-1}+\left(P_l+\left(-j\omega\right)^{\alpha_l}\right)u_l\right]+\sum_{m=1}^{M}\left(L_m\otimes I_l\right)u_1e^{j\omega\tau_m}=0,\tag{19}$$

and it yields that

$$\begin{aligned}u_2&=\left(-j\omega\right)^{\alpha_1}u_1,\\u_3&=\left(-j\omega\right)^{\alpha_2}u_2,\\&\vdots\\u_l&=\left(-j\omega\right)^{\alpha_{l-1}}u_{l-1},\\\sum_{m=1}^{M}\left(L_m\otimes I_l\right)u_1e^{j\omega\tau_m}&=-\left[P_2u_2+P_3u_3+\cdots+P_{l-1}u_{l-1}+\left(P_l+\left(-j\omega\right)^{\alpha_l}\right)u_l\right].\end{aligned}\tag{20}$$

According to (20), we have

$$\begin{aligned}\sum_{m=1}^{M}\left(L_m\otimes I_l\right)u_1e^{j\omega\tau_m}=-\Big[&P_2\left(-j\omega\right)^{\alpha_1}+P_3\left(-j\omega\right)^{\alpha_2+\alpha_1}+\cdots+P_{l-1}\left(-j\omega\right)^{\alpha_{l-2}+\alpha_{l-3}+\cdots+\alpha_1}\\&+P_l\left(-j\omega\right)^{\alpha_{l-1}+\alpha_{l-2}+\cdots+\alpha_1}+\left(-j\omega\right)^{\alpha_l+\alpha_{l-1}+\cdots+\alpha_1}\Big]u_1,\end{aligned}\tag{21}$$

then we can multiply both sides of (21) by u^H (the conjugate transpose of u); the following equation can be obtained:

$$\begin{aligned}\sum_{m=1}^{M}\frac{u^H\left(L_m\otimes I_l\right)u_1}{u^Hu_1}e^{j\omega\tau_m}=-\Big[&P_2\left(-j\omega\right)^{\alpha_1}+P_3\left(-j\omega\right)^{\alpha_2+\alpha_1}+\cdots+P_{l-1}\left(-j\omega\right)^{\alpha_{l-2}+\alpha_{l-3}+\cdots+\alpha_1}\\&+P_l\left(-j\omega\right)^{\alpha_{l-1}+\alpha_{l-2}+\cdots+\alpha_1}+\left(-j\omega\right)^{\alpha_l+\alpha_{l-1}+\cdots+\alpha_1}\Big]\\=-\sum_{k=1}^{l}&\left(-j\omega\right)^{\sum_{i=1}^{k}\alpha_i}P_{k+1},\end{aligned}\tag{22}$$

where $l\geqslant 1, P_{l+1}=1$.

Due to

$$u=\left[u_1,u_2,u_3,\ldots,u_l\right]^T=\left[u_1,\left(-j\omega\right)^{\alpha_1}u_1,\left(-j\omega\right)^{\alpha_1+\alpha_2}\cdot u_1,\ldots,\left(-j\omega\right)^{\alpha_{l-1}+\alpha_{l-2}+\cdots+\alpha_1}u_1\right]^T,$$

$$u_1=\frac{u}{\left\{\left[1,\left(-j\omega\right)^{\alpha_1},\left(-j\omega\right)^{\alpha_1+\alpha_2},\ldots,\left(-j\omega\right)^{\alpha_{l-1}+\alpha_{l-2}+\cdots+\alpha_1}\right]^T\right\}},\tag{23}$$

(22) can be simplified to

$$\begin{aligned}\sum_{m=1}^{M}\frac{u^H\left(L_m\otimes I_l\right)u_1}{u^Hu_1}e^{j\omega\tau_m}&=\sum_{m=1}^{M}\frac{u^H\left(L_m\otimes I_l\right)u}{u^Hu}e^{j\omega\tau_m}\\&=-\sum_{k=1}^{l}\left(-j\omega\right)^{\sum_{i=1}^{k}\alpha_i}P_{k+1}\triangleq F_l\left(\omega\right),\end{aligned}\tag{24}$$

where $l\geqslant 1, P_{l+1}=1$.

Let $u^H(L_m\otimes I_l)u/(u^Hu)=a_m$; we take modulus of both sides of (24). According to Lemma 1, we can get the following inequality:

$$\begin{aligned}M_l\left(\omega\right)=\left|F_l\left(\omega\right)\right|&=\left|\sum_{m=1}^{M}a_me^{j\omega\tau_m}\right|\leq\left|\sum_{m=1}^{M}a_m\right|\\&=\frac{u^H\left(L\otimes I_l\right)u}{u^Hu}\leq M_l\left(\overline{\omega}\right)=\left|F_l\left(\overline{\omega}\right)\right|=\lambda_n.\end{aligned}\tag{25}$$

It is obvious that $M_l(\omega)$ is an increasing function for $\omega>0$, and if $\omega\leq\overline{\omega}$, we can get $M_l(\omega)\leq M_l(\overline{\omega})=|F_l(\overline{\omega})|=\lambda_n$; that is, inequality (25) is true.

According to (24), we can get

$$\begin{aligned}\arg\left[F_l\left(\omega\right)\right]&=\arg\left(\sum_{m=1}^{M}a_me^{j\omega\tau_m}\right)\triangleq\theta_l\left(\omega\right),\\&=\arctan R_l\left(\omega\right),\end{aligned}\tag{26}$$

where $\theta_l(\omega)$ is the principal value of the argument of $F_l(\omega)$, $R_l(\omega)\triangleq \mathrm{Im}[F_l(\omega)]/\mathrm{Re}[F_l(\omega)]=\tan[\theta_l(\omega)]$, and $\mathrm{Re}[F_l(\omega)]$ and $\mathrm{Im}[F_l(\omega)]$, respectively, denote the real part and the imaginary part of $F_l(\omega)$.

According to (26), it is easy to obtain that

$$\theta_l\left(\omega\right)=\arg\left(\sum_{m=1}^{M}a_me^{j\omega\tau_m}\right)\leq\max\left\{\omega\tau_m\right\}.\tag{27}$$

Consider a FOMAS with single integral; we have $F_1(\omega)=-(-j\omega)^{\alpha_1}P_2=\omega^{\alpha_1}e^{j(\pi(2-\alpha_1)/2)}P_2$. It is apparent that $\theta_1(\omega)=\pi(2-\alpha_1)/2$, and $M_1(\omega)=\omega^{\alpha_1}P_2(P_2=1)$. According to (25), we should only consider $\omega\leq\overline{\omega}=\lambda_n^{(1/\alpha_1)}$, and if all $\tau_m<\overline{\tau}=T_1(\overline{\omega})=T_1[\lambda_n^{(1/\alpha_1)}]=(1/\overline{\omega})\theta_1(\overline{\omega})=\pi(2-\alpha_1)/[2\lambda_n^{(1/\alpha_1)}]$, then $\omega\tau_m<\lambda_n^{(1/\alpha_1)}\overline{\tau}=\lambda_n^{(1/\alpha_1)}T_1[\lambda_n^{(1/\alpha_1)}]=\pi(2-\alpha_1)/2=\theta_1(\omega)$, which contradicts to (27). Therefore, when all $\tau_m<\overline{\tau}$, the characteristic eigenvalues of $\det[G_{\tau_m}(s)]$

of the MIFOMAS (10) with symmetric time-delays are all situated in the LHP and the FOMAS with single integral will remain stable and can achieve consensus. On the contrary, the FOMAS with single integral will not remain stable and can not achieve consensus. Theorem 4 is proven for $l = 1$.

In the following, the FOMAS with multiple integral (double integral to sextuple integral) shall be analyzed step by step. For convenience of analysis, we first need to define some symbolic parameters:

$$
\begin{aligned}
z_1 &= \omega^{2\alpha_1} P_2^2,\\
z_2 &= \omega^{2(\alpha_1+\alpha_2)} P_3^2,\\
z_3 &= 2\omega^{(2\alpha_1+\alpha_2)} \cos\frac{\pi\alpha_2}{2} P_2P_3,\\
z_4 &= 2\omega^{(2\alpha_1+\alpha_2+\alpha_3)} \cos\frac{\pi(\alpha_2+\alpha_3)}{2} P_2P_4,\\
z_5 &= 2\omega^{(2\alpha_1+\alpha_2+\alpha_3+\alpha_4)} \cos\frac{\pi(\alpha_2+\alpha_3+\alpha_4)}{2} P_2P_5,\\
z_6 &= 2\omega^{(2\alpha_1+\alpha_2+\alpha_3+\alpha_4+\alpha_5)} \cos\frac{\pi(\alpha_2+\alpha_3+\alpha_4+\alpha_5)}{2}\\
&\quad \cdot P_2P_6,\\
z_7 &= 2\omega^{(2\alpha_1+\alpha_2+\alpha_3+\alpha_4+\alpha_5+\alpha_6)}\\
&\quad \cdot \cos\frac{\pi(\alpha_2+\alpha_3+\alpha_4+\alpha_5+\alpha_6)}{2} P_2P_7,\\
z_8 &= 2\omega^{(2\alpha_1+2\alpha_2+\alpha_3)} \cos\frac{\pi\alpha_3}{2} P_3P_4,\\
z_9 &= 2\omega^{(2\alpha_1+2\alpha_2+\alpha_3+\alpha_4)} \cos\frac{\pi(\alpha_3+\alpha_4)}{2} P_3P_5,\\
z_{10} &= 2\omega^{(2\alpha_1+2\alpha_2+\alpha_3+\alpha_4+\alpha_5)} \cos\frac{\pi(\alpha_3+\alpha_4+\alpha_5)}{2} P_3P_6,\\
z_{11} &= 2\omega^{(2\alpha_1+2\alpha_2+\alpha_3+\alpha_4+\alpha_5+\alpha_6)} \cos\frac{\pi(\alpha_3+\alpha_4+\alpha_5+\alpha_6)}{2}\\
&\quad \cdot P_3P_7,\\
z_{12} &= \omega^{2(\alpha_1+\alpha_2+\alpha_3)} P_4^2,\\
z_{13} &= 2\omega^{(2\alpha_1+2\alpha_2+2\alpha_3+\alpha_4)} \cos\frac{\pi\alpha_4}{2} P_4P_5,\\
z_{14} &= 2\omega^{(2\alpha_1+2\alpha_2+2\alpha_3+\alpha_4+\alpha_5)} \cos\frac{\pi(\alpha_4+\alpha_5)}{2} P_4P_6,\\
z_{15} &= 2\omega^{(2\alpha_1+2\alpha_2+2\alpha_3+\alpha_4+\alpha_5+\alpha_6)} \cos\frac{\pi(\alpha_4+\alpha_5+\alpha_6)}{2}\\
&\quad \cdot P_4P_7,\\
z_{16} &= \omega^{2(\alpha_1+\alpha_2+\alpha_3+\alpha_4)} P_5^2,\\
z_{17} &= 2\omega^{(2\alpha_1+2\alpha_2+2\alpha_3+2\alpha_4+\alpha_5)} \cos\frac{\pi\alpha_5}{2} P_5P_6,\\
z_{18} &= 2\omega^{(2\alpha_1+2\alpha_2+2\alpha_3+2\alpha_4+\alpha_5+\alpha_6)} \cos\frac{\pi(\alpha_5+\alpha_6)}{2} P_5P_7,\\
z_{19} &= \omega^{2(\alpha_1+\alpha_2+\alpha_3+\alpha_4+\alpha_5)} P_6^2,\\
z_{20} &= 2\omega^{(2\alpha_1+2\alpha_2+2\alpha_3+2\alpha_4+2\alpha_5+\alpha_6)} \cos\frac{\pi\alpha_6}{2} P_6P_7,\\
z_{21} &= \omega^{2(\alpha_1+\alpha_2+\alpha_3+\alpha_4+\alpha_5+\alpha_6)} P_7^2,
\end{aligned}
\tag{28}
$$

and

$$
\begin{aligned}
d_1 &= \alpha_2\omega^{(2\alpha_1+\alpha_2-1)} P_2P_3 \sin\frac{\pi\alpha_2}{2},\\
d_2 &= (\alpha_2+\alpha_3)\,\omega^{(2\alpha_1+\alpha_2+\alpha_3-1)} P_2P_4 \sin\frac{\pi(\alpha_2+\alpha_3)}{2},\\
d_3 &= (\alpha_2+\alpha_3+\alpha_4)\,\omega^{(2\alpha_1+\alpha_2+\alpha_3+\alpha_4-1)} P_2P_5\\
&\quad \cdot \sin\frac{\pi(\alpha_2+\alpha_3+\alpha_4)}{2},\\
d_4 &= (\alpha_2+\alpha_3+\alpha_4+\alpha_5)\,\omega^{(2\alpha_1+\alpha_2+\alpha_3+\alpha_4+\alpha_5-1)} \cdot P_2P_6\\
&\quad \cdot \sin\frac{\pi(\alpha_2+\alpha_3+\alpha_4+\alpha_5)}{2},\\
d_5 &= (\alpha_2+\alpha_3+\alpha_4+\alpha_5+\alpha_6)\,\omega^{(2\alpha_1+\alpha_2+\alpha_3+\alpha_4+\alpha_5+\alpha_6-1)}\\
&\quad \cdot P_2P_7 \sin\frac{\pi(\alpha_2+\alpha_3+\alpha_4+\alpha_5+\alpha_6)}{2},\\
d_6 &= \alpha_3\omega^{(2\alpha_1+2\alpha_2+\alpha_3-1)} P_3P_4 \sin\frac{\pi\alpha_3}{2},\\
d_7 &= (\alpha_3+\alpha_4)\,\omega^{(2\alpha_1+2\alpha_2+\alpha_3+\alpha_4-1)} P_3P_5 \sin\frac{\pi(\alpha_3+\alpha_4)}{2},\\
d_8 &= (\alpha_3+\alpha_4+\alpha_5)\,\omega^{(2\alpha_1+2\alpha_2+\alpha_3+\alpha_4+\alpha_5-1)} \cdot P_3P_6\\
&\quad \cdot \sin\frac{\pi(\alpha_3+\alpha_4+\alpha_5)}{2},\\
d_9 &= (\alpha_3+\alpha_4+\alpha_5+\alpha_6)\,\omega^{(2\alpha_1+2\alpha_2+\alpha_3+\alpha_4+\alpha_5+\alpha_6-1)}\\
&\quad \cdot P_3P_7 \sin\frac{\pi(\alpha_3+\alpha_4+\alpha_5+\alpha_6)}{2},\\
d_{10} &= \alpha_4\omega^{(2\alpha_1+2\alpha_2+2\alpha_3+\alpha_4-1)} P_4P_5 \sin\frac{\pi\alpha_4}{2},\\
d_{11} &= (\alpha_4+\alpha_5)\,\omega^{(2\alpha_1+2\alpha_2+2\alpha_3+\alpha_4+\alpha_5-1)} P_4P_6
\end{aligned}
$$

$$\cdot \sin \frac{\pi(\alpha_4+\alpha_5)}{2},$$

$$d_{12} = (\alpha_4+\alpha_5+\alpha_6)\,\omega^{(2\alpha_1+2\alpha_2+2\alpha_3+\alpha_4+\alpha_5+\alpha_6-1)} \cdot P_4P_7 \cdot \sin \frac{\pi(\alpha_4+\alpha_5+\alpha_6)}{2},$$

$$d_{13} = \alpha_5\omega^{(2\alpha_1+2\alpha_2+2\alpha_3+2\alpha_4+\alpha_5-1)}P_5P_6 \sin \frac{\pi\alpha_5}{2},$$

$$d_{14} = (\alpha_5+\alpha_6)\,\omega^{(2\alpha_1+2\alpha_2+2\alpha_3+2\alpha_4+\alpha_5+\alpha_6-1)}P_5P_7 \cdot \sin \frac{\pi(\alpha_5+\alpha_6)}{2},$$

$$d_{15} = \alpha_6\omega^{(2\alpha_1+2\alpha_2+2\alpha_3+2\alpha_4+2\alpha_5+\alpha_6-1)}P_6P_7 \sin \frac{\pi\alpha_6}{2}. \tag{29}$$

For the FOMAS with double integral,

$$\begin{aligned} F_2(\omega) &= -\sum_{k=1}^{2}(-j\omega)^{\sum_{i=1}^{k}\alpha_i}P_{k+1} = -\left[(-j\omega)^{\alpha_1}P_2 + (-j\omega)^{\alpha_1+\alpha_2}P_3\right] \\ &= \omega^{\alpha_1}e^{j(\pi(2-\alpha_1)/2)}P_2 + \omega^{\alpha_1+\alpha_2}e^{j(\pi(2-\alpha_1-\alpha_2)/2)}P_3 \\ &= \left[\omega^{\alpha_1}P_2\cos\frac{\pi(2-\alpha_1)}{2} + \omega^{(\alpha_1+\alpha_2)}P_3\cos\frac{\pi(2-\alpha_1-\alpha_2)}{2}\right] \\ &\quad + j\left[\omega^{\alpha_1}P_2\sin\frac{\pi(2-\alpha_1)}{2} + \omega^{(\alpha_1+\alpha_2)}P_3\sin\frac{\pi(2-\alpha_1-\alpha_2)}{2}\right] \\ &= \mathrm{Re}\left[F_2(\omega)\right] + j\,\mathrm{Im}\left[F_2(\omega)\right]. \end{aligned} \tag{30}$$

$$\left[M_2(\omega)\right]^2 = \left|F_2(\omega)\right|^2 = \omega^{2\alpha_1}P_2^2 + \omega^{2(\alpha_1+\alpha_2)}P_3^2 + 2\omega^{(2\alpha_1+\alpha_2)}\cos\frac{\pi\alpha_2}{2}P_2P_3 = z_1+z_2+z_3. \tag{31}$$

Because of $R_2(\omega) = \mathrm{Im}[F_2(\omega)]/\mathrm{Re}[F_2(\omega)]$, we can get the first derivative of $R_2(\omega)$:

$$R_2'(\omega) = -\frac{\left[\alpha_2\omega^{2\alpha_1+\alpha_2-1}P_2P_3\sin(\pi\alpha_2/2)\right]}{\left[\omega^{\alpha_1}P_2\cos(\pi(2-\alpha_1)/2) + \omega^{(\alpha_1+\alpha_2)}P_3\cos(\pi(2-\alpha_1-\alpha_2)/2)\right]^2} = -\frac{d_1}{\left\{\mathrm{Re}\left[F_2(\omega)\right]\right\}^2} < 0. \tag{32}$$

For the FOMAS with triple integral,

$$\begin{aligned} F_3(\omega) &= -\sum_{k=1}^{3}(-j\omega)^{\sum_{i=1}^{k}\alpha_i}P_{k+1} = -\left[(-j\omega)^{\alpha_1}P_2 + (-j\omega)^{\alpha_1+\alpha_2}P_3 + (-j\omega)^{\alpha_1+\alpha_2+\alpha_3}P_4\right] \\ &= \omega^{\alpha_1}e^{j(\pi(2-\alpha_1)/2)}P_2 + \omega^{\alpha_1+\alpha_2}e^{j(\pi(2-\alpha_1-\alpha_2)/2)}P_3 + \omega^{(\alpha_1+\alpha_2+\alpha_3)}e^{j(\pi(2-\alpha_1-\alpha_2-\alpha_3)/2)}P_4 \\ &= \left[\omega^{\alpha_1}P_2\cos\frac{\pi(2-\alpha_1)}{2} + \omega^{(\alpha_1+\alpha_2)}P_3\cos\frac{\pi(2-\alpha_1-\alpha_2)}{2} + \omega^{(\alpha_1+\alpha_2+\alpha_3)}P_4\cos\frac{\pi(2-\alpha_1-\alpha_2-\alpha_3)}{2}\right] \\ &\quad + j\left[\omega^{\alpha_1}P_2\sin\frac{\pi(2-\alpha_1)}{2} + \omega^{(\alpha_1+\alpha_2)}P_3\sin\frac{\pi(2-\alpha_1-\alpha_2)}{2} + \omega^{(\alpha_1+\alpha_2+\alpha_3)}P_4\sin\frac{\pi(2-\alpha_1-\alpha_2-\alpha_3)}{2}\right] \\ &= \mathrm{Re}\left[F_3(\omega)\right] + j\,\mathrm{Im}\left[F_3(\omega)\right], \end{aligned} \tag{33}$$

$$\begin{aligned} \left[M_3(\omega)\right]^2 &= \left|F_3(\omega)\right|^2 = \omega^{2\alpha_1}P_2^2 + \omega^{2(\alpha_1+\alpha_2)}P_3^2 + 2\omega^{(2\alpha_1+\alpha_2)}\cos\frac{\pi\alpha_2}{2}P_2P_3 + 2\omega^{(2\alpha_1+\alpha_2+\alpha_3)} \\ &\quad \cdot \cos\frac{\pi(\alpha_2+\alpha_3)}{2}P_2P_4 + 2\omega^{(2\alpha_1+2\alpha_2+\alpha_3)}\cos\frac{\pi\alpha_3}{2}P_3P_4 \\ &\quad + \omega^{2(\alpha_1+\alpha_2+\alpha_3)}P_4^2 = z_1+z_2+z_3+z_4+z_8+z_{12}. \end{aligned} \tag{34}$$

Because of $R_3(\omega) = \mathrm{Im}[F_3(\omega)]/\mathrm{Re}[F_3(\omega)]$, we can get the first derivative of $R_3(\omega)$:

$$
\begin{aligned}
&R_3'(\omega)\\
&= -\frac{\left[\alpha_2\omega^{(2\alpha_1+\alpha_2-1)}P_2P_3\sin\left(\pi\alpha_2/2\right)+\left(\alpha_2+\alpha_3\right)\omega^{(2\alpha_1+\alpha_2+\alpha_3-1)}\cdot P_2P_4\sin\left(\pi\left(\alpha_2+\alpha_3\right)/2\right)+\alpha_3\omega^{(2\alpha_1+2\alpha_2+\alpha_3-1)}P_3P_4\sin\left(\pi\alpha_3/2\right)\right]}{\left[\omega^{\alpha_1}P_2\cdot\cos\left(\pi\left(2-\alpha_1\right)/2\right)+\omega^{(\alpha_1+\alpha_2)}P_3\cos\left(\pi\left(2-\alpha_1-\alpha_2\right)/2\right)+\omega^{(\alpha_1+\alpha_2+\alpha_3)}P_4\cdot\cos\left(\pi\left(2-\alpha_1-\alpha_2-\alpha_3\right)/2\right)\right]^2} \qquad (35)\\
&= -\frac{\left(d_1+d_2+d_6\right)}{\left\{\mathrm{Re}\left[F_3(\omega)\right]\right\}^2} < 0.
\end{aligned}
$$

In a similar way, the $[M_l(\omega)]^2$ and $R_l'(\omega)$ of the FOMASs with quadruple integral to sextuple integral can be, respectively, calculated under the appropriate parameters, and they are as follows:

$$
\begin{aligned}
&\left[M_4(\omega)\right]^2 = z_1+z_2+z_3+z_4+z_5+z_8+z_9+z_{12}+z_{13}+z_{16},\\
&R_4'(\omega) = -\frac{\left(d_1+d_2+d_3+d_6+d_7+d_{10}\right)}{\left\{\mathrm{Re}\left[F_4(\omega)\right]\right\}^2} < 0.
\end{aligned} \qquad (36)
$$

$$
\begin{aligned}
&\left[M_5(\omega)\right]^2 = z_1+z_2+z_3+z_4+z_5+z_6+z_8+z_9+z_{10}+z_{12}+z_{13}+z_{14}+z_{16}+z_{17}+z_{19},\\
&R_5'(\omega) = -\frac{\left(d_1+d_2+d_3+d_4+d_6+d_7+d_8+d_{10}+d_{11}+d_{13}\right)}{\left\{\mathrm{Re}\left[F_5(\omega)\right]\right\}^2} < 0.
\end{aligned} \qquad (37)
$$

$$
\begin{aligned}
&\left[M_6(\omega)\right]^2 = z_1+z_2+z_3+z_4+z_5+z_6+z_7+z_8+z_9+z_{10}+z_{11}+z_{12}+z_{13}+z_{14}+z_{15}+z_{16}+z_{17}+z_{18}+z_{19}+z_{20}\\
&\qquad +z_{21},\\
&R_6'(\omega) = -\frac{\left(d_1+d_2+d_3+d_4+d_5+d_6+d_7+d_8+d_9+d_{10}+d_{11}+d_{12}+d_{13}+d_{14}+d_{15}\right)}{\left\{\mathrm{Re}\left[F_6(\omega)\right]\right\}^2} < 0.
\end{aligned} \qquad (38)
$$

In summary, we have found that the first derivatives of $R_l(\omega)$ $(2 \le l \le 6)$ listed above are negative values, and $R_l'(\omega) < 0$ means that $R_l(\omega) = \tan[\theta_l(\omega)]$ are monotonically decreasing with the growth of ω. Then it can be deduced that the arguments $\theta_l(\omega)$ also decrease monotonically and continuously about ω because the values of $F_l(\omega)$ vary smoothly. Evidently, we can analyze the features of $\theta_l(\omega)$ $(2 \le l \le 6)$ together.

If $0 < \omega_1 < \omega_2$, we have $\omega_2/\omega_1 > 1$, and because the arguments $\theta_l(\omega)$ decrease monotonically and continuously about ω, we have $\theta_l(\omega_1) > \theta_l(\omega_2)$; i.e., $\theta_l(\omega_1)/\theta_l(\omega_2) > 1$. Thus,

$$
\frac{T_l(\omega_1)}{T_l(\omega_2)} = \frac{\theta_l(\omega_1)}{\omega_1}\cdot\frac{\omega_2}{\theta_l(\omega_2)} = \frac{\theta_l(\omega_1)}{\theta_l(\omega_2)}\cdot\frac{\omega_2}{\omega_1} > 1, \qquad (39)
$$

so we can get $T_l(\omega_1) > T_l(\omega_2)$, which means $T_l(\omega)$ also decrease monotonically and continuously about ω. When $\omega \le \overline{\omega}$, we have

$$
T_l(\omega) \ge T_l(\overline{\omega}) = \overline{\tau}. \qquad (40)
$$

It is worth noting that inequality (40) can be obtained when the characteristic eigenvalue of $\det[G_{\tau_m}(s)]$ of the MIFOMAS (10) is $s = -j\omega \ne 0$. If we let all $\tau_m < \overline{\tau}$, then we can obtain the following inequality:

$$
\begin{aligned}
T_l(\omega) &= \frac{\theta_l(\omega)}{\omega} = \frac{\arg\left(\sum_{m=1}^{M}a_m e^{j\omega\tau_m}\right)}{\omega} \le \frac{\max\{\omega\tau_m\}}{\omega}\\
&< \frac{\omega\overline{\tau}}{\omega} = \overline{\tau}.
\end{aligned} \qquad (41)
$$

Inequality (41) is in contradiction with inequality (40). Therefore, as long as all $\tau_m < \overline{\tau}$, we can ensure all the characteristic eigenvalues of $\det[G_{\tau_m}(s)]$ of the MIFOMAS (10) with symmetric time-delays are situated in the LHP, and the MIFOMAS (10) with symmetric time-delays will remain stable and can achieve consensus. On the contrary, the MIFOMAS (10) with symmetric time-delays will not be stable and can not achieve consensus. Theorem 4 is proven for $l \in \{2, 3, 4, 5, 6\}$. □

Remark 5. Consensus of the MIFOMAS (10) without symmetric time-delays is necessary for consensus of this system with symmetric time-delays.

Remark 6. Although $l \in \{1, 2, 3, 4, 5, 6\}$ in Theorem 4 due to computational complexity, the value of l may be greater than 6 under the appropriate parameters.

Corollary 7. *If we suppose that a FOMAS with multiple integral is given by MIFOMAS (4) whose corresponding network topology $\mathcal{G}$ satisfies Lemma 1 and $\alpha_1 = \alpha_2 = \cdots = \alpha_l = 1$, then the MIFOMAS (10) with symmetric time-delays can be transformed into high-order MAS with symmetric time-delays whose dynamic model is an integer-order dynamic model and the following functions can be obtained:*

$$\begin{aligned} F_l(\omega) &= -\sum_{k=1}^{l} (-j\omega)^k P_{k+1}, \\ \theta_l(\omega) &= \arg[F_l(\omega)] = \arg\left[-\sum_{k=1}^{l} (-j\omega)^k P_{k+1}\right] \\ &= \arctan R_l(\omega), \\ T_l(\omega) &= \frac{1}{\omega}\theta_l(\omega), \end{aligned} \tag{42}$$

where $l \in \{1, 2, 3, 4, 5, 6\}$, $R_l(\omega) \triangleq \mathrm{Im}[F_l(\omega)]/\mathrm{Re}[F_l(\omega)] = \tan[\theta_l(\omega)]$, and $\mathrm{Re}[F_l(\omega)]$ and $\mathrm{Im}[F_l(\omega)]$, respectively, denote the real part and the imaginary part of $F_l(\omega)$.

For the high-order MAS with symmetric time-delays, if all τ_m satisfy $\tau_m < \overline{\tau} = T_l(\overline{\omega}) = (1/\overline{\omega})\theta_l(\overline{\omega})$, then the control protocol (7) can resolve the consensus problem for the high-order MAS with symmetric time-delays, and on the contrary, then the control protocol (7) can not resolve the consensus problem for the high-order MAS with symmetric time-delays. The value of $\overline{\omega}$ corresponding to l in $T_l(\overline{\omega})$ is determined by the following equation:

$$\left|F_l(\overline{\omega})\right| = \lambda_n, \quad l \in \{1, 2, 3, 4, 5, 6\}, \tag{43}$$

where $|F_l(\omega)|$ is the modulus of $F_l(\omega)$ and λ_n is the maximum eigenvalue of L.

Remark 8. The dynamic model and the control protocol in Corollary 7 were discussed in [21], and the conclusion in Corollary 7 is less conservative than that in [21]. The proof about Corollary 7 is the same as that of Theorem 4.

Theorem 9. *Suppose that a FOMAS with multiple integral is given by MIFOMAS (4) whose corresponding network topology $\mathcal{G}$ satisfies Lemma 2. Define the following functions:*

$$\begin{aligned} B_l(\omega) &= -\sum_{k=1}^{l} (-j\omega)^{\sum_{i=1}^{k}\alpha_i} P_{k+1}, \\ \Theta_l(\omega) &= \arg[B_l(\omega)] = \arg\left[-\sum_{k=1}^{l} (-j\omega)^{\sum_{i=1}^{k}\alpha_i} P_{k+1}\right] \\ &= \arctan R_l(\omega), \\ \Gamma_l(\omega) &= \frac{1}{\omega}\left[\Theta_l(\omega) - \arg(\lambda_i)\right], \end{aligned} \tag{44}$$

where $l \in \{1, 2, 3, 4, 5, 6\}$, $\arg(\lambda_i) \in (-\pi/2, \pi/2)$, λ_i is the i-th eigenvalue of L, $R_l(\omega) \triangleq \mathrm{Im}[B_l(\omega)]/\mathrm{Re}[B_l(\omega)] = \tan[\Theta_l(\omega)]$, and $\mathrm{Im}[B_l(\omega)]$ and $\mathrm{Re}[B_l(\omega)]$ denote the imaginary part and real part of $B_l(\omega)$, respectively.

If all τ_m satisfy $\tau_m < \overline{\tau} = \min_{|\lambda_i|\neq 0}\{\Gamma_l(\overline{\omega}_i)\}$ for the MIFOMAS (10) with asymmetric time-delays, then the control protocol (7) can resolve the consensus problem of the MIFOMAS (10) with asymmetric time-delays, and on the contrary, then the control protocol (7) can not resolve the consensus problem of the MIFOMAS (10) with asymmetric time-delays. The value of $\overline{\omega}_i$ corresponding to l in $\Gamma_l(\overline{\omega}_i)$ is determined by the following equation:

$$\left|B_l(\overline{\omega}_i)\right| = \left|\lambda_i\right|, \quad l \in \{1, 2, 3, 4, 5, 6\}, \tag{45}$$

where $|B_l(\overline{\omega}_i)|$ is the modulus of $B_l(\overline{\omega}_i)$.

Proof. By adopting the proof method similar to Theorem 4, we suppose that $s = -j\omega \neq 0$ is the characteristic eigenvalue of $\det[G_{\tau_m}(s)]$ of the MIFOMAS (10) with asymmetric time-delays on the imaginary axis, $u = u_1 \otimes [1, 0, \ldots, 0, 0]^T + u_2 \otimes [0, 1, 0, \ldots, 0]^T + \cdots + u_{l-1} \otimes [0, \ldots, 0, 1, 0]^T + u_l \otimes [0, \ldots, 0, 0, 1]^T$ is the corresponding eigenvector, and $\|u\| = \mathbf{1}$, $u_1, u_2, \ldots, u_{l-1}, u_l \in \mathbb{C}^n$. According to Lemma 2, we can get the following equation:

$$B_l(\omega) \triangleq \sum_{m=1}^{M} a_m e^{j\omega\tau_m} = -\sum_{k=1}^{l} (-j\omega)^{\sum_{i=1}^{k}\alpha_i} P_{k+1}. \tag{46}$$

Take modulus of both sides of (46); $|B_l(\omega)|$ is an increasing function for $\omega > 0$; thus $\omega(|B_l(\omega)|)$ is also an increasing function for $|B_l(\omega)|$.

Calculate the principal value of the argument of (46); we have

$$\begin{aligned} \Theta_l(\omega) &\triangleq \arg[B_l(\omega)] = \arg\left[-\sum_{k=1}^{l} (-j\omega)^{\sum_{i=1}^{k}\alpha_i} P_{k+1}\right] \\ &= \arctan R_l(\omega), \end{aligned} \tag{47}$$

where $R_l(\omega) \triangleq \mathrm{Im}[B_l(\omega)]/\mathrm{Re}[B_l(\omega)] = \tan[\Theta_l(\omega)]$ and $\mathrm{Im}[B_l(\omega)]$ and $\mathrm{Re}[B_l(\omega)]$ denote the imaginary part and real part of $B_l(\omega)$, respectively.

According to the definition of $B_l(\omega)$ in (46), we have

$$\Theta_l(\omega) \le \arg\left(\sum_{m=1}^{M} a_m\right) + \max(\omega\tau_m), \tag{48}$$

so there is

$$\max(\omega\tau_m) \ge \Theta_l(\omega) - \arg\left(\sum_{m=1}^{M} a_m\right). \tag{49}$$

Due to $\sum_{m=1}^{M} a_m = u^H(L \otimes I_l)u/(u^H u)$, the possible values of $\sum_{m=1}^{M} a_m$ must be nonzero eigenvalues of L of graph $\mathcal{G}$; i.e., $\sum_{m=1}^{M} a_m = \lambda_i$ ($\lambda_i \neq 0$), which makes the delay margin $\overline{\tau}$ minimized. So when $|B_l(\omega)| \le |\lambda_i|$, $\omega(|B_l(\omega)|) \le \omega(|\lambda_i|) = \overline{\omega}_i$. If we let all $\tau_m < \overline{\tau}$, there is

$$\begin{aligned}\max(\omega\tau_m) &< \overline{\omega}_i\overline{\tau} = \overline{\omega}_i \min_{|\lambda_i|\neq 0}\{\Gamma_l(\overline{\omega}_i)\} \\ &= \min_{|\lambda_i|\neq 0}\left\{\frac{[\Theta_l(\overline{\omega}_i) - \arg(\lambda_i)]}{\overline{\omega}_i}\right\}\overline{\omega}_i \\ &\le \Theta_l(\omega) - \arg\left(\sum_{m=1}^{M} a_m\right).\end{aligned} \tag{50}$$

Inequality (50) is in contradiction with inequality (49). Therefore, as long as all $\tau_m < \overline{\tau}$, the characteristic eigenvalues of $\det[G_{\tau_m}(s)]$ of the MIFOMAS (10) with asymmetric time-delays can not reach or pass through the imaginary axis, then the MIFOMAS (10) with asymmetric time-delays will remain stable and can achieve consensus. On the contrary, the MIFOMAS (10) with asymmetric time-delays will not be stable and can not achieve consensus. Theorem 9 is proven. □

Remark 10. Consensus of the MIFOMAS (10) without asymmetric time-delays is necessary for consensus of this system with asymmetric time-delays.

Remark 11. Although $l \in \{1, 2, 3, 4, 5, 6\}$ in Theorem 9 due to computational complexity, the value of l may be greater than 6 under the appropriate parameters.

Corollary 12. *If we suppose that a FOMAS with multiple integral is given by MIFOMAS (4) whose corresponding network topology $\mathcal{G}$ satisfies Lemma 2 and $\alpha_1 = \alpha_2 = \ldots = \alpha_l = 1$, then the MIFOMAS (10) with asymmetric time-delays can be transformed into high-order MAS with asymmetric time-delays whose dynamic model is an integer-order dynamic model and the following functions can be obtained:*

$$\begin{aligned}B_l(\omega) &= -\sum_{k=1}^{l}(-j\omega)^k P_{k+1}, \\ \Theta_l(\omega) &= \arg[B_l(\omega)] = \arg\left[-\sum_{k=1}^{l}(-j\omega)^k P_{k+1}\right] \\ &= \arctan R_l(\omega), \\ \Gamma_l(\omega) &= \frac{1}{\omega}[\Theta_l(\omega) - \arg(\lambda_i)],\end{aligned} \tag{51}$$

where $l \in \{1, 2, 3, 4, 5, 6\}$, $\arg(\lambda_i) \in (-\pi/2, \pi/2)$, λ_i is the i-th eigenvalue of L, $R_l(\omega) \triangleq \mathrm{Im}[B_l(\omega)]/\mathrm{Re}[B_l(\omega)] = \tan[\Theta_l(\omega)]$, and $\mathrm{Im}[B_l(\omega)]$ and $\mathrm{Re}[B_l(\omega)]$ denote the imaginary part and real part of $B_l(\omega)$, respectively.

For the high-order MAS with asymmetric time-delays, if all τ_m satisfy $\tau_m < \overline{\tau} = \min_{|\lambda_i|\neq 0}\{\Gamma_l(\overline{\omega}_i)\}$, then the control protocol (7) can resolve the consensus problem for the high-order MAS with asymmetric time-delays, and on the contrary, then the control protocol (7) can not resolve the consensus problem for the high-order MAS with asymmetric time-delays. The value of $\overline{\omega}_i$ corresponding to l in $\Gamma_l(\overline{\omega}_i)$ is determined by the following equation:

$$|B_l(\overline{\omega}_i)| = |\lambda_i|, \quad l \in \{1, 2, 3, 4, 5, 6\}, \tag{52}$$

where $|B_l(\overline{\omega}_i)|$ is the modulus of $B_l(\overline{\omega}_i)$.

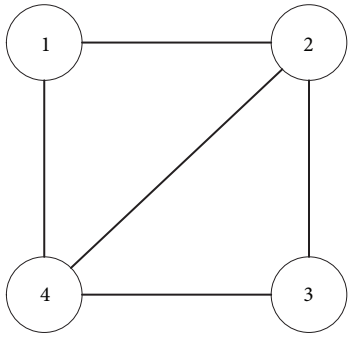

Figure 1: The undirected network topology.

6. Simulation Results

The correctness and validity of the theoretical results for Theorems 4 and 9 will be verified by some numerical simulations in this section. Under different network topologies, the FOMAS with different multiple integral will be considered.

First of all, to validate Theorem 4, we consider a FOMAS composed of 4 agents. Figure 1 shows the network topology depicted with a connected and undirected graph $\mathcal{G}$, and Figure 1 has five different time-delays which are symmetric time-delays and it shows full connectivity. All the delays are marked with τ_{ij}, where i and j are the indexes, which are used to represent the connected agents i and j. If we suppose the weight of each edge of graph $\mathcal{G}$ in Figure 1 is 1, then the adjacency matrix and

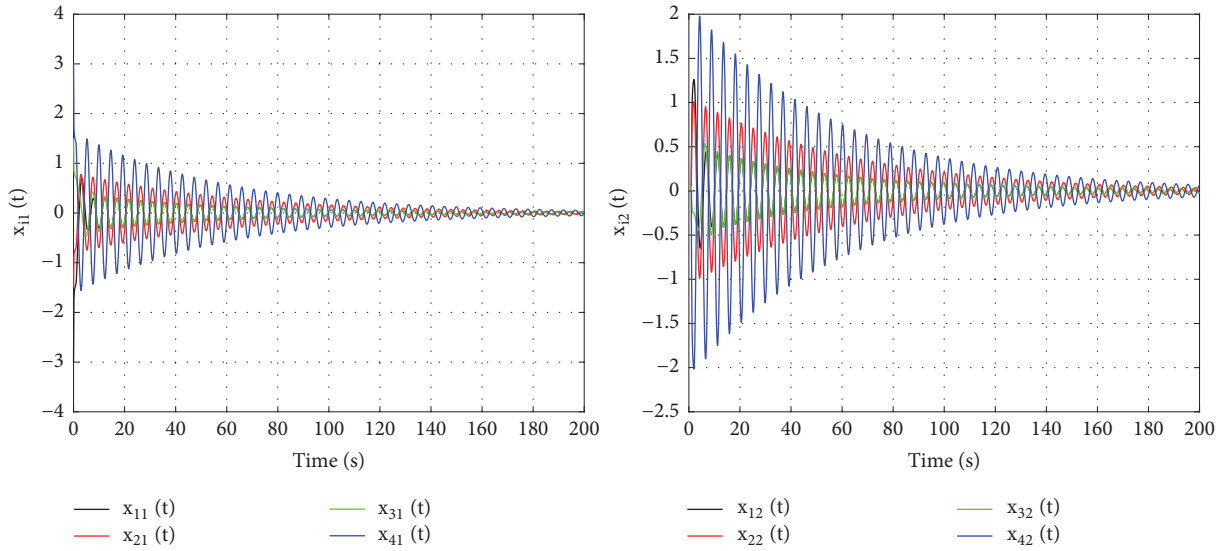

FIGURE 2: The trajectories of all agents' states in the FOMAS with double integral and symmetric time-delays when all $\tau_m < \overline{\tau}$ in Example 1.

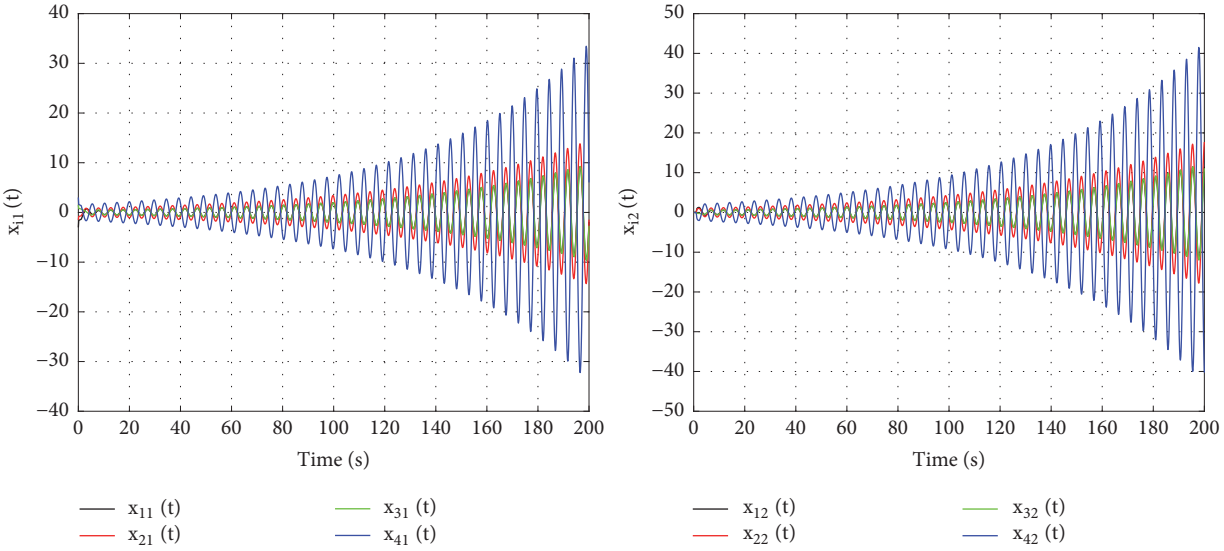

FIGURE 3: The trajectories of all agents' states in the FOMAS with double integral and symmetric time-delays when all $\tau_m > \overline{\tau}$ in Example 1.

the corresponding Laplacian matrix of $\mathcal{G}$ are, respectively,

$$\mathcal{A} = \begin{bmatrix} 2 & 1 & 0 & 1 \\ 1 & 3 & 1 & 1 \\ 0 & 1 & 2 & 1 \\ 1 & 1 & 1 & 3 \end{bmatrix}, \quad L = \begin{bmatrix} 2 & -1 & 0 & -1 \\ -1 & 3 & -1 & -1 \\ 0 & -1 & 2 & -1 \\ -1 & -1 & -1 & 3 \end{bmatrix}, \tag{53}$$

where $\lambda_n = 4$ is the maximum eigenvalue of L.

Example 1. For a FOMAS with double integral and symmetric time-delays under the undirected graph, let us set $\alpha_1 = 0.9$, $\alpha_2 = 0.8$, $\alpha_l = 0$ $(3 \le l \le 6)$, and $P_2 = 2.5$, $P_3 = 1$, $P_4 = P_5 = P_6 = P_7 = 0$; thus the delay margin $\overline{\tau} = 1.015s$ according to Theorem 4. Two groups of symmetric time-delays are set: $\tau_{12} = \tau_{21} = 1.01s$, $\tau_{14} = \tau_{41} = 1.00s$, $\tau_{23} = \tau_{32} = 0.99s$, $\tau_{24} = \tau_{42} = 0.98s$, $\tau_{34} = \tau_{43} = 0.97s$, which are bounded by the delay margin $\overline{\tau}$; $\tau_{12} = \tau_{21} = 1.02s$, $\tau_{14} = \tau_{41} = 1.03s$, $\tau_{23} = \tau_{32} = 1.04s$, $\tau_{24} = \tau_{42} = 1.05s$, $\tau_{34} = \tau_{43} = 1.06s$, which exceed the delay margin $\overline{\tau}$. The simulation results about Example 1 are displayed in Figures 2 and 3: the two subfigures in Figure 2 show the trajectories of all agents' states when all symmetric time-delays are less than the delay margin $\overline{\tau}$, which indicates that the FOMAS with double integral and symmetric time-delays is stable and consensus

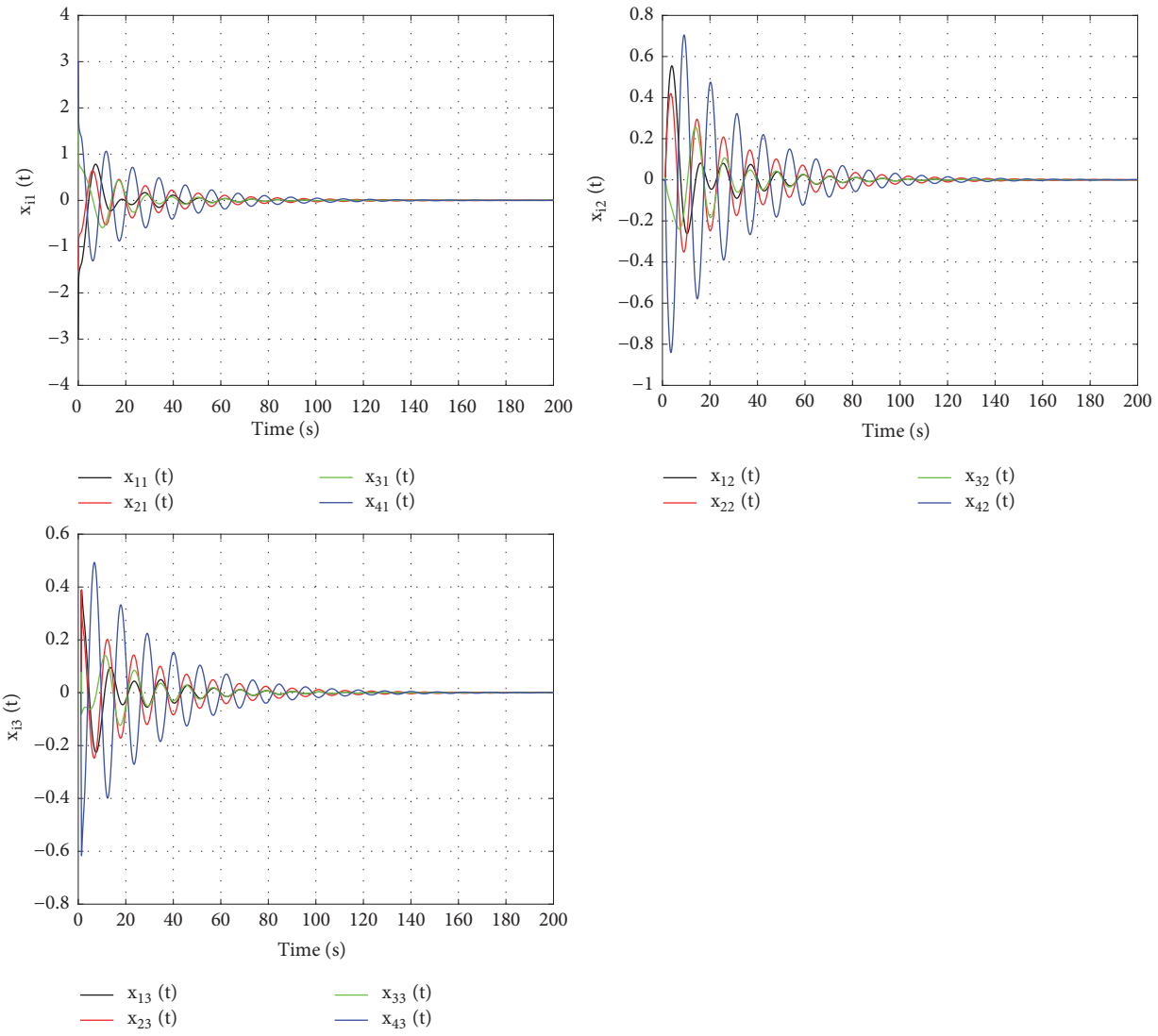

FIGURE 4: The trajectories of all agents' states in the FOMAS with triple integral and symmetric time-delays when all $\tau_m < \overline{\tau}$ in Example 2.

of the FOMAS with double integral and symmetric time-delays can be reached; the two subfigures in Figure 3 show the trajectories of all agents' states when all symmetric time-delays exceed the delay margin $\overline{\tau}$, which indicates that the FOMAS with double integral and symmetric time-delays is unstable and consensus of the FOMAS with double integral and symmetric time-delays can not be reached.

Example 2. For a FOMAS with triple integral and symmetric time-delays under the undirected graph, let us set $\alpha_1 = 0.9$, $\alpha_2 = 0.8$, $\alpha_3 = 0.7$, $\alpha_l = 0$ $(4 \le l \le 6)$, and $P_2 = 2.5$, $P_3 = 9$, $P_4 = 1$, $P_5 = P_6 = P_7 = 0$; thus $\overline{\tau} = 1.398s$ according to Theorem 4. Two groups of symmetric time-delays are set: $\tau_{12} = \tau_{21} = 1.30s$, $\tau_{14} = \tau_{41} = 1.25s$, $\tau_{23} = \tau_{32} = 1.20s$, $\tau_{24} = \tau_{42} = 1.15s$, $\tau_{34} = \tau_{43} = 1.10s$, which are bounded by the delay margin $\overline{\tau}$; $\tau_{12} = \tau_{21} = 1.40s$, $\tau_{14} = \tau_{41} = 1.41s$, $\tau_{23} = \tau_{32} = 1.42s$, $\tau_{24} = \tau_{42} = 1.43s$, $\tau_{34} = \tau_{43} = 1.44s$, which exceed the delay margin $\overline{\tau}$. The simulation results about Example 2 are displayed in Figures 4 and 5: the three subfigures in Figure 4 show the trajectories of all agents' states when all symmetric time-delays are less than the delay margin $\overline{\tau}$, which indicates that the FOMAS with triple integral and symmetric time-delays is stable and consensus of the FOMAS with triple integral and symmetric time-delays can be reached; the three subfigures in Figure 5 show the trajectories of all agents' states when all symmetric time-delays exceed the delay margin $\overline{\tau}$, which indicates that the FOMAS with triple integral and symmetric time-delays is unstable and consensus of the FOMAS with triple integral and symmetric time-delays can not be reached.

Example 3. For a FOMAS with sextuple integral and symmetric time-delays under the undirected graph, let us set $\alpha_1 = 0.9$, $\alpha_2 = 0.8$, $\alpha_3 = 0.7$, $\alpha_4 = 0.6$, $\alpha_5 = 0.5$, $\alpha_6 = 0.4$, and

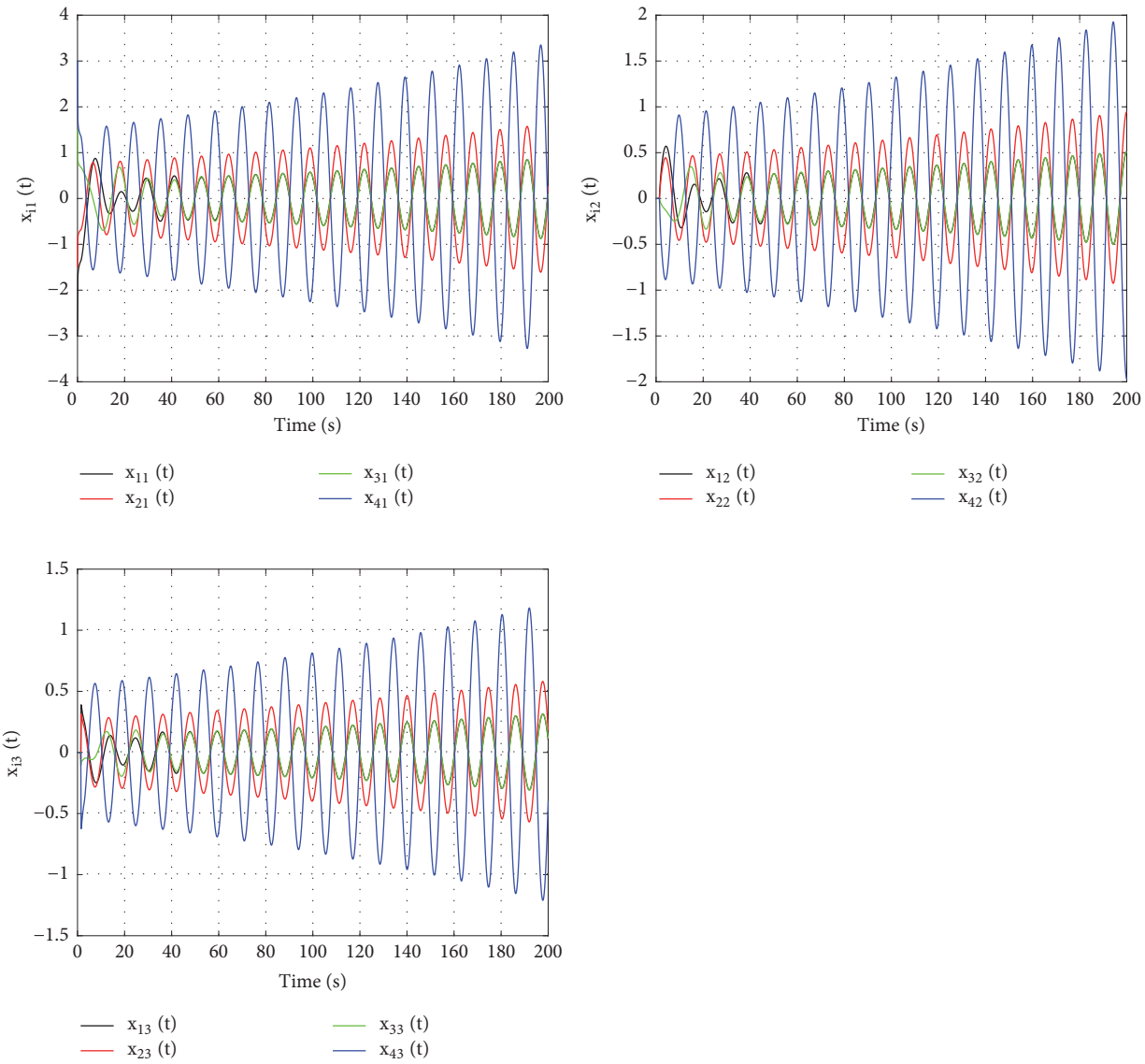

FIGURE 5: The trajectories of all agents' states in the FOMAS with triple integral and symmetric time-delays when all $\tau_m > \overline{\tau}$ in Example 2.

$P_2 = 2.5$, $P_3 = 9$, $P_4 = 4$, $P_5 = 8$, $P_6 = 1.2$, $P_7 = 1$; thus $\overline{\tau} = 0.2515s$ according to Theorem 4. Two groups of symmetric time-delays are set: $\tau_{12} = \tau_{21} = 0.24s$, $\tau_{14} = \tau_{41} = 0.22s$, $\tau_{23} = \tau_{32} = 0.20s$, $\tau_{24} = \tau_{42} = 0.18s$, $\tau_{34} = \tau_{43} = 0.16s$, which are bounded by the delay margin $\overline{\tau}$; $\tau_{12} = \tau_{21} = 0.26s$, $\tau_{14} = \tau_{41} = 0.27s$, $\tau_{23} = \tau_{32} = 0.28s$, $\tau_{24} = \tau_{42} = 0.29s$, $\tau_{34} = \tau_{43} = 0.30s$, which exceed the delay margin $\overline{\tau}$. The simulation results about Example 3 are displayed in Figures 6 and 7: the six subfigures in Figure 6 show the trajectories of all agents' states when all symmetric time-delays are less than the delay margin $\overline{\tau}$, which indicates that the FOMAS with sextuple integral and symmetric time-delays is stable and consensus of the FOMAS with sextuple integral and symmetric time-delays can be reached; the six subfigures in Figure 7 show the trajectories of all agents' states when all symmetric time-delays exceed the delay margin $\overline{\tau}$, which indicates that the FOMAS with sextuple integral and symmetric time-delays is unstable and consensus of the FOMAS with sextuple integral and symmetric time-delays can not be reached.

Next, to examine Theorem 9, we give a network topology described in Figure 8, which is a directed graph $\mathcal{G}$ with a spanning tree. It also contains five different time-delays which are asymmetric time-delays and displays full connectivity. If we suppose the weight of each edge of graph $\mathcal{G}$ in Figure 8 is 1, then the adjacency matrix and the corresponding Laplacian matrix are

$$\mathcal{A} = \begin{bmatrix} 2 & 1 & 0 & 1 \\ 0 & 1 & 0 & 1 \\ 0 & 1 & 1 & 0 \\ 0 & 0 & 1 & 1 \end{bmatrix},$$

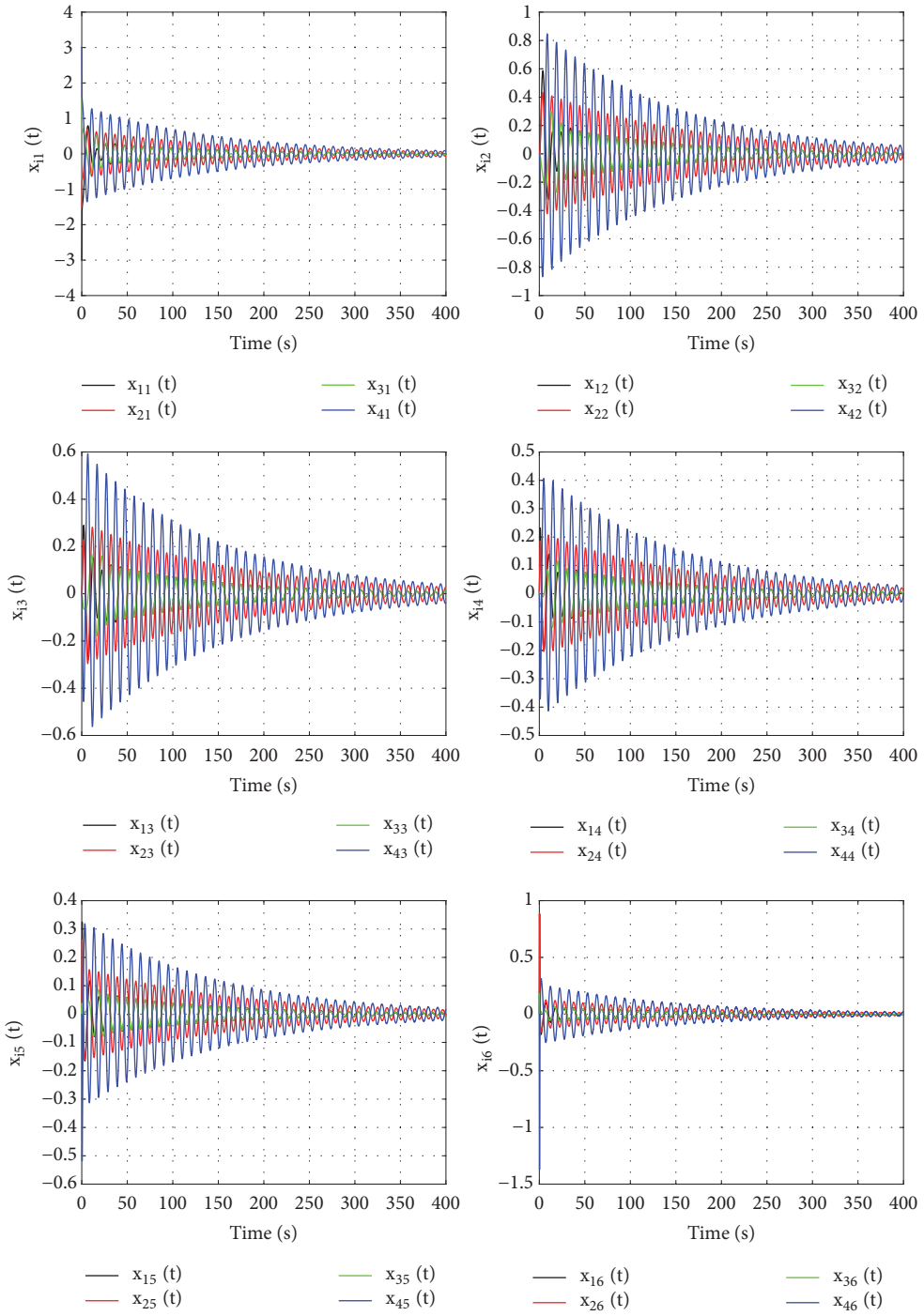

FIGURE 6: The trajectories of all agents' states in the FOMAS with sextuple integral and symmetric time-delays when all $\tau_m < \overline{\tau}$ in Example 3.

$$L = \begin{bmatrix} 2 & -1 & 0 & -1 \\ 0 & 1 & 0 & -1 \\ 0 & -1 & 1 & 0 \\ 0 & 0 & -1 & 1 \end{bmatrix}, \tag{54}$$

where $\lambda_1 = 2, \lambda_2 = 0, \lambda_3 = 1.5 + 0.866i$, and $\lambda_4 = 1.5 - 0.866i$ are all eigenvalues of L.

Example 4. For a FOMAS with double integral and asymmetric time-delays under the directed graph, let us set $\alpha_1 = 0.9$, $\alpha_2 = 0.8$, $\alpha_l = 0$ $(3 \le l \le 6)$, and $P_2 = 2.5$, $P_3 = 1$, $P_4 = P_5 = P_6 = P_7 = 0$; thus $\overline{\tau} = 1.649s$ according to

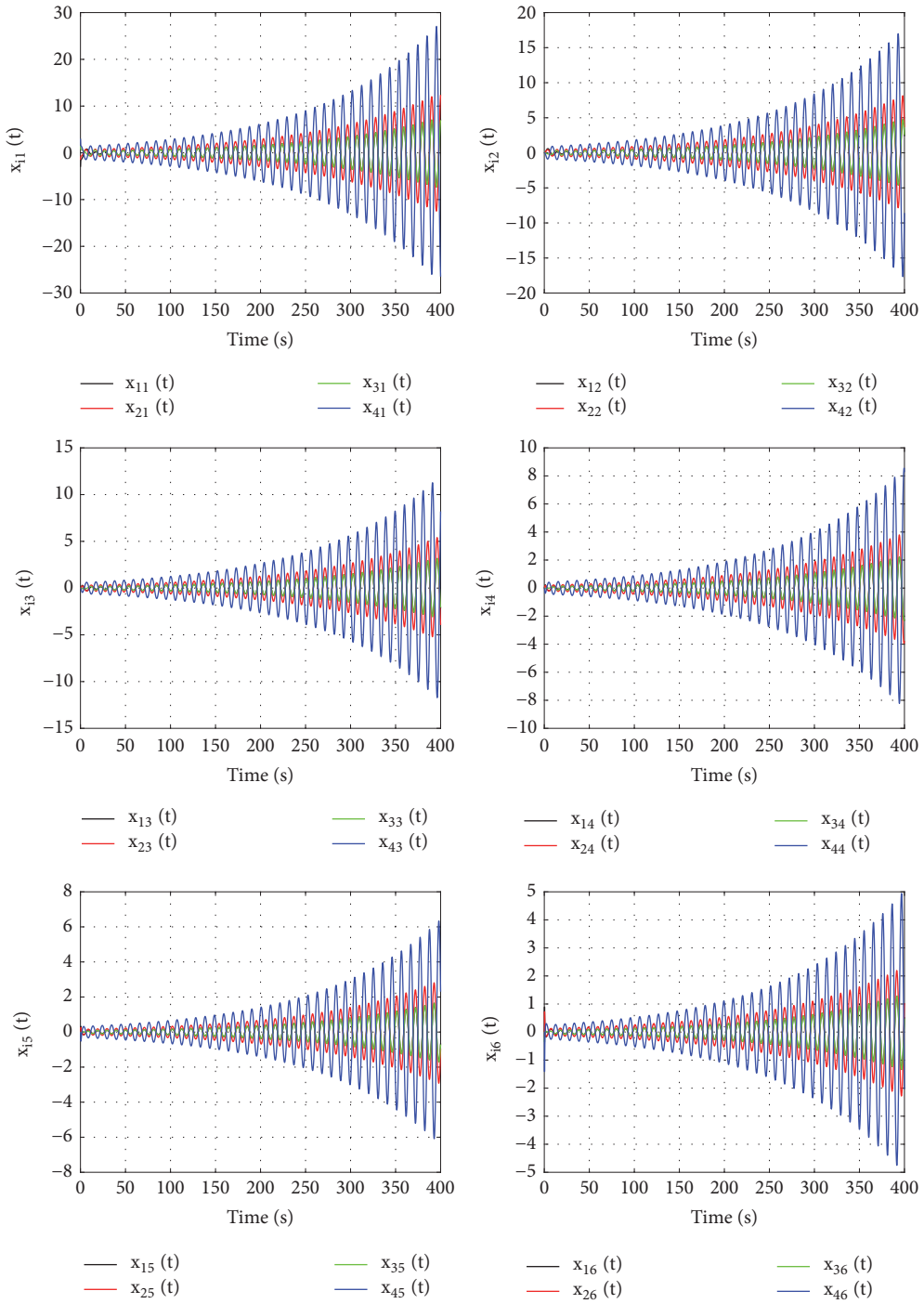

FIGURE 7: The trajectories of all agents' states in the FOMAS with sextuple integral and symmetric time-delays when all $\tau_m > \overline{\tau}$ in Example 3.

Theorem 9. Two groups of asymmetric time-delays are set: $\tau_{12} = 1.64s$, $\tau_{14} = 1.63s$, $\tau_{24} = 1.62s$, $\tau_{32} = 1.61s$, $\tau_{43} = 1.60s$, which are bounded by the delay margin $\overline{\tau}$; $\tau_{12} = 1.66s$, $\tau_{14} = 1.67s$, $\tau_{24} = 1.68s$, $\tau_{32} = 1.69s$, $\tau_{43} = 1.70s$, which exceed the delay margin $\overline{\tau}$. The simulation results about Example 4 are displayed in Figures 9 and 10: the two subfigures in Figure 9 show the trajectories of all agents' states when all asymmetric time-delays are less than the delay margin $\overline{\tau}$, which indicates that consensus of the FOMAS with double integral and asymmetric time-delays can be reached; the two subfigures in Figure 10 show the trajectories of all agents' states when all asymmetric time-delays exceed the

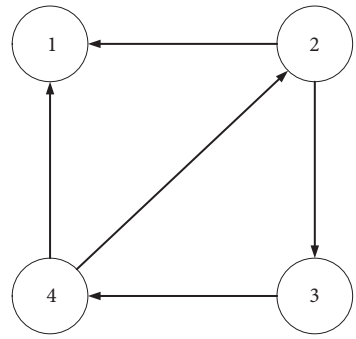

Figure 8: The directed network topology.

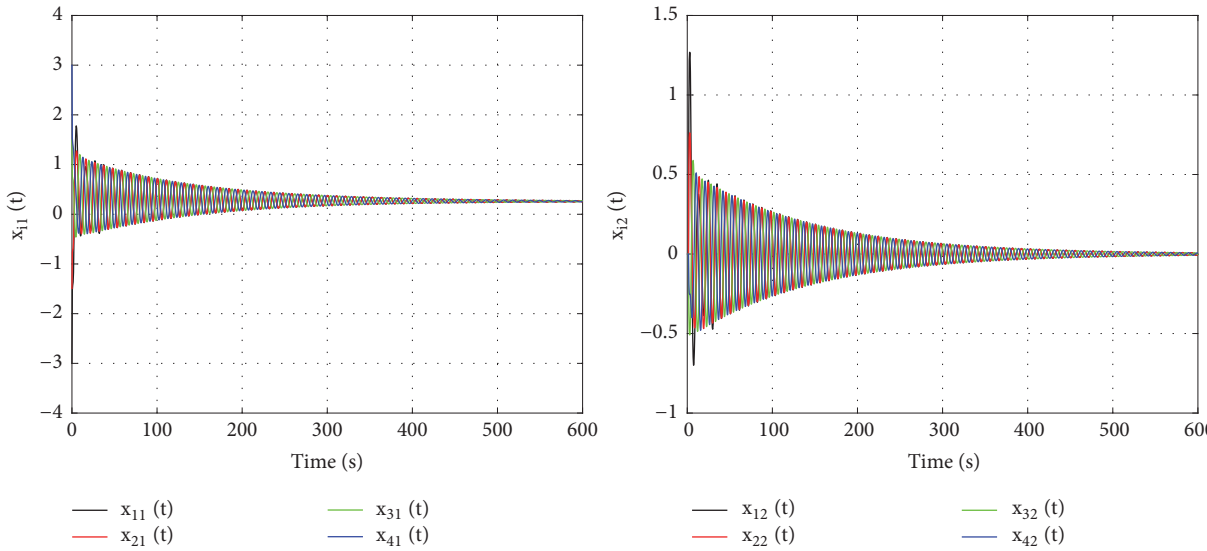

Figure 9: The trajectories of all agents' states in the FOMAS with double integral and asymmetric time-delays when all $\tau_m < \overline{\tau}$ in Example 4.

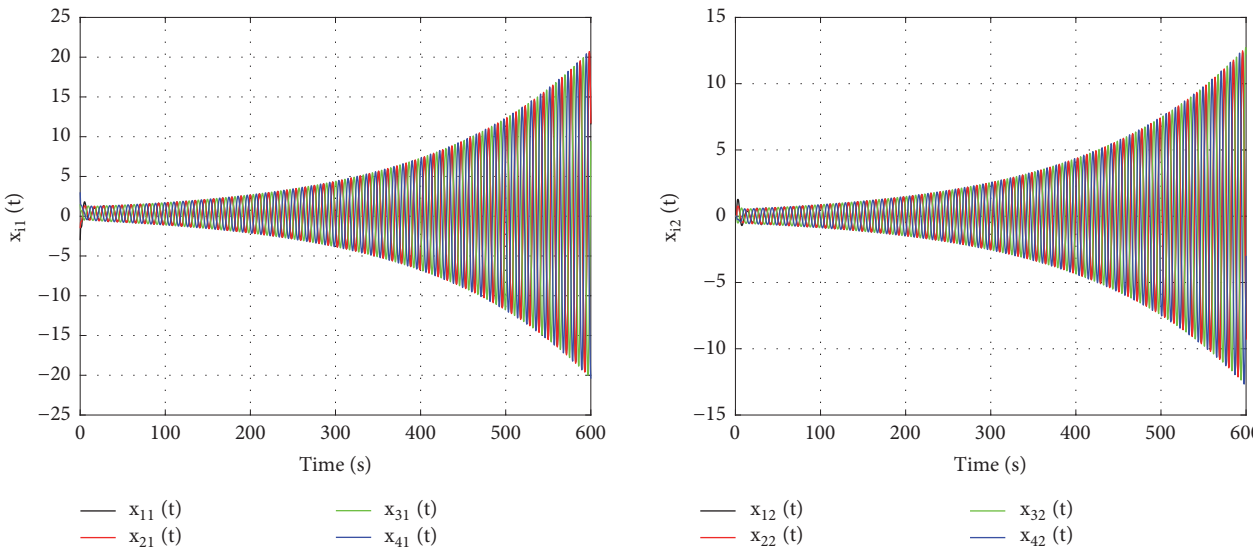

Figure 10: The trajectories of all agents' states in the FOMAS with double integral and asymmetric time-delays when all $\tau_m > \overline{\tau}$ in Example 4.

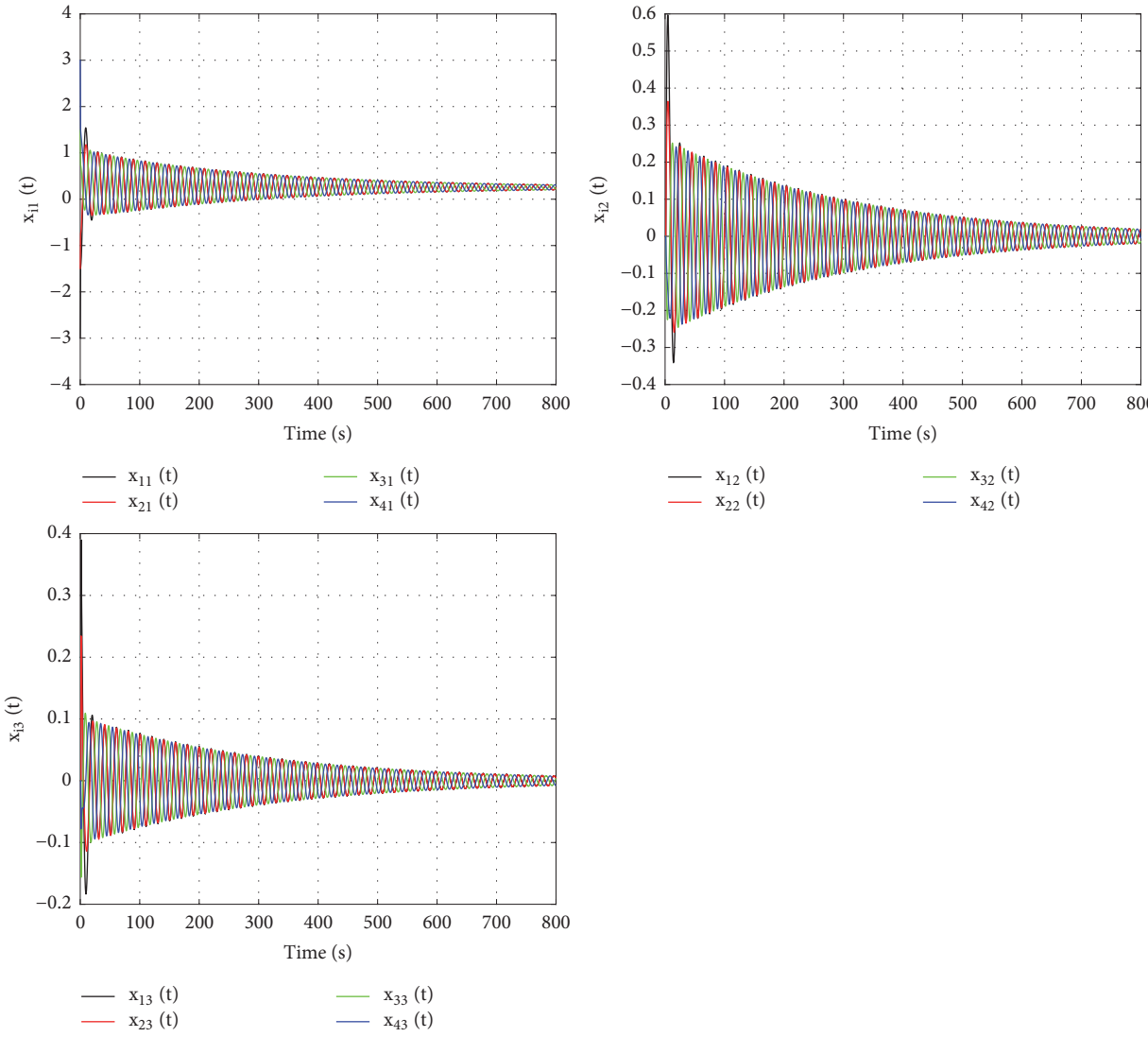

Figure 11: The trajectories of all agents' states in the FOMAS with triple integral and asymmetric time-delays when all $\tau_m < \overline{\tau}$ in Example 5.

delay margin $\overline{\tau}$, which indicates that consensus of the FOMAS with double integral and asymmetric time-delays can not be reached.

Example 5. For a FOMAS with triple integral and asymmetric time-delays under the directed graph, let us set $\alpha_1 = 0.9$, $\alpha_2 = 0.8$, $\alpha_3 = 0.7$, $\alpha_l = 0$ $(4 \leq l \leq 6)$, and $P_2 = 2.5$, $P_3 = 9$, $P_4 = 1$, $P_5 = P_6 = P_7 = 0$; thus $\overline{\tau} = 1.327s$ according to Theorem 9. Two groups of asymmetric time-delays are set: $\tau_{12} = 1.32s$, $\tau_{14} = 1.29s$, $\tau_{24} = 1.26s$, $\tau_{32} = 1.23s$, $\tau_{43} = 1.21s$, which are bounded by the delay margin $\overline{\tau}$; $\tau_{12} = 1.33s$, $\tau_{14} = 1.36s$, $\tau_{24} = 1.39s$, $\tau_{32} = 1.42s$, $\tau_{43} = 1.45s$, which exceed the delay margin $\overline{\tau}$. The simulation results about Example 5 are displayed in Figures 11 and 12: the three subfigures in Figure 11 show the trajectories of all agents' states when all asymmetric time-delays are less than the delay margin $\overline{\tau}$, which indicates that consensus of the FOMAS with triple integral and asymmetric time-delays can be reached; the three subfigures in Figure 12 show the trajectories of all agents' states when all asymmetric time-delays exceed the delay margin $\overline{\tau}$, which indicates that consensus of the FOMAS with triple integral and asymmetric time-delays can not be reached.

Example 6. For a FOMAS with sextuple integral and asymmetric time-delays under the directed graph, let us set $\alpha_1 = 0.9$, $\alpha_2 = 0.8$, $\alpha_3 = 0.7$, $\alpha_4 = 0.6$, $\alpha_5 = 0.5$, $\alpha_6 = 0.4$, and $P_2 = 2.5$, $P_3 = 9$, $P_4 = 4$, $P_5 = 8$, $P_6 = 1.2$, $P_7 = 1$; thus $\overline{\tau} = 0.4335s$ according to Theorem 9. Two groups of asymmetric time-delays are set: $\tau_{12} = 0.43s$, $\tau_{14} = 0.40s$, $\tau_{24} = 0.37s$, $\tau_{32} = 0.34s$, $\tau_{43} = 0.31s$, which are bounded by the delay margin $\overline{\tau}$; $\tau_{12} = 0.44s$, $\tau_{14} = 0.47s$, $\tau_{24} = 0.50s$, $\tau_{32} = 0.53s$, $\tau_{43} = 0.57s$, which exceed the delay margin $\overline{\tau}$. The simulation results about Example 6 are

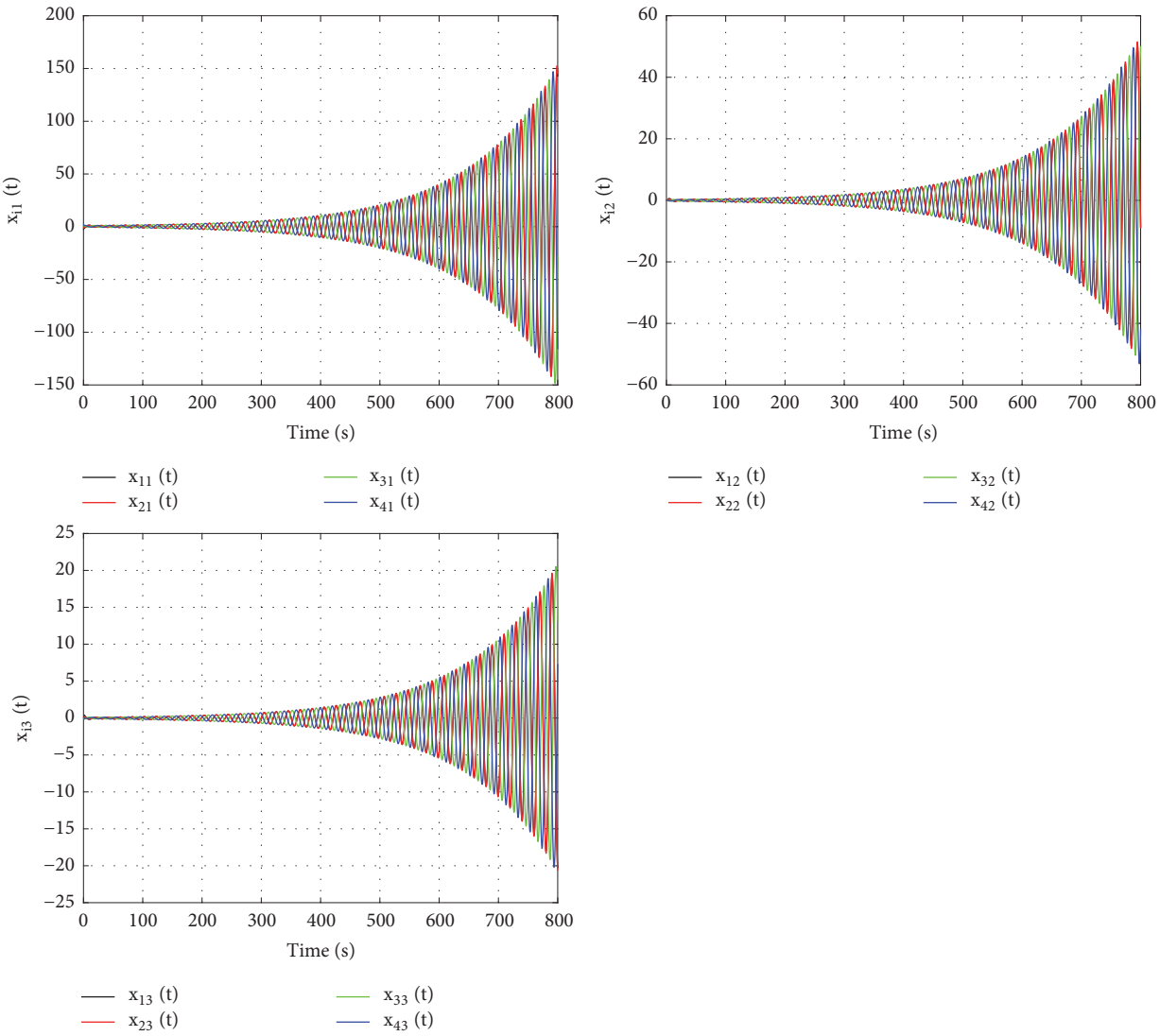

FIGURE 12: The trajectories of all agents' states in the FOMAS with triple integral and asymmetric time-delays when all $\tau_m > \overline{\tau}$ in Example 5.

displayed in Figures 13 and 14: the six subfigures in Figure 13 show the trajectories of all agents' states when all asymmetric time-delays are less than the delay margin $\overline{\tau}$, which indicates that consensus of the FOMAS with sextuple integral and asymmetric time-delays can be reached; the six subfigures in Figure 14 show the trajectories of all agents' states when all asymmetric time-delays exceed the delay margin $\overline{\tau}$, which indicates that consensus of the FOMAS with sextuple integral and asymmetric time-delays can not be reached.

7. Conclusion

The consensus problems of a FOMAS with multiple integral under nonuniform time-delays are studied in this paper. Taking into account two kinds of nonuniform time-delays, the sufficient conditions have been derived in the form of inequalities for the MIFOMAS with nonuniform time-delays. Numerical simulations of the MIFOMAS with nonuniform time-delays over undirected topology and directed topology are performed to verify these theorems. Finally, the simulation results show that the selected examples have achieved the desired results: the MIFOMAS with nonuniform time-delays under given conditions can achieve the consensus. With the help of the above research of this paper, distributed formation control of the MIFOMAS with nonuniform time-delays will be one of the most significant topics, which will be one of our future research tasks.

Data Availability

The data used to support the findings of this study are available from the corresponding author upon request.

Conflicts of Interest

The authors declare that they have no conflicts of interest.

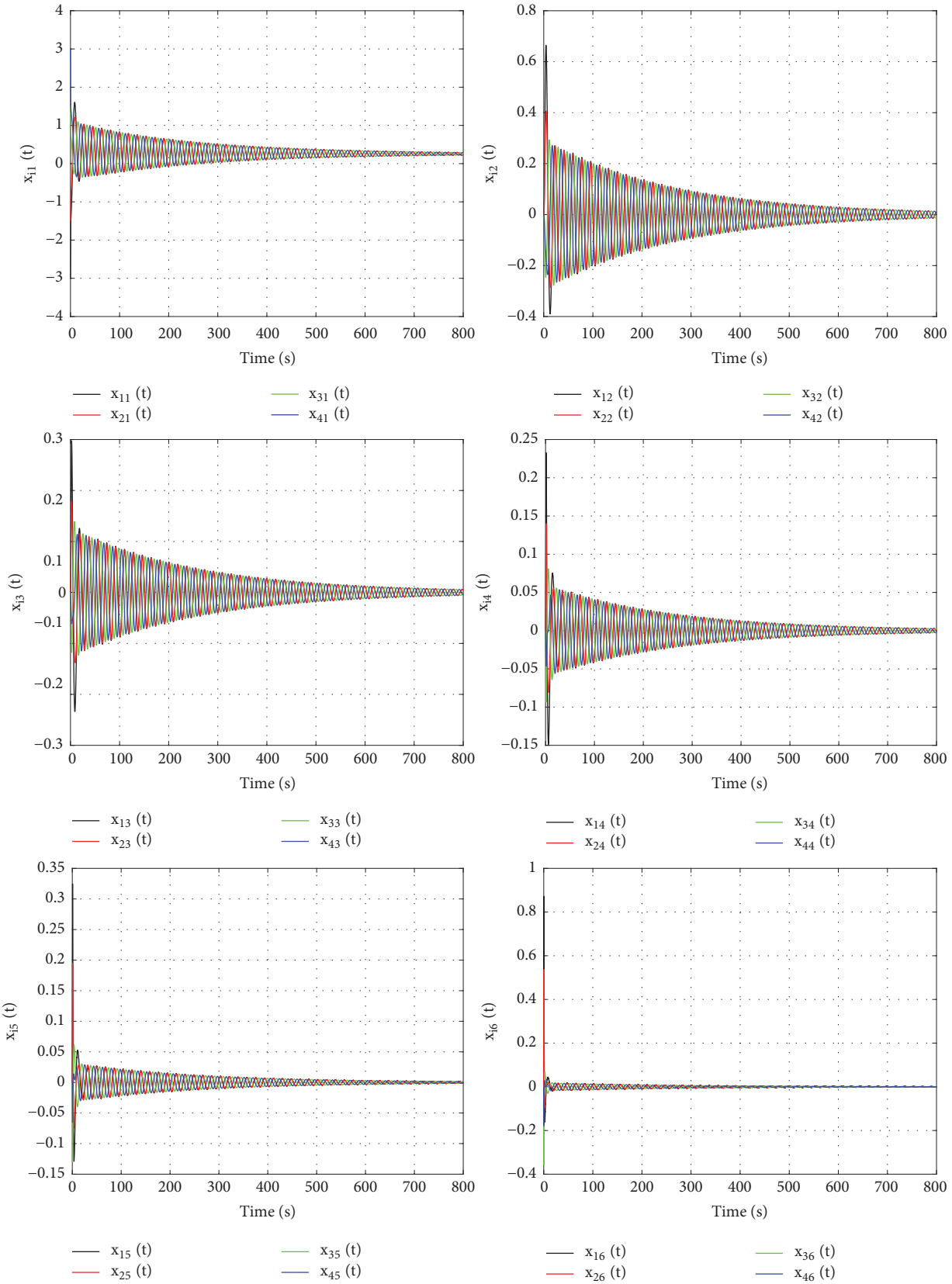

FIGURE 13: The trajectories of all agents' states in the FOMAS with sextuple integral and asymmetric time-delays when all $\tau_m < \overline{\tau}$ in Example 6.

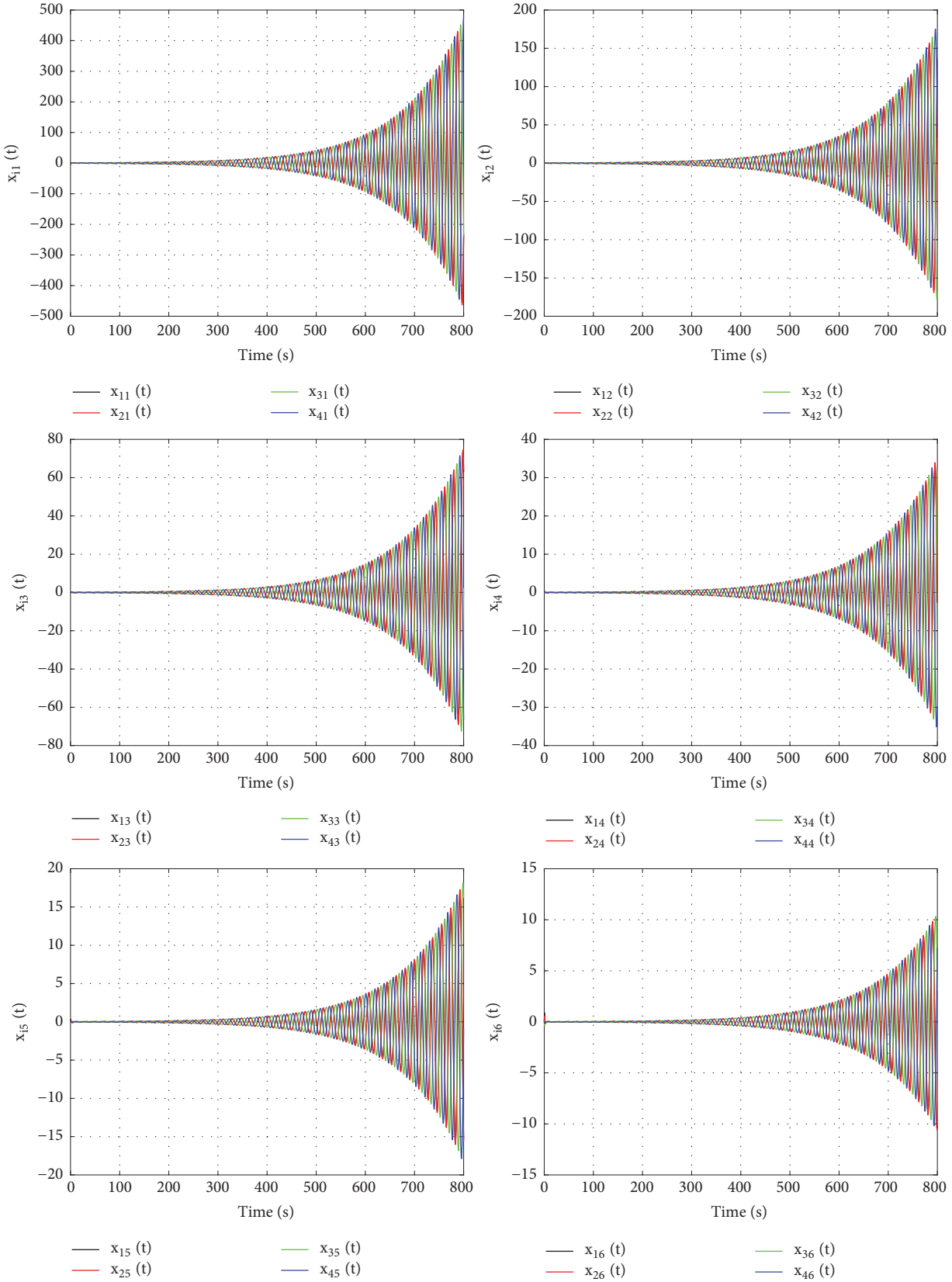

FIGURE 14: The trajectories of all agents' states in the FOMAS with sextuple integral and asymmetric time-delays when all $\tau_m > \overline{\tau}$ in Example 6.

Acknowledgments

This work was supported by the Science and Technology Department Project of Sichuan Province of China (Grants nos. 2014FZ0041, 2017GZ0305, and 2016GZ0220), the Education Department Key Project of Sichuan Province of China (Grant no. 17ZA0077), and the National Natural Science Foundation of China (Grant nos. U1733103, 61802036).

References

[1] M. Shi, K. Qin, and J. Liu, "Cooperative multi-agent sweep coverage control for unknown areas of irregular shape," *Iet Control Theory and Applications*, vol. 18, no. 2, pp. 115–117, 2008.

[2] A. E. Turgut, H. Çelikkanat, F. Gökçe, and E. Şahin, "Self-organized flocking in mobile robot swarms," *Swarm Intelligence*, vol. 2, no. 2-4, pp. 97–120, 2008.

[3] T. R. Krogstad and J. T. Gravdahl, *Coordinated Attitude Control of Satellites in Formation*, Springer Berlin Heidelberg, 2006.

[4] T. Vicsek, A. Czirk, E. Ben-Jacob, I. Cohen, and O. Shochet, "Novel type of phase transition in a system of self-driven particles," *Physical Review Letters*, vol. 75, no. 6, pp. 1226–1229, 1995.

[5] A. Jadbabaie, J. Lin, and A. S. Morse, "Coordination of groups of mobile autonomous agents using nearest neighbor rules," *IEEE Transactions on Automatic Control*, vol. 48, no. 6, pp. 988–1001, 2003.

[6] L. Moreau, "Stability of multiagent systems with time-dependent communication links," *IEEE Transactions on Automatic Control*, vol. 50, no. 2, pp. 169–182, 2005.

[7] W. Ren and R. W. Beard, "Consensus seeking in multiagent systems under dynamically changing interaction topologies," *IEEE Transactions on Automatic Control*, vol. 50, no. 5, pp. 655–661, 2005.

[8] R. Olfati-Saber, J. A. Fax, and R. M. Murray, "Consensus and cooperation in networked multi-agent systems," *Proceedings of the IEEE*, vol. 95, no. 1, pp. 215–233, 2007.

[9] P. Li and K. Qin, "Distributed robust h∞ consensus control for uncertain multiagent systems with state and input delays," *Mathematical Problems in Engineering*, vol. 2017, Article ID 5091756, 15 pages, 2017.

[10] Y. Wu, B. Hu, and Z. Guan, "Exponential Consensus Analysis for Multiagent Networks Based on Time-Delay Impulsive Systems," *IEEE Transactions on Systems, Man, and Cybernetics: Systems*, vol. 99, pp. 1–8, 2017.

[11] Y. Wu, B. Hu, and Z. Guan, "Consensus Problems Over Cooperation-Competition Random Switching Networks With Noisy Channels," *IEEE Transactions on Neural Networks and Learning Systems*, vol. 99, pp. 1–9, 2018.

[12] P. Lin and Y. Jia, "Consensus of a class of second-order multi-agent systems with time-delay and jointly-connected topologies," *IEEE Transactions on Automatic Control*, vol. 55, no. 3, pp. 778–784, 2010.

[13] J. Qin, H. Gao, and W. X. Zheng, "Second-order consensus for multi-agent systems with switching topology and communication delay," *Systems & Control Letters*, vol. 60, no. 6, pp. 390–397, 2011.

[14] H. Li, X. Liao, X. Lei, T. Huang, and W. Zhu, "Second-order consensus seeking in multi-agent systems with nonlinear dynamics over random switching directed networks," *IEEE Transactions on Circuits and Systems I: Regular Papers*, vol. 60, no. 6, pp. 1595–1607, 2013.

[15] P. Li, K. Qin, and M. Shi, "Distributed robust H_∞ rotating consensus control for directed networks of second-order agents with mixed uncertainties and time-delay," *Neurocomputing*, vol. 148, pp. 332–339, 2015.

[16] M. Shi and K. Qin, "Distributed Control for Multiagent Consensus Motions with Nonuniform Time Delays," *Mathematical Problems in Engineering*, vol. 2016, Article ID 3567682, 10 pages, 2016.

[17] Y. Liu and Y. M. Jia, "Consensus problem of high-order multi-agent systems with external disturbances: an h8 analysis approach," *International Journal of Robust & Nonlinear Control*, vol. 20, no. 14, pp. 1579–1593, 2010.

[18] P. Lin, Z. Li, Y. Jia, and M. Sun, "High-order multi-agent consensus with dynamically changing topologies and time-delays," *IET Control Theory & Applications*, vol. 5, no. 8, pp. 976–981, 2011.

[19] Y.-P. Tian and Y. Zhang, "High-order consensus of heterogeneous multi-agent systems with unknown communication delays," *Automatica*, vol. 48, no. 6, pp. 1205–1212, 2012.

[20] J. Liu and B. Zhang, "Consensus Problem of High-Order Multiagent Systems with Time Delays," *Mathematical Problems in Engineering*, vol. 2017, Article ID 9104905, 7 pages, 2017.

[21] M. Shi, K. Qin, P. Li, and J. Liu, "Consensus Conditions for High-Order Multiagent Systems with Nonuniform Delays," *Mathematical Problems in Engineering*, vol. 2017, Article ID 7307834, 12 pages, 2017.

[22] W. Ren and Y. C. Cao, *Distributed Coordination of Multi-agent Networks*, Springer, London, UK, 2011.

[23] R. C. Koeller, "Toward an equation of state for solid materials with memory by use of the half-order derivative," *Acta Mechanica*, vol. 191, no. 3-4, pp. 125–133, 2007.

[24] J. Sabatier, O. P. Agrawal, and J. A. Machado, "Advance in Fractional Calculus: Theoretical Developments and Applications in Physics and Engineering," *Biochemical Journal*, vol. 361, no. 1, pp. 97–103, 2007.

[25] J. Bai, G. Wen, A. Rahmani, X. Chu, and Y. Yu, "Consensus with a reference state for fractional-order multi-agent systems," *International Journal of Systems Science*, vol. 47, no. 1, pp. 222–234, 2016.

[26] G. Ren and Y. Yu, "Consensus of fractional multi-agent systems using distributed adaptive protocols," *Asian Journal of Control*, vol. 19, no. 6, pp. 2076–2084, 2017.

[27] C. Tricaud and Y. Chen, "Time-Optimal Control of Systems with Fractional Dynamics," *International Journal of Differential Equations*, vol. 2010, Article ID 461048, 16 pages, 2010.

[28] Z. Liao, C. Peng, W. Li, and Y. Wang, "Robust stability analysis for a class of fractional order systems with uncertain parameters," *Journal of The Franklin Institute*, vol. 348, no. 6, pp. 1101–1113, 2011.

[29] Y. C. Cao, Y. Li, W. Ren, and Y. Q. Chen, "Distributed coordination of networked fractional-order systems," *IEEE Transactions on Systems, Man, and Cybernetics, Part B: Cybernetics*, vol. 40, no. 2, pp. 362–370, 2010.

[30] H. Y. Yang, X. L. Zhu, and K. C. Cao, "Distributed coordination of fractional order multi-agent systems with communication delays," *Fractional Calculus Applied Analysis*, vol. 17, no. 1, pp. 23–37, 2013.

[31] H. Y. Yang, L. Guo, X. L. Zhu, K. C. Cao, and H. L. Zou, "Consensus of compound-order multi-agent systems with communication delays," *Central European Journal of Physics*, vol. 11, no. 6, pp. 806–812, 2013.

[32] W. Zhu, B. Chen, and Y. Jie, "Consensus of fractional-order multi-agent systems with input time delay," *Fractional Calculus and Applied Analysis*, vol. 20, no. 1, pp. 52–70, 2017.

[33] J. Liu, K. Qin, W. Chen, P. Li, and M. Shi, "Consensus of Fractional-Order Multiagent Systems with Nonuniform Time Delays," *Mathematical Problems in Engineering*, vol. 2018, Article ID 2850757, 9 pages, 2018.

[34] J. Liu, K. Y. Qin, W. Chen, and P. Li, "Consensus of delayed fractional-order multi-agent systems based on state-derivative feedback," *Complexity*, vol. 2018, Article ID 8789632, 12 pages, 2018.

[35] C. Yang, W. Li, and W. Zhu, "Consensus analysis of fractional-order multiagent systems with double-integrator," *Discrete Dynamics in Nature and Society*, 8 pages, 2017.

[36] S. Shen, W. Li, and W. Zhu, "Consensus of fractional-order multiagent systems with double integrator under switching topologies," *Discrete Dynamics in Nature and Society*, 7 pages, 2017.

[37] J. Bai, G. Wen, A. Rahmani, and Y. Yu, "Consensus for the fractional-order double-integrator multi-agent systems based on the sliding mode estimator," *IET Control Theory & Applications*, vol. 12, no. 5, pp. 621–628, 2018.

[38] J. Liu, W. Chen, K. Qin, and P. Li, "Consensus of Fractional-Order Multiagent Systems with Double Integral and Time Delay," *Mathematical Problems in Engineering*, vol. 2018, Article ID 6059574, 12 pages, 2018.

[39] J. Liu, K. Qin, P. Li, and W. Chen, "Distributed consensus control for double-integrator fractional-order multi-agent systems with nonuniform time-delays," *Neurocomputing*, vol. 321, pp. 369–380, 2018.

[40] I. Podlubny, "Fractional differential equations," *Mathematics in Science & Engineering*, vol. 198, no. 3, pp. 553–556, 1999.

[41] C. Godsil and G. Royle, *Algebraic Graph Theory*, World Book Publishing Company Beijing Inc, 2014.

[42] D. Matignon, "Stability properties for generalized fractional differential systems," *Proceedings of the Fractional Differential Systems: Models, Methods and Applications*, vol. 5, pp. 145–158, 1998.

Hindawi
Complexity
Volume 2018, Article ID 3249720, 7 pages
https://doi.org/10.1155/2018/3249720

Research Article

New Iterative Method for the Solution of Fractional Damped Burger and Fractional Sharma-Tasso-Olver Equations

Mohammad Jibran Khan,[1] Rashid Nawaz,[2] Samreen Farid,[2] and Javed Iqbal[2]

[1]*Department of Computer and IT, Sarhad University of Science and Information Technology, Peshawar, Pakistan*
[2]*Department of Mathematics, Abdul Wali Khan University Mardan, Khyber Pakhtunkhwa, Pakistan*

Correspondence should be addressed to Rashid Nawaz; rashid_uop@yahoo.com

Received 14 May 2018; Revised 19 July 2018; Accepted 30 July 2018; Published 5 September 2018

Academic Editor: Jesus M. Muñoz-Pacheco

The new iterative method has been used to obtain the approximate solutions of time fractional damped Burger and time fractional Sharma-Tasso-Olver equations. Results obtained by the proposed method for different fractional-order derivatives are compared with those obtained by the fractional reduced differential transform method (FRDTM). The 2nd-order approximate solutions by the new iterative method are in good agreement with the exact solution as compared to the 5th-order solution by the FRDTM.

1. Introduction

Most of the problems arising in the physical and biological area of science are nonlinear in nature, and it is not always possible to find the exact solution of such problems. These problems become more complicated when they involve fractional derivatives and are modelled through mathematical tools from fractional calculus. Fractional partial differential equations (FPDEs) are tremendous instrument and are widely used to describe many significant phenomena and dynamic processes such as engineering, rheology, acoustic, electrical networks, and viscoelasticity [1–6]. Generally, partial differential equations (PDEs) are hard to tackle, and their fractional-order types are more complicated [7, 8]. Therefore, several analytical and approximate methods can be used for finding their approximate solutions such as Adomian decomposition [9], homotopy analysis [10], tau method [11], residual power series method [12], and optimal homotopy asymptotic method [13]. Though the study of FPDEs has been obstructed due to the absence of proficient and accurate techniques, the derivation of approximate solution of FPDEs remains a hotspot and demands to attempt some dexterous and solid plans which are of interest. Daftardar-Gejji and Jafari proposed an iterative method called the new iterative method (NIM) for finding the approximate solution of differential equations [14]. NIM does not require the need for calculation of tedious Adomian polynomials in nonlinear terms like ADM, the need for determination of a Lagrange multiplier in its algorithm like VIM, and the need for discretization like numerical methods. The proposed method handles linear and nonlinear equations in an easy and straightforward way. Recently, the method has been extended for differential equations of the fractional order [15–17].

In the present study, we have implemented NIM for finding the approximate solution of the following fractional-order damped Burger equation.

$$D_t^{\alpha}u(x,t) + u(x,t)D_x u(x,t) - D_x^2 u(x,t) + \lambda u(x,t) = 0, \quad t > 0, 0 < \alpha \le 1. \tag{1}$$

Second, consider the fractional-order Sharma-Tasso-Olver equation of the following form.

$$D_t^{\alpha}u(x,t) + aD_x u^3(x,t) + \frac{3}{2}aD_x^2 u^2(x,t) + aD_x^3 u(x,t) = 0, \quad t > 0, 0 < \alpha \le 1, \tag{2}$$

where α is the parameter describing the order of fractional derivatives, $u(x,t)$ is the function of x and t, and a, λ are constants. The fractional derivatives are described in the Caputo sense. NIM converges rapidly to the exact solution compared to FRDTM, and only at the 2nd iteration does the proposed method yield very encouraging results. The accuracy of the proposed method can further be increased by taking higher-order approximations.

2. Definitions

In this section, we have stated some definitions which are relevant to our work.

Definition 1. A function $g(y), y > 0$, is said to be in space $C_\eta, \eta \in \Re$, if there exists a real number $p > \eta$, such that $g(y) = y^p g_1(y)$, where $g_1(y) \in C(0, \infty)$. The function $g(y)$, $y > 0$, is said to be in space $C_\eta{}^\lambda$ if only if $g^\lambda \in C_\eta, \lambda \in N$.

Definition 2. The R-L fractional integral operator of order $\alpha \geq 0$ of a function $g \in C_\eta, \eta \geq -1$, is as follows:

$$\begin{aligned} J_a^\alpha g(y) &= \frac{1}{\Gamma(\alpha)} \int_a^y (y-\eta)^{\alpha-1} g(\eta) d\eta, \quad \alpha > 0, y > a, \\ J_a^0 g(y) &= g(y). \end{aligned} \tag{3}$$

Because of certain disadvantages of R-L fractional derivative operator, Caputo proposed modified fractional differential operator ${}_cD^\alpha$ as follow.

Definition 3. Caputo fractional derivative of $g(y)$ takes the following form.

$${}_cD_a^\alpha g(y) = \frac{1}{\Gamma(\lambda-\alpha)} \int_a^y (y-\eta)^{\lambda-\alpha-1} g^\lambda(\eta) d\eta, \tag{4}$$

where

$$\begin{aligned} &\lambda - 1 < \alpha \leq \lambda, \\ &\lambda \in N, \\ &y > a, \\ &g \in C_{-1}^\lambda. \end{aligned} \tag{5}$$

Definition 4. If $\lambda - 1 < \alpha \leq \lambda, \lambda \in N$, and $g \in C_\eta^\lambda, \eta \geq -1$, then ${}_{\mathrm{RL}}D_a^\alpha J_a^\alpha g(y) = g(y)$ and $J_{ac}^\alpha D_a^\alpha g(y) = g(y) - \sum_{k=0}^{\lambda-1} g^{(k)}(a) (y-a)^k/k!, y > a$.

The properties of the operator $J_a{}^\alpha$ are shown as follows:

(i) $J_a^\alpha g(y)$ exists for almost every $y \in [a, b]$.

(ii) $J_a^\alpha J_a^\beta g(y) = J_a^{\alpha+\beta} g(y)$.

(iii) $J_a^\alpha J_a^\beta g(y) = J_a^\beta J_a^\alpha g(y)$.

(iv) $J_a^\alpha (y-a)^\gamma = (\Gamma(\gamma+1)/\Gamma(\alpha+\gamma+1))(y-a)^{\alpha+\gamma}$.

In the equations above, $g \in C_\eta^\lambda$, $\alpha, \beta > 0$, $\eta \geq -1$, and $\gamma \geq -1$.

3. New Iterative Method

The basic mathematical theory of NIM is described as follows.

Let us consider the following nonlinear equation:

$$v(y) = f(y) + \xi(v(y)) + \aleph(v(y)), \tag{6}$$

where $f(y)$, $y = (y_1, y, y_3, \dots, y_n)$, is the known function and ξ and N are the linear and nonlinear functions of $v(y)$, respectively. According to the basic idea of NIM, the solution of the above equation has the series form.

$$v(y) = \sum_{k=0}^{\infty} v_k(y). \tag{7}$$

The linear operator ξ can be decomposed as

$$\sum_{k=0}^{\infty} \xi(v_k) = \xi\left(\sum_{k=0}^{\infty} v_k\right). \tag{8}$$

The decomposition of the nonlinear operator $\aleph$ is as follows:

$$\aleph\left(\sum_{k=0}^{\infty} v_k\right) = \aleph(v_0) + \sum_{k=1}^{\infty} \left\{ \aleph\left(\sum_{i=0}^{k} v_i\right) - \aleph\left(\sum_{i=0}^{k-1} v_i\right) \right\}. \tag{9}$$

Hence, the general equation of (6) takes the following form:

$$\begin{aligned} v(y) = \sum_{k=0}^{\infty} v_k(y) &= f + \xi\left(\sum_{k=0}^{\infty} v_k\right) + \aleph(v_0) \\ &+ \sum_{k=1}^{\infty} \left\{ \aleph\left(\sum_{i=0}^{k} v_i\right) - \aleph\left(\sum_{i=0}^{k-1} v_i\right) \right\}, \end{aligned} \tag{10}$$

From this, we have

$$\begin{aligned} v_0 &= f, \\ v_1 &= \xi(v_0) + \aleph(v_0), \\ v_2 &= \xi(v_1) + \aleph(v_0 + v_1) - \aleph(v_0), \\ v_{m+1} &= \xi(v_m) + \aleph(v_0 + v_1 + \cdots + v_m) \\ &\quad - \aleph(v_0 + v_1 + \cdots + v_{m-1}), \\ &\qquad m = 1, 2, 3 \dots \end{aligned} \tag{11}$$

The k-term series solution of the general equation (6) takes the following form:

$$v = v_0 + v_1 + \cdots + v_{k-1}. \tag{12}$$

4. Applications

Example 1 (damped Burger equation).
Consider the damped Burger equation

$$D_t^{\alpha}u(x,t)+u(x,t)D_xu(x,t)-D_x^2u(x,t)+\lambda u(x,t)=0,\quad t>0,\ 0<\alpha\le 1, \tag{13}$$

together with IC

$$u(x,0)=\lambda x, \tag{14}$$

where λ is a constant. The exact solution of (13) is of the following form:

$$u(x,t)=\frac{\lambda x}{2e^{\lambda t}-1}. \tag{15}$$

Using the operator J^{α} on both sides of (13) using the initial condition and Definition 4 yields

$$u(x,t)=\lambda x+J^{\alpha}\left(-u(x,t)D_xu(x,t)+D_x^2u(x,t)-\lambda u(x,t)\right), \tag{16}$$

where $\xi(u)=J^{\alpha}(D_x^2u(x,t)-\lambda u(x,t))$ and $\aleph(u)=J^{\alpha}(-u(x,t)D_xu(x,t))$.
According to (11), we have

$$\begin{aligned}u_0(x,t)&=\lambda x,\\ u_1(x,t)&=-\frac{2\lambda^2t^{\alpha}x}{\Gamma(\alpha+1)},\\ u_2(x,t)&=\frac{2\lambda^3t^{2\alpha}x\left(3-\left(2\lambda t^{\alpha}(\Gamma(2\alpha+1))^2/(\Gamma(\alpha+1))^2\Gamma(3\alpha+1)\right)\right)}{\Gamma(2\alpha+1)}.\end{aligned} \tag{17}$$

The three-term approximate solution of the above equation is

$$u(x,t)=\lambda x-\frac{2\lambda^2t^{\alpha}x}{\Gamma(\alpha+1)}+\frac{2\lambda^3t^{2\alpha}x\left(3-\left(2\lambda t^{\alpha}(\Gamma(2\alpha+1))^2/(\Gamma(\alpha+1))^2\Gamma(3\alpha+1)\right)\right)}{\Gamma(2\alpha+1)}. \tag{18}$$

Example 2 (Sharma-Tasso-Olver equation).
One can consider

$$D_t^{\alpha}u(x,t)+aD_xu^3(x,t)+\frac{3}{2}aD_x^2u^2(x,t)+aD_x^3u(x,t)=0,\quad t>0,\ 0<\alpha\le 1, \tag{19}$$

together with IC

$$u(x,0)=\sqrt{\frac{1}{a}}\tanh\left(\sqrt{\frac{1}{a}}x\right), \tag{20}$$

where a is a constant. The exact solution of (19) for $\alpha=1$ is of the following form:

$$u(x,t)=\sqrt{\frac{1}{a}}\tanh\left(\sqrt{\frac{1}{a}}(x-t)\right). \tag{21}$$

Using the operator J^{α} on both sides of (19) using the initial condition and Definition 4 yields

$$u(x,t)=\sqrt{\frac{1}{a}}\tanh\left(\sqrt{\frac{1}{a}}x\right)+J^{\alpha}\left(-aD_xu^3(x,t)-\frac{3}{2}aD_x{}^2u^2(x,t)-aD_x^3u(x,t)\right), \tag{22}$$

where $\xi(u)=J^{\alpha}(-aD_x^3u(x,t))$ and $\aleph(u)=J^{\alpha}(-aD_xu^3(x,t)-3/2aD_x^2u^2(x,t))$.
According to (11), we have

$$\begin{aligned}u_0(x,t)&=\sqrt{\frac{1}{a}}\tanh\left(\sqrt{\frac{1}{a}}x\right),\\ u_1(x,t)&=-\frac{t^{\alpha}\sec h^2\left(x/\sqrt{a}\right)}{a\Gamma(1+\alpha)},\\ u_2(x,t)&=\frac{t^{2\alpha}\sec h^2\left(x/\sqrt{a}\right)}{a^{5/2}}\left\{\begin{array}{l}-\dfrac{3\sqrt{a}t^{\alpha}\left(-3+2\cosh\left(2x/\sqrt{a}\right)\right)\Gamma(1+2\alpha)\sec h^4\left(x/\sqrt{a}\right)}{(\Gamma(1+\alpha))^2\Gamma(1+3\alpha)}\\ -\dfrac{2a\tanh\left(x/\sqrt{a}\right)}{\Gamma(1+2\alpha)}-\dfrac{6t^{2\alpha}\Gamma(1+3\alpha)\sec h^4\left(x/\sqrt{a}\right)\tanh\left(x/\sqrt{a}\right)}{(\Gamma(1+\alpha))^3\Gamma(1+4\alpha)}\end{array}\right\}.\end{aligned} \tag{23}$$

The three-term approximate solution of the above equation is as follows:

$$u(x,t) = \sqrt{\frac{1}{a}}\tanh\left(\sqrt{\frac{1}{a}}x\right) - \frac{t^{\alpha}\sec h^{2}\left(x/\sqrt{a}\right)}{a\Gamma(1+\alpha)} + \frac{t^{2\alpha}\sec h^{2}\left(x/\sqrt{a}\right)}{a^{5/2}} \cdot \left\{ \begin{array}{l} -\dfrac{3\sqrt{a}t^{\alpha}\left(-3+2\cosh\left(2x/\sqrt{a}\right)\right)\Gamma(1+2\alpha)\sec h^{4}\left(x/\sqrt{a}\right)}{\left(\Gamma(1+\alpha)\right)^{2}\Gamma(1+3\alpha)} \\ -\dfrac{2a\tanh\left(x/\sqrt{a}\right)}{\Gamma(1+2\alpha)} - \dfrac{6t^{2\alpha}\Gamma(1+3\alpha)\sec h^{4}\left(x/\sqrt{a}\right)\tanh\left(x/\sqrt{a}\right)}{\left(\Gamma(1+\alpha)\right)^{3}\Gamma(1+4\alpha)} \end{array} \right\}. \tag{24}$$

Table 1: Comparison of numerical results of NIM and FRDTM at $\alpha = 1$ and $\lambda = 1$.

x	t	5th-order FRDTM [18]	2nd-order NIM	Exact solution	Absolute error
−5	0.002	−4.980060	−4.98006	−4.98006	1.19501×10^{-7}
	0.004	−4.960239	−4.96024	−4.96024	9.52046×10^{-7}
	0.006	−4.940535	−4.94054	−4.94054	3.19985×10^{-7}
	0.008	−4.920949	−4.92096	−4.92095	7.55346×10^{-6}
−3	0.002	−2.988036	−2.98804	−2.98804	7.17009×10^{-8}
	0.004	−2.976143	−2.97614	−2.97614	5.71228×10^{-7}
	0.006	−2.964321	−2.96432	−2.96432	1.91991×10^{-6}
	0.008	−2.952569	−2.95257	−2.95257	4.53208×10^{-6}
3	0.002	2.988036	2.98804	2.98804	7.17009×10^{-8}
	0.004	2.976143	2.97614	2.97614	5.71228×10^{-7}
	0.006	2.964321	2.96432	2.96432	1.91991×10^{-6}
	0.008	2.952569	2.95257	2.95257	4.53208×10^{-6}
5	0.002	4.980060	4.98006	4.98006	1.19501×10^{-7}
	0.004	4.960239	4.96024	4.96024	9.52046×10^{-7}
	0.006	4.940535	4.94054	4.94054	3.19985×10^{-6}
	0.008	4.920949	4.92096	4.92095	7.55346×10^{-6}

Table 2: Comparison of numerical results of the 2nd-order NIM and the 5th-order FRDTM for different values of α.

x	t	FRDTM [18] ($\alpha = 0.5$)	FRDTM [18] ($\alpha = 0.75$)	NIM ($\alpha = 0.5$)	NIM ($\alpha = 0.75$)
−5	0.002	−4.211841	−4.876244	−4.55366	−4.89911
	0.004	−3.938004	−4.794473	−4.4015	−4.8326
	0.006	−3.744961	−4.724456	−4.29706	−4.7758
	0.008	−3.592556	−4.661485	−4.21704	−4.72486
−3	0.002	−2.527105	−2.925746	−2.7322	−2.93946
	0.004	−2.362803	−2.876684	−2.6409	−2.89956
	0.006	−2.246977	−2.834674	−2.57824	−2.86548
	0.008	−2.155534	−2.796891	−2.53022	−2.83492
3	0.002	2.527105	2.925746	2.7322	2.93946
	0.004	2.362803	2.876684	2.6409	2.89956
	0.006	2.246977	2.834674	2.57824	2.86548
	0.008	2.155534	2.796891	2.53022	2.83492
5	0.002	4.211841	4.876244	4.55366	4.89911
	0.004	3.938004	4.794473	4.4015	4.8326
	0.006	3.744961	4.724456	4.29706	4.7758
	0.008	3.592556	4.661485	4.21704	4.72486

5. Results and Discussion

We have implemented NIM for finding the approximate solutions of the fractional damped Burger equation and fractional Sharma-Tasso-Olver equation. Tables 1 and 2 show the numerical results of the 2nd-order NIM which are compared with those of the 5th-order fractional reduced differential transform method (FRDTM) solution [18] for the fractional-order damped Burger equation. Tables 3 and 4 show the comparison of the proposed scheme with the FRDTM for the fractional-order Sharma-Tasso-Olver equation. Figure 1 shows the comparison of 2D plot of the approximate and exact solution by NIM for the classical damped Burger equation. Figure 2 shows the comparison of the approximate solution for different values of α with the exact solution at $t = 0.01$. In Figures 3 and 4, 3D plots of approximate and exact solutions by NIM for the damped Burger equation are given. In Figure 5, the 2D plots of the approximate and exact solution for the classical Sharma-Tasso-Olver equation are given. Figure 6 shows the comparison of the approximate solution for different values of α with the exact solution at $t = 0.1$. The 3D plots of approximate and exact solutions for the Sharma-Tasso-Olver equation are given in Figures 7 and 8. Throughout computations, we take $\lambda = 1$ and $a = 4$.

By forming the numerical values and graphs, it is clear that NIM is a very powerful tool for the solution of fractional partial differential equations. The accuracy of the NIM can further be increased by taking higher-order approximations.

Table 3: Comparison of numerical results of NIM and FRDTM at $\alpha = 1$ and $a = 4$.

x	t	5th-order FRDTM [18]	2nd-order NIM	Exact solution	Absolute error
−5	0.002	−0.493320	−0.49332	−0.49332	7.13918×10^{-12}
	0.004	−0.493334	−0.493334	−0.493334	5.70817×10^{-11}
	0.006	−0.493347	−0.493347	−0.493347	1.92542×10^{-10}
	0.008	−0.493360	−0.49336	−0.49336	4.56141×10^{-10}
−3	0.002	−0.452664	−0.452664	−0.452664	6.65773×10^{-12}
	0.004	−0.452755	−0.452755	−0.452755	5.333×10^{-11}
	0.006	−0.452844	−0.452844	−0.452844	1.80218×10^{-10}
	0.008	−0.452934	−0.452934	−0.452934	4.27726×10^{-10}
3	0.002	0.452484	0.452484	0.452484	6.64085×10^{-12}
	0.004	0.452393	0.452393	0.452393	5.30587×10^{-11}
	0.006	0.452302	0.452302	0.452302	1.78845×10^{-10}
	0.008	0.452211	0.452211	0.452211	4.23386×10^{-10}
5	0.002	0.493294	0.493294	0.493294	7.14723×10^{-12}
	0.004	0.493281	0.493281	0.493281	5.721×10^{-11}
	0.006	0.493267	0.493267	0.493267	1.93192×10^{-10}
	0.008	0.493254	0.493254	0.493254	4.58194×10^{-10}

Table 4: Comparison of numerical results of the 2nd-order NIM and the 5th-order FRDTM for different values of α.

x	t	FRDTM [18] ($\alpha = 0.5$)	FRDTM [18] ($\alpha = 0.75$)	NIM ($\alpha = 0.5$)	NIM ($\alpha = 0.75$)
−5	0.002	−0.493876	−0.49339	−0.49363	−0.493375
	0.004	−0.494098	−0.493447	−0.493755	−0.493421
	0.006	−0.494262	−0.493496	−0.493849	−0.493461
	0.008	−0.494397	−0.49354	−0.493926	−0.493497
−3	0.002	−0.456455	−0.453141	−0.454774	−0.453036
	0.004	−0.457972	−0.453523	−0.455639	−0.453348
	0.006	−0.459102	−0.453856	−0.456286	−0.45362
	0.008	−0.460032	−0.45416	−0.456819	−0.453867
3	0.002	0.448366	0.452001	0.450211	0.452106
	0.004	0.446521	0.451607	0.449182	0.451784
	0.006	0.445064	0.451259	0.448372	0.4515
	0.008	0.443806	0.450937	0.447674	0.451237
5	0.002	0.492686	0.493223	0.492959	0.493238
	0.004	0.492412	0.493165	0.492806	0.493191
	0.006	0.492194	0.493113	0.492687	0.493149
	0.008	0.492007	0.493066	0.492583	0.49311

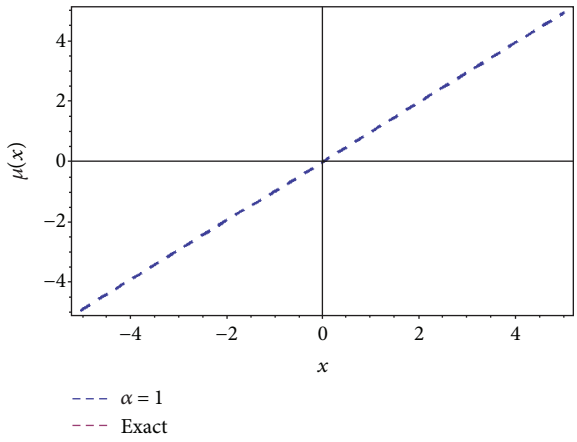

Figure 1: Numerical solution of the classical damped Burger equation with the exact solution at $t = 0.01$.

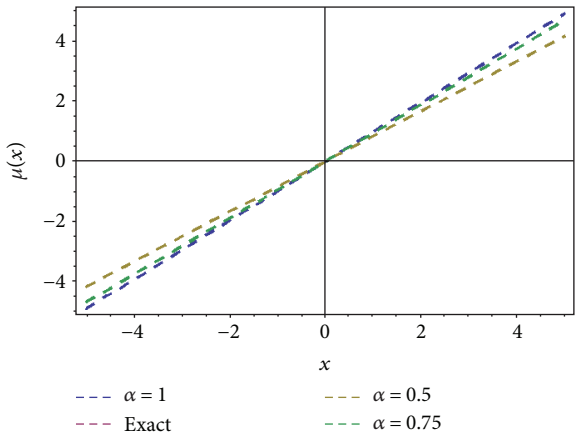

Figure 2: Numerical solution of the fractional damped Burger equation with the exact solution for different values of α at $t = 0.01$.

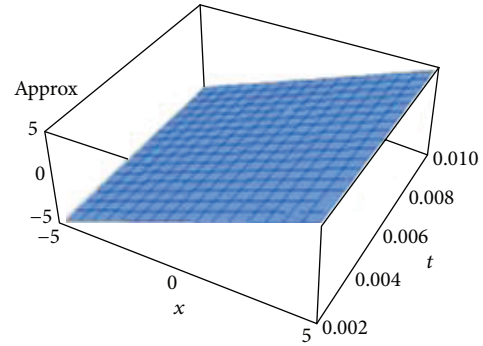

Figure 3: 3D plot of $u(x, t)$ for (DB) equation at $\alpha = 1$.

6. Conclusion

We have successfully applied NIM to time fractional (DB) and (STO) equations. Results reveal that NIM converges to the desired solution in lesser iteration compared to FRDTM. We can conclude that NIM computationally handles many physical and engineering problems in a simple and straightforward way. The accuracy of this method is also better than that of many methods which are computationally difficult to use.

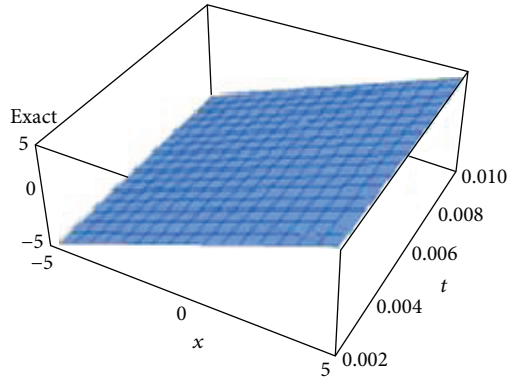

Figure 4: 3D plot of the exact solution for the DB equation.

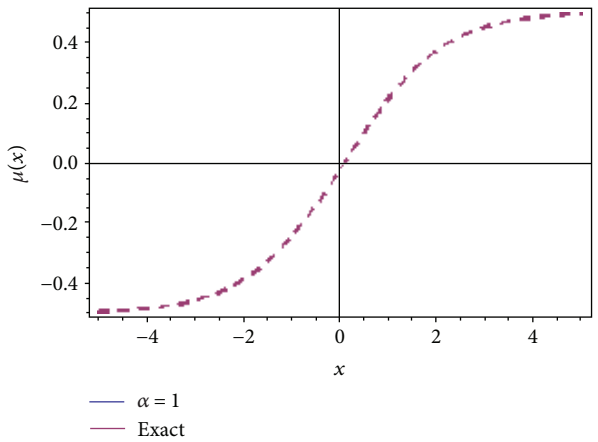

Figure 5: Numerical solution of the classical Sharma-Tasso-Olver equation with the exact solution at $t = 0.1$.

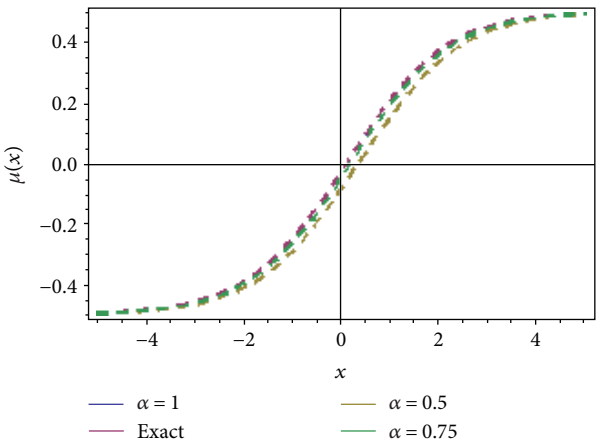

Figure 6: Numerical solution of the fractional Sharma-Tasso-Olver equation with the exact solution for different values of α at $t = 0.1$.

Data Availability

All the data and the metadata regarding the finding of the manuscript have been given in the research manuscript.

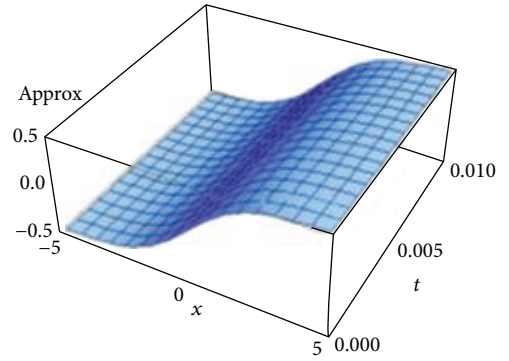

Figure 7: 3D plot of $u(x, t)$ for the STO equation at $\alpha = 1$.

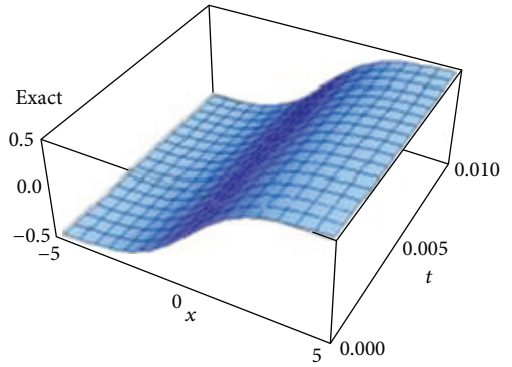

Figure 8: 3D plot of the exact solution of the STO equation.

Conflicts of Interest

The authors declare that they have no conflicts of interest.

Acknowledgments

Sarhad University of Science and Information Technology, Peshawar, Pakistan, will pay the publication charges of the manuscript.

References

[1] I. Podlubny, *Fractional Differential Equations, Mathematics in Science and Engineering*, Academic Press, San Diego, California, USA, 1999.

[2] X.-J. Yang, J. A. Tenreiro Machado, and H. M. Srivastava, "A new numerical technique for solving the local fractional diffusion equation: two-dimensional extended differential transform approach," *Applied Mathematics and Computation*, vol. 274, pp. 143–151, 2016.

[3] R. S. Sengar, M. Sharma, and A. Trivedi, "Fractional calculus applied in solving instability phenomenon in fluid dynamics," *Journal Impact Factor*, vol. 6, no. 5, pp. 34–44, 2015.

[4] X. J. Yang, F. Gao, and H. M. Srivastava, "New rheological models within local fractional derivatives," *Romanian Reports in Physics*, vol. 69, no. 113, 2017.

[5] Y. Yu, P. Perdikaris, and G. E. Karniadakis, "Fractional modeling of viscoelasticity in 3D cerebral arteries and aneurysms," *Journal of Computational Physics*, vol. 323, pp. 219–242, 2016.

[6] V. Gill, K. Modi, and Y. Singh, "Analytic solutions of fractional differential equation associated with RLC electrical circuit," *Journal of Statistics and Management Systems*, vol. 21, no. 4, pp. 575–582, 2018.

[7] S. Das, "Analytical solution of a fractional diffusion equation by variational iteration method," *Computers & Mathematics with Applications*, vol. 57, no. 3, pp. 483–487, 2009.

[8] A. Elsaid, "The variational iteration method for solving Riesz fractional partial differential equations," *Computers & Mathematics with Applications*, vol. 60, no. 7, pp. 1940–1947, 2010.

[9] M. Ahmad, A. A. Bhat, and R. Jain, "Space time fractional telegraph equation and its application by using Adomian decomposition method," *Journal of New Theory*, vol. 22, pp. 73–81, 2018.

[10] F. Mabood, W. A. Khan, and A. I. M. Ismail, "MHD flow over exponential radiating stretching sheet using homotopy analysis method," *Journal of King Saud University - Engineering Sciences*, vol. 29, no. 1, pp. 68–74, 2017.

[11] S. Salahshour, T. Allahviranloo, and S. Abbasbandy, "Solving fuzzy fractional differential equations by fuzzy Laplace transforms," *Communications in Nonlinear Science and Numerical Simulation*, vol. 17, no. 3, pp. 1372–1381, 2012.

[12] S. Momani, O. Abu Arqub, M.'m. Abu Hammad, and Z. S. Abo-Hammour, "A residual power series technique for solving systems of initial value problems," *Applied Mathematics & Information Sciences*, vol. 10, no. 2, pp. 765–775, 2016.

[13] S. Sarwar and M. M. Rashidi, "Approximate solution of two-term fractional-order diffusion, wave-diffusion and telegraph models arising in mathematical physics using optimal homotopy asymptotic method," *Waves in Random and Complex Media*, vol. 26, no. 3, pp. 365–382, 2016.

[14] V. Daftardar-Gejji and H. Jafari, "An iterative method for solving nonlinear functional equations," *Journal of Mathematical Analysis and Applications*, vol. 316, no. 2, pp. 753–763, 2006.

[15] A. M. S. Mahdy and N. A. H. Mukhtar, "New iterative method for solving nonlinear partial differential equations," *Journal of Progressive Research in Mathematics*, vol. 11, no. 3, pp. 1701–1711, 2017.

[16] M. S. Al-Luhaibi, "New iterative method for fractional gas dynamics and coupled Burger's equations," *The Scientific World Journal*, vol. 2015, Article ID 153124, 8 pages, 2015.

[17] B. R. Sontakke and A. Shaikh, "Approximate solutions of time fractional Kawahara and modified Kawahara equations by fractional complex transform," *Communications in Numerical Analysis*, vol. 2016, no. 2, pp. 218–229, 2016.

[18] M. S. Rawashdeh, "An efficient approach for time-fractional damped Burger & time-Sharma-Tasso-Olver equation using the FRDTM," *Applied Mathematics & Information Sciences*, vol. 9, no. 3, pp. 1239–1246, 2015.

Hindawi
Complexity
Volume 2018, Article ID 4192824, 7 pages
https://doi.org/10.1155/2018/4192824

Research Article

A Fractional-Order System with Coexisting Chaotic Attractors and Control Chaos via a Single State Variable Linear Controller

Ping Zhou,[1,2] **Meihua Ke**,[2] **and Peng Zhu**[2]

[1]*Center of System Theory and Its Applications, Chongqing University of Posts and Telecommunications, Chongqing 400065, China*
[2]*Key Laboratory of Network Control and Intelligent Instrument of Ministry of Education, Chongqing University of Posts and Telecommunications, Chongqing 400065, China*

Correspondence should be addressed to Ping Zhou; zhouping@cqupt.edu.cn

Received 23 March 2018; Accepted 16 April 2018; Published 25 June 2018

Academic Editor: Viet-Thanh Pham

A 3D fractional-order nonlinear system with coexisting chaotic attractors is proposed in this paper. The necessary condition of the existence chaos is $q \geq 0.8477$. The fractional-order system exhibits chaotic attractors with the order as low as 2.5431. The largest Lyapunov exponent varying as fractional order q is given. Furthermore, there are the coexisting "positive attractor" and "negative attractor" in this fractional-order chaotic system, and the necessary condition for "positive attractor" and "negative attractor" is obtained. Meanwhile, a control scheme for the stabilization of the unstable equilibrium is suggested via a single state variable linear controller. Numerical results show that the control scheme is valid.

1. Introduction

Chaotic behaviors in nonlinear is a very interesting phenomenon. The high irregularity, unpredictability, and complexity in chaotic systems [1, 2] have been widely used in the field of engineering and technology such as secure communications, image steganography, authenticated encryption, motor control, and power system protection. Recently, coexisting chaotic attractors have been found in chaotic systems [3–9]. For example, the coexisting chaotic attractors in a 3D no-equilibrium system were reported by Pham et al. [3], the coexisting multiple attractors in Hopfield neural network were found by Bao et al. [4], the coexisting chaotic attractors in a hyperchaotic hyperjerk system were given by Wang et al. [5], the coexisting "positive attractor" and "negative attractor" in a 3D autonomous continuous chaotic system were found by Zhou and Ke [6], and so on [7–9]. Therefore, more and more attention has been focused on the coexisting chaotic attractors in nonlinear chaotic systems.

On the other hand, the fractional-order differential equations [10–12] can be accurately described in the real-world physical systems such as viscoelasticity, dielectric polarization, electrode-electrolyte polarization, electromagnetic waves, heat conduction, diffusion-wave, and superdiffusion. Chaotic behaviors have been found in many real-world physical fractional-order nonlinear systems, for example, the fractional-order chaotic brushless DC motor [13], the fractional-order electronic circuits [14], the fractional-order microelectromechanical system [15], and the fractional-order gyroscopes [16]. Therefore, more and more attention has been paid to the chaotic behaviors in fractional-order nonlinear systems.

Motivated by the above discussions, based on a 3D autonomous continuous chaotic system reported by Zhou and Ke [6], we suggested a 3D autonomous continuous fractional-order system. We have shown that the chaotic system reported by Zhou and Ke [6] can be extended to its fractional-order version where the coexisting "positive attractor" and "negative attractor" can be observed. We obtained that the fractional-order system with the order as low as 2.5431 exhibits chaotic attractors. Moreover, we obtained the largest Lyapunov exponent varying as fractional order. Finally, for the stabilization of the unstable equilibrium, one control scheme is proposed via a single state variable linear controller.

The outline of this paper is organized as follows. In Section 2, based on a 3D autonomous continuous chaotic system reported by Zhou and Ke [6], the fractional-order version nonlinear system is given, and some basic dynamical properties of this fractional-order version nonlinear system are obtained including the necessary condition of the existence chaos, the largest Lyapunov exponent varying as fractional order, and the coexisting "positive attractor" and "negative attractor." In Section 3, by a single state variable, stabilization of the unstable equilibrium points of the fractional-order chaotic system is discussed. Finally, the conclusions are given in Section 4.

2. System Model and Basic Characteristics

In this paper, the Caputo definition of the fractional derivative will be used in next. The Caputo definition of the fractional derivative is described as

$$ {}_0^cD_t^q g(t) = \frac{1}{\Gamma(k-q)} \int_0^t \frac{g^{(k)}(\tau)}{(t-\tau)^{q+1-k}} d\tau, \quad k-1 < q < k, \tag{1} $$

where ${}_0^cD_t^q$ is the Caputo operator, k is the first integer which is not less than q, and $g^{(k)}(t)$ is the k-order derivative in usual sense of $g(t)$.

Next, based on the 3D autonomous continuous chaotic system reported by Zhou and Ke [6], a fractional-order system is addressed as

$$ \begin{aligned} {}_0^cD_t^q x_1 &= -x_1 + 0.5x_1x_3 + x_2x_3, \\ {}_0^cD_t^q x_2 &= 4x_2 - 1.2x_1x_3, \\ {}_0^cD_t^q x_3 &= x_1x_2 - 6x_3, \end{aligned} \tag{2} $$

where fractional order $0 < q < 1$. Fractional-order system (2) has five equilibrium points. They are $S_0 = (0,0,0)$, $S_1^+ = (4.4721, -1.5745, 1.1736)$, $S_1^- = (-4.4721, 1.5745, 1.1736)$, $S_2^+ = (4.4721, 3.8106, -2.8403)$, and $S_2^- = (-4.4721, -3.8106, -2.8403)$, respectively.

Now, we can obtain the eigenvalues of the five equilibrium points. The eigenvalues of equilibrium point S_0 are $(-6, -1, 4)$. Thus, equilibrium point S_0 is an unstable saddle point of index one. The eigenvalues of equilibrium points S_1^+ and S_1^- are $(-5.3957,\ 1.4912 + 3.2168j,\ 1.4912 - 3.2168j)$. Thus, equilibrium points S_1^+ and S_1^- are unstable saddle points of index two. The eigenvalues of equilibrium points S_2^+ and S_2^- are $(-6.7558,\ 1.1678 + 4.7892j,\ 1.1678 - 4.7892j)$. Thus, equilibrium points S_2^+ and S_2^- are unstable saddle points of index two.

Tavazoei and Haeri [17] have obtained that a necessary condition for a fractional-order nonlinear system to exist chaotic is

$$ q \geq \frac{2}{\pi} \left| \arctan \frac{\mathrm{Im}(\lambda)}{\mathrm{Re}(\lambda)} \right|, \tag{3} $$

where λ is the eigenvalues of saddle equilibrium point of index two in fractional-order nonlinear system.

Now, we can obtain the necessary condition of the existence chaos in fractional-order system (2). According to (3), we have the following:

$$ \begin{aligned} q &\geq \frac{2}{\pi} \left| \arctan \frac{\mathrm{Im}(\lambda)}{\mathrm{Re}(\lambda)} \right| \\ &= 0.7237 \text{ for equilibrium points } S_1^+ \text{ and } S_1^-; \\ q &\geq \frac{2}{\pi} \left| \arctan \frac{\mathrm{Im}(\lambda)}{\mathrm{Re}(\lambda)} \right| \\ &= 0.8477 \text{ for equilibrium points } S_2^+ \text{ and } S_2^-. \end{aligned} \tag{4} $$

Thus, the necessary condition of existence chaos in fractional-order system (2) is $q \geq 0.8477$. This result indicates that fractional-order system (2) with the order as low as 2.5431 can exhibit chaotic attractors.

In this paper, the improved version of Adams-Bashforth-Moulton [18] (denoted by IVABM) numerical algorithm is used to deal with fractional-order system (2). The IVABM numerical algorithm will be introduced next. Now, consider the fractional-order system

$$ \begin{aligned} {}_0^cD_t^{q_1} x_1 &= g_1(x_1, x_2, x_3), \\ {}_0^cD_t^{q_2} x_2 &= g_2(x_1, x_2, x_3), \\ {}_0^cD_t^{q_3} x_3 &= g_3(x_1, x_2, x_3) \end{aligned} \tag{5} $$

with initial condition $(x_1(0), x_2(0), x_3(0))$. Let $l = T/N$, and $t_n = nl$ $(n = 0, 1, 2, \ldots, N)$. By IVABM numerical algorithm, system (5) can be discretized as follows:

$$ \begin{aligned} x_1(n+1) &= x_1(0) \\ &\quad + \frac{h^{q_1}}{\Gamma(q_1+2)} \left[g_1\left(x_1^p(n+1), x_2^p(n+1), x_3^p(n+1)\right) \right. \\ &\quad \left. + \sum_{j=0}^{n} \alpha_{1,j,n+1} g_1(x_1(j), x_2(j), x_3(j)) \right], \\ x_2(n+1) &= x_2(0) \\ &\quad + \frac{h^{q_2}}{\Gamma(q_2+2)} \left[g_2\left(x_1^p(n+1), x_2^p(n+1), x_3^p(n+1)\right) \right. \\ &\quad \left. + \sum_{j=0}^{n} \alpha_{2,j,n+1} g_2(x_1(j), x_2(j), x_3(j)) \right], \\ x_3(n+1) &= x_3(0) \\ &\quad + \frac{h^{q_3}}{\Gamma(q_3+2)} \left[g_3\left(x_1^p(n+1), x_2^p(n+1), x_3^p(n+1)\right) \right. \\ &\quad \left. + \sum_{j=0}^{n} \alpha_{3,j,n+1} g_3(x_1(j), x_2(j), x_3(j)) \right], \end{aligned} \tag{6} $$

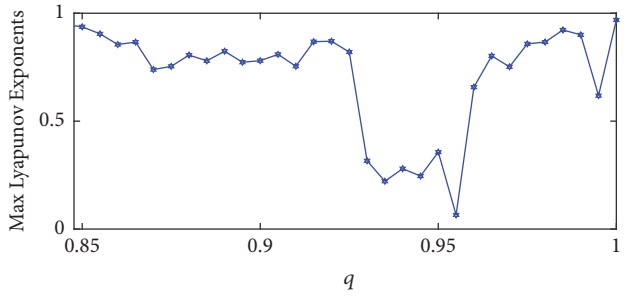

Figure 1: The largest Lyapunov exponent varying as fractional order q.

where

$$
\begin{aligned}
&x_1^p(n+1) \\
&= x_1(0) + \frac{1}{\Gamma(q_1)} \sum_{j=0}^{n} \beta_{1,j,n+1} g_1(x_1(j), x_2(j), x_3(j)), \\
&x_2^p(n+1) \\
&= x_2(0) + \frac{1}{\Gamma(q_2)} \sum_{j=0}^{n} \beta_{2,j,n+1} g_2(x_1(j), x_2(j), x_3(j)), \\
&x_3^p(n+1) \\
&= x_3(0) + \frac{1}{\Gamma(q_3)} \sum_{j=0}^{n} \beta_{3,j,n+1} g_3(x_1(j), x_2(j), x_3(j)),
\end{aligned} \tag{7}
$$

$$
\begin{aligned}
&\alpha_{i,j,n+1} \\
&= \begin{cases} n^{q_i+1} - (n-q_i)(n+1)^{q_i}, & j = 0 \\ (n-j+2)^{q_i+1} + (n-j)^{q_i+1} - 2(n-j+1)^{q_i+1}, & 1 \le j \le n \\ 1, & j = n+1, \end{cases} \\
&\qquad (i = 1, 2, 3),
\end{aligned}
$$

$$
\begin{aligned}
&\beta_{i,j,n+1} = \frac{h^{q_i}}{q_i} \left[(n-j+1)^{q_i} - (n-j)^{q_i} \right], \\
&\qquad 0 \le j \le n, \ (i = 1, 2, 3).
\end{aligned}
$$

The error of this IVABM numerical algorithm is

$$
\begin{aligned}
&\left| x_i(t_n) - x_i(n) \right| = o\left(h^{p_i}\right), \\
&\qquad p_i = \min\left(2, 1 + q_i\right), \ (i = 1, 2, 3).
\end{aligned} \tag{8}
$$

We can yield the largest Lyapunov exponent varying as q via IVABM numerical algorithm, which is shown in Figure 1, where $0.8477 \le q \le 1$ and the initial condition is $(-5, 2, 5)$.

According to Figure 1, we can obtain that the largest Lyapunov exponent is larger zero for $0.8477 \le q \le 1$. This result indicates that the chaotic attractor is emerged in fractional-order system (2) for $0.8477 \le q \le 1$. For example, let $q = 0.8477$, the largest Lyapunov exponent is 0.9853, and the chaotic attractor in fractional-order system (2) with initial condition $(-5, 2, 5)$ is shown as Figure 2.

Same as the results reported by Zhou and Ke [6], there are coexisting "positive attractor" and "negative attractor" in fractional-order system (2). The chaotic attractor in fractional-order system (2) can be decided by the initial conditions; that is, the chaotic attractor depends on the distance from the initial point (initial condition $x_0 = (x_1(0), x_2(0), x_3(0))$ to the unstable points [6]. Next, the distances from the initial point to points S_1^+, S_1^-, S_2^+, and S_2^- are denoted by L_1^+, L_1^-, L_2^+, and L_2^-, respectively. Same as [6], the following results can be obtained:

(1) If the initial point (initial condition) is near the unstable S_1^+ or S_2^+, there is the same chaotic attractor in fractional-order chaotic system (2), which is called "positive attractor" by Zhou and Ke [6], where the "positive attractor" means $x_1(t) > 0$ and a necessary condition for "positive attractor" is $x_1(0) > 0$ [6].

(2) If the initial point (initial condition) is near the unstable S_1^- or S_2^-, there is the same chaotic attractor in fractional-order chaotic system (2), which is called "negative attractor" by Zhou and Ke [6], where the "positive attractor" means $x_1(t) < 0$ and a necessary condition for "negative attractor" is $x_1(0) < 0$ [6].

Next, some numerical simulations are given for $q = 0.9$. Here, the largest Lyapunov exponent is 0.763 for $q = 0.9$.

Case 1 (the initial point is near unstable saddle point S_1^+ or S_1^-). For example, choose the initial conditions as $(4, -1, 1)$. Therefore, L_1^+, L_1^-, L_2^+, and L_2^- are 0.7636, 8.8563, 6.1735, and 9.7172, respectively. Therefore, the initial point $(4, -1, 1)$ is near unstable saddle point S_1^+. Therefore, the fractional-order system (2) has the "positive attractor," which is shown as Figure 3.

For example, choose the initial conditions as $(-4, 1, 1)$. Therefore, L_1^+, L_1^-, L_2^+, and L_2^- are 8.8563, 0.7636, 9.7172, and 6.1735, respectively. Therefore, the initial point $(-4, 1, 1)$ is near unstable saddle point S_1^-. Thus, fractional-order system (2) has the "negative attractor," which is shown as Figure 3.

Case 2 (the initial point is near unstable saddle point S_2^+ or S_2^-). For example, choose the initial conditions as $(4, 3, -2)$. Therefore, L_1^+, L_1^-, L_2^+, and L_2^- are 5.5875, 9.1586, 1.2594, and 10.9026, respectively. Therefore, the initial point $(4, 3, -2)$ is close to unstable saddle point S_2^+. Thus, fractional-order system (2) has the "positive attractor," which is shown as Figure 4.

For example, choose the initial conditions as $(-4, -3, -2)$. Therefore, L_1^+, L_1^-, L_2^+, and L_2^- are 9.1586, 5.5875, 10.9026, and 1.2594, respectively. Therefore, the initial point $(-4, -3, -2)$ is close to unstable saddle point S_2^-. Thus, fractional-order system (2) has the "negative attractor," which is shown as Figure 4.

According to Figures 3 and 4, the coexisting chaotic attractors are found in fractional-order chaotic system (2). These results indicate that the chaotic system reported by Zhou and Ke [6] can be extended to its fractional-order version where the coexisting "positive attractor" and "negative attractor" can be observed.

Remark 1. There are overlaps between the coexisting chaotic attractors in [3–5, 7–9]. However, there are two isolated chaotic attractors in fractional-order chaotic system

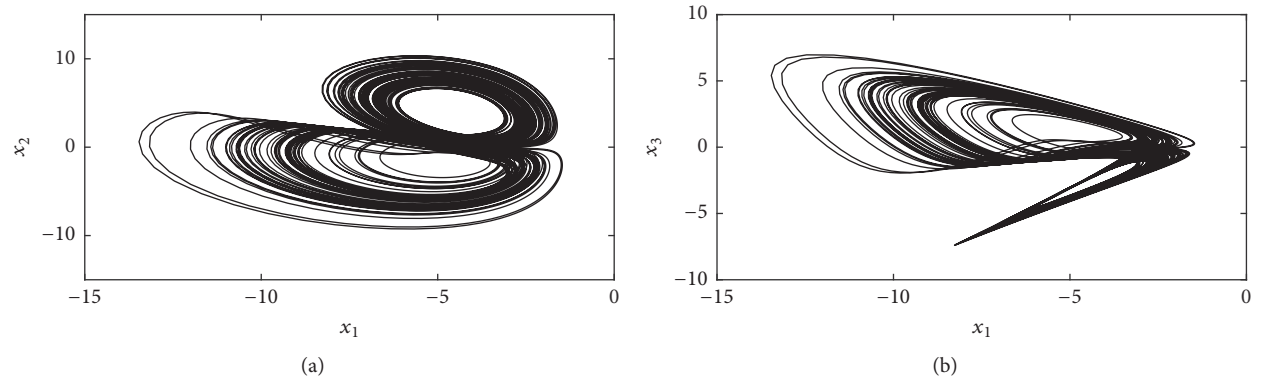

Figure 2: The chaotic attractor in fractional-order system (2).

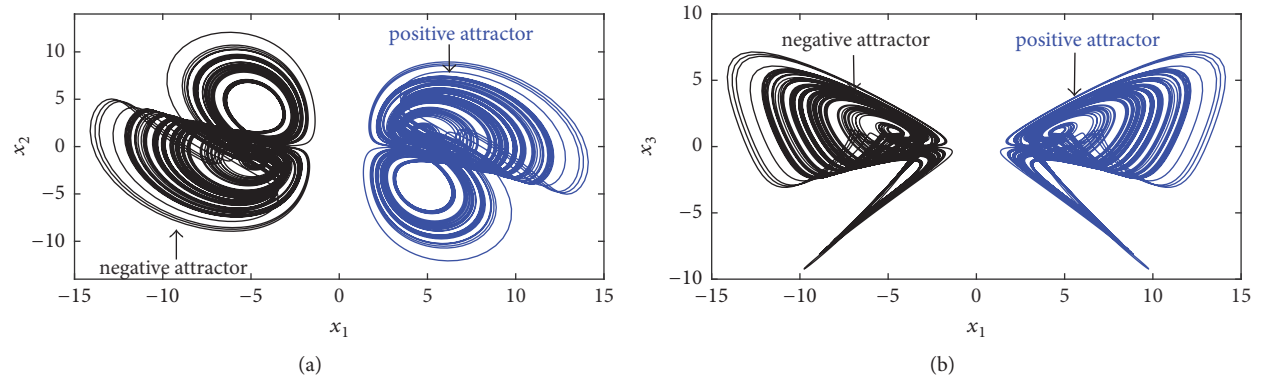

Figure 3: The "positive attractor" and "negative attractor" in fractional-order system (2).

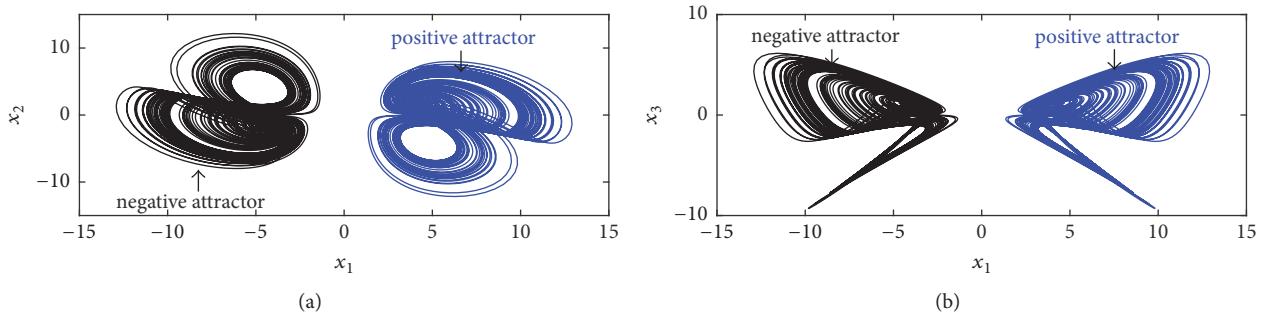

Figure 4: The "positive attractor" and "negative attractor" in fractional-order system (2).

(2); that is, there are no overlaps between the coexisting chaotic attractors in fractional-order chaotic system (2).

3. Stabilization of the Unstable Equilibrium Points of the Fractional-Order Chaotic System (2)

First, a result on stability of fractional-order nonlinear system is recalled. Consider the fractional-order nonlinear system as follows:

$$ {}_0^c D_t^q y(t) = H(y(t)) = My(t) + f(y(t)), \quad (9) $$

where $0 < q \leq 1$, $y(t) = (y_1(t), y_2(t), \ldots, y_n(t))^T \in R^n$ denotes the state vector, $H : R^n \to R^n$ is a nonlinear vector field, $M \in R^{n\times n}$ is a constant matrix, and $f(y(t))$ and $My(t)$ denote the nonlinear and linear parts of $H(y(t))$.

Lemma 2 (for more details, see [19]). *Fractional-order nonlinear system (9) is said to be asymptotically stable if the next two conditions hold:*

(i) $f(y(t))|_{y(t)=0} = 0$, *and* $\lim_{y(t)\to 0}(\|f(y(t))\|/\|y(t)\|) = 0$,

(ii) $|\arg \lambda_i(M)| > 0.5q\pi (i = 1, 2, \ldots, n)$, *and* $q\|M\| > 1$,

where $\lambda_i(M)$ *and* $\|M\|$ *denote the eigenvalues and the* l_2*-norm with respect to matrix* M*, respectively.*

Next, we discuss how to stable the unstable equilibrium point in fractional-order chaotic system (2) via single state variable linear controller. Now, let the unstable equilibrium points in system (2) be $(\overline{x}_1, \overline{x}_2, \overline{x}_3)$, and the controlled fractional-order system is shown as follows:

$$\begin{aligned} {}_0^cD_t^q x_1 &= -x_1 + 0.5x_1x_3 + x_2x_3 + k_1\left(x_2 - \overline{x}_2\right), \\ {}_0^cD_t^q x_2 &= 4x_2 - 1.2x_1x_3 + k_2\left(x_2 - \overline{x}_2\right), \\ {}_0^cD_t^q x_3 &= x_1x_2 - 6x_3 + k_3\left(x_2 - \overline{x}_2\right), \end{aligned} \tag{10}$$

where $0.8477 \le q \le 1$ and $k_i(x_2 - \overline{x}_2)$ $(i = 1, 2, 3)$ is a linear controller determined by a single state variable x_2. k_i $(i = 1, 2, 3) \in R$ are feedback gains determined later.

Theorem 3. *Let real matrix be*

$$A = \begin{pmatrix} -\left(1 - 0.5\overline{x}_3\right) & \left(\overline{x}_3 + k_1\right) & \left(0.5\overline{x}_1 + \overline{x}_2\right) \\ -1.2\overline{x}_3 & \left(4 + k_2\right) & 1.2\overline{x}_1 \\ \overline{x}_2 & \left(\overline{x}_1 + k_3\right) & -6 \end{pmatrix}, \tag{11}$$

and choose suit feedback gains k_i $(i = 1, 2, 3)$; if $|\arg\lambda_i(A)| > 0.5q\pi$ $(i = 1, 2, 3)$, then the unstable equilibrium points $(\overline{x}_1, \overline{x}_2, \overline{x}_3)$ of fractional-order chaotic system (2) in controlled system (10) are asymptotically stable.

Proof. Let $y_1 = x_1 - \overline{x}_1$, $y_2 = x_2 - \overline{x}_2$, and $y_3 = x_3 - \overline{x}_3$; then controlled system (10) can be changed as

$$\begin{aligned} {}_0^cD_t^q y_1 &= -\left(1 - 0.5\overline{x}_3\right) y_1 + \left(\overline{x}_3 + k_1\right) y_2 \\ &\quad + \left(0.5\overline{x}_1 + \overline{x}_2\right) y_3 + 0.5y_1y_3 + y_2y_3, \\ {}_0^cD_t^q y_2 &= -1.2\overline{x}_3 y_1 + \left(4 + k_2\right) y_2 - 1.2\overline{x}_1 y_3 - 1.2y_1y_3, \\ {}_0^cD_t^q y_3 &= \overline{x}_2 y_1 + \left(\overline{x}_1 + k_3\right) y_2 - 6y_3 + y_1y_2. \end{aligned} \tag{12}$$

Thus, the unstable equilibrium points $(\overline{x}_1, \overline{x}_2, \overline{x}_3)$ in fractional-order chaotic system (2) are changed as the point $(y_1, y_2, y_3) = (0, 0, 0)$ in system (12).

One can easily obtain that point $(y_1, y_2, y_3) = (0, 0, 0)$ is the origin of system (12). Therefore, the problem of stabilization of the unstable equilibrium points in fractional-order chaotic system (2) is turned to the problem of stabilization of fractional-order system (12). If the origin of system (12) is asymptotically stable, then the unstable equilibrium points $(\overline{x}_1, \overline{x}_2, \overline{x}_3)$ of fractional-order chaotic system (2) in controlled system (10) are asymptotically stable.

Now, controlled system (12) can be rewritten as

$${}_0^cD_t^q y(t) = Ay(t) + f\left(y(t)\right), \tag{13}$$

where $f(y(t)) = \left((0.5y_1 + y_2)y_3 \;\; -1.2y_1y_3 \;\; y_1y_2\right)^T$.

First, it is easy to obtain that $f(y(t))|_{y(t)=0} = 0$, and

$$\begin{aligned} &\frac{\left\|f\left(y(t)\right)\right\|}{\left\|y(t)\right\|} \\ &= \sqrt{\frac{\left[\left(0.5y_1 + y_2\right)y_3\right]^2 + \left(-1.2y_1y_3\right)^2 + \left(y_1y_2\right)^2}{y_1^2 + y_2^2 + y_3^2}} \\ &\le \sqrt{\left[\left(0.5y_1 + y_2\right)\right]^2 + \left(-1.2y_3\right)^2 + \left(y_2\right)^2}, \\ &\lim_{y(t)\to 0} \frac{\left\|f\left(y(t)\right)\right\|}{\left\|y(t)\right\|} \\ &\le \lim_{y(t)\to 0} \sqrt{\left[\left(0.5y_1 + y_2\right)\right]^2 + \left(-1.2y_3\right)^2 + \left(y_2\right)^2} = 0. \end{aligned} \tag{14}$$

Thus, the first condition in Lemma 2 is satisfied.

Second, according to

$$A = \begin{pmatrix} -\left(1 - 0.5\overline{x}_3\right) & \left(\overline{x}_3 + k_1\right) & \left(0.5\overline{x}_1 + \overline{x}_2\right) \\ -1.2\overline{x}_3 & \left(4 + k_2\right) & 1.2\overline{x}_1 \\ \overline{x}_2 & \left(\overline{x}_1 + k_3\right) & -6 \end{pmatrix}, \tag{15}$$

$q\|A\| > 1$, and using $|\arg\lambda_i(A)| > 0.5q\pi (i = 1, 2, 3)$, we can yield that the second condition in Lemma 2 is satisfied.

Therefore, according to Lemma 2, the origin of system (12) is asymptotically stable. That is, the unstable equilibrium points $(\overline{x}_1, \overline{x}_2, \overline{x}_3)$ of fractional-order chaotic system (2) in controlled system (10) are asymptotically stable. The proof is finished. □

Remark 4. In our control scheme, the linear controller is only determined by one single state variable, so our control scheme is different from many previous control schemes.

4. Numerical Simulations Results

Next, in order to show the effectiveness of the proposed control approach, the numerical simulations are performed for $q = 0.9$.

For the unstable equilibrium point $S_0 = (0, 0, 0)$, if we choose $k_1 = k_3 = 0$, $k_2 = -7$, then $A = \begin{pmatrix} -1 & 0 & 0 \\ 0 & -3 & 0 \\ 0 & 0 & -6 \end{pmatrix}$. Thus, we obtain $\lambda_1 = -1$, $\lambda_2 = -3$, $\lambda_3 = -6$, and $q\|A\| > 1$. According to Theorem 3, the unstable equilibrium point S_0 in controlled system (10) is asymptotically stable. Figure 5 displays the time evolution of state variables. Here, the initial conditions be $(7, 6, 3)$.

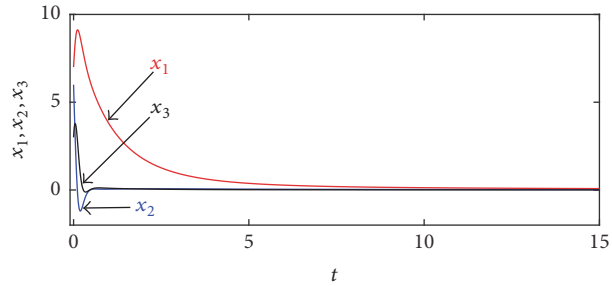

FIGURE 5: The time evolution of state variables x_i $(i = 1, 2, 3)$.

For the unstable equilibrium point $S_1^+ = (4.4721, -1.5745, 1.1736)$, if we choose $k_1 = k_3 = 0$, $k_2 = -8$, then $A = \begin{pmatrix} -0.4132 & 1.1736 & 0.66155 \\ -1.40832 & -4 & 5.36652 \\ -1.5745 & 4.4721 & -6 \end{pmatrix}$. Thus, we obtain $\lambda_1 = -0.5726$, $\lambda_{2,3} = -4.9203 \pm 4.9982j$, and $q\|A\| > 1$. According

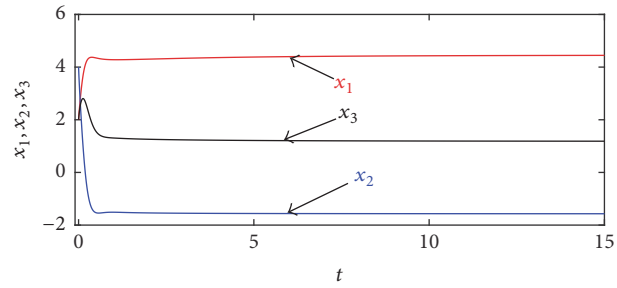

FIGURE 6: The time evolution of state variables x_i $(i = 1, 2, 3)$.

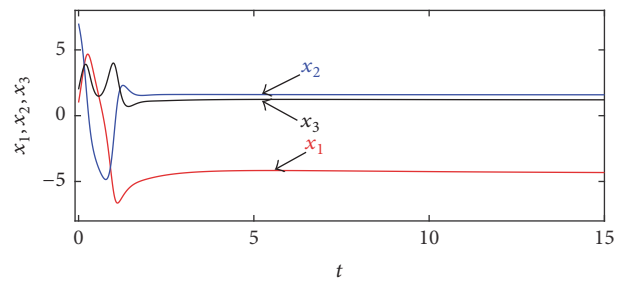

FIGURE 7: The time evolution of state variables x_i $(i = 1, 2, 3)$.

to Theorem 3, the unstable equilibrium point S_1^+ in controlled system (10) is asymptotically stable. Figure 6 shows the time evolution of state variables. Here, the initial conditions are $(2, 4, 2)$.

For the unstable equilibrium point $S_1^- = (-4.4721, 1.5745, 1.1736)$, if we choose $k_1 = k_3 = 0$, $k_2 = -4$, then $A = \begin{pmatrix} -0.4132 & 1.1736 & -0.66155 \\ -1.40832 & 0 & -5.36652 \\ 1.5745 & -4.4721 & -6 \end{pmatrix}$. Therefore, we obtain $\lambda_1 = -0.5418$, $\lambda_{2,3} = -2.9357 \pm 4.1682j$, and $q\|A\| > 1$. According to Theorem 3, the unstable equilibrium point S_1^- in controlled system (10) is asymptotically stable. Figure 7 shows the time evolution of state variables. Here, the initial conditions are $(1, 7, 2)$.

For the unstable equilibrium point $S_2^+ = (4.4721, 3.8106, -2.8403)$, if we choose $k_1 = -2.1597$, $k_2 = -7$, $k_3 = -9.4721$, then $A = \begin{pmatrix} -2.42015 & -5 & 6.04665 \\ 3.40836 & -3 & 5.36652 \\ 3.8106 & -5 & -6 \end{pmatrix}$. Thus, we obtain $\lambda_1 = -10.8877$, $\lambda_{2,3} = -0.2662 \pm 1.040j$, and $q\|A\| > 1$. According to Theorem 3, the unstable equilibrium point S_2^+ in controlled system (10) is asymptotically stable. Figure 8 shows the time evolution of state variables. Here, the initial conditions are $(5, 4, -3)$.

For the unstable equilibrium point $S_2^- = (-4.4721, -3.8106, -2.8403)$, if we choose $k_1 = -7.1597$, $k_2 = -7$, $k_3 = 9.9721$, then $A = \begin{pmatrix} -2.42015 & -10 & -6.04665 \\ 3.40836 & -3 & -5.36652 \\ -3.8106 & 5.5 & -6 \end{pmatrix}$. Thus, we obtain $\lambda_1 = -9.3229$, $\lambda_{2,3} = -1.0486 \pm 0.8095j$, and $q\|A\| > 1$. According to Theorem 3, the unstable equilibrium point S_2^- in controlled system (10) is asymptotically stable. Figure 9 shows the time evolution of state variables. Here, the initial conditions are $(-7, -6, -2)$.

The simulative results in Figures 5–9 show the effectiveness of our control scheme.

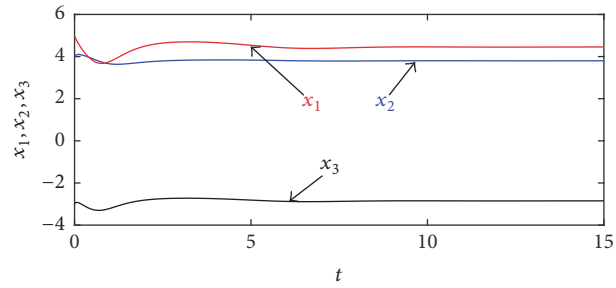

FIGURE 8: The time evolution of state variables x_i $(i = 1, 2, 3)$.

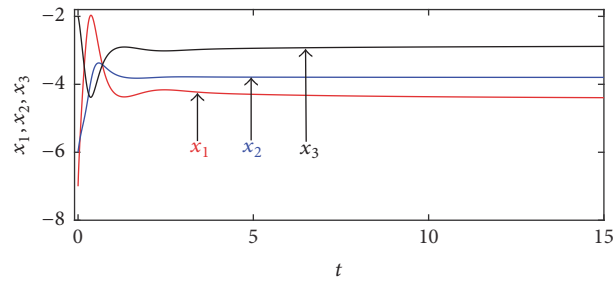

FIGURE 9: The time evolution of state variables x_i $(i = 1, 2, 3)$.

5. Conclusions

In this paper, a fractional-order chaotic system is proposed. The necessary condition of existence chaos in this fractional-order chaotic system is $q \geq 0.8477$. The largest Lyapunov exponent varying as fractional order q is given. The coexisting "positive attractor" and "negative attractor" can be observed, and the necessary conditions for "positive attractor" and "negative attractor" are obtained. Meanwhile, by a single state variable, a linear controller is used for the stabilization of the unstable equilibrium points of the fractional-order chaotic system. The numerical results show that the control approach is effective.

Data Availability

The data used to support the findings of this study are available from the corresponding author upon request.

Conflicts of Interest

The authors declare no conflicts of interest.

References

[1] G. R. Chen and X. Dong, *From Chaos to Order Perspectives, Methodologies and Applications*, World scientific, Singapore, 1998.

[2] J. C. Sprott, *Chaos and Time-Series Analysis*, Oxford University Press, Oxford, UK, 2003.

[3] V.-T. Pham, C. Volos, S. Jafari, and T. Kapitaniak, "Coexistence of hidden chaotic attractors in a novel no-equilibrium system," *Nonlinear Dynamics*, vol. 87, no. 3, pp. 2001–2010, 2017.

[4] B. Bao, H. Qian, J. Wang et al., "Numerical analyses and experimental validations of coexisting multiple attractors in Hopfield neural network," *Nonlinear Dynamics*, vol. 90, no. 4, pp. 2359–2369, 2017.

[5] X. Wang, S. Vaidyanathan, C. Volos, V.-T. Pham, and T. Kapitaniak, "Dynamics, circuit realization, control and synchronization of a hyperchaotic hyperjerk system with coexisting attractors," *Nonlinear Dynamics*, vol. 89, no. 3, pp. 1673–1687, 2017.

[6] P. Zhou and M. Ke, "A new 3d autonomous continuous system with two isolated chaotic attractors and its topological horseshoes," *Complexity*, vol. 2017, Article ID 4037682, 7 pages, 2017.

[7] F. Yuan, G. Y. Wang, and Y. R. Shen, "Coexisting attractors in a memcapacitor-based chaotic oscillator," *Nonlinear Dynamics*, vol. 85, no. 1, pp. 37–50, 2016.

[8] Q. Lai and S. Chen, "Coexisting attractors generated from a new 4D smooth chaotic system," *International Journal of Control, Automation, and Systems*, vol. 14, no. 4, pp. 1124–1131, 2016.

[9] J. Kengne, Z. T. Njitacke, and H. B. Fotsin, "Dynamical analysis of a simple autonomous jerk system with multiple attractors," *Nonlinear Dynamics*, vol. 83, no. 1-2, pp. 751–765, 2016.

[10] R. Hilfer, *Applications of Fractional Calculus in Physics*, World Scientific, Singapore, 2000.

[11] I. Podlubny, *Fractional Differential Equations*, Academic Press, San Diego, Calif, USA, 1999.

[12] P. Zhou and P. Zhu, "A practical synchronization approach for fractional-order chaotic systems," *Nonlinear Dynamics*, vol. 89, no. 3, pp. 1719–1726, 2017.

[13] P. Zhou, R. J. Bai, and J. M. Zheng, "Stabilization of a fractional-order chaotic brushless DC motor via a single input," *Nonlinear Dynamics*, vol. 82, no. 1-2, pp. 519–525, 2015.

[14] T. T. Hartley, C. F. Lorenzo, and H. K. Qammer, "Chaos in a fractional order Chua's system," *IEEE Transactions on Circuits and Systems I: Fundamental Theory and Applications*, vol. 42, no. 8, pp. 485–490, 1995.

[15] M. P. Aghababa, "Chaos in a fractional-order micro-electromechanical resonator and its suppression," *Chinese Physics B*, vol. 21, no. 10, Article ID 100505, 9 pages, 2012.

[16] M. P. Aghababa and H. P. Aghababa, "The rich dynamics of fractional-order gyros applying a fractional controller," *Proceedings of the Institution of Mechanical Engineers, Part I: Journal of Systems and Control Engineering*, vol. 227, no. 7, pp. 588–601, 2013.

[17] M. S. Tavazoei and M. Haeri, "A necessary condition for double scroll attractor existence in fractional-order systems," *Physics Letters A*, vol. 367, no. 1-2, pp. 102–113, 2007.

[18] C. Li and G. Peng, "Chaos in Chen's system with a fractional order," *Chaos, Solitons & Fractals*, vol. 22, no. 2, pp. 443–450, 2004.

[19] L. Chen, Y. Chai, R. Wu, and J. Yang, "Stability and stabilization of a class of nonlinear fractional-order systems with caputo derivative," *IEEE Transactions on Circuits and Systems II: Express Briefs*, vol. 59, no. 9, pp. 602–606, 2012.

Hindawi
Complexity
Volume 2018, Article ID 6570560, 14 pages
https://doi.org/10.1155/2018/6570560

Research Article

Robust Fractional-Order PID Controller Tuning Based on Bode's Optimal Loop Shaping

Lu Liu [1] **and Shuo Zhang** [2]

[1] *School of Marine Science and Technology, Northwestern Polytechnical University, Xi'an 710072, China*
[2] *Department of Applied Mathematics, Northwestern Polytechnical University, Xi'an 710072, China*

Correspondence should be addressed to Shuo Zhang; zhangshuo1018@nwpu.edu.cn

Received 11 February 2018; Accepted 2 April 2018; Published 25 June 2018

Academic Editor: Viet-Thanh Pham

This paper presents a novel fractional-order PID controller tuning strategy based on Bode's optimal loop shaping which is commonly used for LTI feedback systems. Firstly, the controller parameters are achieved based on flat phase property and Bode's optimal reference model, so that the controlled system is robust to gain variations and can achieve desirable transient performance according to various control requirements. Then, robustness analysis of the controlled system is carried out to support the results. Furthermore, the parameter setting is analyzed to demonstrate the superiority of the proposed controller. At last, some simulation examples are shown to verify the accuracy and usefulness of the proposed control strategy. The proposed fractional-order PID controller does not have any restriction on the controlled plant, so it can be widely applied on both integer-order and fractional-order systems.

1. Introduction

Fractional calculus was first mentioned in a letter between Leibniz and L'Hospital about 300 years ago [1]. Not until the last few decades had the related studies been generalized to various fields instead of pure theoretical derivation. A number of studies have revealed the potentialities of fractional calculus, such as engineering [2–4], physics [5], applied mathematics [6, 7], and bioengineering [8]. Among these research fields, fractional-order control technology and fractional-order modeling develop quite fast. Many physical phenomena were proved to be better described by fractional-order models [9, 10]. The additional integral and differential orders in fractional-order control algorithms offer more possibilities in enhancing system robustness, stability, and transient performance.

In the control field, PID control is undoubtedly the most widely used control algorithm in industrial applications [11]. So there are abundant reasons to investigate control algorithm which owns the superiorities of both PID controller and fractional calculus. The earliest attempt was made by Podlubny who proposed the fractional-order PID ($PI^{\lambda}D^{\mu}$ or FOPID) controller [12]. There are two more parameters, that is, integral order λ and differential order μ, in FOPID controller compared with traditional PID controller. These extra parameters can serve as additional tuning knobs which may provide more flexibilities in improving system control performance. Petras presented a digital version FOPID controller which was implemented in a DC motor [13]. Fractance circuits and microprocessors were used to achieve the analogue transformation and implementation of the digital FOPID controller. An optimal FOPID controller was designed based on particle swarm optimization and applied to an automatic voltage regulator by Zamani et al. [14]. A frequency domain tuning scheme of FOPID controller was proposed by Vinagre et al. [15]. Hamamci investigated an FOPID controller which can stabilize fractional-order systems with time delay [16]. The proposed controller can also be tuned to meet gain and phase margins requirements. The design method of FOPID controller which is suitable to be used in industrial applications was demonstrated by Monje et. al [2]. Moreover, some novel control technologies

which combined FOPID controller and intelligent control algorithms together have been investigated and were proved to be effective in improving system transient performance [4, 17].

Going a step further, there are many FOPID controllers proposed for enhancing system robustness. One of the notable works is CRONE controller with three generations, developed by Oustaloup to deal with different model uncertainties including zero and pole misplacement [18]. Another frequently used method is achieving the flat phase property which is done by making the derivative of the phase to be zero at gain crossover. A PID control scheme based on this property was presented in [19]. Later, the fractional-order PD/PI controllers, which have already been successfully applied in motion control systems, were also designed according to the same isodamping property [20–22]. The extension of this method which can guarantee the system robustness with respect to different parameters variations was studied by Liu et al. [23]. Moreover, Feliu-Batlle et al. presented a Smith predictor based robust fractional-order controller with the application to water distribution [24]. The author has also proposed a robust fractional-order control scheme used in oscillatory systems with large uncertainties in their parameters [25]. A note on FOPID controller design which proposed a robust parameter tuning algorithm using Bode envelopes can be found in [26]. Besides, a robust fractional-order cascade PD and PI controller was investigated based on fuzzy control technology by Kumar et al. and has been applied to the speed control of a hybrid electric vehicle [27].

In this paper, we focus on the robust FOPID controller design based on Bode's optimal loop shaping which is commonly used for LTI (Linear Time Invariant) feedback systems [28]. Bode's ideal transfer function is served as a reference model in the parameter optimization process. Some related fractional-order controller tuning algorithms were discussed in [29–31]. However, most of them have a specified controlled system type and cannot be widely applied to different kinds of systems. In [29], a PID controller is proposed based on Bode's ideal transfer function, but it only aims at integer-order controlled plants; a similar work can be found in [30], where a robust fractional-order PI controller is designed; however, according to the derivation process, only one certain type of fractional-order controlled plant has been taken into consideration; moreover, the Bode loop shaping with CRONE compensator is discussed in [31], but it only emphasizes the loop shaping accuracy instead of controller tuning algorithm. The application domain of these studies is quite limited. Therefore, a robust fractional-order PID controller tuning algorithm based on Bode's optimal loop shaping which can be widely applied on both integer-order and fractional-order controlled systems is worth exploring in this paper. The controlled system with the proposed controller is robust to gain variations because the phase curve is flat within a certain frequency limit. The effectiveness of the presented robust FOPID controller is demonstrated by the simulation results of several controlled systems including integer-order and fractional-order ones.

The rest of this paper is organized as follows: in Section 2, some preliminaries of fractional calculus are given; detailed analysis of Bode's optimal loop shaping is presented in Section 3; Section 4 illustrates the proposed controller tuning process as well as robustness analysis of the controlled system; simulation results to verify the effectiveness of the proposed algorithm are presented in Section 5; finally, conclusions are made in Section 6.

2. Preliminaries

2.1. Fractional-Order Derivative. The fractional-order integral-differential operator ${}_{t_0}D_t^{\alpha}$ can be defined as

$$ {}_{t_0}D_t^{\alpha} = \begin{cases} \int_{t_0}^{t} f(\tau)\, d\tau^{-\alpha}, & \alpha < 0 \\ f(t), & \alpha = 0 \\ \dfrac{d^{\alpha}}{dt^{\alpha}} f(t), & \alpha > 0, \end{cases} \tag{1} $$

where $\alpha \in R$ is the integral or differential order and t, t_0 are upper and lower limits of the operator, respectively.

So far, there is still no unified definition of fractional-order derivative. But there have been three generally accepted definitions, that is, Caputo definition, Riemann-Liouville definition, and Grunwald-Letnikov [1]. Each of the three definitions has its own properties. In this paper, we use Caputo definition because it has been extensively used in engineering applications [6, 7]. The Caputo derivative of order α for a function $f(t) \in C^{n+1}([t_0, +\infty], R)$ is defined as [6]

$$ {}_{t_0}D_t^{\alpha} f(t) = \frac{1}{\Gamma(n-\alpha)} \int_{t_0}^{t} \frac{f^{(n)}(\tau)}{(t-\tau)^{\alpha+1-n}} d\tau, \tag{2} $$

where n is a positive integer, such that $n - 1 < \alpha \le n$.

The Laplace transform based on Caputo definition can be expressed as

$$ \mathscr{L}\left\{ {}_{t_0}D_t^{\alpha} f(t) \right\} = s^{\alpha} F(s) - \sum_{k=0}^{n-1} s^{\alpha-k-1} f^{(k)}(t_0), \tag{3} $$

where $\mathscr{L}\{\cdot\}$ represents the Laplace transform, $n - 1 < \alpha < n$, and s is the Laplace transform operator.

2.2. Mittag-Leffler Function. The Mittag-Leffler (ML) function is a generalized form of exponential function. It is widely used in solving fractional-order differential equations [1]. An ML function with two parameters can be written as a power series as [1]

$$ E_{\alpha,\beta}(x) = \sum_{k=0}^{\infty} \frac{x^k}{\Gamma(\alpha k + \beta)}, \tag{4} $$

where $\alpha > 0$, $\beta > 0$ and $x \in C$. When $\alpha = \beta = 1$, $E_{1,1}(x) = e^x$.

When $\beta = 1$, the ML function in (4) simplifies to a one-parameter form as

$$ E_{\alpha}(x) = E_{\alpha,1}(x) = \sum_{k=0}^{\infty} \frac{x^k}{\Gamma(\alpha k + 1)}. \tag{5} $$

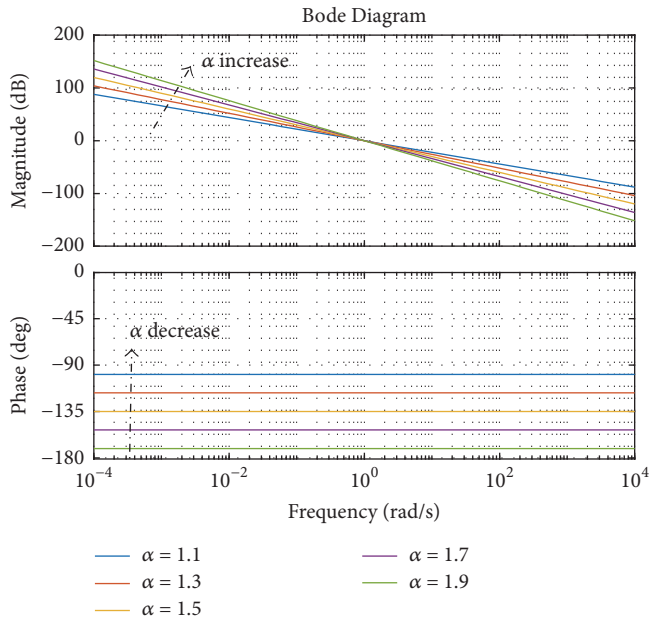

Figure 1: Bode diagram with different α.

The Laplace transform of (4) is

$$\mathscr{L}\left\{t^{\beta-1}E_{\alpha,\beta}\left(-\theta t^{\alpha}\right)\right\} = \frac{s^{\alpha-\beta}}{s^{\alpha}+\theta}, \quad \left(\mathrm{Re}\,(s) > |\theta|^{1/\alpha}\right), \tag{6}$$

where $t \geq 0$ and $\mathrm{Re}(s)$ is the real part of s.

3. Analysis of Bode's Optimal Loop Shaping

Consider a system whose open-loop transfer function is

$$F(s) = \frac{A}{s^{\alpha}}, \tag{7}$$

where $\alpha \in R$, $A = {\omega_c}^{\alpha}$, and ω_c is the crossover frequency of amplitude curve in Bode diagram which satisfies $\lg|F(j\omega_c)| = 0$. System (7) is a typical elementary fractional-order system. The resonance condition of this kind of system is $1 < \alpha < 2$, which has been proved in [32]. Therefore, we only take $1 < \alpha < 2$ into consideration in this paper. The Bode diagrams of system (7) with $\alpha = 1.1, 1.3, 1.5, 1.7, 1.9$ are shown as Figure 1. The amplitude curves are straight lines with the slopes of -20α dB/dec, and the corresponding phase curves are horizontal lines with $-\alpha\pi/2$ rad. Therefore, the phase margin of system (7) is $(1-\alpha/2)\pi$. That is to say, the phase margin will not change along with the change of A. So system with the open-loop transfer function in (7) is robust to gain variations. This is the optimal loop shaping suggested by Bode in [28].

The closed-loop transfer function corresponding to the open-loop one in (7) is

$$F(s) = \frac{A}{s^{\alpha}+A} = \frac{1}{Ts^{\alpha}+1}, \tag{8}$$

where $1 < \alpha < 2$ and $T = 1/A = {\omega_c}^{-\alpha}$ is the time constant of the system. The closed-loop system in (8) will be a reference model in the controller parameters optimization process in next section. Therefore, parameters α, T can be tuned to satisfy different performance requirements.

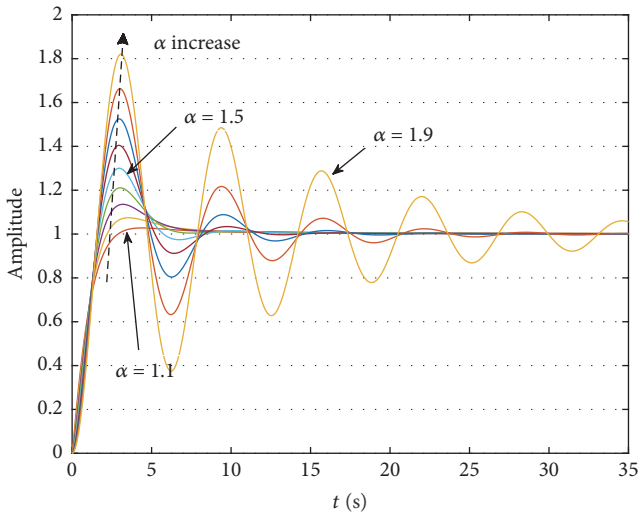

Figure 2: Step responses with different α.

When a unit step signal is fed into system (8), the time response of the system can be achieved as [1]

$$y(t) = L^{-1}\left[\frac{1}{s\left(Ts^{\alpha}+1\right)}\right] = 1 - \sum_{n=0}^{\infty}\frac{\left[-T^{-1}t^{\alpha}\right]^{n}}{\Gamma(\alpha n+1)} = 1 - E_{\alpha,1}\left(-T^{-1}t^{\alpha}\right). \tag{9}$$

Figure 2 gives the step responses of system (8) with $\alpha = 1.1, 1.2, \ldots, 1.9$. Some important time response performance indicators are derived as follows.

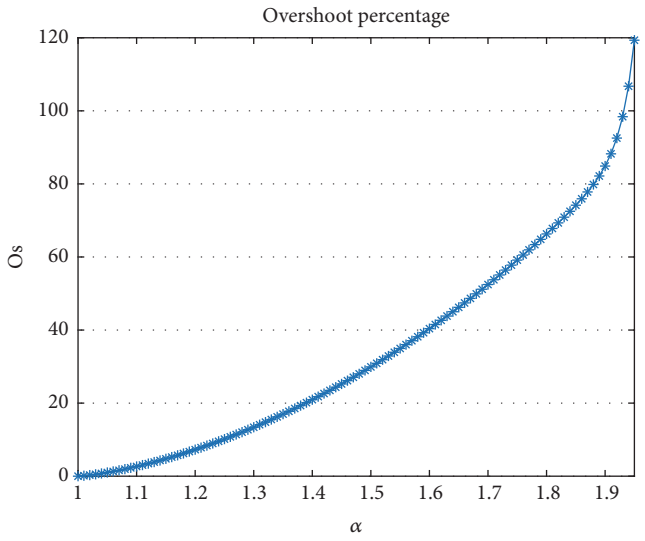

Figure 3: Overshoot percentage with different α.

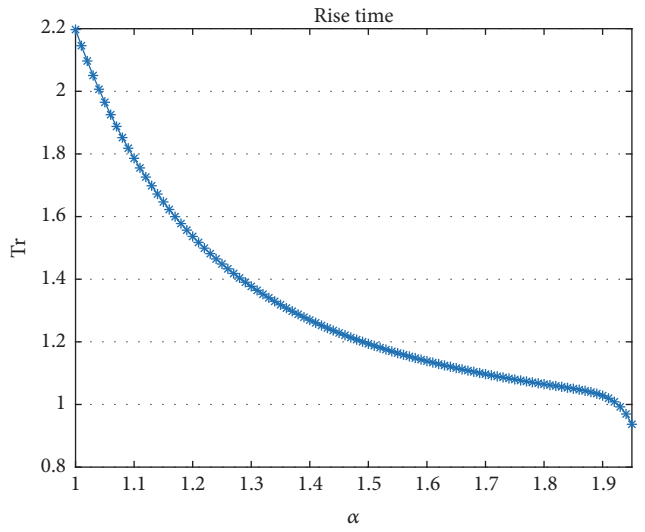

Figure 4: Rise time with different α.

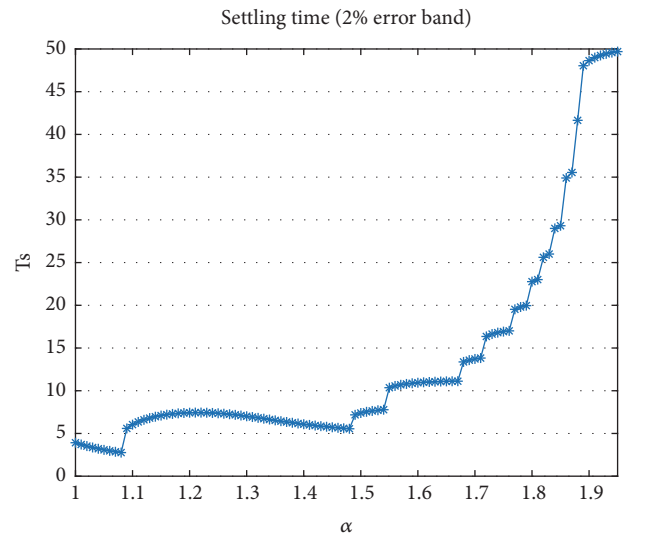

Figure 5: Setting time with different α (2%).

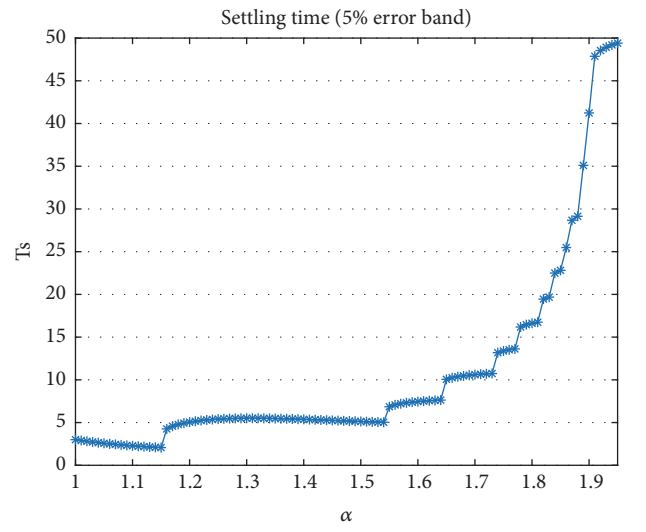

Figure 6: Setting time with different α (5%).

(1) Overshoot percentage M_p

$$M_p = \frac{y_{\max} - y_{\text{final}}}{y_{\text{final}}} \times 100\%. \tag{10}$$

(2) Rise time T_r (the time for the output to rise from 10% to first time 90% of the final value).

(3) 2% or 5% error band settling time T_s (the time for the output to reach and stay within a 2% or 5% error band of the final value).

These indicators cannot be achieved explicitly. Therefore, we express the relations between them and parameter α in Figures 3–6. The relationship curves have been approximated numerically into some nonlinear functions in [33]. However, the approximate accuracies may not be satisfactory enough. Hence, we recommend referring to the results we got in the figures. In this way, the controller parameters can be tuned by choosing different α values according to the required time domain indicators.

Moreover, frequency domain response specifications should also be taken into consideration. As it was demonstrated above, the phase margin of system (8) which has correspondence with time domain response overshoot is $(1 - \alpha/2)\pi$. The closed-loop frequency domain responses of system (8) with different T are illustrated in Figure 7. It can be seen from Figure 7 that the bandwidth of the system increases along with the value of T. On the other hand, the wider the bandwidth is in a system frequency domain response, the smaller the rise time will be in the corresponding time domain response. Namely, the controller parameters can also be tuned according to frequency domain specifications by changing the values of α and T. Moreover, the curves attenuate fast at high frequencies, which means that the system is not sensitive to high frequency disturbance.

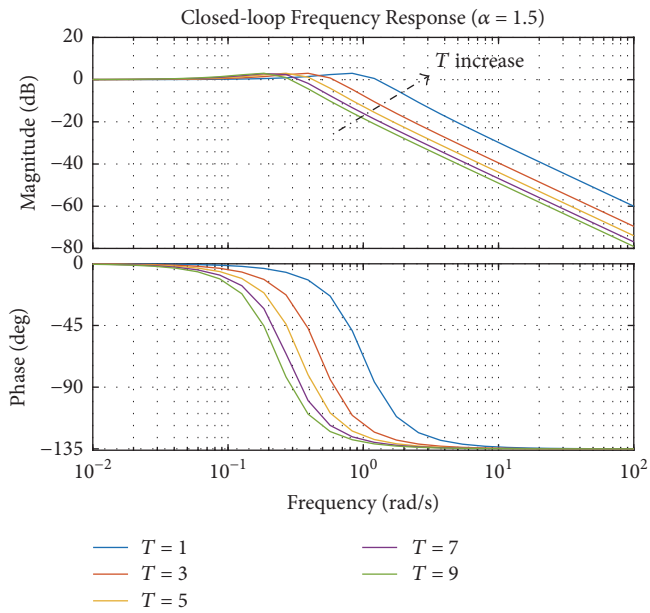

Figure 7: Frequency responses with different T ($\alpha = 1.5$).

It should be noted that there are some conflict relations between different design specifications. For instance, parameters chosen according to small rise time will lead to large overshoot. Therefore, wise trade-offs should be made on the selection of reference model.

4. Controller Tuning

4.1. Fractional-Order PID Controller. FOPID ($PI^{\lambda}D^{\mu}$) controller is an extension of conventional PID controller with extra two parameters, that is, integral order λ and differential order μ [12]. It can be expressed in frequency domain as

$$G_c(s) = K_p + \frac{K_i}{s^{\lambda}} + K_d s^{u}, \quad (0 < \lambda,\ \mu < 2) \tag{11}$$

where K_p, K_i, K_d are proportional, integral, and differential coefficients, respectively. When $\lambda = \mu = 1$, FOPID controller is equal to conventional PID controller. Figure 8 gives the comparison of controller parameters tuning domains between FOPID and PID controllers in geometrical perspective. The two extra parameters make the controller parameter tuning domain extend from a few points into a partial quarter plane. Meanwhile, the slope of amplitude curve in open-loop system frequency response at crossover frequency updates from -20 dB/dec into -20λ dB/dec. These provide more possibilities in improving control system robustness as well as transient performance, especially for fractional-order systems. However, the regulating process may become more complicated at the same time. The detailed analysis of the influence of λ, μ on control system performance can be found in [4].

4.2. Fractional Operator Realization. The fractional operators in (11) can be realized by several approaches [1]. In this paper, taking system (7) into consideration, we choose the

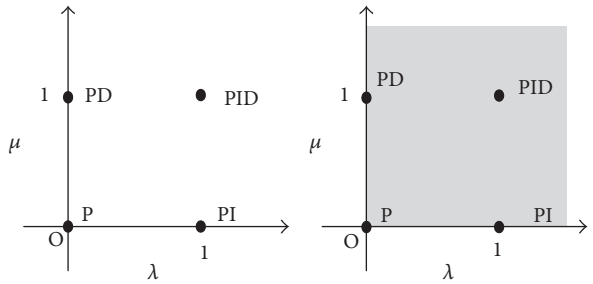

Figure 8: Comparison of PID and FOPID controllers.

Oustaloup approximation method which is widely used in this field [34]. A generalized fractional operator can be expressed as

$$H(s) = \left(\frac{s}{\omega_i}\right)^{\alpha}, \quad \alpha \in R^{+}. \tag{12}$$

Consider the expected approximate frequency range as (ω_a, ω_b); the operator s/ω_i can be substituted by

$$K_0 \frac{1 + s/\omega_s}{1 + s/\omega_l}, \tag{13}$$

where $K_0 = \omega_s/\omega_i = \omega_i/\omega_l$, $\omega_s < \omega_a$, $\omega_l > \omega_b$. Therefore, (12) can be updated as

$$H(s) = K\left(\frac{1 + s/\omega_s}{1 + s/\omega_l}\right)^{\alpha}, \tag{14}$$

where $C = {C_0}^{\alpha}$. Transform the transfer function above into the zero-pole form; it is obtained that

$$H(s) = \lim_{n\to\infty} \hat{H}(s), \tag{15}$$

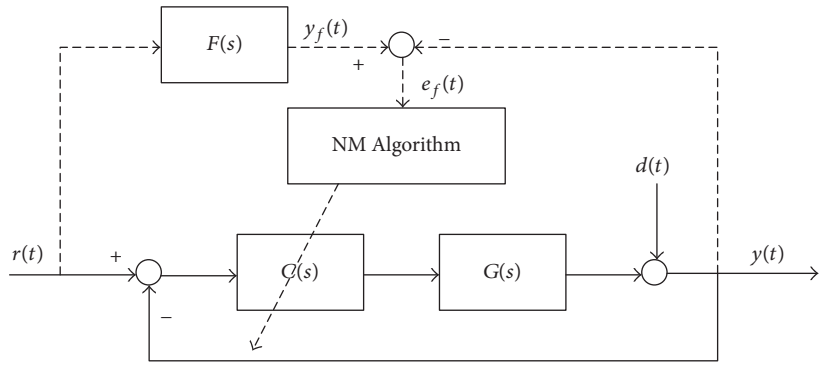

Figure 9: Tuning structure.

where

$$\hat{H}(s) = \left(\frac{\omega_i}{\omega_l}\right)^{\alpha} \prod_{k=-N}^{N} \frac{1 + s/\omega_k}{1 + s/\omega_k'},$$
$$\omega_k = \omega_s \left(\frac{\omega_l}{\omega_s}\right)^{((1/2)(1-\alpha)+k+N)/(2N+1)}, \quad (16)$$
$$\omega_k' = \omega_s \left(\frac{\omega_l}{\omega_s}\right)^{((1/2)(1+\alpha)+k+N)/(2N+1)}.$$

In this paper, we use the 7th approximation with interested frequency range $(10^{-3}, 10^{3})$.

4.3. Parameter Optimization. Normally, controller parameter optimization is proceeded based on the objective function which includes error between reference signal and actual output. However, this tuning method can only randomly get satisfactory control performance. It may make the rise time or overshoot of the controlled system quite small, but it cannot guarantee meeting any specific requirement. Besides, large times of trial and error are needed in the tuning process. In this paper, the Bode's optimal loop shaping transfer function is used as a nominal reference model in the optimization process to help the controlled system satisfy different control performance requirements. The tuning structure of the controlled system is represented in Figure 9, where $r(t)$, $y(t)$, $d(t)$ are reference signal, actual output signal, and disturbance signal, $e_f(t)$, $y_f(t)$ are nominal error signal and desire output signal which satisfy $e_f(t) = y_f(t) - y(t)$, and $C(s)$, $G(s)$, $F(s)$ are controller, controlled plant, and nominal reference model, respectively. In this way, the robustness and other transient performance requirements can be improved by tuning the controller parameters as well as the parameters of the nominal reference model $F(s)$ which was discussed in Section 3. The ITAE (Integral Time Absolute Error) indicator is chosen as the objective function in this paper. Therefore, according to Figure 9, the objective function can be expressed as

$$J = \int_0^{\infty} t \left|e_f(t)\right| dt = \int_0^{\infty} t \left|y_f(t) - y(t)\right| dt. \quad (17)$$

After getting the objective function, the Nelder-Mead (NM) simplex search algorithm is used to optimize the controller parameters according to the value of the objective function [35]. The fundamental principle of NM algorithm is constructing a rough search direction according to the initial parameter values first and updating the search direction constantly according to the objective function value until the optimal result is achieved. NM algorithm is widely applied in optimization processes, but the initial values influence the optimization result a lot. Therefore, suitable initial values should be selected before optimization.

4.4. Robustness Analysis. In this subsection, the robustness of a typical fractional-order system controlled by the proposed controller is analyzed. Consider a fractional-order transfer function described by

$$P(s) = \frac{k}{a_1 s^{\alpha_1} + a_2 s^{\alpha_2} + 1}, \quad (18)$$

where $k > 0$ is the system gain, a_1 and a_2 are positive constant coefficients, and the fractional-orders satisfy $1 < \alpha_1 \leq 2$, $0 < \alpha_2 \leq 1$.

Next we consider the corresponding FOPID controller designed as (11), where the fractional-orders are chosen as $\lambda = \alpha_2$ and $\mu = \alpha_1 - \alpha_2$ and the controller parameters are set as $k_p = a_2/b$, $k_i = 1/b$, and $k_d = a_2/b$. The constant b satisfies $b = k\omega_c^{-\alpha_2}$, and ω_c represents the gain crossover frequency of the open-loop transfer function $L(s) = P(s)G_c(s)$.

Based on (11) and (18), the open-loop transfer function can be obtained as

$$L(s) = \frac{k}{bs^{\alpha_2}} = \left(\frac{\omega_c}{s}\right)^{\alpha_2}. \quad (19)$$

Then we analyze the robustness of the controlled system with designed FOPID controller by employing the small gain theorem which has been widely used in FOPID control [36–38]. According to the small gain theorem, the robust stability condition can be represented by

$$\delta_p(\omega) < V(\omega, \alpha_2) \triangleq \frac{|1 + P(\omega i) C(\omega i)|}{|P(\omega i) C(\omega i)|}, \quad \text{for } \forall \omega > 0, \quad (20)$$

where $\delta_p(\omega)$ denotes the multiplicative norm-bound uncertainty of transfer function $P(s)$. Thus, larger $V(\omega, \alpha_2)$ means

Table 1: Controller parameters of $P_1(s)$.

$\phi_m = 45^\circ$	K_p	K_i	K_d	λ	μ
$\omega_c = 0.5$	0.4576	4.8570	0.0051	1.3814	1.8969
$\omega_c = 1.0$	0.2174	1.8775	0.0125	1.4226	0.0653
$\omega_c = 1.5$	0.1494	1.0816	0.0032	1.4226	2.1905
$\phi_m = 60^\circ$	K_p	K_i	K_d	λ	μ
$\omega_c = 0.5$	0.4197	4.7618	0.0907	1.2399	0.0468
$\omega_c = 1.0$	0.0649	1.8576	0.1888	1.2794	0.0023
$\omega_c = 1.5$	0.1719	1.0697	0.0328	1.2957	1.2878
$\phi_m = 90^\circ$	K_p	K_i	K_d	λ	μ
$\omega_c = 0.5$	0.9640	4.3890	0.0063	0.9969	0.2621
$\omega_c = 1.0$	0.3930	1.7269	0.0150	0.9976	1.1411
$\omega_c = 1.5$	0.2327	1.003	0.0080	0.9981	2.1141

that bigger modeling uncertainty may occur without breaking the robust stability of the controlled system.

Due to (11), (18), and (20), we achieve $V(\omega, \alpha_2)$ as

$$V(\omega, \alpha_2) = \frac{\left|1 + (\omega_c/\omega i)^{\alpha_2}\right|}{\left|(\omega_c/\omega i)^{\alpha_2}\right|} = \frac{\left|1 + i^{(-\alpha_2)}(\omega_c/\omega)^{\alpha_2}\right|}{(\omega_c/\omega)^{\alpha_2}} = \left(\left(\frac{\omega}{\omega_c}\right)^{2\alpha_2} + 2\left(\frac{\omega}{\omega_c}\right)^{\alpha_2}\cos\left(\frac{\alpha_2\pi}{2}\right) + 1\right)^{1/2}. \quad (21)$$

Besides, we calculate the derivatives of $V(\omega, \alpha_2)$ with respect to α_2 and obtain

$$\frac{dV(\omega, \alpha_2)}{d\alpha_2} = \frac{\ln(\omega/\omega_c)\left[(\omega/\omega_c)^{\alpha_2} + \cos(\alpha_2\pi/2)\right] - (\pi/2)\sin(\alpha_2\pi/2)}{\sqrt{\left(1 + 2(\omega_c/\omega)^{\alpha_2}\cos(\alpha_2\pi/2) + (\omega_c/\omega)^{2\alpha_2}\right)}}. \quad (22)$$

It is obvious that $dV(\omega, \alpha_2)/d\alpha_2 < 0$ when $\omega \le \omega_c$ and $0 < \alpha_2 \le 1$. Thus, $V(\omega, \alpha_2)$ is monotone decreasing with respect to $\alpha_2 \in (0, 1]$. In other words, for the same control system, FOPID controller owns better robust performance than PID controller in the low or even medium frequency ranges, which is established by the gain crossover frequency $\omega \le \omega_c$, and has no connection with the fractional-order α_2. In the simulation part, the obtained robust analysis result will be verified by some numerical examples.

5. Simulation

In this section, we take three typical kinds of systems, including fractional-order system and integer-order system, into consideration to illustrate the effectiveness of the proposed control strategy. Firstly, consider a fractional-order system whose transfer function is similar to the widely used first-order system [30]:

$$P_1(s) = \frac{0.5856}{0.2318s^{0.985} + 1}. \quad (23)$$

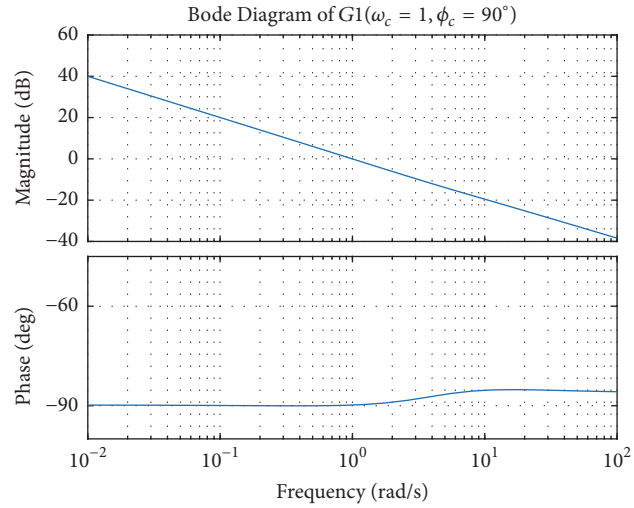

Figure 10: Bode diagram of $P_1(s)$.

The reference parameters in (8) and controller parameters in (11) tuned by the proposed algorithm are shown in Table 1. The Bode diagram of $P_1(s)$ controlled by the proposed controller with reference model parameters $\omega_c = 1$, $\phi_m = 90^\circ$ is depicted in Figure 10. It can be seen that the phase curve at crossover frequency is almost flat and the phase margin is $\pi/2$ which satisfies the controller design requirements. The step responses of $P_1(s)$ controlled by FOPID controllers tuned with the fixed phase margin $\phi_m = 60^\circ$ and different crossover frequencies $\omega_c = 0.5$, $\omega_c = 1$, $\omega_c = 1.5$ are shown in Figure 11. Correspondingly, Figure 12 demonstrates the step responses of $P_1(s)$ controlled by FOPID controllers tuned with the fixed crossover frequency $\omega_c = 1$ and varying phase margins $\phi_m = 45^\circ$, $\phi_m = 60^\circ$, $\phi_m = 90^\circ$. The unchanged overshoot and different settling times in Figure 11 and the similar settling time and different overshoots in Figure 12 illustrate the impact of reference model with varying parameters. Therefore, different control requirements can be fulfilled by varying reference model parameters ω_c, ϕ and controller parameters. In order to check the robustness of the controlled

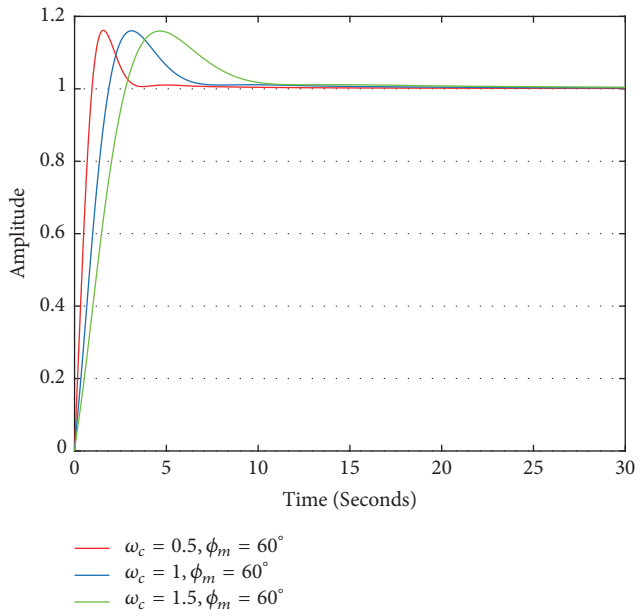

Figure 11: Step responses of $P_1(s)$ with different ω_c.

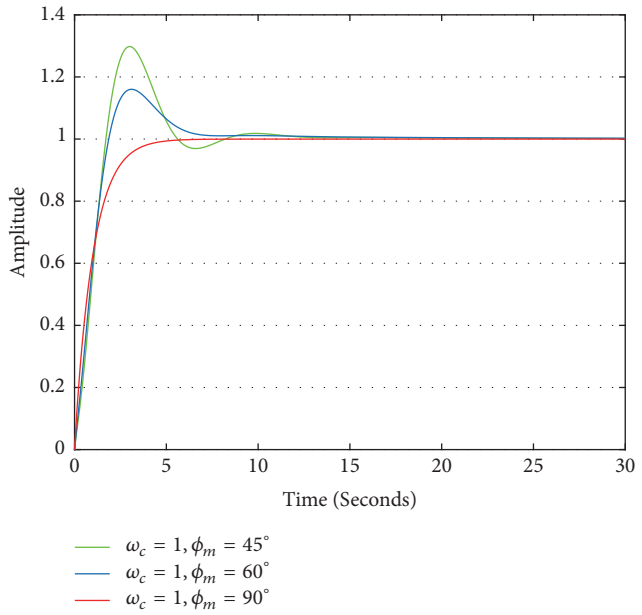

Figure 12: Step responses of $P_1(s)$ with different ϕ_m.

system, step responses comparisons of systems tuned by different reference parameters under ±30% gain variations are demonstrated in Figures 13 and 14, respectively. The overshoots of the step responses in each subfigures remain almost the same. These phenomena show that system $P_1(s)$ controlled by the proposed controller is robust to high amplitude gain variations. The step response comparison of $P_1(s)$ controlled by the proposed FOPID controller and the FOPID controller used in [30] is shown in Figure 15. The performance of system controlled by the proposed controller outperforms the other one with better robustness, lower overshoot, and smaller settling time. Figure 16 illustrates the ITAE indices values of $P_1(s)$ with different tuning parameters. All the indices are small enough to meet the optimization requirements.

Then, consider a fractional-order system [1] which is relatively complicated as

$$P_2(s) = \frac{1}{s^{2.6} + 3.3s^{1.5} + 2.9s^{1.3} + 3.32s^{0.9} + 1}. \quad (24)$$

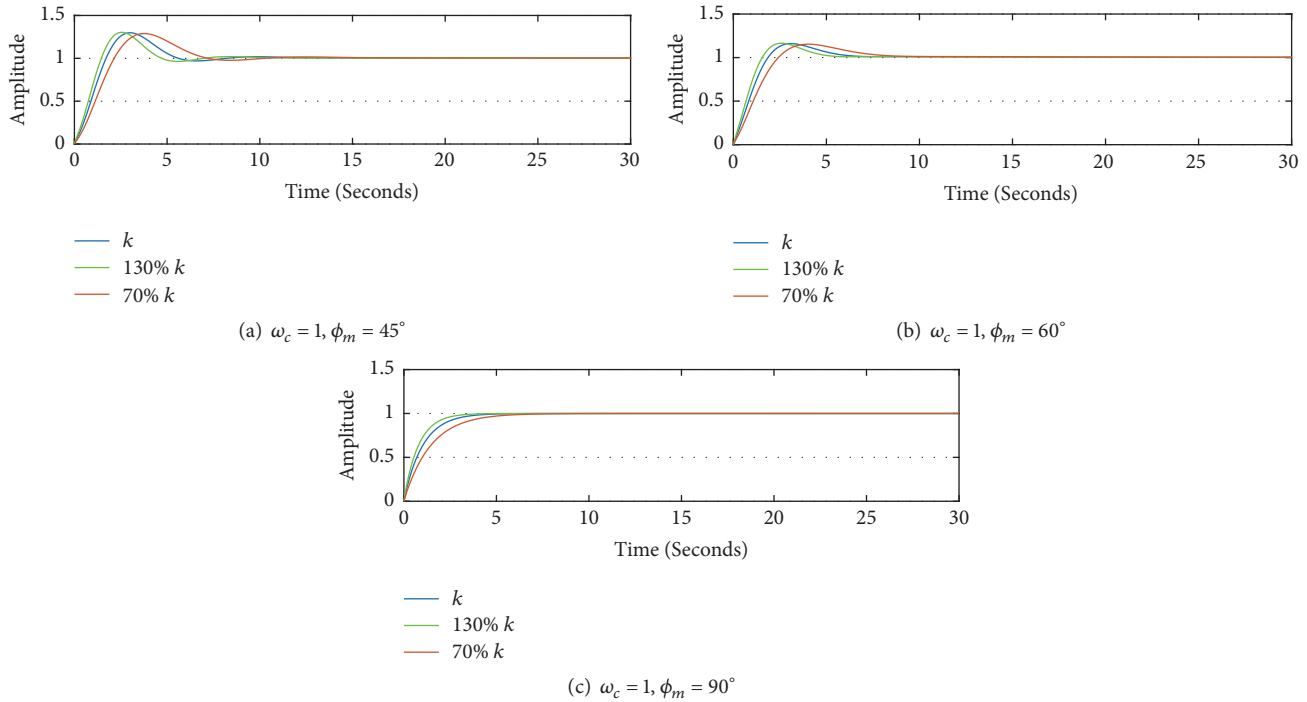

(a) $\omega_c = 1, \phi_m = 45^\circ$

(b) $\omega_c = 1, \phi_m = 60^\circ$

(c) $\omega_c = 1, \phi_m = 90^\circ$

Figure 13: Step responses of $P_1(s)$ with different ϕ_m.

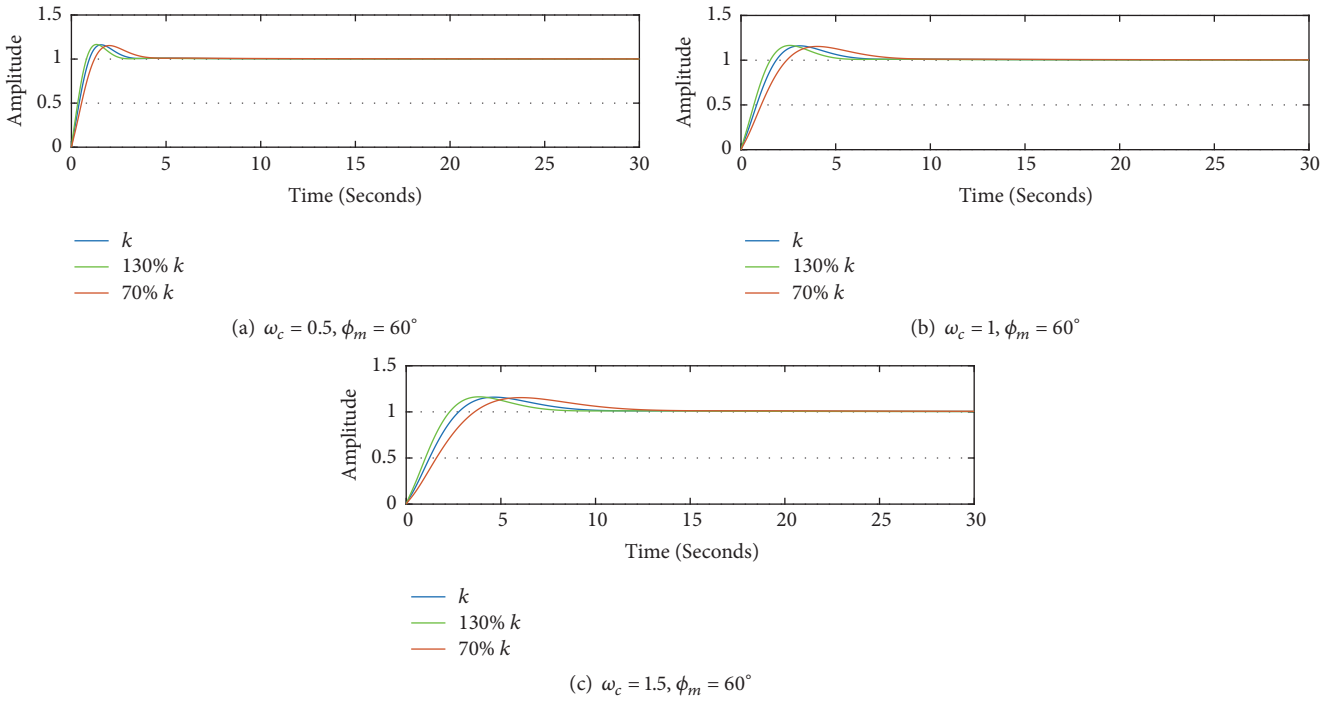

(a) $\omega_c = 0.5, \phi_m = 60^\circ$

(b) $\omega_c = 1, \phi_m = 60^\circ$

(c) $\omega_c = 1.5, \phi_m = 60^\circ$

Figure 14: Step responses of $P_1(s)$ with different ω_c.

The reference parameters and the obtained the controller parameters are shown in Table 2. Figures 17 and 18 demonstrate the step responses of $P_2(s)$ controlled by the proposed controllers tuning with different ω_c and ϕ_m. Similarly, the results show that different control performance can be satisfied by varying reference model parameters. The ITAE indices of $P_2(s)$ in Figure 19 are also small enough for optimization.

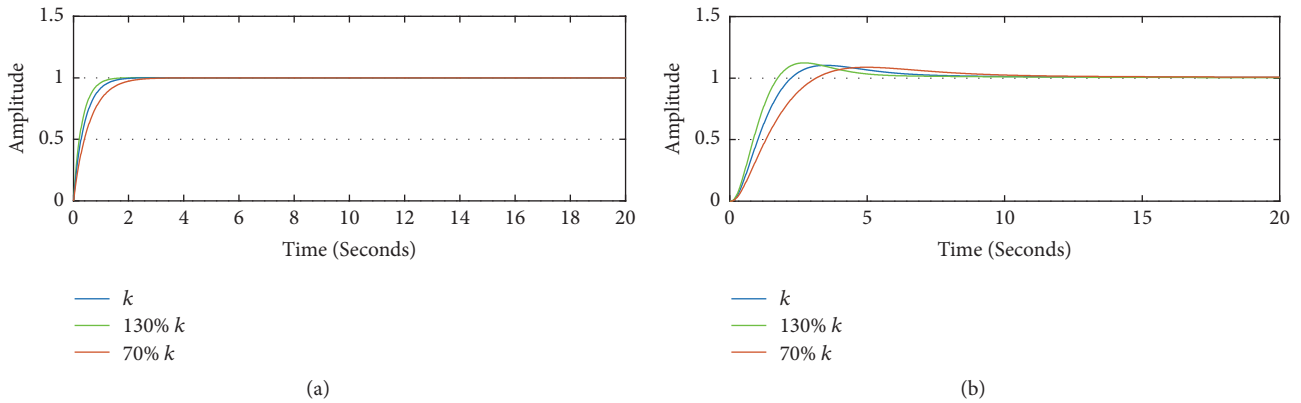

Figure 15: Step responses of $P_1(s)$ with different FOPID controllers ((a) FOPID controller proposed in this paper, (b) FOPID controller in [30]).

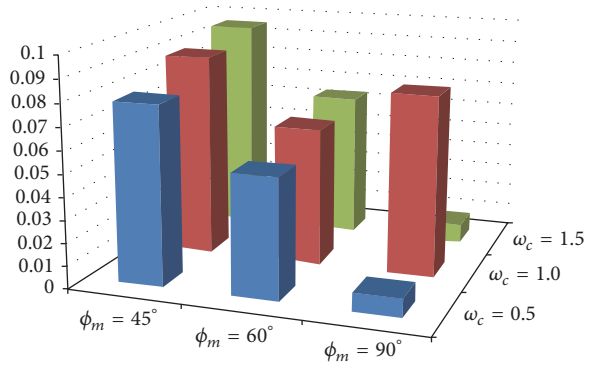

Figure 16: ITAE indices values of $P_1(s)$.

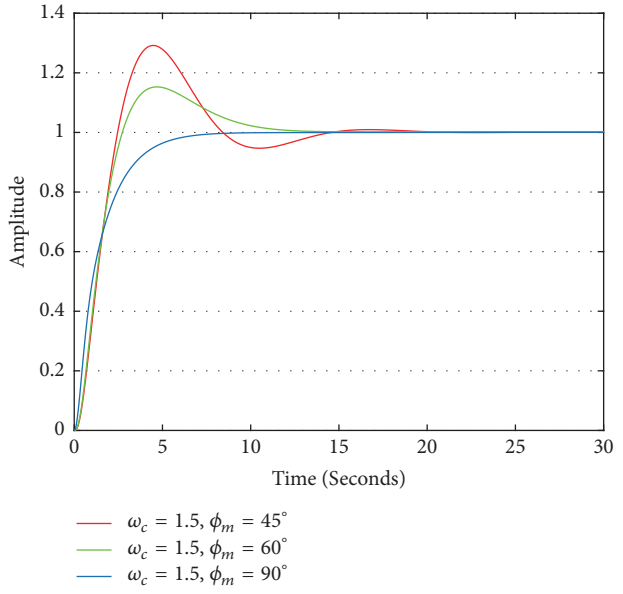

Figure 17: Step response of $P_2(s)$ with the same ω_c.

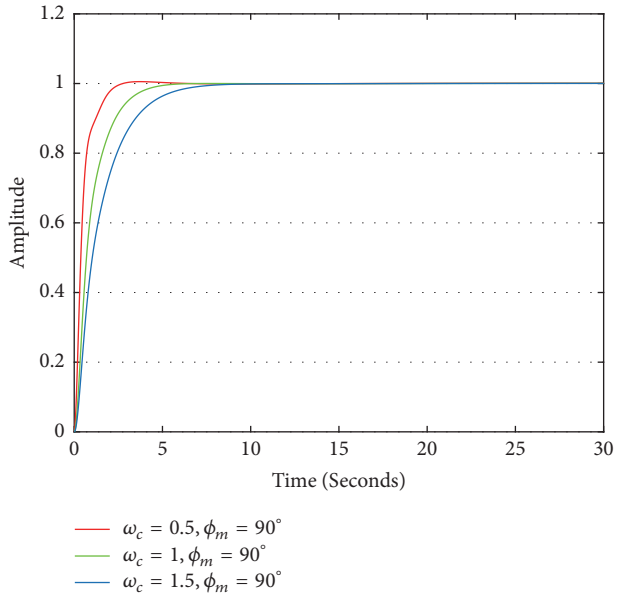

FIGURE 18: Step response of $P_2(s)$ with the same ϕ_m.

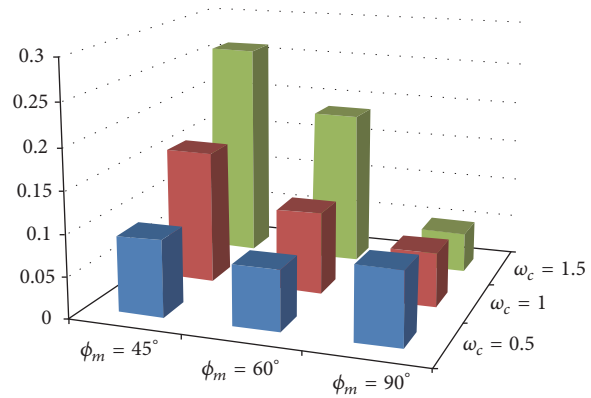

FIGURE 19: ITAE indices values of $P_2(s)$.

TABLE 2: Controller parameters of $P_2(s)$.

$\phi_m = 45^\circ$	K_p	K_i	K_d	λ	μ
$\omega_c = 0.5$	18.3282	9.9945	1.5199	0.9742	1.3785
$\omega_c = 1.0$	7.9000	3.4213	0.5194	1.0581	1.6645
$\omega_c = 1.5$	3.4053	1.7451	0.8343	1.0783	0.0200
$\phi_m = 60^\circ$	K_p	K_i	K_d	λ	μ
$\omega_c = 0.5$	19.9228	4.6069	2.0377	1.0861	1.3092
$\omega_c = 1.0$	8.7852	1.9719	0.9068	1.1120	1.4516
$\omega_c = 1.5$	2.6270	1.0729	2.2338	1.1239	0.0068
$\phi_m = 90^\circ$	K_p	K_i	K_d	λ	μ
$\omega_c = 0.5$	13.1618	1.6627	6.6312	1.0474	0.8915
$\omega_c = 1.0$	5.8327	0.9930	3.7246	1.0143	0.6984
$\omega_c = 1.5$	3.7370	0.6459	2.5961	1.0057	0.6438

Table 3: Controller parameters of $P_3(s)$.

$\phi_m = 45^\circ$	K_p	K_i	K_d	λ	μ
$\omega_c = 0.5$	2.4905	4.3983	0.0580	1.2311	1.5110
$\omega_c = 1.0$	0.9355	1.4819	0.0018	1.2690	0.6910
$\omega_c = 1.5$	0.6170	0.7823	0.0267	1.3210	2.0922
$\phi_m = 60^\circ$	K_p	K_i	K_d	λ	μ
$\omega_c = 0.5$	2.7170	3.4615	0.1476	1.1772	1.3201
$\omega_c = 1.0$	1.1504	1.3321	0.0444	1.2078	1.5853
$\omega_c = 1.5$	0.7038	0.7593	0.0268	1.2262	1.7678
$\phi_m = 90^\circ$	K_p	K_i	K_d	λ	μ
$\omega_c = 0.5$	2.4535	1.9657	0.4621	1.0005	1.0355
$\omega_c = 1.0$	1.2374	0.9942	0.2407	1.0002	1.0212
$\omega_c = 1.5$	0.8273	0.6647	0.1628	1.0001	1.0157

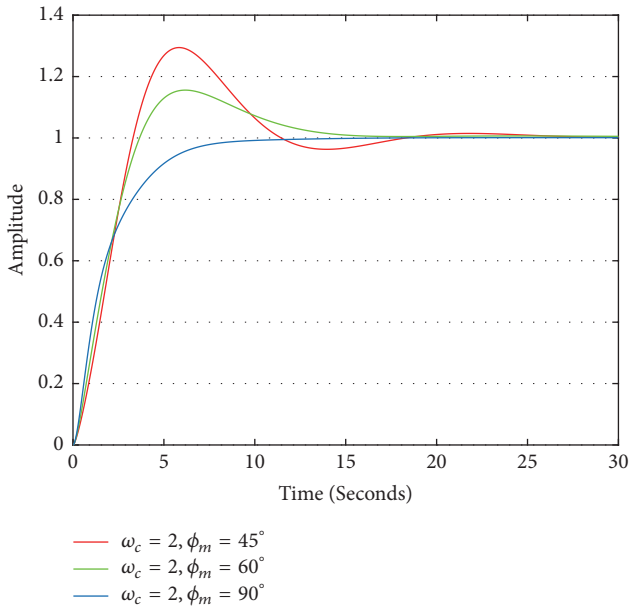

Figure 20: Step response of $P_3(s)$ with the same ω_c.

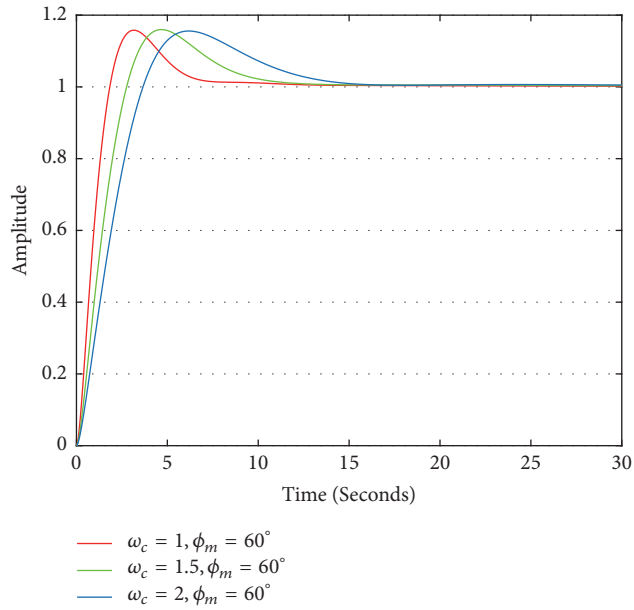

Figure 21: Step response of $P_3(s)$ with the same ϕ_m.

Finally, take an integer-order system [31], whose transfer function is shown as below, into consideration:

$$P_3(s) = \frac{1}{(s+1)(0.2s+1)(0.04s+1)(0.008s+1)}. \quad (25)$$

Table 3 shows the tuned controller and reference model parameters of $P_3(s)$. Step responses of $P_3(s)$ controlled by different controllers in Table 3 are depicted in Figures 20 and 21. It is shown that the step responses of integer-order system can also be shaped by the proposed FOPID controller according to different design requirements. The ITAE indices of $P_3(s)$ in Figure 22 also satisfy the optimization criterion. The simulation results verify the effectiveness of the proposed controller used on both fractional-order and integer-order systems. The systems controlled by the proposed algorithm achieve better robustness and transient control performance compared with other controllers.

6. Conclusion

In this paper, a novel tuning methodology of robust fractional-order PID controller is proposed. The controlled system output can be shaped by varying reference model parameters according to different control performance requirements. The phase curve can be flat within a certain frequency limit. Therefore, the system has the desirable characteristic of being robust to gain variations. Robustness analysis which supports the robust tuning specification is also carried out. The proposed fractional-order PID controller does not have any restriction on the controlled plant. So it can be widely applied on both integer-order and fractional-order systems.

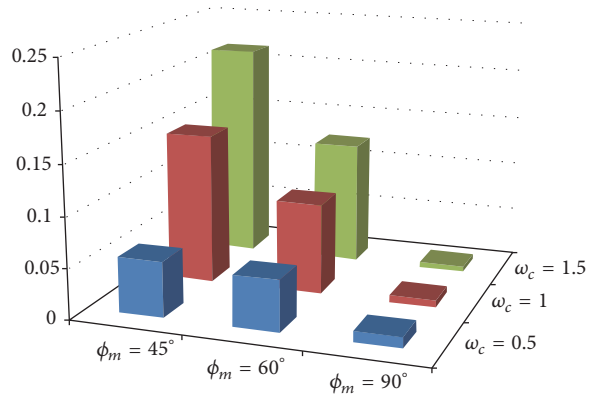

FIGURE 22: ITAE indices values of $P_3(s)$.

Three design examples including different kinds of controlled plants are presented to verify the effectiveness of the proposed algorithm.

Conflicts of Interest

The authors declare that they have no conflicts of interest.

Acknowledgments

This work is supported by the Fundamental Research Funds for the Central Universities of China (under Grant nos. G2018KY0305, G2018KY0302, and 3102017OQD069) and the National Natural Science Foundation of China (NSFC) (under Grant no. 61703335).

References

[1] D. Xue, *Fractional-order Control Systems: Fundamentals and Numerical Implementations*, De Gruyter, Berlin, 2017.

[2] C. A. Monje, B. M. Vinagre, V. Feliu, and Y. Chen, "Tuning and auto-tuning of fractional order controllers for industry applications," *Control Engineering Practice*, vol. 16, no. 7, pp. 798–812, 2008.

[3] L. Liu, S. Tian, D. Xue, T. Zhang, and Y. Chen, "Continuous fractional-order Zero Phase Error Tracking Control," *ISA Transactions*, vol. 75, pp. 226–235, 2018.

[4] L. Liu, F. Pan, and D. Xue, "Variable-order fuzzy fractional PID controller," *ISA Transactions*, vol. 55, pp. 227–233, 2015.

[5] A. Lassoued and O. Boubaker, "Dynamic analysis and circuit design of a novel hyperchaotic system with fractional-order terms," *Complexity*, vol. 2017, Article ID 3273408, 10 pages, 2017.

[6] S. Zhang, Y. Yu, and H. Wang, "Mittag-Leffler stability of fractional-order Hopfield neural networks," *Nonlinear Analysis: Hybrid Systems*, vol. 16, pp. 104–121, 2015.

[7] S. Zhang, Y. Yu, and Q. Wang, "Stability analysis of fractional-order Hopfield neural networks with discontinuous activation functions," *Neurocomputing*, vol. 171, pp. 1075–1084, 2016.

[8] R. L. Magin, "Fractional calculus in bioengineering, part 3," *Critical Reviews in Biomedical Engineering*, vol. 32, no. 1, pp. 1–104, 2004.

[9] T. J. Freeborn, "A survey of fractional-order circuit models for biology and biomedicine," *IEEE Journal on Emerging and Selected Topics in Circuits and Systems*, vol. 3, no. 3, pp. 416–424, 2013.

[10] F. Ge, Y. Chen, and C. Kou, "On the regional gradient observability of time fractional diffusion processes," *Automatica*, vol. 74, pp. 1–9, 2016.

[11] K. J. Strm and T. Hgglund, *PID controllers: Theory, Design and Tuning*, 1995.

[12] I. Podlubny, "Fractional-order systems and $PI^{\lambda}D^{\mu}$-controllers," *IEEE Transactions on Automatic Control*, vol. 44, no. 1, pp. 208–214, 1999.

[13] I. Petras, "Fractional-order feedback control of a DC motor," *Journal of Electrical Engineering*, vol. 60, no. 3, pp. 117–128, 2009.

[14] M. Zamani, M. Karimi-Ghartemani, N. Sadati, and M. Parniani, "Design of a fractional order PID controller for an AVR using particle swarm optimization," *Control Engineering Practice*, vol. 17, no. 12, pp. 1380–1387, 2009.

[15] B. Vinagre, I. Podlubny, L. Dorcak, and V. Feliu, "On fractional PID controllers: A frequency domain approach," in *Proceedings of the IFAC Workshop on Digital Control Past*, 2000.

[16] S. E. Hamamci, "An algorithm for stabilization of fractional-order time delay systems using fractional-order PID controllers," *Institute of Electrical and Electronics Engineers Transactions on Automatic Control*, vol. 52, no. 10, pp. 1964–1968, 2007.

[17] H. U. Hai-Bo and Y. R. Huang, "Self-tuning fractional order PID based on hybrid PSO neural networks," in *Microelectronics & Computer*, 2010.

[18] A. Oustaloup, J. Sabatier, P. Lanusse et al., "An overview of the CRONE approach in system analysis, modeling and identification, observation and control," *IFAC Proceedings Volumes*, vol. 41, no. 2, pp. 14254–14265, 2008.

[19] Y. Chen and K. L. Moore, "Relay feedback tuning of robust PID controllers with iso-damping property," *IEEE Transactions on Systems, Man, and Cybernetics, Part B: Cybernetics*, vol. 35, no. 1, pp. 23–31, 2005.

[20] H. S. Li, Y. Luo, and Y. Q. Chen, "A fractional order proportional and derivative (FOPD) motion controller: tuning rule and experiments," *IEEE Transactions on Control Systems Technology*, vol. 18, no. 2, pp. 516–520, 2010.

[21] Y. Luo, Y. Q. Chen, C. Y. Wang, and Y. G. Pi, "Tuning fractional order proportional integral controllers for fractional order systems," *Journal of Process Control*, vol. 20, no. 7, pp. 823–831, 2010.

[22] Y. Chen, H. Dou, B. M. Vinagre, and C. A. Monje, "A robust tuning method for fractional order PI controllers," *IFAC Proceedings Volumes*, vol. 39, no. 11, pp. 22–27, 2006.

[23] L. Liu, S. Zhang, D. Xue, and Y. Chen, "General robustness analysis and robust fractional-order PD controller design for fractional-order plants," *IET Control Theory Application*, 2018.

[24] V. Feliu-Batlle, R. Rivas Pérez, F. J. Castillo García, and L. Sanchez Rodriguez, "Smith predictor based robust fractional order control: application to water distribution in a main irrigation canal pool," *Journal of Process Control*, vol. 19, no. 3, pp. 506–519, 2009.

[25] V. Feliu-Batlle, "Robust isophase margin control of oscillatory systems with large uncertainties in their parameters: a fractional-order control approach," *International Journal of Robust and Nonlinear Control*, vol. 27, no. 12, pp. 2145–2164, 2017.

[26] C. Yeroglu and N. Tan, "Note on fractional-order proportional-integral-differential controller design," *IET Control Theory & Applications*, vol. 5, no. 17, pp. 1978–1989, 2011.

[27] V. Kumar, K. P. Rana, and P. Mishra, "Robust speed control of hybrid electric vehicle using fractional order fuzzy PD and PI controllers in cascade control loop," *Journal of The Franklin Institute*, vol. 353, no. 8, pp. 1713–1741, 2016.

[28] H. W. Bode, *Network Analysis and Feedback Amplifier Design*, Van Nostrand, 1945.

[29] A. Banos, J. n. Cervera, P. Lanusse, and J. Sabatier, "Bode optimal loop shaping with CRONE compensator," *Journal of Vibration and Control*, vol. 17, no. 13, pp. 1964–1974, 2011.

[30] R. Azarmi, M. Tavakoli-Kakhki, A. K. Sedigh, and A. Fatehi, "Robust Fractional Order PI Controller Tuning Based on Bode's Ideal Transfer Function," *IFAC-PapersOnLine*, vol. 49, no. 9, pp. 158–163, 2016.

[31] K. Amoura, R. Mansouri, M. Bettayeb, and U. M. Al-Saggaf, "Closed-loop step response for tuning PID-fractional-order-filter controllers," *ISA Transactions*, vol. 64, pp. 247–257, 2016.

[32] R. Malti, X. Moreau, F. Khemane, and A. Oustaloup, "Stability and resonance conditions of elementary fractional transfer functions," *Automatica*, vol. 47, no. 11, pp. 2462–2467, 2011.

[33] R. S. Barbosa, J. A. T. Machado, and I. M. Ferreira, "Tuning of PID controllers based on bode's ideal transfer function," *Nonlinear Dynamics*, vol. 38, no. 1-4, pp. 305–321, 2004.

[34] A. Oustaloup, P. Melchior, P. Lanusse, O. Cois, and F. Dancla, *The CRONE toolbox for MATLAB*, 2000.

[35] M. A. Luersen and R. le Riche, "Globalized nelder-mead method for engineering optimization," *Computers & Structures*, vol. 82, no. 23–26, pp. 2251–2260, 2004.

[36] R. Azarmi, A. K. Sedigh, M. Tavakoli-Kakhki, and A. Fatehi, "Design and implementation of smith predictor based fractional order PID controller on MIMO flow-level plant," in *Proceedings of the 23rd Iranian Conference on Electrical Engineering, ICEE 2015*, pp. 858–863, Iran, May 2015.

[37] F. Padula, R. Vilanova, and A. Visioli, "H_{∞} optimization-based fractional-order PID controllers design," *International Journal of Robust and Nonlinear Control*, vol. 24, no. 17, pp. 3009–3026, 2014.

[38] D. Wang and X. Gao, "H_{∞} design with fractional-order PD^{μ} controllers," *Automatica*, vol. 48, no. 5, pp. 974–977, 2012.